Characterizing the SUMOylation of APC4 and the Function of APC4 Within Neurons

Dissertation

for the award of the degree
“Doctor of Philosophy"
at the Georg-August-Universität Göttingen

within the doctoral program Biology
Georg-August University School of Science (GAUSS)

Submitted by
Jennifer L. Day
From Boise, Idaho, USA

Göttingen, 2021

Thesis Committee

Dr. Nils Brose
Department of Molecular Biology
Max Planck Institute for Experimental Medicine

Dr. Holger Bastians
Section for Cellular Oncology, Institute of Molecular Oncology
University Medical Center Göttingen

Members of the Examination Board

Reviewer: Dr. Nils Brose
Department of Molecular Biology
Max Planck Institute for Experimental Medicine

Second Reviewer: Dr. Holger Bastians
Section for Cellular Oncology, Institute of Molecular Oncology
University Medical Center Göttingen

Further Members of the Examination Board

Dr. Markus Bohnsack
Department of Molecular Biology
University Medical Center Göttingen

Dr. Thomas Dresbach
Department of Anatomy and Embryology
University Medical School Göttingen

Dr. Tiago Fleming Outeiro
Department of Experimental Neurodegeneration
University Medical Center Göttingen

Dr. Ira Milosevic
Synaptic Vesicle Dynamics, European Neuroscience Institute
Current affiliation:
Wellcome Centre for Human Genetics, Nuffield Department of Medicine
NIHR Oxford Biomedical Research Centre

Date of the oral examination: June 2, 2021

Declaration

I declare that this thesis was written independently and with no other sources than those cited.

Jennifer L. Day

April 14, 2021

Table of Contents

Abstract

The Anaphase Promoting Complex (APC/C) is an E3 ubiquitin ligase that is involved in multiple molecular processes in eukaryotic cells. It is regulated by an intricate system of post-translational modifications that enables the complex to quickly target different sets of proteins for degradation by the proteasome. The APC/C is best known for its function in regulating the cell cycle, but it is also expressed in non-dividing cells like neurons, where its function is less clear. In the present study, I first sought to elucidate the function of the SUMOylation of APC4, a component of the APC/C, in HEK293 cells and in neurons. In the second part of my study, I tried to determine the function of APC4 in neurons. In regards to the first research focus, I show that APC4 is SUMOylated, and I found that this SUMOylation does not influence the subcellular localization of APC4 or the assembly of the APC/C. I show further that endogenous APC4 is localized to the nucleus and to the cytoplasm of HEK293 cells and neurons, and I found that APC4 is more heavily SUMOylated in the nucleus of HEK293 cells and in the cytoplasm of cortical neurons obtained from a mouse brain. My attempts to determine the role of APC4 SUMOylation in the regulation of the neuronal APC/C were confounded by the fact that my experimental results challenged the earlier notions of the current list of candidate neuronal substrates of the APC/C. In regards to my second research direction, I knocked out the gene encoding APC4, *ANAPC4*, in cultured neurons and conducted biochemical and morphological analyses of the mutant neurons. In contrast to prior publications, I found that FEZ1, ID1, and NEUROD2 are not substrates of the cortical APC/C. ID1 levels were instead depleted in *ANAPC4* knockout cultures, indicating that ID1 is downstream of a substrate of the APC/C. I further show that *ANAPC4* knockout neurons have an increase in the number of primary neurites, but they had no changes in the length of their neurites or in their number of branches. Altogether, these *ANAPC4* knockout data indicate that many of the previously proposed neuronal substrates of the APC/C are in fact not targeted by the APC/C. Future studies must focus on elucidating the function of the APC/C in neurons and in determining how the SUMOylation of APC4 influences the ubiquitylation of these substrates. In general, the information contained in the present thesis may be important for the development of novel drug targets to treat cancer and possibly diseases of the nervous system.

List of Figures

List of Tables

List of Key Abbreviations

Aβ	Amyloid beta
AMPA	α-amino-3-hydroxy-5-methyl-4-isoxazolepropionic acid receptor
ANAPC4	Gene encoding APC4
APC/C	Anaphase Promoting Complex
APC#	Anaphase Promoting Complex Subunit #
bp	Base pairs
C. *elegans*	*Caenorhabditis elegans*
CaMKIIβ	Calcium/calmodulin-dependent protein kinase II
Cdc20	Cell Division Cycle Protein 20
Cdh1	Cadherin 1
D box	Destruction box
D. melanogaster	*Drosophila melanogaster*
DAPI	4',6-Diamidino-2-Phenylindole, Dihydrochloride
DHPG	3,5-dihydroxyphenylglycine
FEZ1	Fasciculation and elongation protein zeta 1
FMRP	Fragile X Mental Retardation Protein
HDAC6	Histone deacetylase 6
HECT	Homologous to E6-AP C-terminus
HCMV	Human Cytomegalovirus
ICC	Immunocytochemistry
ID1	Inhibitor of DNA binding 1
ID2	Inhibitor of DNA binding 2
IP	Immunoaffinity purification
IPSC	Inhibitory Postsynaptic Potentials
LTD	Long Term Depression
LTP	Long Term Potentiation
MPIEM	Max Planck Institute for Experimental Medicine
NEUROD2	Neuronal Differentiation 2
NMDA(R)	N-methyl-D-aspartate (Receptor type)
PFA	Paraformaldehyde
PFKFB3	6-Phosphofructo-2-kinase/fructose-2,6-bisphosphatase-3
PSD	Post Synaptic Density
RING	Really Interesting New Gene
ROCK	Rho-associated protein kinase 2
S. cerevisiae	*Saccharomyces cerevisiae*
S. pombe	*Saccharomyces pombe*
SDS/PAGE	Sodium Dodecyl Sulfate Polyacrylamide Gel
SEM	Standard Error of the Mean
SENP	Sentrin-Specific Protease
SHANK	SH3 And Multiple Ankyrin Repeat Domains
SIM	SUMO interacting motif
SPM	Crude PSD Fraction
SUMO	Small Ubiquitin-Like Modifier
tm1a	Knockin first allele *ANAPC4* conditional knockout mouse line
tm1c	*ANAPC4* conditional knockout mouse line
tm1d	*ANAPC4* conditional knockout mouse line, after Cre expression
TPR	Tetratricopeptide Repeats
WB	Western Blotting

1. Introduction

A plethora of different signaling pathways control the ability of cells to survive, adapt, and function. This is achieved by a complex system that regulates all of these pathways at a variety of different levels within each pathway. First of all, the genes that encode the pathway-relevant proteins must be transcribed and translated at the proper time and at the proper levels. Second, the proteins must be correctly folded in order for it to have the proper functions and the proper interactions with other proteins in the cell. Third, all relevant proteins must be localized to the proper cellular subcompartment at the correct time. Finally, the levels of protein expression must be tightly regulated by the controlled degradation of all of the proteins in the pathway. Cells utilize a variety of different post-translational modifications to achieve the miraculous feat of controlling all of these different signaling pathways. Post-translational modifications function at all levels of this process, where they help to modulate transcription, translation, protein interactions, protein function, protein localization, protein stability, and protein turnover (reviewed in Chen et al., 2017).

There are many different types of post-translational modifications within a cell, and each type of modification serves a distinct function. In many cases, a small chemical group is attached to the protein. One of the best-studied examples of this type of modification is phosphorylation, which involves the attachment of a phosphate group to serine, threonine, or tyrosine residues of a protein. Other chemical groups may be added to proteins, which is the case with glycosylation (carbohydrate group), acetylation (acetyl group), and methylation (methyl group; reviewed in Chen et al., 2017). Ubiquitylation and SUMOylation, which is an ubiquitin-like modification, are unique among the major post-translational modifications, because they involve the attachment of a small polypeptide to a lysine residue of a protein through a cascade of E1, E2, and E3 enzymes (Figures 1 and 2). Ubiquitylation and SUMOylation serve a diverse array of functions within a cell (reviewed in Chen et al., 2017; reviewed in Gareau and Lima, 2010), and they are the primary focus of this present study.

1.1 Ubiquitylation

1.1.1 The Different Types of Protein Ubiquitylation

Ubiquitylation involves the formation of an isopeptide bond between the C-terminus of ubiquitin and lysine residues on substrate proteins, but other types of linkages may also occur within cells (reviewed in Oh et al., 2018). While we normally associate ubiquitylation with the attachment of a chain of ubiquitin moieties to a substrate protein, the attachment of a single ubiquitin moiety through monoubiquitylation does frequently occur too, and this type of modification is important for regulating both protein function and protein-protein interactions (reviewed in Yau and Rape, 2016). The regulation of the histone code by the monoubiquitylation of Histone H2A is a prominent example of this type of monoubiquitylation (Borchert et al., 2010; Zhou et al., 2008).

Ubiquitin itself is a 76 amino acid protein that has 7 lysine residues (K6, K11, K27, K29, K33, K48, and K63) within its sequence, and each of these can be ubiquitylated to form chains of ubiquitin (reviewed in Oh et al., 2018). The chain nomenclature is based on the specific lysine residue that is ubiquitylated within the chain, and this same lysine residue is ubiquitylated on each individual ubiquitin moiety within that chain. The most prevalent type of chain is the K48 chain, which, along with K11 chains, triggers degradation by the 26S proteasome. The second most common type of chain is K63, which is involved, for instance, in the activation of kinases, the regulation of endocytosis, and the regulation of the NF-κB transcription factor (reviewed in Erpapazoglou et al., 2014). Recently, it is becoming more evident that chains with mixed linkages or branches are formed, and these are important for a variety of different biological processes, including proteasomal degradation. Due to the sheer number of different combinations of ubiquitin connections that can be achieved within a chain, these complex chains seem to serve a diverse array of functions within a cell (reviewed in Yau and Rape, 2016).

1.1.2 A Cascade Of Enzymes Ubiquitylates Substrate Proteins

A cascade of enzymes is required for the attachment of ubiquitin to a substrate protein (Figure 1). First, an E1 enzyme forms a thioester bond with ubiquitin (Figure 1 A), and then the ubiquitin is transferred to a catalytic cysteine residue on an E2 ligase (Figure 1 B). Finally, one of two classes of E3 ligases helps to transfer ubiquitin from the E2 enzyme to the substrate protein (Figure 1 C and D; reviewed in Saritas-Yildirim and Silva, 2014).

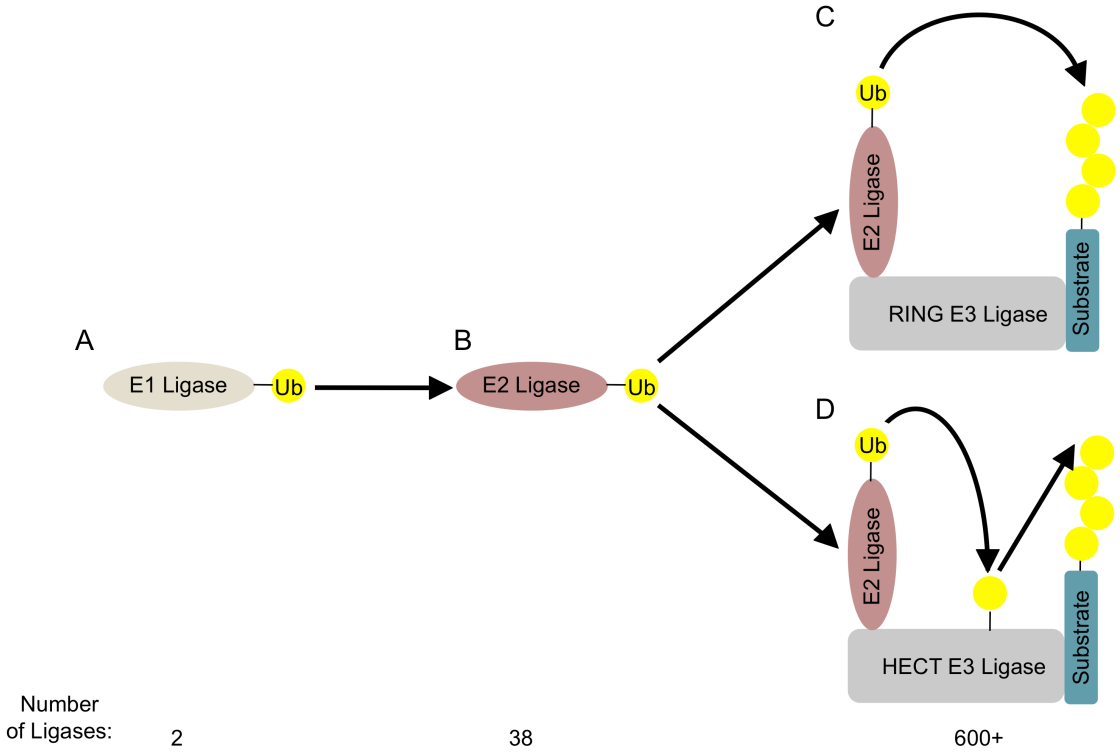

Figure 1. Ubiquitylation Involves the Attachment of an Ubiquitin Moiety to a Substrate Protein Through a Cascade of E1, E2, and E3 Ligases. Ubiquitin (Ub; yellow) is first attached to an E1 ligase (**A**) before it is transferred to the E2 ligase (**B**) and then finally to the substrate protein by an E3 ligase (**C** and **D**). There are two main types of E3 ligases that differ in their mechanism of transferring ubiquitin to the substrate protein. RING E3 ligases (**C**) directly transfer the ubiquitin to the growing ubiquitin chain, but HECT ligases (**D**) instead use an intermediary step that involves the transfer of ubiquitin to itself before this same ubiquitin is then transferred to the substrate. There are multiple different enzymes that function within each step of this process, accumulating with over 600 E3 ligases in the final step of this pathway. This diverse array of E3 ligases is responsible for generating the substrate specificity within the ubiquitin pathway.

Substrate specificity within the ubiquitin pathway is achieved by its many E3 ligases, which each bind to their own set of substrates and help to transfer ubiquitin to them. There are two main classes of E3 ligases that function within the ubiquitin pathway: RING and HECT (Figure 1 C and D). The most striking difference between these two classes of ligases is that ubiquitin is directly transferred from the E2 enzyme to the substrate protein by RING ligases, but HECT ligases instead use an intermediary step that involves the transfer of ubiquitin to itself before this same ubiquitin moiety is then transferred to the substrate protein (reviewed in Saritas-Yildirim and Silva, 2014).

1.2 SUMOylation

More recently, SUMOylation emerged as a novel ubiquitin-like post-translational modification that is important for regulating cellular physiology. It involves the covalent attachment of a SUMO moiety to a lysine residue on target proteins. SUMOylation affects protein interactions, stability, and localization of predominately nuclear proteins (reviewed by Geiss-Friedlander and Melchior, 2007).

1.2.1 Four Different SUMO Paralogs Are Found in Mammalian Cells

SUMO is expressed in all eukaryotes. The mammalian genome contains four genes that encode SUMO1 through SUMO4. SUMO2 and SUMO3 differ only by 3 amino acids, while SUMO1 has only 50% homology to SUMO2 and SUMO3 (reviewed in Everett et al., 2013). Unfortunately, the SUMO2 and SUMO3 sequences were switched when they were entered into NCBI, complicating discussions within this field. In this study, I use the original naming system, which is opposite of what is used by NCBI. SUMO4 differs from SUMO2 by 14 amino acids, but it may not be utilized within cells, as the known SENPs are unable to process it (Figure 2; Owerbach et al., 2005). A fifth SUMO gene was identified in primates (Liang et al., 2016). While SUMOylation typically involves the attachment of a single SUMO moiety to a lysine of a target protein, SUMO2 and SUMO3 each have an internal lysine residue that can be SUMOylated, allowing for the formation of SUMO chains.

However, SUMO chain formation is not well understood and it does not seem to be as prevalent as ubiquitin chain formation (Tatham et al., 2001).

Endogenous SUMO2 and SUMO3 are too similar to be distinguished with antibodies, so it has been impossible to study their specific function and possible redundancy in mammalian systems until recently. Additionally, the available antibodies have a poor specificity for SUMO. To resolve all of these issues, scientists typically overexpressed tagged forms of the SUMO paralogs. To study endogenous SUMO1, my lab generated a SUMO1 knockin mouse line, in which wildtype *SUMO1* is replaced with His_6-HA-SUMO1 at the *SUMO1* locus (Tirard and Brose, 2016; Tirard et al., 2012). Furthermore, HA-SUMO2 and V5-SUMO3 knockin mouse lines were generated, but they unfortunately were not available to be used in this present study. Recently, *SUMO1*, *SUMO2*, and *SUMO3* knockout mice were also generated. Interestingly, *SUMO1* knockout mice are viable, and they do not show an increase in SUMO2/3 expression (Zhang et al., 2008). In another study, *SUMO2* and *SUMO3* were knocked out in mice individually, and they found that SUMO3 is more dominantly expressed. *SUMO3* knockout mice die at around embryonic day 10.5, but *SUMO2* knockout mice are completely viable (Wang et al., 2014). In a recent study, a *SUMO3* conditional knockout mouse was generated, and the authors showed that *SUMO3* is required within neurons of the forebrain for episodic memory, fear conditioning, and LTP (Yu et al., 2020). All of these knockin and knockout lines will be instrumental for our further understanding of mammalian SUMOylation.

1.2.2 A Cascade of E1, E1, and E3 Enzymes SUMOylates Target Proteins

Analogous to the Ubiquitylation pathway, SUMOylation utilizes a cascade of E1, E2, and E3 enzymes to attach a SUMO moiety to a target protein (Figure 2; reviewed in Gareau and Lima, 2010). Before entering this cascade, SUMO is processed to a mature form by a family of enzymes called SENPs. The enzymes SENP1, SENP2, and SENP5 hydrolyze the C-terminus of SUMO, processing SUMO to a mature form that terminates with a diglycine motif (Figure 2, Step 1). This motif is adenylated by an E1 complex, consisting of SAE1 and UBA2, and then it is transferred to UBA2 (Figure 2, Step 2). Next, SUMO is transferred to the E2 conjugating enzyme, UBC9 (Figure 2, Step 3). Finally, one of a few E3 ligases facilitates the transfer of SUMO from the E2 enzyme to the target protein (Figure 2, Step 4). SENPs (SENP 1-3, 5-7)

deconjugate the mature SUMO from substrates, freeing SUMO to be used again in subsequent reactions (Figure 2, Step 5; reviewed in Gareau and Lima, 2010; reviewed in Kumar and Zhang, 2015).

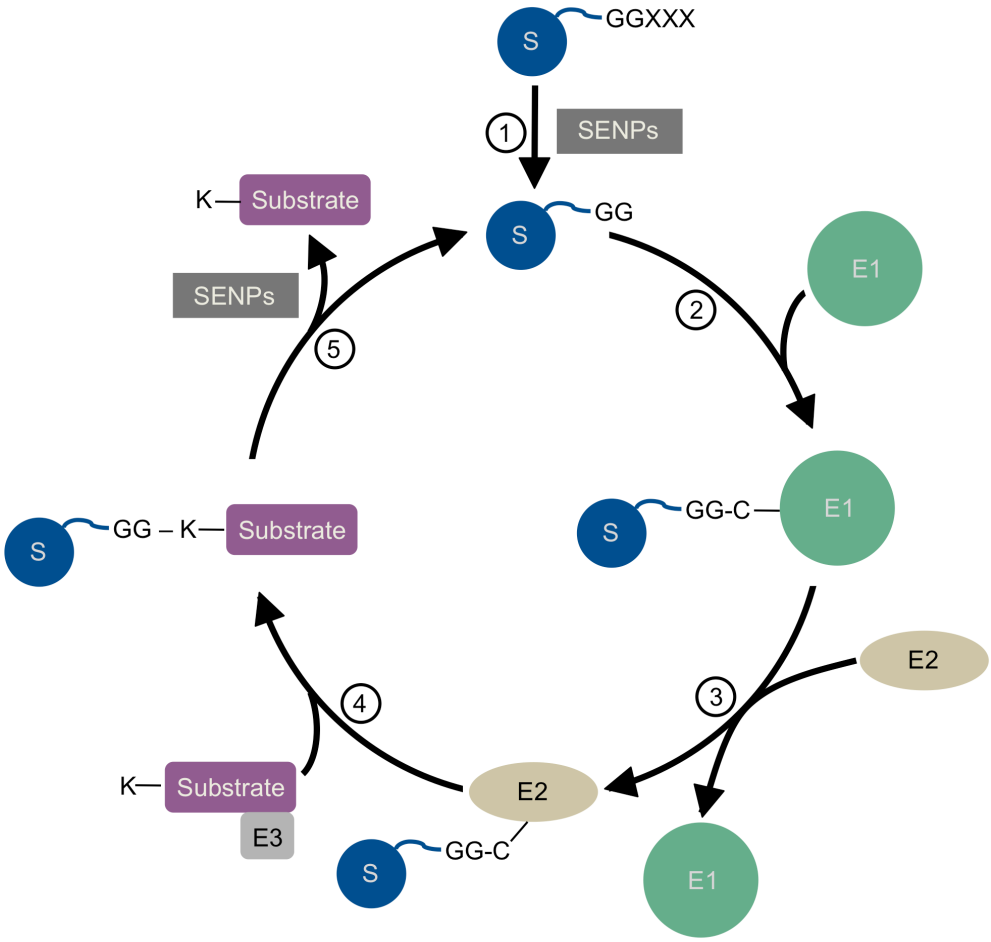

Figure 2. The Cycle of SUMO Conjugation and Deconjugation is Analogous to the Ubiquitylation Pathway. SUMO is processed into an active form by SENP enzymes (**1**). SUMO is then conjugated to target proteins via a cascade of enzymes that include E1 (**2**), E2 (**3**), and E3 ligases (**4**). Target proteins may then be deconjugated by SENP enzymes (**5**).

1.2.3 Identification of APC4-SUMO Conjugates in Proteomic Screens

His_6-HA-SUMO1 knockin mice were used to systematically screen for SUMO1-conjugated proteins *in vivo*, specifically in the brain (Tirard and Brose, 2016; Tirard et al., 2012). A subsequent screen for SUMO1 substrates in a soluble fraction of brains obtained from these mice yielded APC4, an APC/C subunit, as a potential SUMO1

substrate (Tirard et al., unpublished). Independent studies also identified APC4 in proteomic screens for target proteins that are conjugated to SUMO2 (Cubeñas-Potts et al., 2015; Hendriks et al., 2018; Matic et al., 2010; Schimmel et al., 2014). While all of these studies identified APC4 as a candidate SUMO2 substrate, they did not provide a biochemical validation that APC4 was indeed SUMOylated.

1.3 The Anaphase Promoting Complex (APC/C)

1.3.1 The APC/C is an E3 Ubiquitin Ligase that Ubiquitinates Proteins and Targets Them for Destruction by the Proteasome

The APC/C was originally discovered simultaneously in yeast (Sudakin et al., 1995) and Xenopus oocyte extracts (King et al., 1995). It was named the Cyclosome in yeast and the APC/C in higher organisms. The APC/C is conserved in all eukaryotes from yeast to humans, and it has at least 11 different subunits. The subunits were independently discovered in numerous organisms, often with distinct naming systems. The naming system of APC/C subunits, activators, and related proteins is listed in Table 1 (reviewed in Peters, 2006; reviewed in Sivakumar and Gorbsky, 2015, 2015; reviewed in Manchado et al., 2010; reviewed in McLean et al., 2011). With the exception of Cdc27, which is also often referred to as Cdc27 even in the vertebrate literature, I am using the vertebrate nomenclature in the present study. However, when I describe a paper that uses a different model organism, I mention the corresponding naming system first and the vertebrate name in parenthesis.

The APC/C is a Cullin-RING E3 ubiquitin ligase that assists in the transfer of ubiquitin from an E2 ligase to target proteins, resulting in ubiquitin-dependent proteasomal degradation of the target proteins (Figure1 C). The APC/C is best known for regulating the cell cycle with its oscillating ubiquitylation of cell cycle proteins. Different sets of proteins are degraded by the proteasome during different stages of the cell cycle after being ubiquitylated by a complex that was either activated by Cdc20 at the M/G1 transition or by Cdh1 at the G1/S transition (Figure 3; reviewed in Peters, 2006; reviewed in Sivakumar and Gorbsky, 2015).

Table 1. APC/C Subunits, Activators, and Substrates Across Different Species

Vertebrate	*S. cerevisiae*	*S. pombe*	Drosophila	Function
APC/C Subunits				
APC1	APC1	CUT4	shattered	Scaffold
APC2	APC2	APC2	morula	Catalytic, APC11/ DOC1 binding
APC3	CDC27	NUC2	Cdc27; makos	Scaffold; binds APC10, Cdh1, CDC20
APC4	APC4	CUT20	APC4	Scaffold; also Lid1
APC5	APC5	APC5	Ida	Scaffold
APC6	CDC16	CUT9	Cdc16	Scaffold
APC7	-	-	APC7	Scaffold
APC8	CDC23	CUT23	Cdc23	Scaffold, binds CDC20
-	APC9	-	-	-
APC10	DOC1	APC10	APC10	Substrate recognition
APC11	APC11	APC11	Lemming A	Catalytic; E2 recruitment and E3 activity
APC12	CDC26	HCN1	-	Stabilizes APC6
APC13	SWM1	APC13	-	Stabilizes APC3, APC6, and APC8
-	MND2	APC15	-	Ama 1 inhibitor; promotes CDC20 ubiquitination
APC16	-	-	-	Stabilizes APC3, APC7
APC/C Activators				
CDC20	CDC20	CDC20	fizzy	Activator and substrate recognition
Cdh1	CDH1	CDH1	fizzy-related	Activator and substrate recognition
-	-	-	Rap1	Substrate recognition
-	-	-	cortex	Substrate recognition
-	AMA1	-	-	Substrate recognition
E2 Ligases Associated with the APC/C				
UBE2K	UBC1	(predicted)	-	K48 chain formation
UBCH5	UBC4	UBC4	Dmel	Monoubiquitylation
UBCH10	UBC11	UBC11	-	Monoubiquitylation; Also called UBE2C
UBE2S	-	-	Ube2S	K11 chain formation
APC/C Substrates				
Cyclin B	CLB2	CDC13	Cyclin B	Mitotic cyclin
Securin	PDS1	CUT2	pim	Metaphase-anaphase transition

APC/C subunits, activation partners, E2 ligases, and two of the most prominent substrates (reviewed in Manchado et al., 2010; reviewed in McLean et al., 2011; Rodrigo-Brenni and Morgan, 2007; reviewed in Peters, 2006; reviewed in Sivakumar and Gorbsky, 2015).

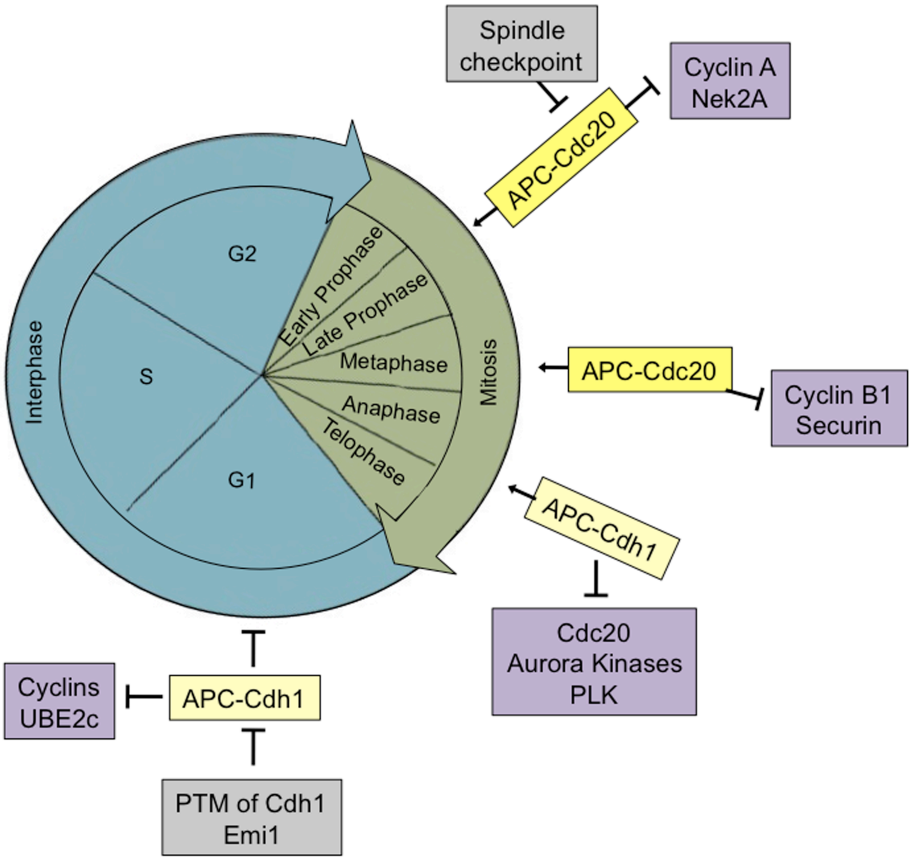

Figure 3. Regulation of the Cell Cycle by the APC/C. Upon activation of the APC/C by Cdc20 (dark yellow) and Cdh1 (light yellow), the APC/C ubiquitinates different subsets of proteins (purple). Each activation pathway functions at different stages of the cell cycle (Interphase is teal and Mitosis is green). This leads to the degradation of different sets of proteins at different stages of the cell cycle, triggered by the APC/C (purple). This cyclic degradation of cell cycle proteins is required for the cell cycle to persist. The APC/C and its activators are shown adjacent to the phase of the cycle that they regulate. If the complex activates the transition from one phase to the next phase, an arrow is drawn from the complex. If the complex inhibits the progression of the cycle at this phase, an inhibitory symbol is drawn from the complex. Grey boxes show some inhibitory signals that each affect different stages of the cell cycle.

1.3.2 The APC/C Regulates the Destruction of Proteins During the Cell Cycle

Activation of the APC/C is tightly regulated during the cell cycle by activators, post-translational modifications, and inhibitory binding partners (Figure 3; reviewed in Peters, 2006; reviewed in Sivakumar and Gorbsky, 2015, 2015). During early mitosis, Cyclin dependent kinases (Cdks) phosphorylate some APC/C subunits, promoting

the binding of Cdc20 to the complex (Kraft et al., 2003; Shteinberg et al., 1999). At this step, Cdh1 is also phosphorylated to prevent it from binding to and activating another complex (Zachariae et al., 1998). The Cdc20-activated APC/C ubiquitylates mitotic cyclins and Securin, causing their proteasomal degradation. The consequent loss of cyclins induces a decrease in the activity of Cdks, resulting in Cdh1 dephosphorylation. Cdh1 is then able to bind and activate other APC/Cs, resulting in the degradation of different sets of proteins that push the cell into the subsequent stage of the cell cycle (reviewed in Peters, 2006; reviewed in Sivakumar and Gorbsky, 2015, 2015). The Cdh1-activated APC/C ubiquitinates Cdc20 and prevents the simultaneous activation of both complexes (Robbins and Cross, 2010; Pfleger and Kirschner, 2000). Due to this intricate system of APC/C activation, the complex is able to regulate the cell cycle and likely many other cellular processes (reviewed in Peters, 2006; reviewed in Sivakumar and Gorbsky, 2015; Zachariae et al., 1998).

1.3.3 The APC/C Uses Several Different E2 Ligases in Mammals to Ubiquitylate Substrate Proteins with a Diverse Array of Ubiquitin Chain Types

While the yeast APC/C adds K48 linked ubiquitin chains (Rodrigo-Brenni and Morgan, 2007), the mammalian APC/C primarily adds K11 linked chains to substrates (Meyer and Rape, 2014; Kirkpatrick et al., 2006), but it is also able to generate K48, K63 (Kirkpatrick et al., 2006), and branched chains that have a mixture of K11 and K48 chains (Meyer and Rape, 2014; Kirkpatrick et al., 2006). Independent of the chain type, the main function of this ubiquitylation is to initiate the proteasomal degradation of proteins (Chau, et al., 1989; Meyer and Rape, 2014).

Yeast utilize two different E2 enzymes for the initiation and the elongation of chains, UBC4 (UBCH5) and UBC1 (UBE2K) respectively (Rodrigo-Brenni and Morgan, 2007). The human APC/C uses two E2 enzymes, UBCH5 (Garnett et al., 2009) and UBCH10 (Garnett et al., 2009; Jin et al., 2008), to add a single ubiquitin to the target protein. Utilizing a binding site distinct from the prior E2 enzymes, a third E2 ligase, UBE2S, binds the APC/C and attaches K11 linked chains to the previously attached ubiquitin (Figure 4; Garnett et al., 2009; Kelly et al., 2014). While a fourth E2 ligase, UBE2K, can generate K48 chains in conjunction with the mammalian APC/C *in vitro*, this E2 enzyme does not seem to be regularly used by the mammalian APC/C within cells (Rodrigo-Brenni and Morgan, 2007). The distinct

binding sites for the E2 enzymes allow for the APC/C inhibitor, MCC, to block the activity of UBCH10 but not UBE2S (Figure 4; Alfieri et al., 2016). There are several additional inhibitors of the APC/C that each block different aspects of the activity of the complex (Figure 4 A and B; Burton et al., 2011; reviewed in Yamano, 2019).

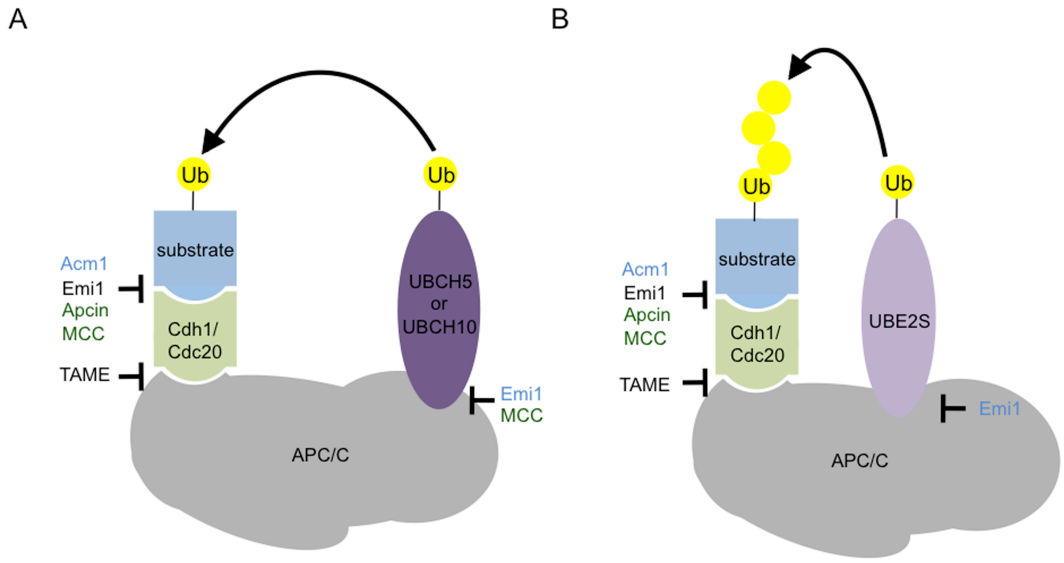

Figure 4. The Mechanism of Ubiquitin Attachment by the APC/C. (**A**) First the E2 ligases UBCH5 or UBCH10 bind to a Cdh1- or Cdc20-activated APC/C and transfer a single ubiquitin moiety to the substrate protein. (**B**) Next Ube2S binds a distinct spot on the APC/C, transfers ubiquitin to the monoubiquitinated substrate, and extends the ubiquitin chain. In addition to regulation by post-translational modifications, a variety of inhibitors are able to inhibit different aspects of this process, such as the E2 enzymes binding to the APC/C or the substrate binding to the activators. Most of these inhibitors within the cell are specific to one type of activated complex (Burton et al., 2011; reviewed in Yamano, 2019). Cdc20 inhibitors are shown in green and Cdh1 inhibitors are shown in blue. Emi1 (black) is the only inhibitor that can block the binding of the substrate to both the Cdh1- and Cdc20-activated APC/C.

The subunits in the APC/C are categorized into several subcomplexes: a catalytic unit, a specificity arm, and a structural unit (Figure 5). Within the catalytic unit (Figure 5, green), the Cullin domain of APC2 and the ring domain of APC11 catalyze the transfer of ubiquitin to target proteins. APC10 within this subcomplex helps to mediate the recruitment of the activators and the substrate proteins to the APC/C. The specificity arm (Figure 5, gray) consists of APC7, APC3, APC6, and APC8. These proteins have TPRs that facilitate the recruitment of substrates and possibly the assembly of the complex. This arm is further stabilized by APC12, APC13, and APC16. Finally, all of the core components of the APC/C are stabilized

by the structural unit (Figure 5, blue), which includes APC4, APC1, and APC5 (reviewed in Peters, 2006; reviewed in Sivakumar and Gorbsky, 2015).

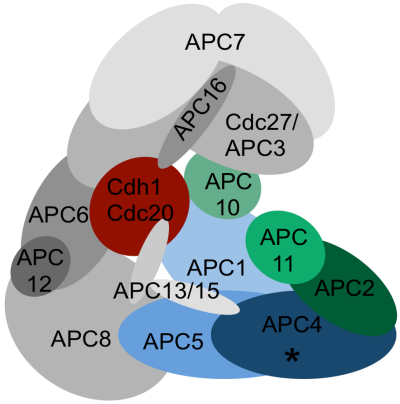

Figure 5. The Structure of the APC/C. The APC/C is a complex of 11 or more proteins that catalyzes the attachment of ubiquitin to target proteins, thereby causing their degradation. The activity of the complex requires an activator such as Cdh1 or Cdc20 (red). The complex consists of a structural stability unit (blue), a catalytic unit (green), and a specificity arm (gray). APC4 (asterisk) is mainly thought to be required for the structure or assembly of the complex.

1.4 Anaphase Promoting Complex Subunit 4 (APC4)

Little is known about the role of APC4 within the APC/C. APC4 was proposed to be an adaptor protein that connects several functional domains of APC/C (Figure 4; Barford, 2011). In support of this idea, it was found that HCMV infection is associated with the inactivation of the APC/C and the degradation of APC4 and APC5 protein levels (Tran et al., 2010). It is not known whether this degradation precedes or follows the inactivation of APC/C. A subsequent study showed that the viral protein, UL21A, is necessary and sufficient to induce the degradation of APC4, APC5, and APC1. The authors also showed that the knockdown of APC4 with siRNA results in the loss of APC4, APC5, and APC1 protein expression. Similarly, knockdown of APC5 or APC1 resulted in the degradation of all three of these structural proteins (Clark and Spector, 2015). A similar relationship was observed with all three of these proteins within the yeast APC/C (Thorton et al., 2006). Together these data imply that APC4 is required for the stability and the function of the APC/C. To date, only a few other studies have addressed the function of APC4 within the complex or during the cell cycle. *ANAPC4* mutations arrested cells in metaphase in yeast (Yamashita et al., 1999) and *C. elegans* (Furuta et al., 2000).

Human cell lines have a delay in the transition from metaphase to anaphase (Eifler et al., 2018; Lee et al., 2018). In Arabidopsis, the APC4 homolog is also required for APC/C dependent gametogenesis and embryogenesis (Wang et al., 2012).

1.5 SUMOylation of APC4

1.5.1 SUMOylation is Required for APC/C-Dependent Cell Cycle Processes in Yeast and in Other Model Organisms

Authors of several studies in yeast initially showed that the SUMOylation pathway contributes to different aspects of the cell cycle, but they neglected to show the involvement of the APC/C in this context. In *S. pombe*, *HUS5* (UBC9) mutants had defects in mitotic arrest and DNA damage recovery during S phase, independent of the *CHK1+* (checkpoint kinase1) DNA damage response pathway. Epistasis experiments indicate that *HUS5* (UBC9) is in the same pathway as *RAD17* (al-Khodairy et al., 1995), a checkpoint protein ubiquitylated by the Cdh1-activated APC/C (Zhang et al., 2010). Another study found that *SMT3* (yeast SUMO) mutants had a loss in cell survival after UV irradiation in *S. pombe*. The mutant cells also had defects in telomere length and chromosome segregation. The authors found that SMT3 (yeast SUMO) is localized near the kinetochore and likely required there for chromosome segregation (Tanaka et al., 1999). While these studies did not tie these phenotypes to the APC/C, many of the detected effects may involve the APC/C and its various substrates that regulate the cell cycle (reviewed in de Boer et al., 2016).

The first major hint that SUMOylation was actually important for the function of the APC/C came from a study on the function of UBC9 in *S. pombe*, where it was found that cyclin (CLB5 and CLB2) degradation requires *UBC9* after S phase and during G2/M, while the loss of *UBC9* alone was not sufficient to regulate this degradation. When *UBC9* was mutated in yeast, the spores were able to germinate but the cells stopped dividing after a few rounds of cell division. Arrested cells were characterized as large budded cells with an increased cell volume and a single nucleus located at the neck of the bud. While the DNA was replicated in these cells, their spindles were shorter and failed to undergo mitosis. Although the authors originally thought that UBC9 is an E2 ligase required for the ubiquitylation of target

proteins, possibly through the APC/C (Seufert et al., 1995), it was later shown that UBC9 was instead an E2 ligase required for the SUMOylation of proteins (Johnson and Blobel, 1997). In a subsequent study, it was found that *CDC23* (APC8) and *SMT3* (yeast SUMO) mutants also had shortened spindle lengths when compared to their wildtype counterparts. After four hours, the *SMT3* (yeast SUMO) mutant lines also had an accumulation of cells that had budded but did not finish dividing. When the cells were arrested in G1 and then released, *SMT3* (yeast SUMO) mutants were delayed in entering mitosis. While 80% of their chromosomes eventually separated, the distance between the chromosomes after separation was decreased in the mutants (Biggins *et al*., 2001).

The depletion of *SUMO1* or *UBC9* in oocytes resulted in a loss of cell maturity, including a decrease in the number of cells with germinal-vesicle breakdown and a decrease in the number of cells with a polar body extrusion. None of these effects were seen when SUMO1 was overexpressed. The polar body extrusion effect was only present if the cells were injected before Anaphase 1. As seen in yeast, the depletion of *SUMO1* or *UBC9* also resulted in a decrease in the condensation of chromosomes, defects in spindle lengths and organization, and the loss of proper microtubule-kinetochore interactions. The chromosomes did not always line up at the metaphase plate, resulting in an increased rate of aneuploidy when SUMO1 or UBC9 were depleted. Likely, some of these effects could involve the APC/C, but the authors never addressed this specifically (Yuan et al., 2014).

1.5.2 The SUMOylation Pathway Is Required for APC/C-Dependent Degradation of Securin in Yeast but Not in Higher Organisms

An older study indicated that SUMOylation is important for the function of the APC/C (Dieckhoff et al., 2004). This study showed that *SMT3* (yeast SUMO) is required for the APC/C-dependent proteolysis of cell cycle proteins and the progression of the cell cycle. The authors demonstrated that when *SMT3* (yeast SUMO) and *UBC9* were knocked out in yeast, the cells arrested in mitosis and had shortened spindles. Arrest of these cells at G2/M was independent of the MAD2 checkpoint, but this arrest was partially rescued by deleting *PDS1* (Securin). This indicated that the arrest depends on the Cdc20-activated APC/C. In yeast, the components of APC/C were primarily localized to the nucleus, and depleting *UBC9* or *SMT3* (yeast SUMO)

did not alter the localization of the tested APC/C components. The same authors also measured the degradation of APC/C-regulated proteins and showed that the levels of proteins like CLB2 (Cyclin) and PDS1 (Securin) were reduced in the SUMOylation mutants. No changes were detected in other proteins degraded by the proteasome, such as GCN4, indicating that SUMOylation affects the activity of the APC/C specifically instead of the activity of the proteasome. Deleting *UBC9* resulted in a smaller increase in PDS1 (Securin) and CLB2 (Cyclin) levels than deleting the other APC/C components, indicating that SUMOylation is likely regulating the function of the complex but it is not vital for all APC/C function. Substrates of both the Cdc20- and Cdh1-activated APC/C were affected, so this SUMOylation does not seem to be activator specific (Dieckhoff et al., 2004).

In yeast, the loss of *UBC9* resulted in an increase in Securin, but the link between SUMO, the APC/C, and Securin is more complicated in mice. WB data from mice oocytes indicated that the expression levels of Securin or its downstream target Rec8 remain unaltered after UBC9 depletion. However, imaging data showed that UBC9 depletion instead led to a loss of Securin and Rec8 colocalization, indicating that SUMOylation affects the localization of Securin but not its expression in mice (Yuan et al., 2014). As APC/C-dependent ubiquitylation typically induces protein degradation, this localization effect likely does not involve the APC/C.

As seen in the case of mouse Securin (Yuan et al., 2014), the ability of the SUMOylation pathway to affect the cell cycle is probably not limited to the APC/C, since other cell cycle proteins can be SUMOylated. In *C. elegans*, BUB-1, a checkpoint kinase, is SUMOylated *in vitro* and its localization is changed when *SMO1* (yeast SUMO) or its E3 ligase, *GEI-17*, is knocked down. During metaphase and anaphase, SMO1 (yeast SUMO) and GEI-17 concentrate together in the area between the separating chromosomes, and their expression levels peak during early anaphase. When *SMO1* (yeast SUMO) was knocked down in cells, the expression of BUB-1 at the kinetochore was not altered, indicating that BUB-1 SUMOylation is not required for the localization of the protein specifically at the kinetochore. All of these data lead to the notion that SMO1 (yeast SUMO) is required for the localization of BUB-1 between the chromosomes but not at the kinetochore. While the SMO1 localization matched the BUB-1 localization, the authors did not actually confirm that BUB-1 is SUMOylated, and they did not rule out the possibility that other proteins, like APC4, could also be SUMOylated (Pelisch et al., 2019).

1.5.3 Identification of APC4 as the SUMOylated Component of the APC/C

His_6-HA-SUMO1 KI mice were generated to systematically screen for SUMO1-conjugated proteins *in vivo* in the brain (Tirard and Brose, 2016; Tirard et al., 2012), and a subsequent screen for substrates in a soluble fraction of brain cells obtained from these mice identified APC4 as a candidate SUMOylated protein (Tirard et al., unpublished). Independent studies also identified APC4 in proteomic screens for proteins conjugated to SUMO2 (Cubeñas-Potts et al., 2015; Hendriks et al., 2018; Matic et al., 2010; Schimmel et al., 2014). In this first published study, human HeLa cells provided the evidence that the sites of SUMO2 attachment are likely lysines 772 and 798 on APC4 (Matic et al., 2010), corresponding to lysines 772 and 797 in mice. The second study completed a proteomic screen for proteins that were differentially SUMOylated during various phases of the cell cycle, and they found that APC4 SUMOylation was enriched specifically in cells arrested at the G2/M checkpoint (Schimmel et al., 2014; Yatskevich et al., 2021).

Before these SUMO1 and SUMO2 proteomic screens, the SUMOylated component of the APC/C was unknown. Previously it was shown that CDC16 (APC6) and CDC23 (APC8) are not SUMOylated in yeast (Dieckhoff et al., 2004). APC7 was found to be SUMOylated only under heat shock conditions (Golebiowski, et al. 2009), but this does not explain the APC/C-related cell cycle effects that were seen in yeast under normal conditions (Dieckhoff et al., 2004; Seufert et al., 1995; Yuan et al., 2014). By purifying the APC/C, it was recently shown that the only complex component that is SUMOylated under normal conditions is APC4, while after heat shock both APC4 and APC7 are SUMOylated. Unfortunately, the SUMOylated residues implicated in mice and humans is not conserved in yeast APC4, so further studies are still required to better understand how the APC/C is SUMOylated within yeast (Eilfer et al., 2018).

1.5.4 Recent Studies Showed that APC4 SUMOylation is Required for Timely Metaphase to Anaphase Transition

In three studies that were published after the start of this thesis, the authors sought to address the importance of APC4 SUMOylation for the function of the APC/C and the role of this process in regulating the cell cycle. Two studies showed that mutating

lysines 772 and 798 of APC4 generated a SUMOylation-deficient mutant. When APC4 was depleted in cells, the cells took longer to progress from metaphase to anaphase. This effect was fully rescued by expressing wildtype APC4 but not SUMOylation-deficient APC4 (Eifler et al., 2018; Lee et al., 2018). *APC4* knockdown also resulted in abnormal mitosis and increased cell death, but these effects did not require APC4 SUMOylation. This indicates that APC4 SUMOylation is required for the ubiquitylation of some but not all APC/C substrates. SUMOylation also did not affect the cellular localization of spindle checkpoint proteins or other components of the APC/C (Lee et al., 2018).

Consistent with the fact that a SUMOylation-deficient mutant could rescue some but not all of the cell cycle phenotypes found upon APC4 loss, a proteomic screen showed that different sets of proteins bind to the SUMOylated and the non-SUMOylated APC/C. The SUMOylated APC/C bound to LYST, KIF18B, BAX, COPS7A, HSP90AB4P, FAM91A1, and TUBB2B. The non-SUMOylated APC/C bound to TUBA3C, TUBA1A, TUBB4A, NUP35, RACGAP1, TIMM13, SMG8, UBL4A, GPHN, and Nbla03646 (Eifler et al., 2018). While many of these proteins may be ubiquitylated by the APC/C, some of these proteins are likely not direct targets of the complex**.** For example, MOAP-1 binds to and activates BAX, thereby inducing apoptosis. While BAX is not known to be ubiquitylated by the APC/C, its binding partner, MOAP-1, is a known target that could be preferentially ubiquitylated by the SUMOylated APC/C. Hence, I suspect that BAX was likely found in this study due to the fact that it normally binds to MOAP-1 (Huang et al., 2012), which potentially preferentially binds to the SUMOylated APC/C.

APC4 SUMOylation seems to affect the ability of the APC/C to ubiquitylate a subset but not all of its target proteins (Eifler et al., 2018; Lee et al., 2018; Yatskevich et al., 2021). *In vitro* ubiquitylation assays were conducted with purified APC/C that contained either wildtype or SUMOylation-deficient APC4, and they were able to detect changes in the ubiquitylation of Hsl1 (Eifler et al., 2018) but not with Securin (Eifler et al., 2018; Lee et al., 2018). However, Hsl1 ubiquitylation was affected by only the Cdh1-activated APC/C and not the Cdc20-activated APC/C (Yatskevich et al., 2021). The SUMOylation-deficient APC/C was also unable to ubiquitylate KIF18B well (Eifler et al., 2018). Interestingly, APC4 SUMOylation seems to affect the binding of the MCC to the Cdc20-activated APC/C; while SUMOylation does not seem to affect the ubiquitylation process itself, it seems to change the confirmation

of the complex to allow for ubiquitylation of substrates. However, it is still not known how APC4 SUMOylation affects the Cdh1-activated APC/C (Yatskevich et al., 2021).

Human APC4 has two phosphorylation sites that are proximal to the sites of SUMOylation, and one of these (Serine 779) is phosphorylated during mitosis but not S-phase (Kraft et al., 2003; Qiao et al., 2016). The second adjacent phosphorylation site (Serine 777) is phosphorylated when the APC/C is activated by Cdc20 (Qiao et al., 2016). To address the interplay between these phosphorylation and SUMOylation sites, the phosphorylation sites were mutated, resulting in a decrease of APC4 SUMOylation (Eifler et al., 2018; Yatskevich et al., 2021) that is rescued by expressing a phosphorylation mimic mutant (Eifler et al., 2018). These data indicate that there is interplay between the phosphorylation and the SUMOylation of APC4, but this connection is not well understood (Eifler et al., 2018; Yatskevich et al., 2021).

While several labs recently published cryo-EM structures of the APC/C, the C-terminal end of APC4, which contains the SUMOylated residues, is disordered and was deleted for these studies (Alfieri et al., 2016; Cronin et al., 2015; Yamaguchi et al., 2016; Zhang et al., 2016). Based on the available published structures, it was however predicted that this C-terminal end of APC4 could interact with APC2. More specifically, it was hypothesized that this site of APC4 SUMOylation may interact with a proposed SIM on APC2. To test for this, the authors generated a SIM mutant and showed that APC2 was no longer able to bind SUMO in an *in vitro* assay. The authors also expressed an APC4-SUMO fusion construct that was mutated to prevent it from being recognized by the SIM motif of APC2, and showed that cells expressing this construct had similar delays in the onset of metaphase as the SUMO-deficient mutant. The authors proposed a model where SUMOylated APC4 interacts with APC2 and changes the confirmation of the APC/C, thereby changing the APC/C from a closed to an open conformation. This ultimately allows the binding of an E2 enzyme to APC2. However, the authors did not test whether any of the known E2 enzymes actually have a preference to bind to either the SUMOylated or non-SUMOylated APC/C (Lee et al., 2018). However, a recent paper suggested that this SIM site is not important for the activity of the Cdc20-activated APC/C, and they instead identified other sites of interaction between APC2 and APC4 (Yatskevich et al., 2021). All of this data could be explained though by SUMOylated APC4 potentially interacting with two separate regions of APC2 when it is bound to either

Cdc20 or Cdh1. Further studies are required to fully understand the function of APC4 SUMOylation on the APC/C and its corresponding affect on cellular physiology.

1.6 Function of APC/C in Mature and Developing Neurons

The first hint that the APC/C has a function outside of regulating the cell cycle came from a study that showed that most of the components of the APC/C are highly expressed in most tissues, including ones that contain mostly non-dividing cells like in the brain. Cdc20 was the only component not identified by WB of these tissues (Gieffers et al., 1999). However, later studies showed that Cdc20 is expressed weakly in neurons, and it is present at the centrosome and its expression increases with the age of the neurons (Kim et al., 2009). Like in dividing cells, the neuronal components of the APC/C all co-IP together, and this corresponding purified APC/C is a fully functional E3 ligase that is able to ubiquitylate Cyclin B1 *in vitro* (Gieffers et al., 1999).

The APC/C is subject to a remarkably complex system of regulation, allowing for the fast degradation of different sets of proteins in each phase of the cell cycle (reviewed in Peters, 2006; reviewed in Sivakumar and Gorbsky, 2015; Pfleger and Kirschner, 2000; Robbins and Cross, 2010). Its ability to do this is controlled through a complex system of post-translational modifications that are starting to be elucidated within the context of the cell cycle. These modifications likely affect the ability of the complex to bind to proteins such as the activators, E2 ligases, and the substrates of the complex (Kraft et al., 2003). Additionally, the cellular localization also seems to play a role in regulating the activity of the complex, but this phenomenon is still poorly understood (Huang and Raff, 2002). In total this complex APC/C regulatory system allows the complex to very quickly degrade different sets of proteins at specific times during the cell cycle (reviewed in Peters, 2006; reviewed in Sivakumar and Gorbsky, 2015).

Like proliferating cells, neurons also require mechanisms to quickly degrade different sets of proteins in order to control, for instance, synaptic plasticity and other aspects of neuron physiology (reviewed in Cajigas et al., 2010). Due to the ability of the APC/C to regulate complex signaling pathways (reviewed in Peters, 2006; reviewed in Sivakumar and Gorbsky, 2015), the high expression levels of the

complex within the brain (Gieffers et al., 1999), and its possible localization at synapses (Pick et al., 2012; Distler et al., 2014), the APC/C is a formidable candidate E3 ligase that may be responsible for degrading multiple proteins within the complicated signaling pathways of neurons. Compared to other known E3 ligases, the APC/C could be particularly relevant for the rapid degradation of different sets of proteins within the complex signaling pathways that regulate neuron physiology. While some substrates of the complex have been identified in neurons (Sections 1.6.1 to 1.6.9; reviewed in Eguren et al., 2011), very little is known about the function of the APC/C within neurons.

1.6.1 Cdh1 Regulates Axon Length Through a Variety of Mechanisms

While the Cdh1-activated APC/C has no effect on the length of dendrites, it was shown to promote the growth of axons by ubiquitylating a variety of different substrate proteins in neurons (Kannan et al., 2012b; Konishi et al., 2004; Lasorella et al., 2006; Stegmüller et al., 2006). Some of the most well established substrates of the neuronal APC/C are the nuclear transcription factors SnoN (Li et al., 2019; Stegmüller et al. 2006; Stegmüller et al., 2008) and ID2 (Lasorella et al., 2006). While ID2 inhibits the expression of genes that block axon growth (Lasorella et al., 2006), SnoN activates the transcription of *Ccd1*, which in turn induces axon growth by activating JNK kinase within the axon (Ikeuchi et al., 2009). Epistasis experiments showed that the TGFß-Smad2 signaling pathway is upstream of the APC/C-SnoN pathway, and it is involved in regulating axon length (Stegmüller et al., 2016; Stegmüller et al., 2008). SnoN and Cdh1 co-IP together and SnoN ubiquitylation requires a D box motif (Stegmüller et al., 2016; Wu et al., 2007). Upon Cdc27-IP, ID2 was co-immunoaffinity purified in a HeLa cell overexpression assay (Lasorella et al., 2006). The regulation of the ubiquitylation of these proteins may be important for therapeutic reasons, as both ID2 and SnoN promote axon regeneration after tissue injury (Do et al., 2013; Yu et al., 2011). Surprisingly, no changes in SnoN expression levels were detected when *APC2* was conditionally knocked out in excitatory neurons in the forebrain (Kuczera et al., 2010).

SMURF1 was initially proposed to be a substrate of the Cdh1-activated APC/C, as depletion of *Cdh1* led to an accumulation of SMURF1. SMURF1 is an ubiquitin E3 ligase that is expressed within the cytosol and the nucleus. Cytosolic

SMURF1 ubiquitylates RhoA, a GTPase that restrains axon growth (Kannan et al. 2012b; Wang et al. 2013). Initially SMURF1 was suggested to be a substrate of the APC/C (Kannan et al. 2012b), but it later was shown that SMURF1 does not co-IP with the APC/C in HEK293 cells. The same study showed that the dimerization of SMURF1 inhibits its E3 ligase activity, and the study found that Cdh1 inhibits this dimerization via an APC/C-independent mechanism (Wan et al., 2011). However, this mechanism does not fully explain why SMURF1 protein expression increased when *Cdh1* was depleted. Strikingly, SMURF1 degradation required a D box motif, which is typically required by the APC/C to bind to its substrates (Kannan et al., 2012b). In theory, Cdh1 could actually act upstream of SMURF1 in both APC/C-dependent and -independent modes. If it were in fact only using an APC/C-independent mechanism, this would actually indicate that Cdh1 binds to substrate proteins both in the presence and the absence of the APC/C by using a D box motif. Structural studies aimed to identify the mechanism by which the APC/C binds to the D box of substrate proteins, and they showed that Cdh1 and APC10 are together responsible for this binding (da Fonseca et al., 2011). Hence, it is feasible that Cdh1 could also bind to D box motif in signaling pathways that do not involve the APC/C.

The same authors that identified SMURF1 as a substrate of the APC/C also suggested that p250GAP, a RhoA GAP, is ubiquitylated by the Cdh1-activated APC/C and affects axon length. While it was shown that p250GAP ubiquitylation is required for restraining axon growth, the authors failed to show that the APC/C is the E3 ligase responsible for this ubiquitylation. The corresponding ubiquitylation of p250GAP did not lead to its destruction, which alone argues against the notion that the APC/C ubiquitylates p250GAP (Kannan et al. 2012a). Further studies are required to determine if the APC/C is indeed acting upstream of p250GAP.

1.6.2 The APC/C is Important for Maintaining Cells in G0 and for Proper Neuronal Development

The activity of the APC/C is important for maintaining neurons in G0 phase (Almeida et al., 2005) and for maintaining proper cell division in neuroblasts (García-Higuera et al., 2008; Slack et al., 2007). The Cdh1-activated APC/C maintains neurons in G0 phase by constantly degrading Cyclin B1, preventing the cells from entering S phase and dying (Almeida et al., 2005). Mice heterozygous for the deletion of Cdh1 have

an increased number of neuronal progenitors within the subventricular zone (García-Higuera et al., 2008). One proposed substrate of the APC/C in this context is Miranda, a protein that associates with myosin motors and helps to control asymmetrical cell division in Drosophila neuroblasts. Miranda is mislocalized in neuroblasts when *Ida* (APC5) is knocked out, but the corresponding study did not assess the expression levels of Miranda upon *Ida* (APC5) knockout. The authors then went on to IP ubiquitin and co-IP Miranda in order to show that Miranda is ubiquitylated. While this IP did seem to work, only a single Miranda band was detected instead of smeared bands, leading to the argument that Miranda is only monoubiquitylated (Slack et al., 2007). The study apparently did not use NEM to inhibit the cysteine peptidases that are involved in deubiquitylation proteins, which might explain the lack of the visible smear. Moreover, the authors did not test whether APC/C is in fact the E3 ligase that ubiquitylates Miranda. Overall, the evidence provided is not sufficient to conclude that Miranda is an actual substrate of the APC/C. While Cyclin B1 monoubiquitylation can induce protein degradation *in vitro*, (Dimova et al., 2012), there is no strong evidence for this regularly occurring with other APC/C substrates or *in vivo* (Garnett et al., 2009; Jin et al., 2008).

Due to the fact that the APC/C regulates cell division, the APC/C is expected to be important for proper brain development. As the focus of my own research has been on APC/C function in postmitotic neurons, here I will only provide one more example from Drosophila that shows the importance of the complex during neuronal development. Knocking down *fzr* (Cdh1) and *fzy* (Cdc20) resulted in an excess migration of glial cells in the eye during development (Neuert et al., 2017; Silies et al., 2010). The substrate of the Cdh1-activated APC/C that was controlling this was proposed to be Fasciclin2. It is believed that a gradient of Fasciclin2 forms along the length of axons, but this gradient is lost when *fzr* (Cdh1) is knocked down, resulting in defects in glial cell migration (Silies et al., 2010). A similar glial migration phenotype was seen when *morula* (APC2) was knocked down in the eye (Neuert et al., 2017). Knockdown of *fzr* (Cdh1) also resulted in a change in the distribution and in the clustering of photoreceptors within the basal layer of the eye disk (Neuert et al., 2017). When *morula* (APC2), *Lemming A* (APC11), and *ida* (APC5) are completely knocked out, there was an initiation of eye disk formation, but the eye fails to grow (Bentley et al., 2002; Neuert et al., 2017). Probably due to the methodological limitations of addressing this issue in Drosophila, Fasciclin2 has not

been confirmed as an actual substrate of the APC/C, and any other substrates of the APC/C that might regulate eye development are unknown. In contrast to what was found in the eye, Drosophila larval brains showed an increase in the total number of glia when *Cdh1* was depleted and a decrease in the number of glia when it was overexpressed (Kaplow et al., 2008). The discrepancies seen between these Drosophila studies could be explained by the fact that the APC/C might influence different substrates in different cell types and during different developmental stages.

1.6.3 The APC/C Regulates Glycolysis and Cell Death Pathways in Neurons

The Cdh1-activated APC/C is also responsible for maintaining the low glycolysis rate of neurons by constantly ubiquitylating PFKFB3, a stimulator of glycolysis (Herrero-Mendez et al.; 2009; Rodriguez-Rodriguez et al., 2012). Upon depletion of Cdh1, the levels of PFKFB3 accumulate and the neurons undergo apoptosis. Activation of NMDA receptors, a subtype of glutamate receptors, inactivated the Cdh1-activated APC/C, stabilizing PFKFB3 and allowed for the release of PFKFB3 from the nucleus into the cytosol. Increased NMDA receptor activation is associated with increased neuronal cytotoxicity and cell death, and this effect is likely partially due to the inactivation of the Cdh1-activated APC/C and the stabilization of PFKFB3 (Rodriguez-Rodriguez et al., 2012).

In addition to regulating glycolysis (Almeida et al., 2005; Rodriguez-Rodriguez et al., 2012), constant activity of the Cdh1-APC/C prevented neurons from entering the apoptosis pathway (Li et al., 2017, Zhang et al., 2019; Li et al., 2020). Depletion of the APC/C activator, Cdh1, increased cell death *in vitro* (Almeida et al., 2005; Huang et al., 2012; Rodriguez-Rodriguez et al., 2012) and *in vivo* (Bobo-Jiménez et al., 2017; Li et al., 2017; Li et al., 2020). The Cdh1-activated APC/C ubiquitylates MOAP-1, but when *Cdh1* was depleted, MOAP-1 accumulated and induced the translocation of BAX from the cytosol to mitochondria where it was activated and induced apoptosis (Huang et al., 2012). While it is unknown if MOAP-1 actually activates BAX in neurons, it is highly expressed in neurons and may play a similar function there (Chan et al., 2019).

The Cdh1-activated APC/C also induced cell death in an *in vivo* model for trigeminal neuropathic pain. Rats in this model have increased apoptosis after tissue injury, and this was accompanied by an increase in the expression of BAX and

Cleaved Caspase 3. These changes in protein expression are partially rescued by injecting Cdh1 into the site of injury 7 days after the initial surgery (Li et al., 2020). Similar effects were seen in a neuropathic pain mechanical allodynia rat model, which is also partially rescued by microinjecting a virus overexpressing Cdh1 (Tan et al., 2015). Related effects were found in the hippocampus, as young rats treated for a long time with isoflurane, a volatile anaesthetic, had a decrease in Cdh1 expression and an increase in the amount of apoptosis. These apoptotic effects observed after the treatment with isoflurane were entirely rescued by injecting Cdh1 in the hippocampus (Li et al., 2017). Another study confirmed that Cdh1 expression itself was depleted after glutamate- or Aβ-induced excitotoxicity (Fuchsberger et al., 2016). Interestingly, the Cdc20-activated APC/C may also ubiquitylate a necrosis activator in neuroblasts of *D. melanogaster*, but its substrate was not identified and it is not known if this occurs in other organisms (Kuang et al., 2014).

Studying a model of NMDA-mediated excitotoxicity, the authors showed that Cdh1 was phosphorylated by CDK5, causing it to be sequestered in the cytosol. The authors argued that the cell death initiated after this treatment is entirely due to the APC/C substrate Cyclin B1 (Maestre et al., 2008). Overexpressing Cyclin B1 in the nucleus, but not in the cytosol, was sufficient to induce apoptosis within a fibroblast cell line (Porter et al., 2003). While overexpressing Cyclin B1 in cells depleted of *Cdh1* rescued about 33% of the cell death effect observed in neurons (Almeida et al., 2005), it is obvious that other substrates of the complex are likely mediating this cell death too. The regulation of the cell death pathway seems to be mainly controlled by the localization of Cyclin B1 and not by its total expression levels (Porter et al., 2003). The APC/C would most likely only affect the total expression levels of Cyclin B1 and not its localization; therefore, it is really difficult to determine how involved the APC/C really is here. One potential explanation is that when Cdh1 is overexpressed, CDK5 is overwhelmed and unable to phosphorylate the population of Cyclin B1, thereby allowing more of it to enter the nucleus and trigger cell death. While CDK5 activity is required for cell death after treatment with sevoflurane, a volatile anesthetic, this death seems to be independent of PFKFB3, indicating that this other neuronal substrate of the APC/C is specifically not mediating this cell death effect (Liu et al., 2019).

1.6.4 The Involvement of the Cdh1-Activated APC/C in Regulating Neurite Development and General Brain Development

In addition to a loss in the numbers of neurons in conditional *Cdh1* knockout mice, there is a large-scale disruption of the proper development of neurites in the hippocampus and in the cortex of these mice, resulting in a decrease in the number and length of neurites in the affected neurons. ROCK2 was proposed to be the substrate responsible for generating these phenotypes. The reasoning for this conclusion is that ROCK2 is ubiquitylated, ROCK2 binds to the APC/C, and the developmental phenotypes in *Cdh1* knockout mice were partially rescued by treatment with a ROCK1/2 inhibitor. ROCK2 is a protein kinase that helps to regulate cell polarity and the actin cytoskeleton. ROCK1, on the other, hand does not seem to be a substrate of the APC/C (Bobo-Jiménez et al., 2017).

The expression of MAP2 was substantially decreased in neurons lacking Cdh1 (Bobo-Jiménez et al., 2017). MAP2 is a protein that binds to microtubules and F-actin and is required for neurite formation in cultured neurons (Roger et al., 2004). Inhibiting ROCK1/2 pharmacologically in placental-derived multipotent stem cells increased both the gene and the protein expression levels of MAP2. These data indicate that ROCK1 may be functioning upstream of MAP2, thereby controlling its expression through an undetermined mechanism (Bobo-Jiménez et al., 2017; Wang et al., 2013). Finally, the loss of MAP2 expression in *Cdh1* conditional knockout mice seems to be partially responsible for the developmental defects seen in the cortex and the CA1 region of the hippocampus in *Cdh1* knockout mice (Bobo-Jiménez et al., 2017), as MAP2 helped to initiate the formation of neurites in neuron cultures (Roger et al., 2004).

1.6.5 The Cdc20-Activated APC/C Regulates Dendritic Length

While many of the well-characterized substrates of the neuronal APC/C are nuclear proteins, the Cdc20-activated APC/C also appears to ubiquitylate proteins at the neuronal centrosome (Kim et al., 2009; Watanabe et al., 2014). At the centrosome, the Cdc20-activated APC/C regulates the length of dendrites by ubiquitylating ID1 (Kim et al., 2009) and FEZ1 (Watanabe et al., 2014). ID1 binds transcription factors and inhibits their function (reviewed in Ling et al., 2014). Upon Cdc27-IP, ID1 was

co-immunoaffinity purified in a HeLa cell overexpression assay (Lasorella et al., 2006). FEZ1 is an adhesion molecule that is involved in the development of neurites and the transport of proteins within neurites (Gunaseelan et al., 2021; Watanabe et al., 2014). Cdc20 overexpression increased the length of dendrites, and this effect was partially rescued by knocking down *FEZ1* (Watanabe et al., 2014). *Cdc20* depletion resulted in a decrease in the length of dendrites in neurons, and this effect was partially rescued by expressing FEZ1 (Watanabe et al., 2014) and it was fully rescued by expressing ID1 (Kim et al., 2009). While there were defects in the total length of dendrites in both studies, the FEZ1 study also found defects in the complexity of the dendrites (Watanabe et al., 2014).

The mechanisms by which these proteins regulate the length of dendrites are not clear. In contrast to knocking down *Cdh1* (Huang et al., 2012; Kannan et al., 2012a; Kannan et al., 2012b; Konishi et al., 2004; Lasorella et al., 2006; Stegmüller et al., 2006), there were no changes in axon length or cell survival in cells depleted of *Cdc20* (Kim et al., 2009). HDAC6, a protein localized to the centrosome, co-IPs with the APC/C and is required for the ubiquitylation of Cdc20 and for APC/C activity at the centrosome of neurons (Kim et al., 2009). The phosphorylation of Cdc20 by CaMKII β also seems to regulate dendritic length (Puram et al., 2011). In total, these studies all lead to a model where the Cdc20-activated APC/C ubiquitylates both ID1 and FEZ1 within neurons, which then in turn regulates the length of dendrites through two separate mechanisms (Kim et al., 2009; Watanabe et al., 2014).

1.6.6 The Involvement of the APC/C in Regulating Synapse Formation Through the Transcription Factor, NEUROD2, is Highly Debated

While Cdh1 is the prominent APC/C activator expressed in the brain (Gieffers et al., 1999), Cdc20 is also weakly expressed there (Kim et al., 2009). One of the most highly debated substrates of the Cdc20-activated APC/C is the transcription factor NEUROD2. In a first relevant study, the authors knocked down *Cdc20* in primary cerebellar granule neurons, identified NEUROD2 as a possible substrate of the Cdc20-activated APC/C, and suggested that the APC/C operates upstream of a pathway regulating synaptogenesis. More specifically, neurons depleted of *Cdc20* showed a decrease in Synapsin clustering (a pre-synaptic marker) and a decrease in

the co-localization of Synapsin with other synaptic markers, such as Syntaxin1 (a pre-synaptic marker) and PSD-95 (a post-synaptic component marker). The authors also showed that *Cdc20* knockdown resulted in the loss of Munc13 clustering and induced a phenotype similar to the one seen upon *NEUROD2* depletion. When the authors demonstrated that Complexin 2 overexpression reversed the phenotype seen with a *NEUROD2* knockdown, they proposed a model where the APC/C-dependent degradation of NEUROD2 acts through Complexin 2 to regulate the clustering of Synapsin and general synapse formation (Yang et al., 2009).

In a second study, the authors developed a *Cdc20* hypomorphic mouse line with decreased Cdc20 expression. Strikingly, cultured granule neurons from this mouse line showed no changes in Synapsin expression, in dendrite length, or in NEUROD2 expression levels. However, other cell types obtained from these mice showed clear defects in the processes regulated by the complex, including prolonged metaphase, defects in chromosome alignment, and an accumulation of Cyclin B1 expression. To explain the discrepancy with the prior study, the authors proposed that NEUROD2 is a substrate of the APC/C in rats but not in mice (Malureanu et al., 2010); however, there are other potential explanations for the differences observed between these two studies.

The original model proposed in the first study entails a role of Complexin 2 in regulating synapse formation, but past studies focusing on complexins showed that this family of protein is not involved in synapse formation. *Complexin 2* knockout mice show normal synaptogenesis and synapse function (Reim et al., 2001), and even neurons devoid of all complexins show no synaptogenesis effects (López-Murcia et al., 2019). Hence, it is unlikely that Complexin 2 functions in regulating synapse formation. It is still unclear if NEUROD2 is a substrate of the APC/C and is involved in synaptogenesis via a mechanism unrelated to Complexin 2.

1.6.7 The Role of APC/C in Regulating FMRP and LTD

LTD is characterized by the loss of synaptic strength, likely due to a mechanism involving the removal of glutamate receptors from the surface of postsynapses. The induction of mGluR-dependent LTD can be achieved by DHPG, a group1 mGluR agonist (reviewed in Collingridge et al., 2010). FMRP, a mRNA binding protein that regulates the translation of specific mRNAs, is rapidly translated, ubiquitylated, and

degraded during DHPG-induced LTD (Hou et al., 2006). Based on studies that utilized a conditional *Cdh1* knockout mouse, the Cdh1-activated APC/C was implicated as the E3 ligase involved in the ubiquitylation of FMRP during mGluR-dependent LTD (Huang et al., 2015). Previously, *Cdh1* knockout mice were shown to have defects neurogenesis (Delgado-Esteban et al., 2013), but this problem was avoided in this study by using an EMX-Cre driver to knockout *Cdh1* later during development, resulting in no noticeable changes in the size or structure of the hippocampus (Hou et al., 2006; Huang et al., 2015).

The conditional *Cdh1* knockout mice showed impaired mGluR-dependent LTD in two different LTD-induction paradigms, but they did not detect changes in early LTP. LTD-induction was achieved independently by treatment with DHPG and by low frequency stimulation, accompanied by treatment with the NMDAR antagonist, AP5. In both cases a drastic impairment in the induction of LTD in *Cdh1* conditional knockout mice was detected, and this effect was rescued in the DHPG paradigm by overexpressing a Cdh1 construct that is only expressed in the cytosol. The overexpression of Emi1, an APC/C inhibitor, also resulted in impaired DHPG-induced LTD. Similarly, the authors showed that the *Cdh1* conditional knockout mice lacked the long-term down regulation of FMRP protein expression that was typically seen after treatment with DHPG. Finally they showed that FMRP co-IP with both Cdc27 and the Cdh1 activator, indicating that FMRP is likely ubiquitylated by the Cdh1-activated APC/C (Huang et al., 2015). A later unrelated study also implicated FMRP, through the activity of the APC/C, in the formation of stress granules in neurons (Valdez-Sinon et al., 2020). Altogether, these data imply a model where the Cdh1-activated APC/C ubiquitylates FMRP, a protein that regulates protein synthesis, and this is all required for the induction of LTD.

1.6.8 Additional Roles of the APC/C in Regulating Synapses, Synaptic Transmission, and Behavior

The APC/C was shown to regulate the expression of AMPA receptor subunits in rats (Fu et al., 2011) and in *C. elegans* (Juo and Kaplan, 2004). A first study showed that GluR1, a subunit of AMPA receptors, was ubiquitylated and was likely a substrate of the Cdh1-activated APC/C in rats. The authors showed GluR1 co-immunoaffinity purifies with the APC/C obtained from synaptosome and whole brain lysates.

Additionally, purified APC/C was shown to ubiquitylate GluR1 *in vitro*. Finally, the study showed that mutating the D box motif of GluR1 led to an accumulation of GluR1 within the neurons (Fu et al., 2011). However, there were no changes in the expression levels of GluR1 when *APC2* was conditionally knocked out in excitatory neurons of the forebrain (Kuczera et al., 2010). In a second study, the authors found that the APC/C regulates the expression of *Glr-1*, an AMPA-type receptor in *C. elegans*, but this receptor is likely not a direct target of the APC/C because Glr-1 does not have a D or a KEN box motif that would allow it to bind to the APC/C. When the authors depleted different components of the APC/C, they observed an accumulation of Glr-1 puncta, but this effect was not seen with other synaptic proteins. The overexpression of ubiquitin also resulted in a decrease in Glr-1 puncta density, which was partially rescued by depleting different components of the APC/C. The study was unable to determine the actual APC/C substrate responsible for regulating the expression of Glr-1 (Juo and Kaplan, 2004).

One of the most interesting potential substrates of the APC/C at the synapse is SHANK1. SHANK1 is ubiquitylated in an activity dependent manner (Jarome et al., 2011). A subsequent study used an ICC approach, where the authors stained for the total SHANK1 signal in order to screen for the E3 ligase responsible for the ubiquitylation of SHANK1. While TRIM3 depletion induced a much greater increase in SHANK1 expression in neurons, *APC2* knockdown also resulted in a significant increase in SHANK1 expression (Hung et al., 2010). An additional study showed that SHANK1 expression was increased after high frequency stimulation in the amygdala and the hippocampus of *Cdh1* conditional knockout mice (Pick et al., 2012), but this effect was not seen without LTP stimulation in *Cdh1* or *APC2* conditional knockout mice (Kuczera et al., 2010; Pick et al., 2012). This indicates a scenario where high frequency stimulation induces SHANK1 ubiquitylation and degradation, and this is potentially regulated in an APC/C-dependent manner because the degradation was lost when *Cdh1* was depleted (Pick et al., 2012). SHANK1 has a D box, which would allow it to theoretically be a substrate of the APC/C, but further studies are needed to determine if SHANK1 is actually a substrate of the APC/C.

The APC/C is important for fear conditioning and late phase LTP within the amygdala. Several groups generated constitutive *Cdh1* knockout mouse lines, but constitutive *Cdh1* knockouts show massive developmental defects by E8.5 and die around E9.5 to 10.5 (García-Higuera et al., 2008; Li et al., 2008). Interestingly, mice

heterozygous for the constitutive *Cdh1* knockout showed defects in contextual fear conditioning, novel object recognition, and late phase LTP (Li et al., 2008). To resolve the issue of embryonic lethality, conditional *Cdh1* knockout mice were crossed to mice expressing a CaMKII Cre driver, and the resulting mice were shown to exhibit impaired fear conditioning and impaired late phase LTP in the amygdala. The authors detected an increase in the expression of SHANK1 and NR2A in the amygdala of these mice, but only after high frequency stimulation. These mice also showed an anxiety phenotype and enhanced reversal learning in several different learning assays, but interestingly they had no changes in early or late phase LTP in the hippocampus. In a cell fractionation experiment that utilized hippocampus tissue, it was shown that Cdh1 is present in all fractions, including the PSD (Pick et al., 2012), and a proteomic screen for proteins in the PSD also identified APC1, APC7, and APC12 within this fraction (Distler et al., 2014). All of this evidence indicates that Cdh1 could possibly have a physical function at the synapse.

Subsequent studies focused on knockout of various components of the APC/C in different cell types to identify the function of the complex in controlling behavior and synaptic transmission. When *Cdh1* was conditionally knocked out with an excitatory neuron specific Cre driver, late phase LTP was impaired in the hippocampus, but there again were no effects on early-phase LTP. There also still were detected defects in late-phase LTP within the amygdala of these mice. Finally these mice still had defects in their ability to modify memories during an associative fear conditioning assay and a water maze behavioral assay (Pick et al., 2013). While the conditional knockout mice did not have motor defects (Kuczera et al., 2010; Pick et al., 2012; Pick et al., 2013), mice heterozygous for the constitutive *Cdh1* knockout had motor defects, indicating that the motor effects might be due to the lack of Cdh1 expression in the peripheral nervous system or in another non-neuronal cell type (García-Higuera et al., 2008). A final study focused on the knockout of *APC2* in excitatory neurons of the forebrain, where they detected defects in the reversal of learning but no defects in the acquisition of fear conditioning. No changes in brain morphology were detected in these mice that lacked *APC2*. Surprisingly, there were no changes in the expression of the proposed APC/C substrates GluR1, SHANK1, and SnoN. To explain why no such changes were seen, the authors stated that they only knocked out *APC2* in the excitatory neurons of the forebrain and this occurred later in development. They assumed that APC/C might transiently regulate

substrates under different conditions, at different times during development, and within different cell types (Kuczera et al., 2010). An APC2 knockout in hematocytes resulted in the loss of function of the APC/C though (Wirth et al., 2004), suggesting that APC2 was required for APC/C function in other cell types.

As discussed in Section 1.6.3, many neurological disorders are characterized by decreased Cdh1 expression, which include ischemia (Zhang et al., 2019), pain disorders (Li et al., 2020; Tan et al., 2015), and Alzheimer's disease (Fuchsberger et al., 2016). Overexpression of Cdh1 rescued a variety of behavioral and neuronal phenotypes in a rat model of ischemia. After ischemia, rats have symptoms of mild cognitive impairment, anxiety, and depression. This was accompanied by a loss of dendritic spine length, reduced spine density, and changes in the expression of synaptic markers. Many of these phenotypic changes were rescued by injecting Cdh1, but this was not the case with the memory defects or with the alterations in the expression of synaptic proteins (Zhang et al., 2019).

Studies in *D. melanogaster* and *C. elegans* also indicate a function for the APC/C in synapses. When *Fzr* (Cdh1) was depleted from neurons in Drosophila, the neurons showed a decrease in the total number of synaptic boutons and an increase in the average area of their boutons. There are also changes in the staining patterns of synaptic markers like GluRIIa and anti-Bruchpilot (Elks-1 homolog) in *Fzr* (Cdh1) mutants. Transmission electron microscopy data obtained from the neuromuscular junction of larvae from this line had a decrease in the quantity of docked vesicles. The mutants also had an increase in the frequency of spontaneous miniature excitatory junctional potentials (Wise et al., 2013). The opposite effect was seen in Drosophila when *Morula* (APC2) was mutated, as these mutants had an increase in the number of synaptic boutons. Liprin-α was suggested to be ubiquitylated by the APC/C in this second study, but biochemical validation was not completed. Neurons with a mutated form of *APC2* also had an increase in the excitatory junctional potential amplitude (van Roessel et al., 2004). Finally, *C. elegans* with mutated APC/C components showed an increase in "seizure" activity. When the *APC4* homolog was mutated, neurons had an increase in the intensity of synaptotagmin puncta. When the *APC6* homolog was mutated, neurons had a decrease in the rate and an increase in the amplitude of IPSCs. They proposed that the APC/C regulates neuronal signaling at inhibitory synapses (Kowalski et al., 2014).

1.6.9 Summary of the APC/C's Function within Neurons

While the APC/C components and activators are expressed in neurons (Gieffers et al., 1999), the function of the complex within these post-mitotic cells remains poorly understood. Many of the mammalian neuronal substrates are summarized in Table 16 in the Discussion. There is some evidence that the complex may function within distinct compartments within neurons in order to regulate the physiology of neurons, but this has not been systematically studied (Huang and Raff, 2002). Unfortunately, most of the studies in this field focused on the function of the activators of the APC/C in neurons, but lacked the stringent experiments required to show ubiquitylation of a candidate substrate by the APC/C (reviewed in Peters, 2006; reviewed in Sivakumar and Gorbsky, 2015). Indeed, SMURF1 is one protein that may be regulated by Cdh1 in an APC/C-independent manner, although even this aspect still remains unresolved (Wan et al., 2011). Further studies are required to confirm all of the proposed neuronal substrates of the APC/C and to possibly identify novel substrates of the complex. While little is known about the function of the APC/C within non-dividing neurons, it remains a highly interesting ubiquitin E3 ligase to study in neurons, in particular, due to its ability to quickly degrade different sets of proteins within complex signaling pathways. This remarkable ability itself is achieved by an extremely complex regulatory system whose mechanisms and effects are just beginning to emerge (Kraft et al., 2003).

1.7 The Aims and Rationale of This Study

My thesis work had two related aims. First, I wanted to stringently verify that APC4 is SUMOylated. Once I had confirmed this, I wanted to characterize the function of this SUMOylation. Second, I attempted to determine the function of the APC/C within neurons by knocking out *ANAPC4* (the gene encoding APC4) in neuron cultures.

1.7.1 Aim 1: Determine if APC4 is SUMOylated and Identify the Function of This SUMOylation

While the function of APC4 is not clear, its position in the complex indicates that it is likely required for the maintenance of a functional complex (Barford, 2011). Hence,

the discovery that APC4 is SUMOylated in the cytoplasm of brain cells (Tirard et al., unpublished) was of particular interest, as it might affect the function of the complex in neurons. Other post-translational modifications like phosphorylation are important for regulating the activity of the APC/C during the cell cycle (Kraft et al., 2003; Qiao et al., 2016), so I hypothesized that APC4 SUMOylation could also regulate protein interactions that occur between APC4 and the other proteins that make up the APC/C, thereby regulating the localization, the activation, or the function of the complex. This notion was supported by the fact that SUMOylation is required for APC/C-dependent cell cycle progression in yeast (Dieckhoff et al., 2004). For these reasons, I tried to verify that APC4 is SUMOylated. After confirming this, I sought to determine if the SUMOylation of APC4 affects the formation, the localization, or the function of the complex.

1.7.2 Aim 2: Determine the Function of APC4 and the APC/C Within Neurons

While the APC/C is thought to regulate various aspects of neuron cell biology and physiology (reviewed in Eguren et al., 2011), our understanding of the function of the neuronal APC/C is limited. The function of APC4 within the complex is also not clear. The majority of studies that addressed the function of the APC/C in neurons relied on an approach to knockdown of the activators, Cdc20 and Cdh1, and then to identify the corresponding phenotype (reviewed in Eguren et al., 2011). However, it was rarely confirmed that any of these phenotypes actually required the activity of the APC/C itself. SMURF1 is one proposed neuronal target of the APC/C that was recently suggested to be regulated by Cdh1 through an APC/C-independent mechanism (Wan et al., 2011), so further studies are required to determine if other proposed substrates also could be regulated by Cdh1 in a similar manner. For this reason, I obtained a conditional *ANAPC4* (the gene encoding APC4) knockout mouse line, and I characterized this line to potentially identify novel functions of the APC/C and to further clarify which of the proposed substrates of the APC/C are in fact targets of the APC/C.

2. Materials and Methods

2.1 Materials

2.1.1 Chemicals and Reagents

Table 2. Chemicals and Reagents Used

Reagent	Manufacturer
1X PBS for Cell Culture	Gibco
30% Acrylamide/Bis Solution	Biorad
4-(2-hydroxyethyl)-1-piperazineethanesulfonic acid (HEPES)	Roth
4',6-Diamidino-2-Phenylindole, Dihydrochloride (DAPI)	Thermo
6x loading dye	Thermo
Acetic acid, glacial	Merck
Agarose	BioFroxx
Amersham ECL Western Blotting Detection Reagents	GE Healthcare
Amersham Hyperfilm ECL	GE Healthcare
Ammonium acetate ($NH_4CH_3CO_2$)	Merck
Ammonium persulfate (APS)	Merck
Ampicillin, 50 mg/mL	Roche
Anti-c-Myc Agarose Affinity Gel antibody produced in rabbit	Sigma
Aprotinin, 1000x	Roche Diagnostics
Aqua-Poly/Mount (mounting solution)	Polyscience Inc
AscI	NEB
B27 serum	Gibco
Bacto agar	BD
BamHI and BamHI HF	NEB
BCA Protein Assay	Pierce
Bovine Serum Albumin (BSA)	Pierce, Thermo, NEB, sigma
Bromophenol blue	Pierce
Calcium cloride ($CaCl_2$)	Merck
ChromPure mouse IgG, whole molecule	Jackson Immuno Research
Cloned Pfu Polymerase AD	Agilent Technologies
Dimethyl sulfoxide (DMSO)	Sigma, Applichem
Dimethylenastron	Santa Cruz
Dismozon	Hartmann
Disodium hydrogen phosphate ($Na_2HPO_4\ 2H_2O$)	Merck
Dithiothreitol (DTT)	Biomol
DMEM	Gibco
DMEM + glutamax	Gibco
dNTPs	Bioline

DpnI	NEB
EndoFree Plasmid Maxi Kit	Qiagen
Ethanol	Sigma
Ethidium bromide	Carl Roth
Ethylenediaminetetraacetic acid (EDTA)	Sigma
Fetal bovine serum, heat inactivated	Gibco
Fish skin gelatin	Sigma
Gel extraction kit	Bioline, Invitrogen
GelRed	Biotum
Generuler 1kb	Thermo
Geneticin	Gibco
Glucose	Sigma
Glutamax	Gibco
Glycerol	Sigma
Glycine	Sigma
Goat serum	Gibco
Hank's balanced salt solution	Gibco
HEK293FT cells	Invitrogen
HiMark protein ladder	Invitrogen
Hydrochloric acid (HCl)	Merck
Immersol Immersion Oil 518F	Carl Zeiss
Isopropanol	Solvay
Kanamycin, 20 mg/mL	Sigma
L-Cystein	Sigma
L-glutamine	Gibco
Leupeptin, 1000x	Roche Diagnostics
Lipofectamine 2000	Invitrogen
Luria Broth- Millers Modification	Sigma
Lysozyme	Sigma
Magnesium chloride ($MgCl_2$)	Merck
Magnesium sulfate ($MgSO_4$)	Merck
MemCode reversible protein stain kit	Thermo
Methanol	JT Baker
Midi-prep DNA isolation kit	Invitrogen
Milk powder	Ferma
Mini-prep DNA isolation kit	Invitrogen
Monoclonal HA-agarose antibody produced in mouse A2095-1 mL	Sigma
Mytaq HS	Bioline
N-ethylamaleimide E1271-5g (NEM)	Sigma
NE-PER nuclear and cytoplasmic extraction reagents	Thermo
Neurobasal A medium	Gibco
Nexttec genomic DNA isolation kit	Nexttec
NheI and NheI HF	NEB
Nitrocellulose membranes	Protran BA, GE Healthcare
NNN'N' tetramethylethylenediamine (TEMED)	OmniPur, Serva
NZ amine (casein hydrolysate) (NZY+ browth)	Fluka Analytical

Opti-MEM medium	Gibco
Papain	Worthington Biomedical Corp
Paraformaldehyde (PFA)	Serva
Penicillin/Streptomycin	Gibco
Phenylmethylsulfonyl Fluoride (PMSF), 1000x	Roche Diagnostics
Poly-L-lysine	Sigma
Potassium chloride	Merck
Potassium dihydrogen phosphate (KH_2PO_4)	Merck
Pre-stained protein ladder	Fermentas
Protein G Sepharose	GE Healthcare
Protogel 30% w/v acrylamide	National Diagnostics
Quick Ligation Kit	Promega
Red taq	Sigma
RNase A	Roche
Sodium acetate ($C_2H_3NaO_2$)	Merck
Sodium butyrate ($C_4H_7NaO_2$)	Merck
Sodium chloride (NaCl)	Merck
Sodium dodecyl sulfate (SDS)	GERBU GmBH
Sodium hydroxide (NaOH)	Merck
Sucrose ($C_{12}H_{22}O_{11}$)	Merck
Supersignal west dura extended duration substrate (ECL)	GE Healthcare
T4 DNA ligase	NEB
TempliPhi 100	GE Healthcare
TOPO kit 2.1	Invitrogen
Triton x100	Roche Diagnostics
Trizma (Tris)	Sigma
Trypsin EDTA, 0.05%	Gibco
Trypsin Inhibitor from chicken egg white (type II)	Sigma
Tween-20	Sigma
Whatman paper	GE Healthcare
Yeast extract	Sigma

2.1.2 Consumables

Table 3. Consumable Items Used

Item	**Manufacturer**
0.22 filters	Merck
0.45 µm filters	Merck
10 cm tissue culture plate	Greiner Bio-One
12 mm coverslips #1.0 (for 24 and 6 well plates, 10 cm dishes)	Thermo
12 well tissue culture plate	Greiner Bio-One
150 mL filters	Corning
15cm tissue culture plate	Greiner Bio-One

18 mm coverslips #1.5 (for 12 and 6 well plates, and 10 cm dishes)	Thermo
24 well tissue culture plate	Greiner Bio-One
25 and 50 mL pipettes	Corning
5, 10, 15, and 20 mL pipettes	Greiner Bio-One
500 mL filters	Corning
6 well tissue culture plate	Greiner Bio-One
96 well PCR plates and 8 well strip tubes	4titude
96 well plates for the plate reader	Greiner Bio-One
Amicon Ultra-15 Centrifugal Filter	Millipore
Bacterial culture tubes	BD Falcon
Bacterial Spreaders (melted pipettes)	VWR
Cell scrapers	VWR
Centrifuge tubes (15 and 50 mL)	BD Falcon
Electroporation cuvette (0.1 cm)	Biorad
Eppendorf tubes (1.5 mL)	Eppendorf
Luer Lock syringes	VWR
Microscopy slides	Thermo
Needles: 27 gauge	Becton Dickson
Petri dishes	Greiner Bio-One
Razors	A. Hartenstein
Strip tubes for tail preparations	Corning
Syringes (1 mL, 5 mL, and 20 mL)	Becton Dickson
T75 Tissue Culture Flask	Sarstedt
Tubes for bacteria freezing: 1.5 mL	Therm
Tubes for virus freezing: 1.5 mL	Sarstedt

2.1.3 Equipment

Table 4. Equipment Used

Equipment Name	**Manufacturer**
Bacterial incubator	Heraeus Instruments
Bacterial shaker	Innova
Benchtop plate shaker	GFL
Centrifuges, large	Beckman, Sorvall, Thermo
Centrifuges, small table top	Eppendorf
Cold rooms	Viessman
DNA electrophoresis chamber	Horizon
DNA sequencer	Applied Biosystems, Sanger
DNA/RNA synthesizer	Applied Biosystems
Electrical supplies for electrophoresis	Amersham
Electrophoresis power supply	Amersham Biosciences
Electroporation pulser	Biorad
Freezer, -80°C	New Brunswick Scientific
Glass tubes (fractionation experiment)	Beckman

Hemocytometer	Marienfeld
Intas ECL Chemostar	Intas
IP rotator	CMV
Microscopes	Axiovert
Oligonucleotide Synthesizer	Biolytic Lab Performance Inc
PCR machines (MPIEM DNA Facility)	Biorad, Applied Biosystems
PCR machine: Gene Amp 9700 PCR Cycler	Applied Biosystems
pH meter	Knick
Plate reader	Molecular Devices
Potter S, Dounce homogenizer	B. Braun
Shacker, bench top	GFL, Shutt Labortechnik
Sonicator	Bandelin
Sonicator bath	Bandelin
Spectrophotometer	Amersham Biosciences
Thermomixer compact	Eppendorf
Tissue culture hood	LaminAir
Tissue culture incubators	Thermo Scientific
Ultracentrifuge and TLA 100.3 rotor	Beckman Coulter
UV gel documentation system	Intas
Vortex	Bender and Hobein AG
Western blotting electrophoresis system	Biorad
Western blotting transfer system	Hoefer Scientific Instruments

2.1.4 Primary and Secondary Antibodies

Table 5. Primary Antibodies Used for WB and ICC

Name	Manufacturer	Catalogue #	Species	Dilution WB	Dilution ICC
APC4	Novus Biologicals	A2095-1mL; Lot A1	Rabbit	1:5000 1:2000 (higher for co-IP/ knockout)	1:500
APC5	Bethyl	A301-026A-M	Rabbit	1:500	
Aurora-A/Ark-1	Santa Cruz	sc-25425 sc-398814	Mouse	1:200	
Beta Tubulin 2.1	Sigma	T4026	Mouse	1:2000	
Beta III-Tubulin	Synaptic Systems	302 304	Guinea pig		1:2000
Cdc27	BD Biosciences	610455	Mouse	1:300; 10ul/IP	
Cdh1	Sigma	C7855	Mouse	1:1000	

Cmyc	Sigma	C3956	Rabbit	1:2000	
Cmyc	Sigma	M5546	Mouse	1:2000	
Complexin 3	Synaptic Systems	122 302	Rabbit	1:2000	
Cre	Sigma	C7988	Mouse		1:2000
Cre	Synaptic Systems	257 003	Rabbit	1:1000	
Cyclin E	Santa Cruz	sc-481	Mouse	1:200	
FEZ1	Gift of Dr. John Chua	NA	Rabbit	1:1000	
Flag	Sigma	F3165	Mouse	1:2000	
GAPDH	Abcam	ab8245	Mouse	1:2000	
GFP	Synaptic Systems	132 005	Guinea pig		1:2000
GFP	Roche	11 814 460 001	Mouse	1:1000	1:2000
GFP	Synaptic Systems	132 002	Rabbit		1:2000
GluR1	Calbiochem	PC246	Rabbit	1:2000	
HA	Covance, Biolegend	MMS-101R-500	Mouse	1:2000	
HA	Invitrogen	71-5500	Rabbit	1:2000	
Histone 3	Abcam (Gift from Dr. Klaas Nave)	ab18521	Rabbit	1:1000	
ID1	Biocheck	BCH-1/37-2	Rabbit	0.1 µg/mL	
MAP2	Novus Biologicals	NB300-213	Chicken		1:600
NeuN	Millipore	MAB377	Mouse	1:1000	
NeuroD2	Abcam	109406	Rabbit	1:500	
p55 CDC (E-7; cdc 20) 55	Santa Cruz	sc-13162	Mouse	1:200	
PSD95	Abcam	ab2723	Mouse	1:2000	
Rab GDI	Synaptic Systems	130 011	Mouse	1:2000	
RFP	Synaptic Systems	390 004	Guinea pig		1:2000
SHANK1	Synaptic Systems	162 002	Rabbit	1:1000	
SMI-312	HISS Diagnostics	SMI-312R	Mouse		1:1000
SUMO1	Marilyn Tirard	NA	Mouse	1:100	
SUMO1	Santa Cruz	sc-5308	Mouse	1:50	
SUMO2	Marilyn Tirard	NA	Mouse	1:30	

SUMO2/3	Abcam	ab81371	Mouse	1:1000	
Synapsin 1/2	Synaptic Systems	106 002	Rabbit	1:2000	1:2000
Synaptophysin	Generated in the Brose lab	p611; homemade	Rabbit	1:2000	

Table 6. Secondary Antibodies Used for WB and ICC

Name	Manufacturer	Catalogue #	Species	Dilution WB	Dilution ICC
Anti-chicken IgG; Alexa 405	Abcam	ab175674	Goat		1:1000
Anti-chicken IgG; Alexa 633	Thermo Fisher	A-21103	Goat		1:1000
Anti-guinea pig IgG; Alexa 488	Thermo Fisher	A-11073	Goat		1:1000
Anti-guinea pig IgG; Alexa 555	Thermo Fisher	A-21435	Goat		1:1000
Anti-guinea pig IgG; Alexa 633	Mobitec	A21105	Goat		1:1000
Anti-mouse HRP	Biorad	172-1011	Goat	1:5000	
Anti-mouse IgG; Alexa 405	Abcam	ab175660	Goat		1:1000
Anti-mouse IgG; Alexa 488	Thermo Fisher	A-11029	Goat		1:1000
Anti-mouse IgG; Alexa 555	Thermo Fisher	A-21424	Goat		1:1000
Anti-mouse IgG; Alexa 633	Thermo Fisher	A-21052	Goat		1:1000
Anti-rabbit HRP	Biorad	172-1019	Goat	1:5000	
Anti-rabbit IgG; Alexa 488	Thermo Fisher	A-11008	Goat		1:1000
Anti-rabbit IgG; Alexa 555	Thermo Fisher	A-21429	Goat		1:1000
Anti-rabbit IgG; Alexa 633	Thermo Fisher	A-21071	Goat		1:1000
Peroxidase AffiniPure Goat Anti-Mouse IgG (H+L; HRP)	Jackson Immuno Research	115 035 146	Goat	1:5000	
Peroxidase AffiniPure Goat Anti-Rabbit IgG (H+L; HRP)	Jackson Immuno Research	111-035-144	Goat	1:5000	

2.1.5 Bacterial Strains and Competent Cell lines

The technicians in my lab generated competent cells using a glycerol stocks for each of these lines.

Table 7. Competent Cell Lines Used

Bacterial Strain	Manufacturer
E. coli Electro10-Blue Competent Cells	Stratagene
E. coli XL-1 Blue Competent Cells	Stratagene
JM110 electrocompetent cells	Agilent

2.1.6 Vectors and cDNA

Table 8. Vectors and cDNA Used

Name	Obtained From
pcDNA3.1-	Invitrogen
HA SUMO1 pCRUZ	Dr. Frauke Melchior (unpublished)
HA SUMO2 pCRUZ	Dr. Frauke Melchior (unpublished)
His SUMO2 pCRUZ	Dr. Frauke Melchior (unpublished)
SUMO3 cDNA	Dr. Frauke Melchior
HA-SUMO3 pcDNA3.1-	Generated with primers 009/013
Myc-SUMO3 pcDNA3.1-	Generated with primers 010/013
APC4 pSPORT	Origene
APC4 cDNA	Mouse cDNA prepared by Dr. Marilyn Tirard
HA-APC4 pcDNA3.1-	Generated from HA-APC4 pCR2.1 TOPO
HA-APC4 K772R pcDNA3.1-	Generated with primers 014/015
HA-APC4 K797R pcDNA3.1-	Generated with primers 016/017
HA-APC4 K772R/K797R pcDNA3.1-	Generated with primers 014-017
Myc-APC4 pcDNA3.1-	Generated from HA-APC4 pCR2.1 TOPO
Myc-APC4 K772R pcDNA3.1-	Generated with primers 014/015
Myc-APC4 K797R pcDNA3.1-	Generated with primers 016/017
Myc-APC4 K772R/K797R pcDNA3.1-	Generated with primers 014-017
pCR2.1-TOPO	Invitrogen
HA-APC4 pCR2.1-TOPO	Generated with primers 001/004
Myc-APC4 pCR2.1-TOPO	Generated with primers 003/004
pEGFP-N1	Clontech

iCre NLS RFP (Referred to as Cre NLS RFP)	Dr. Hong Jun Rhee
His Ubiquitin prK5	Dr. Hiroshi Kawabe
HA Ubiquitin prK5	Dr. Hiroshi Kawabe
HA Cdh1 pCS2+	Dr. Marc Kirschner (Pfleger et al., 2001)
HA Cdc20 pCS2+	Dr. Marc Kirschner (Pfleger et al., 2001)
EGFP pc2+	Generated from EGFP-N1 and HA Cdc20 pCS2+
NLS RFP	Dr. Hong Jun Rhee
f(syn)w-iCreRFP p2A (TT) (Referred to as Cre RFP P2A)	Dr. Christian Rosenmund (Vardar et al., 2016)
pVSVG- (Lentivirus envelope)	pMD2.G was a gift from Dr. Didier Trono (Addgene plasmid # 12259, unpublished)
pCMV R8.9 (Lentivirus packaging)	pCMV delta R8.2 was a gift from Dr. Didier Trono (Addgene plasmid # 12263, unpublished)
prK5r-GluR1iQ	Dr. Aleksandra Ivanovic
Flag-ID2 pcDNA3.0	Dr. Judith Stegmueller (Lasorella et al., 2006)
f(syn)w-rbn.sbd	Dr. Marilyn Tirard
HA-APC4 K772R/K797R f(syn)w-rbn.sbd	Generated from f(syn)w-rbn.sbd and HA-APC4 K772R/K797R pcDNA3.1-
FUGW	Anja Günther (Lois et al., 2002)
HA-APC4 f(syn)w-rbn.sbd	Generated from f(syn)w-rbn.sbd and HA-APC4 pcDNA3.1-

2.1.7 Primers Generated for Cloning

I generated many primers in order to clone and sequence the APC4 and SUMO3 constructs described in this study. The primers used for mouse genotyping are listed and in 2.2.15. The primer number listed here are the numbers used in my lab notebooks.

Table 9. List of All Primers Generated

Primer #	Primer Usage	Primer Sequence
001	HA APC4 cloning primer forward	GACAGCTAGCACCATGTACCCATACGATG TTCCAGATTACGCTCTGCGCTTTCCGACCT G
003	Myc APC4 cloning primer forward	GACAGCTAGCACCATGGAACAAAAACTCA TCTCAGAAGAGGATCTGCTGCGCTTTCCG ACCTG
004	APC4 cloning primer reverse	CGGTCGGGATCCTCATCACGAGTCCAACT CAGGGTCAAG

007	pcDNA3.1 forward sequencing primer	CAAATGGGCGGTAGGCGT
008	pcDNA3.1 reverse sequencing primer	GCAACTAGAAGGCACAGTCG
009	Ha-SUMO3 cloning primer forward	GACAGCTAGCACCATGTACCCATACGATG TTCCAGATTACGCTGCCGACGAAAAGCCC AAG
010	Myc-SUMO3 cloning primer forward	GACAGCTAGCACCATGGAACAAAAACTCA TCTCAGAAGAGGATCTGGCCGACGAAAAG CCCAAG
013	SUMO3 cloning primer reverse	GCCTCGCTGGATCCTCAACCTCCCGTCTG CTGTTGGAAC
014	Lysine 1 mutagenesis primer forward	GAAGCCTGTGAAGATCAGGGAGGAAGTAC TGTCAGAGTCAGAG
015	Lysine 1 mutagenesis primer reverse	CTCTGACTCTGACAGTACTTCCTCCCTGAT CTTCACAGGCTTC
016	Lysine 2 mutagenesis primer forward	CTGCTGCCCTAGATCCGGACGTAGTCATC AGAGTGGAGCTTGACC
017	Lysine 2 mutagenesis primer reverse	GGTCAAGCTCCACTCTGATGACTACGTCC GGATCTAGGGCAGCAG
018	APC4 sequencing primer1	GGAACTTGTATTGCTCTG
019	APC4 sequencing primer2	CTGTATGTAGCAATGCTG
020	APC4 sequencing primer3	CTGCCTCAGCTGACAAGG

2.1.8 Lentiviral Constructs

I generated all of the Lentivirus using the protocol in Section 2.3.6. All of the government rules for working with, documenting, and storing lentivirus were followed.

Table 10. All Lentivirus Particles Generated

Lentivirus Lab Number	Lentivirus Name
191	FUGW (EGFP-expressing control)
412	HA APC4 wt f(syn)w-rbn.sbd

392	HA APC4 double f(syn)w-rbn
473	f(syn)w-rbn.sbd
482	Cre-RFP-P2A
483	iCre NLS RFP
484	NLS RFP

2.1.9 Computer Software

I used the following computer programs: Finch TV (Version 1.5.0, Geospiza Inc), Fiji (Image analysis; Schindelin et al., 2019), Seq Builder (DNASTAR), Image J (WB Analysis; Abramoff et al., 2004; Schneider et al., 2012), Igor Pro (Calculating protein half-life; Gomez et al., 2002), Inkscape (Inkscape, n.d.), Microsoft Word, Microsoft Excel, Microsoft Powerpoint, and Photoshop Elements 13 (Adobe). Most statistical analysis was completed with Excel, but SPSS (IBM, version 27) was instead used for the neuron morphology analysis.

2.2 Molecular Biology Methods

2.2.1 General Cloning Protocol

Cloning of constructs was completed using standard methods (Schell and Wilson, 1979). The insert and vector DNA were digest ran on 0.8% agarose gels and gel extracted. To quantify the amount of DNA and determine the success of the gel extraction, I briefly ran the DNA on an agarose gel. Approximately 200 ng of DNA total were used in each ligation reaction. The insert to vector ratio ranged from 1:5 to 20:1. The ligation reaction was incubated overnight at 16 °C.

All ligation reactions were ethanol precipitated before transformation. To ethanol precipitate ligation reactions, 20 µL of ligation reaction, 2 µL of 5 M sodium acetate, and 55 µL of 100% ethanol were mixed together and stored at -20 °C for 2 to 16 hours. Then the reaction was centrifuged at 23,100 x *g* for 30 minutes and the supernatant was removed. 10 µL of water was added to the dried DNA pellets and then 1 µL of the DNA

was typically electroporated into Electro10 Competent Cells that were generated by our lab.

Twenty to forty colonies were selected when I was screening the colonies for the correct vector, and DNA was generated from these colonies using Templiphi, commercial Mini-prep kits, or a crude boiling method (see Section 2.2.7). The colonies were analyzed by restriction digestion to identify correct colonies, and the DNA from these colonies was sequenced. One correct construct was stored as a bacterial glycerol stock, which was generated by mixing 500 µL of culture and 500 µL of autoclaved 30% glycerol and then storing it in a tube at -80 °C.

2.2.2 Cloning the SUMO3 and APC4 pcDNA 3.1- Constructs

Mouse APC4 and human SUMO3 were cloned into pcDNA3.1- using standard cloning methods described in Section 2.2.1. The SUMO construct sequence was prematurely ended after the double glycine motif, so that the construct would not need to be processed by SENPs. Depending on the size of the insert, it was either amplified with Redtaq or Pfu. A BamHI site was added to the 3' end and a NheI site was added to the 5' end of the insert with primer overhangs and PCR. APC4 constructs were first cloned into pCR2.1-TOPO using a TOPO cloning kit and the manufacturer's protocol (Fontes et al., 2013), and this was then digested and cloned into pcDNA3.1-.

2.2.3 Site Directed Mutagenesis to Generate a SUMO-Deficient Mutant Construct

A proteomic screen identified two lysines that were likely SUMOylated within human APC4 (Matic et al., 2010). After comparing the human and mouse APC4 sequences, I determined that likely correlates in mouse were lysines 772 and 797. Hence, these sites were each mutated to arginine individually and then a double mutant was also generated using standard mutagenesis procedures (Uemura et al.,1988).

Primers of approximately 40 bp were designed and included the desired lysine to arginine mutation and an insertion of a new restriction site to the sequence, and these mutations were placed within in the center of the primer sequence. Pfu DNA

polymerase was used to generate the mutated construct using this reaction: 50 ng of Myc-APC4 pcDNA3.1-, 1.3 µL of forward and reverse primers (50 pmol/µL), 4 µL of dNTP (100 mM), 5 µL of 10 x reaction buffer, 0.6 µL of Pfu (2.5 U/µL), and water up to 50 µL. The cycling parameters were as follows: (1) 95 °C for 10 minutes (2) 95 °C for 30 seconds (3) 60 °C or 62 °C for 1 minute (4) 68 °C for 18 minutes (5) Repeat steps 2 to 4, 17 times (6) 68 °C for 10 minutes (7) 10 °C until the sample was recovered. Following PCR, the reaction was ethanol precipitated by adding 5 µL of 3 M ammonium acetate and 140 µL of 100% ethanol to the 50 µL PCR reaction. This solution was stored overnight at -20 °C. The DNA was centrifuged at 23,100 x *g* for 30 minutes at 4 °C. The supernatant was removed and the pellet was air-dried and then resuspended in 8 µL of water.

To cut the template plasmid before transformation, the ethanol precipitated PCR reaction was mixed with 1 µL of DpnI and 1 µL of the digestion buffer. The plasmid was digested for two hours at 37 °C. 2 to 5 µL of the digested plasmid was electroporated into Electro10 Competent Cells. DNA was obtained from colonies using TempliPhi, and the DNA was digested with BamH1 and NheI to identify the correct colonies. Potential colonies were sequenced and stored as glycerol stocks.

2.2.4 Cloning Scheme and Protocol for Generating the HA-APC4 Lentivirus Constructs

An Asc1 site was added to the C-terminus of the wildtype and mutant APC4 constructs by mutagenesis. Approximately 40 to 60 bp primers were designed to include 15 to 20 bp of the C-terminal sequence of APC4, followed by the restriction site AscI. Pfu DNA polymerase was used in the reaction to generate APC4-expressing plasmids with the additional AscI site. The following is the 50 µL reaction mixture used for mutagenesis: 50 ng of Myc-APC4 pcDNA3.1-, 1.3 µL of forward and reverse primers (50 pmol/ µL), 4 µL of dNTP (100 mM), 5 µL of 10 x reaction buffer, 0.6 µL of Pfu (2.5 U/µL), and water up to 50 µL. The cycling parameters were as follows: (1) 95 °C for 10 minutes (2) 95 °C for 30 seconds (3) 60 °C or 62 °C for 1 minute (4) 68°C for 18 minutes (5) Repeat steps 2 to 4, 17 times (6) 68 °C for 10 minutes (7) 10 °C until the sample was recovered.

Following PCR, the reaction was ethanol precipitated by adding 5 µL of ammonium acetate and 140 µL of 100% ethanol to the 50 µL of PCR reaction. This solution was stored at -20 °C overnight. The DNA was pelleted by centrifugation at 23,100 x *g* for 30 minutes at 4 °C. The supernatant was removed and the pellet was air-dried. The pellet was then re-suspended in 8 µL of water and 1 µL was transformed into Electro10 competent cells. Colonies were screened to identify colonies that had the new AscI site, and these were then fully sequenced. Correct colonies were stored as glycerol stocks.

The lentivirus vector f(syn)w-rbn.sbd and the APC4 constructs flanked by a N-terminal NheI and a C-terminal AscI sites were digested for 3 hours with NheI and AscI at 37 °C. The cloning protocol proceeded as described in Section 2.2.1. DNA from colonies was digested with NheI and AscI to identify the correct colonies before they were sequenced and stored as glycerol stocks.

2.2.5 Cloning Protocol for Generating the EGFP pCS2+ Control Plasmid

In addition to a pcDNA3.1- empty vector, I wanted a control vector to use in HEK293 cell experiments that expressed EGFP. To generate this control vector, I replaced Cdc20 within my HA-Cdc20 pCS2+ vector with EGFP. EGFP-N1 was transformed into JM110 electrocompetent cells, a Dam- competent cell line prepared in our lab. HA-Cdc20 pCS2+ and EGFP-N1 were digested with BamHI and XbaI for 3 hours, and the vector and insert bands were gel extracted and ligated together using the standard protocol (see Section 2.2.1). DNA from colonies was screened with BamHI and PvuI digestions, and then the DNA was sequenced. A glycerol stock was prepared for the correct construct.

2.2.6 Bacterial Transformation

A 50 µL aliquot of electro-competent cells was thawed on ice and transferred to a pre-cooled electroporation cuvette. Between 0.5 and 4 µL of a DNA sample or a ligation reaction was gently pipetted into the cuvette. An electrical pulse of 1.8 kV was applied

to the cuvette. Between 0.7 and 1 mL of NZY+ broth was added to the cuvette to recover the bacteria. The culture was moved to a new Eppendorf tube and the bacteria were allowed to recover for an hour at 37 °C with moderate shaking. The *E. coli* were pelleted at 3,000 x *g* for 1 minute, and the pellet was resuspended in 50 µL of LB medium and plated on pre-warmed LB plates that contained the appropriate antibiotic (Schell and Wilson, 1979).

LB Plates:

25 g of LB Browth (Miller's Modification) and 15 g Bacto-agar were added to 1 L of distilled water and autoclaved. Appropriate antibiotics were added to cultures before plates were poured.

LB Medium:

25 g of LB Browth (Miller's Modification) was dissolved in distilled water and autoclaved. Appropriate antibiotics were added to cultures immediately before use.

NZY+ Medium:

10 g of NZ amino (casein hydrolysate), 5 g of yeast extract, and 5 g of NaCl were dissolved in 1 L of distilled water and autoclaved. Immediately before use, a 10 mL aliquot of NZY+ was supplemented with the following: 125 µL of 1 M $MgCl_2$, 125 µL of 1 M $MgSO_4$, and 100 µL of 2 M glucose.

2.2.7 Plasmid DNA Preparations

Mini-prep and maxi-prep plasmid DNA purification utilized 4 mL and 200 mL of a bacterial culture respectively. Manufacturer's protocols were used for isolation by the kit. All DNA was stored in 1X TE or water.

A boiling method was also used to isolate small amounts of DNA in some bacterial colony screens. Cells were suspended in 250 µL of STET buffer and vortexed. 25 µL of 10 mg/mL lysozyme was added and the tube was vortexed again. The tube was boiled for 45 seconds at 100 °C and then centrifuged at maximum speed for 10

minutes at room temperature. 50 µL of 7.5 M ammonium-acetate and 500 µL of 100% Ethanol were added to each tube sequentially and the tubes were mixed. The tubes were centrifuged at 23,100 x *g* for 30 minutes and the supernatant was discarded. The pellet was washed with 500 µL of 70% ethanol and centrifuged at 23,100 x *g* for 5 minutes at room temperature. The supernatant was removed and the pellet was air-dried. The pellet was resuspended in 50 µL of 1X TE buffer supplemented with RNase A (20 µg/mL).

TempliPhi preparation of DNA was often used to prepare DNA for bacterial colony screens. A single colony was picked and put into 50 µL of LB media and grown for 4 hours at 37°C without shaking. 1 µL of bacterial culture was added to 5 µL of TempliPhi Denature Buffer in a PCR tube and heated to 95 °C for three minutes, and then the tubes were cooled on ice. 5 µL of TempliPhi Premix was added to each tube and incubated at 30 °C for 18 hours. The reaction was heat inactivated at 65 °C for 10 minutes and stored at -20 °C until used. Before using the reaction in restriction digestions or sequencing reactions, the reaction was diluted with 20 µL of water.

STET Buffer:

8% Sucrose, 0.5 M Triton X-100, 10 mM Tris HCl pH 8.0, 50 mM EDTA pH 8.0

TE Buffer:

10 mM Tris-HCl pH 7.4, 1 mM EDTA

2.2.8 DNA Quantification

Plasmid DNA was quantified using a spectrophotometer. Digested DNA and PCR products were quantified on agarose gels by comparing various quantities of DNA sample to a ladder containing known quantities of DNA. After running the agarose gel, it was post-stained with ethidium bromide for 30 minutes to provide more reliable DNA quantification results than with GelRed (Boulet et al., 2010).

2.2.9 DNA Sequencing

All DNA sequence analysis was done by the MPIEM DNA Core Facility on an Applied Biosystems 373 DNA Sequencer using the standard protocols published by the manufacturer. Sequences were analyzed with NCBI Blast and the sequencing data was viewed with Finch TV (Version 1.5.0, Geospiza Inc).

2.2.10 Primer Generation

All primers were generated using the MPIEM DNA Core Facility and an Abi 5000 DNA/RNA synthesizer or a Dr. Oligo 48 Automated Chemistry Instrument from Biolytic Lab Performance Inc. Primer designs were analyzed using IDT's online Oligo Analyzer Software. See the list of primers in Section 2.1.7.

2.2.11 DNA Digestions with Restriction Endonucleases

To characterize plasmids and cloned constructs, DNA was digested with NEB endonucleases using the manufacter's protocols (Schell and Wilson, 1979). Briefly, 200 ng to 2 µg of DNA was digested with a total of 0.5 to 2 µL of enzyme in a reaction volume of 30 to 50 µL for 1 to 16 hours at 37 °C. Heat inactivation was used when indicated by the NEB website (Boulet et al., 2010).

2.2.12 DNA Electrophoresis and Imaging of the DNA Gels

DNA was loaded into a TBE-based 0.8 to 2% agarose gel and ran in 1X TBE running buffer at 100 to 150 V for one hour. After running the gel, the gel was post-stained for 30 to 60 minutes with ethidium bromide or GelRed. To determine the molecular weight or to quantity the DNA fragment within a lane, 0.5 µg of GeneRuler 1 kb DNA ladder was added to a lane for comparison. The DNA was visualized using UV light and a Gel Documentation System (Boulet et al., 2010).

2.2.13 Purification of DNA Fragments

Following the separation of DNA by electrophoresis, fragments of interest were excised using a razor and stored in Eppendorf tubes. The fragments were purified using a PureLink Gel Extraction Kit (Invitrogen) and the manufacturer's protocol. The purified DNA was run on an agarose gel to determine the purity and the quantity of the DNA (Boulet et al., 2010).

2.2.14 Polymerase Chain Reaction (PCR)

DNA fragments of interest were amplified in 20 to 50 µL of a reaction mixture. Pfu was used to generate the 2.4 kb inserts needed for cloning the APC4 constructs, but Red Taq was used in all other cases. The PCR reaction composition and cycling protocol varied by the reaction but followed the manufacturer's protocol (Boulet et al., 2010). The primers used are given in Section 2.1.7.

2.2.15 Mouse Genotyping

The technical staff in our lab and in the MPIEM DNA Core Facility performed all of the mouse genotyping. DNA was isolated from the tails of mice when they were 2 to 3 weeks old. The DNA was isolated using a Nexttec genomic DNA isolation kit. The PCR reaction mixture was 1X MyTaq Reaction buffer, 5.5 mM $MgCl_2$, 1 mM dNTPs, 0.2 nM primers, 0.05 U/µL MyTaq HS DNA Polymerase, and 1 to 2 µL of tail DNA. The cycling parameters were as followed: (1) 96 °C for 3 minutes (2) 94 °C for 30 seconds (3) 62 °C for 1 minute (4) 72 °C for 1 minute (5) Repeat steps 2 to 4, 32 times (6) 72 °C for 7 minutes (7) 12 °C until the sample was recovered.

Table 11. Mouse Genotyping Primers Used

Institute's Primer Number	Primer Description	Primer Sequence
38002	Forward primer for all mice	CCCCTCATGAAGAACTACAGG
38003	Reverse Primer for knockout first target region	ATCGCTTTTGCCTTGACG
26716	Reverse Primer for tm1a knockout first mice	CACCCAACTGACCTTGGGCAAG
29796	Reverse primer for tm1c allele	CCGCCTACTGCGACTATAGA
12112	Forward primer for FLIR mice	FAM-GTGACAGAGACAAAGACAAGCGTTAG
12113	Reverse primer for FLIR mice	AATTGCCGGTCCTATTTACTCGTT
29470	Intron 3/4 amplicon (forward actin)	TGTGGCTTTCTGAACTTGACA
35539	Magali primer ms-mRNA-UPL#64-Actb-R (reverse actin)	ACCAGAGGCATACAGGGACA

Table 12. PCR Results for Each Mouse Genotype

Mouse Genotype	Primer Numbers Used	Band Size (base pairs)
Wildtype (*ANAPC4*)	38002, 38003	316 bp
tm1a	38002, 26716	455 bp
tm1c	38002, 38003	512 bp
FLIR (Flip)	12112, 12113	139 bp
Actin (Wildtype control for FLIR)	29470, 35539	119 bp

2.2.16 Buffers and Solutions

Unless specifically listed, all buffers and solutions were generated using standard laboratory protocols. Solutions were in general made more acidic with HCl and more basic with NaOH. However, care was taken to not introduce new ions to the solution so other acids and bases were used when required.

2.3 Tissue Cultures, Transfections, and Lentivirus Transduction

2.3.1 HEK293 Cell Tissue Culture

Standard tissue culture techniques were used to grow HEK293FT up to passage 40 in DMEM Complete Media. Cells were plated on 10 cm dishes, 12 well plates, or 6 well plates at around 20% confluency. Cells were grown in an incubator held at 37 °C and 5% CO_2. For passaging, cells were treated with 0.05% trypsin for 1 to 3 minutes to detach them and to transfer them to new plates (Graham et al., 1977). This procedure was modified when the cells were grown to harvest lentivirus, as discussed in Section 2.3.6.

DMEM Complete Media:
DMEM media, 1.45 g/L glucose, Penn/Strep, and 10% FBS

2.3.2 HEK 293 Cell Transfections

HEK293FT cells were plated at 20% confluency. After 12 to 24 hours, the cells were transfected with DNA using lipofectamine 2000 according to the manufacturer's protocol (Felgner et al., 1987). See Section 2.1.6 for a list of constructs used. For a 6 well plate, 0.5 µg of DNA and 1 µL of lipofectamine were used. For a 10 cm dish, 2 to 5 µg of total DNA was used. For every 1 µg of DNA, 2 µL of lipofectamine was also used. The media was not changed before or after the transfection unless otherwise specified. An EGFP-expressing vector was used as a control to determine the transfection efficacy at around 48 to 72 hours after the transfection. Media was removed after 48 to 72 hours, and the plates were stored at -20 °C for up to two weeks before being lysed. For IP experiments, the plates were processed on the same day that they were harvested. The transfection procedure for HEK293 cells was different when used to produce lentivirus (see Section 2.3.6).

2.3.3 Neuron Cultures

Neuron cultures were generated using standard procedures (Swaiman et al., 1982). The hippocampus was dissected from the brains of P0 mice, and the cortex was dissected from the brains of E16 embryos. While the brains were dissected, they were submerged in Hanks' Balanced Salt Solution. The tissue from one mouse was digested in 500 µL papain working solution for 40 to 50 minutes at 37 °C with gentle agitation (450 revolutions per minute). To stop the digestion, the papain solution was replaced with pre-warmed stop solution, and it was incubated for another 20 minutes at 37 °C with gentle agitation (450 revolutions per minute). Then the tissue was mechanically triturated with 100 µL of pre-warmed Complete Neurobasal Medium using a plastic P100 pipette tip. This was repeated one additional time and the solution of cells was adjusted to a volume of 1.2 mL. If the genotypes were all identical, all samples were combined at this step to make a master stock for plating.

The dissociated neurons were plated on coverslips or wells that had been coated with poly-L-lysine and subsequently washed four times with water before plating. If the isolated cells were used for imaging, approximately 25,000 to 50,000 cells were seeded in each well of a 24 well plate. For biochemical analysis, around 1.2 million cells were seeded in each well of a 6 well plate. Neurons were cultured in complete Neurobasal medium in a tissue culture incubator held at 37 °C with 5% CO_2. Medium was changed 18 to 24 hours after plating to pre-warmed complete Neurobasal medium to promote the survival of a high number of cells.

Complete Neurobasal Medium:
Neurobasal A medium, 2% B27, penicillin (50 U/ml), and streptomycin (50 µg/ml), and 1% GlutaMAX

Stop solution:
1250 mg Bovine Serum Albumin, 1250 mg Trypsin Inhibitor from chicken egg white (Type II), 10% FBS, 450 mL of DMEM

Papain working solution:

papain stock solution, 25 units/mL of papain enzyme

I heated the stock solution at 37°C for 30 minutes. To solubilize the enzyme, the solution was bubbled with saturated carbogen (95% oxygen and 5% carbon dioxide) and then was filtered with a 0.22 µm syringe filter.

Papain stock solution:

1.65 mM L-Cysteine, 1 mM CaCl2, 0.5 mM EDTA, in 500mL of DMEM

2.3.4 Neuron Culture Transfections

While higher percentages of neurons express a construct after lentiviral infection, expression rates of less than 5% can be obtained by using calcium phosphate transfection (Jiang and Chen, 2006). This technique is in particular useful for imaging questions that require young neurons to overexpress a construct of interest. Briefly, 1 µg of plasmid DNA was diluted in water to a final volume of 21.9 µL, and 3.1 µL of 2 M $CaCl_2$ was added in drops and the solution was mixed by briefly hitting the tube on the bench four times after each drop. Up to 4 transfection reactions could be done inside one tube. This mixture was then added in drops to 25 µL of 2x HBS, and the mixture was vortexed after each drop for 2 to 3 seconds at the lowest setting. The mixture was incubated in the dark for 20 minutes at room temperature. During the incubation, the media was removed from the DIV1 neurons and replaced with pre-warmed Neurobasal that lacked supplements. The removed media was saved and added back to cells after the transfection. The transfection reaction was pipetted up and down 5 times and 50 µL of the reaction was added to each well of a 24 well plate. The cells were then incubated at 37 °C and 5% CO_2 for 20 minutes, until the formation of aggregates started. The cells were then washed 2 times for 7 minutes in an incubator held at 37 °C and 10% CO_2. The washing solution was 2X HBS that was pre-equilibrated for 24 hours in an incubator at 37 °C and 10% CO_2. The formation and the dissolution of aggregates were monitored with a microscope. The original media was returned and the neurons were grown under standard conditions until they were fixed at DIV5.

HBS 2x:

274 mM NaCl, 10 mM KCl, 1.4 mM Na_2HPO_4, 15 mM Glucose-D, 42 mM HEPES The final pH was adjusted to 7.08 with NaOH.

2.3.5 Cell Synchronization in G2/M

Cells were synchronized in G2/M using established procedures (Ertych et al., 2014). HEK293 cells were plated on Poly-L-Lysine coated 10 cm dishes. When they reached 70% confluency, the media was changed to pre-warmed DMEM Complete media and the cells were transfected using the protocol in 2.3.2. After 8 hours, 2 μM Dimethylenastron, an inhibitor of the mitotic kinesin, Eg5, was added to the media and the plates were gently swirled and returned to the incubator for 16 hours. Then the media was changed to pre-heated DMEM Complete Media. After 8 hours, the inhibitor was added again for 14 to 16 hours. The cells were washed before being harvested. Aurora-A and Cyclin E antibodies were used to confirm that the cells were in G2/M via WB during several experiments. However, this was later deemed to not be necessary, as you could easily identify cells in G2/M arrest by observing their cellular morphology. It was not a primary aim of the study to obtain cells purely at this checkpoint, but I instead was just trying to increase the proportion of the cells at this checkpoint to boost the amount of APC4 SUMOylation.

2.3.6 Preparation of Lentivirus and Lentivirus Transduction

I prepared lentivirus using standard methods (Naldini et al., 1996). Low passage (passage 10 to 25) HEK293FT cells were maintained in media that contained 0.4 μg/μL Geneticin. Prior to seeding the cells, 15 cm plates were coated with Poly-L-Lysine (1:12 dilution in 1X PBS) for 1 to 48 hours, washed, and stored in water or 1X PBS until used. When cells were around 70 - 100% confluent, they were transfected with 40 μg of vector, 16 μg of packaging, and 16 μg of envelope DNA. The transfection reactions also used 6 mL of Opti-MEM medium and 60 μL of Lipofectamine 2000. The reaction was incubated at room temperature in the S2 lab for 60 minutes before it was added to the cells

(Felgner et al., 1987). The media of the cells was changed to pre-warmed 10% FBS in Opti-MEM medium, prior to the addition of the transfection mixture. After 6 hours, the media was changed to pre-warmed Virus Media, and then the virus was harvested after about 44 to 48 hours.

To harvest virus, media from plates was transferred to 50 mL centrifuge tubes and centrifuged at 2000 x *g* for 10 minutes at 4 °C. All steps of this protocol took place with pre-chilled tubes and solutions. The media was filtered with a 0.45 µm filter attached to a Luer Lock syringe, and the solution was transferred to an Amicon filter system where it was centrifuged at 3500 x *g* for 10 minutes at 4 °C. The virus was washed two times each with Neurobasal A media and 1X TBS. For each wash, the tube was centrifuged at 4000 x *g* for 18 minutes and the wash was discarded. The remaining virus was diluted in 1X TBS to a volume of 500 µL, aliquoted, froze in liquid nitrogen, and stored at -80 °C.

The virus titer was determined by infecting wildtype primary hippocampal neuron cultures grown on a 24 well plate with 5, 10, 15, 20, or 25 µL of virus. The percentage of cells infected was determined on a confocal microscope by comparing the number of cells with DAPI stain to those with RFP or GFP stain. Typically 90 to 100% infection rates were achieved by adding around 5 to 10 µL of virus into each well of a 24 well plate. For biochemistry experiments, each well was typically infecting with around 100 µL of virus, which resulted in infection rates over 90%.

1X TBS:

50 mM Tris HCl (pH = 7.40), 150 mM NaCl

Virus Media:

DMEM, 1% Penn/Strep, 2% goat Serum, and 10 mM sodium butyrate

2.4 Biochemistry Methods

All biochemistry experiments utilized standard procedures for the lysis of cells, quantification of protein, SDS/PAGE electrophoresis, and WB (Kumar et al., 1985).

2.4.1 Lysis of Cell Cultures

Cells were lysed using standard methods in lysis buffer. Tissue culture plates containing cells were frozen at -80 °C if they were not lysed immediately. If the cells were used for IP experiments, they were lysed immediately. For HEK293 cells, 1.4 mL of Lysis Buffer was added to a 10 cm dish and 200 to 300 µL of Lysis Buffer was added to each well of a six well plate. For neuron cultures, I lysed a single well of a six well plate with 80 µL of Lysis Buffer. If more than one well of the same conditions were lysed together, all plates were lysed sequentially with a volume of equal to about 60 µL of Lysis Buffer per well. For neurons plated on a 10 cm dish, 800 to 1000 µL of lysis buffer was used. Cells were scraped off with a cell scraper and transferred to a centrifuge tube stored on ice.

HEK293 cells lysates were briefly sonicated for 4 seconds with a sonicator probe set on power level 60, but this step was avoided for neuron cultures when an IP was not conducted. If a neuron cultures needed sonication, this was immediately done before the lysate was ran on the gel with either a sonicator probe using the same settings as before or for 30 minutes in a sonicator bath. When HEK293 cells were synchronized in G2/M arrest or cell fractionated, they also typically needed an additional sonication step that was done after the addition of Laemmli buffer by sonicating it in a water bath for 30 minutes. NEM was added to the Lysis Buffer of all IPs and SUMO expression experiments, but it was left out of most APC4 knockout and APC/C IP experiments.

Lysis Buffer:
150 mM NaCl, 10 mM Tris pH 7.4, 1% Triton X-100
Protease inhibitors: 1 µg/mL aprotinin, 0.5 µg/mL leupeptine, and 17.4 µg/mL PMSF
NEM: 20 mM NEM dissolved in DMSO if required

2.4.2 Determining Protein Concentration

To determine the protein concentration, I used the Bicinchoninic Acid (BCA) method and the manufacturer's protocol. The BCA reagents were mixed at a 1:50 ratio and 1 to 5 µL of protein were added to 200 µL of the BCA mix in each well of a 96 well plate. 10

µL of known concentrations of BSA were added to control wells in order to create a control curve. This curve was then used to estimate the concentration of the protein in all of the lysates. Protein stock solutions were immediately generated at concentrations of less than 2 µg/µL. Lysate were also diluted to this range for IPs.

2.4.3 SDS/PAGE Gel Electrophoresis

To separate proteins based on their molecular weights, lysates were run on SDS/PAGE gels consisting of an upper stacking gel and a lower resolving gel. Mini protein gels were casted on a Biorad gel casting system. The resolving gel was typically an 8% gel. A 15% gel was used to show unconjugated SUMO or other proteins that have a lower molecular weight. If higher molecular weight proteins above 150 kDa were being probed, a 6% gel was used. The recipes are shown below. The National Diagnostics Acrylamide was used for all experiments, except for the neuron culture and cell fractionation experiments. With the exception of using the HiMark Protein Ladder on the 6% gels, the Pageruler Prestained ladder was used to determine the size of the proteins on the gels. Lysates were dissolved in Laemmli buffer. Typically, samples were boiled for 3 min at 95°C before loading onto the gel. In general, 25 µg of protein were loaded per well. To compare molecular weights, 5 µL of Protein Prestained Ladder was added to a well. The gels were run in 1x Running Buffer for 1.5 to 3 hours at 20 to 25 mA per the number of gels within the chamber at that time.

<u>3X Laemmli Buffer:</u>
150 mM Tris pH 6.8, 30% glycerol, 0.6 g SDS, bromophenol blue
100 mM DTT was added fresh to each sample

<u>1X Running Buffer:</u>
25 mM Tris-HCl, 240 mM glycine, 0.1% SDS (pH 8.8)

<u>Upper Stacking Gels:</u>
0.17 mL of 30% acrylamide, 0.13 mL of 1 M Tris pH 6.8, 10 µL of 10% SDS, 10 µL of 10% APS, 1 µL TEMED, 0.68 mL water.

Lower Resolving Gels:

6% gels: 2 mL of 30% acrylamide, 2.5 mL of 1.5 M Tris pH 8.8, 100 µL of 10% SDS, 100 µL of 10% APS, 8 µL of TEMED, 5.3 mL of water.

8% gels: 2.7 mL of 30% acrylamide, 2.5 mL of 1.5 M Tris pH 8.8, 100 µL of 10% SDS, 100 µL of 10% APS, 4 µL of TEMED, 4 mL of water.

15% gels: 5 mL of 30% acrylamide, 2.5 mL of 1.5M Tris pH 8.8, 100 µL of 10% SDS, 100 µL of 10% APS, 2 µL of TEMED, 2.3 mL of water.

2.4.4 Western Blotting (WB)

After protein samples were ran on a SDS/PAGE gel, they were transferred at 45 mA for 16 hours onto Nitrocellulose membranes using a tank blotting system. To verify the transfer, membranes were briefly stained with Ponceau S. All of the APC4 knockout experiments were instead stained with Memcode Reversible Stain. I obtained an image to document the transfer by either scanning or copying it, and the membrane was dried overnight before it was blotted.

All WB steps were completed at room temperature with shaking. Membranes were blocked with 5% milk for 20 to 60 minutes. Then the membrane was incubated with primary antibody in 5% milk. The experiments to determine if APC4 was SUMOylated used a primary incubation time of 3 hours, but the remaining experiments used an incubation time of 4 hours. The membrane was rinsed 3 times and then washed once with milk for 10 to 30 minutes. Secondary antibody was applied in 5% milk for 1 to 1.5 hours. Finally, the membrane was quickly washed three times followed by an additional wash for 30 to 60 minutes in 1X PBS or 1X PBST. All antibodies used are listed in Section 2.1.4.

To visualize the antibody, ECL reagent was applied using the manufacturer's protocol. Briefly, the reagents were mixed at a 1:1 ratio, and 2 mL of the mixture were pipetted over each membrane. Excess liquid was removed with a paper towel. For the

APC4 SUMOylation, ubiquitylation assays, and the APC/C HEK293 cell IP experiments, membranes were exposed to film for up to an hour after the addition of ECL. The following exposures were typically acquired: 30 seconds, 1 minute, 5 minutes, and 30 minutes. At times when the signal was very weak, I would try to boost it using the Supersignal West Dura ECL. The majority of other experiments were processed on our Intas Imaging System for 60 minutes with a variety of intermediate exposures instead of film. After ECL treatment, the membranes were washed in water before they were dried overnight.

Membranes were regularly re-blotted, often after waiting for 24 to 48 hours to decrease the signal left over from the prior antibodies. If the signal was really strong, I stripped the membrane by incubating it with 200 mM NaOH at 37 ºC for 10 minutes. I then washed it several times with 1x PBS and water, and then I dried them over night. Membrane stripping was generally done only once per membrane

To quantify the protein levels on a membrane, the band intensity of the protein of interest was quantified using ImageJ's Analyze Gels tool. This value was typically normalized to tubulin in the figures, unless otherwise noted, but values normalized to the memcode stain were compared when available. Each experiment was typically repeated at least three times, and the average value of the protein's expression was determined. When several different experiments were quantified (Figures 14 and 24), 2 to 4 lanes on the same or different gels were typically used to determine the normalized protein values for that one experiment. These experimental averages were then averaged together for all of the different experiments.

10x PBS:

80 g of NaCl, 2 g of KCl, 14.4 g of Na_2HPO_4, 2.4 g of K_2PO_4

1X PBST:

1X PBS + 0.1% Tween 20

Milk

5 g of powdered milk dissolved in 100 mL of 1X PBS or 1X PBST right before use

2.4.5 Immunoaffinity Purification (IP)

The standard protocol was adapted for all IP experiments (Tomomori-Sato et al., 2013). For SUMOylation and ubiquitylation IPs, cells were lysed in buffer containing NEM. Lysates were sonicated with a probe sat to power level 60 for 4 seconds and then the lysates were transferred to new tubes. Next the lysates were centrifuged at 106,000 x *g* for 30 minutes at 4°C using an ultracentrifuge. After the centrifugation, 100 µL input samples were aliquoted from the eluate and stored on ice until the IPs were completed. The remaining supernatant was transferred to a tube that contained 40 µL of pre-washed HA or Myc beads. The beads were washed two times with Lysis Buffer containing NEM, and then fresh NEM and protease inhibitors were added to all IP samples. Samples were then incubated with mixing by rotation at 4 °C for 4 hours. The beads were then washed 2 times in Lysis Buffer that contained fresh NEM. The protein was then eluted off the beads with 70 µL of 1X Laemmli Buffer at room temperature for 10 to 30 minutes. For the SUMOylation studies, no samples were boiled before loading, as the overexpressed APC4 aggregated a lot at higher temperatures. The ubiquitylation IPs were boiled for 3 minutes at 100 ºC. Each lane of an SDS/PAGE gel was loaded with 15 µL of inputs and 20 µL of IP eluates, and then I analyzed all of the samples by WB. The protein concentration was not typically quantified before the lysates were added to the beads.

The APC/C co-IP protocol required substantial optimization, as the APC/C tended to stick non-specifically to all types of the beads that I tested. I tested a variety of different buffering conditions and protocols, eventually finding reliable conditions. However, the APC/C co-IP only worked in the absence of NEM, and as such NEM was not used in these experiments. For APC/C co-IP experiments, I used lysates from DIV11 neuron cultures or HEK293 cells. The HEK293 cells were transfected two days before lysis. The cells were lysed in Lysis Buffer containing all of our protease inhibitors (but no NEM). The lysate was then sonicated at a power level of 60 for 4 seconds and then the lysate was transferred to a new tube. Lysates were ultracentrifuged at 106,000 x *g* for 30 minutes at 4°C, and the eluate was transferred to a new tube and then the ultracentrifugation step was repeated. Finally, the eluates were transferred to new tubes

containing 40 µL of pre-washed and packed Protein G Sepharose, or commercially available HA or Myc beads.

To IP the endogenous APC/C, 10 µL of anti-Cdc27 antibody was added to the eluates with Protein G Sepharose. As a negative control for the Cdc27 IPs, the beads were incubated with an equal amount of an IgG isotype control. All samples were incubated with rotation at 4 °C for 4 hours. Beads were then washed 4 times with Lysis Buffer containing all of the protease inhibitors, and the beads were spun down at 110 x *g* for one minute at 4 °C after each wash. The protein was then eluted off the beads with 50 µL of 1X Laemmli Buffer and boiled at 100 °C for 3 minutes. 15 µL of inputs and 15 µL of IPs were loaded in each lane of an SDS/PAGE gel and analyzed by WB using the standard procedure.

2.4.6 Subcellular Fractionation of the Mouse Cortex

I used standard protocols to fractionate samples (Carlin et al., 1980), and all of the samples were kept on ice or at 4 °C during this entire process. The final fractions were frozen in liquid nitrogen and stored at -80 °C. The cortex was dissected from the brain of an eight week-old wildtype C57/N mouse. To obtain the Homogenate (H), the cortex was then homogenized in 5 mL of Solution A with 12 strokes of a Dounce homogenizer at 900 rpm (collected 100 µL for analysis). The solution was centrifuged for 10 minutes at 1400 x *g*, and the supernatant was collected for the S1 fraction (saved 100 µL for analysis). The pellet from this first centrifugation was dissolved in 3 mL of Solution A to generate the P1 fraction (saved 1 mL for analysis).

The S1 fraction was centrifuged for 10min at 13,800 x *g*, and the supernatant was collected as the S2 fraction (saved 1 mL for analysis). To generate the P2 fraction, the pellet from the second spin was disassociated in 2 mL of Solution B and homogenized with 4 strokes a Dounce homogenizer at 900 rpm (saved 100 µL for analysis). To generate the Syn fraction, 2 mL of the P2 fraction was added to the top of a column with a sucrose gradient and centrifuged at 82,500 x *g*. About 700 µL of solution was collected from the interphase between 1 M and 1.2 M sucrose, and the volume of this fraction was adjusted to 1.5 mL with solution B to generate the Syn

fraction (collected 100 µL for analysis). To generate the SPM fraction, 1.5 mL of Solution C was added to the Syn fraction and the solution was incubated with mild shaking for 15 minutes before it was ultracentrifuged at 32000 x *g* for 20 minutes. The pellet was re-suspended in a 50 µL of a 1:1 mixture of Solutions B and C. After 5 minutes of incubation, the pellet was resuspended by pipetting to generate the SPM fraction.

The protein concentration was determined for all fractions, except the SPM, and 20 µg of protein was added to an 8% gel. I added 25 µL of 3x Laemmli to the SPM fraction and 25 µL was loaded to the gel. While the Laemmli stain was visible, the gel was cut at around 70 kDa to allow for simultaneous blotting with multiple antibodies. Standard methods were used to the analyze the fractions by SDS/PAGE followed by WB using antibodies against APC4, APC5, Rab-GDI, Synaptophysin, NeuN, and PSD-95. The membrane was stripped between WB experiments with 200mM NaOH for 20 minutes at 37 °C, and then the membrane was washed with 1X PBS and dried overnight.

Solution A:

0.32 M Sucrose, 1 mM HEPES pH 7.4, 1 mM $MgCl_2$, 0.5 mM $CaCl_2$.

Solution B:

0.32 M Sucrose, 1 mM HEPES pH 7.4

Solution C:

0.32 M Sucrose, 1% Triton x100, 12 mM Tris, pH 8.1

Syn Gradients Columns:

These columns were generated by adding 4 ml of 1.2 M Sucrose, 3 mL of 1 M Sucrose, and 3 mL of 0.85 M Sucrose in layers (all Sucrose layers also had 1 mM HEPES. pH 7.4)

2.4.7 Cellular Fractionation of HEK293 Cells

HEK293 cells were transfected using the standard transfection protocol in Section 2.3.2. Cells were trypsinized and spun at 1500 x *g* to pellet the cells. The pellet was washed in room temperature 1X PBS and then placed on ice for the remainder of the protocol. The fractionation was then completed using the manufacturer's protocol and kit: Thermo Scientific's NE-PER Nuclear and Cytoplasmic Extraction Reagents. Protease inhibitors and NEM were added using the same concentrations as lysis buffer. To try to boost purity, I washed the nuclear pellet with ice cold 1X PBS three times. After the protocol was completed, lysates were quantified and run on SDS/PAGE gels using the standard procedures. The amount of protein ran on the membrane was identical in mass in the Equal Protein Loading sample (E) or equal in the percent of cell volume in the Cell Equivalent samples (C).

To identify the cellular fraction in HEK293 cells that contain SUMOylated endogenous APC4, this protocol was completed three different times. The average value of these experiments was compared to a predicted value of 0 using a paired sample t-test in Excel. The experiment to determine if the overexpressed Myc-APC4 construct enters the nucleus was completed a single time.

2.5 Immunocytochemistry (ICC)

2.5.1 Preparation of Coverslips for ICC

Coverslips were incubated at room temperature overnight in 100% ethanol, washed 10 times with water, and then single coverslips were added to either 10 cm dishes, 6 well, 12 well, or 24 well plates. These dishes were then UV treated for 1 hour and then stored in sealed plastic bags. For both HEK293 cells and neuron cultures, coverslips were treated with Poly-L-Lysine for 1 hour at 37 °C, washed 4 times with water and then the coverslips were covered in water and stored in the tissue culture incubator until used.

To prepare coverslips for imaging, I used a standard protocol in my host lab (Daniel et al., 2017). HEK293 cells and neurons cultures were washed with 1X PBS, fixed for 10 minutes in 4% PFA at room temperature, and then washed 4 times with 1X PBS. Coverslips were blocked for 30 minutes at room temperature with Imaging Solution. The plates at this step were covered with aluminum foil to keep them in the dark. With the exception of the APC4 antibody, coverslips were incubated overnight with Imaging Solution that contained all primary antibodies for 16 to 21 hours at 4 °C. They were then washed 4 times with 1X PBS and blocked in Imaging Solution for 30 minutes. The secondary antibodies were diluted at a 1:1000 ratio in Imaging Solution and incubated with the coverslips for 1 hour at room temperature. DAPI was diluted at a 1:10,000 ratio in 1X PBS and incubated at room temperature with the coverslips for 10 minutes. The coverslips were then washed quickly four times and then for a longer 30 minutes wash in 1X PBS. Coverslips were then mounted to slides and allowed to dry at room temperature over night or in the fridge if they were not imaged within 24 hours. Slides were stored at 4 °C until they were imaged. When RFP was not stained with an antibody, the imaging was completed within 10 days unless noted. All other imaging was typically completed within 8 weeks and the coverslips were stored at 4 °C until they were ready to be imaged.

The APC4 antibody staining required extensive optimization, and I settled on a protocol where the coverslips were incubated in Imaging Solution for 24 hours at 4 °C before the other antibodies were added. After 24 hours, I incubated the coverslips in imaging solution that contained a new stock of APC4 antibody and the other remaining antibodies, and this was incubated at 4 °C for 16 to 21 hours. For the secondary only control, the APC4 antibody was omitted and the coverslips were just incubated with the Imaging Solution for the first 24 hours. I unfortunately could never detect APC4 staining with only 20 hours of incubation. To try to boost the staining seen after incubating for 40 to 45 hours, I also tested different fixing conditions (2% PFA, 1% formalin, 100% methanol, 2 minutes of 4% PFA followed by 5% acetic acid in methanol) and a second APC4 antibody, but I was unable to ever boost the levels of APC4 staining.

Imaging Solution:

1x PBS pH 7.4, 0.1% fish skin gelatin, 1% goat serum, 0.3% triton X100

4% Paraformaldehyde (PFA) pH 7.4:

4% sucrose, 4% paraformaldehyde. Used drops of 1 M NaOH to dissolve the PFA.

2.5.2 Fluorescence Microscopy and Image Analysis

Images were acquired on using a Leica TCS SP2 confocal microscope at the MPIEM's microscopy facility. I used the microscope's 63x oil-immersion objective, an image format size of 1024 x 1024, a zoom of 1.2, a voxel size of 193.74 nm x 193.74 nm, and a 4-line average during the acquisitions. The neuron morphology and the knockout mouse experiment images were 12-bit images, but the other images were all 8-bit images. With the exception of the neuron morphology experiment, all images were taken as a single plane that passed through the center of the cell body. The microscope settings (power, gain, and laser offset) were adjusted at the beginning of each session and kept constant throughout the session. With the exception of the morphology analysis, all images were acquired during one session. In the rare case that the image intensity needed to be adjusted, this was done in Photoshop Elements 13 by adjusting the adjusting the lighting levels to a set numerical value for all images in the experiment.

For the morphological analysis, data from two entirely different experiments were pooled together. Each of these experiments was imaged during two separate sessions, where I imaged around 15 to 25 cells from each condition every day. A program was created with all the microscope settings to try to ensure that the settings were similar between each day of one experiment. Some minor adjustments had to be made to the settings during the second experiment, but this was avoided in the channels that were being used for the analysis. The sample labels for the morphology study were taped over and coded randomly to ensure that the study was blinded.

For the morphological analysis, Z-stacks were taken of neurons using a step size of 92 to 108 nm (4 to 15 slices per neuron) for both the Beta III-Tubulin and MAP2 channels. A single plane image was also taken that showed all of the staining for each

cell: RFP, SMI-312, Beta III-Tubulin, and MAP2. Several neurons were thrown out of the morphological analysis experiment from each condition, because the neurites were not clearly defined and distinguishable from the other neurons. Additionally, a few neurons from each condition had a huge swelling off the soma that made the soma hard to define, so these cells were also thrown out out of the analysis.

For the morphological analysis, a single maximum intensity projection was created for all of the planes of a neuron's Beta III-Tubulin stain. To fit a whole neuron into one image, often several overlapping images were taken and they were stitched together using the program called Pairwise Stitching of Images (Linear Blending Method, Check peaks = 5, Compute overlap; Preibisch et al., 2009) in Fiji (Schindelin et al., 2019). Scaled images were then manually traced with Fiji's SNT plugin (Tavares et al., 2017; used Hessian-based analysis settings of $\sigma = 0.484$ and max = 3.69). Primary neurites were labeled as the main neurite exiting the soma. Neurites branching off these neurites were labeled as secondary neurites, and neurites branching off the secondary neurites were tertiary neurites. All neurites of less than 3 μm were excluded from the analysis. One example neuron from each condition that resembled the average data for all of the measurements acquired was selected, and the traces from these neurons were skeletonized using the SNT program (Figure 23 A). Sholl Analysis was completed using the Sholl Analysis 3.1.110 plugin and a starting radius of 5 μm and step size of 5 μm (Sholl, 1953). Fiji was used for all steps of this analysis (Schindelin et al., 2019).

2.5.3 Statistical Analysis For Neuron Morphology Experiments

Cre NLS RFP- and NLS RFP-infected samples were analyzed as described in Section 2.5.2 and Statistical Analysis was preformed using SPSS (IBM, version 27). While the majority of my morphology data did not have a Gaussian distribution, there was also unequal variance between the Cre NLS RFP- and NLS RFP-infected samples, which complicated the statistical analysis. As my data fit a heavy-tailed distribution with unequal variance, I chose to use a Welch's t-test instead of using a non-parametric test, as a Welch's t-test was found to be the most accurate type of test for similar sets of data (Fagerland and Sandvik, 2009; Kroeger et al., 2021; Skovlund and Fenstad, 2001).

2.6 Animals

All animals were maintained, generated, and acquired from the MPIEM's Animal Facility. The guidelines for the welfare of experimental animals that was issued by the federal government of Germany and the Max Planck Society was used to conduct all experiments and maintain the mouse lines. All mice were maintained in the C57/N background, and mice from the C57/N background were also used when my experiments required a wildtype mouse.

2.6.1 Generation of the *tm1c* Conditional *ANAPC4* Knockout Mouse Line

In order to deplete APC4 protein expression within neuron cultures, I tried to acquire a mouse line that to knockout *ANAPC4*, the gene encoding APC4. The *tm1a* knockout-first *ANAPC4* mouse (EUCOMM, MGI: 1098673; EUCOMM, MGI: 1098673; IMPC, n.d.) was first generated by the Sanger Genome Research Institute, and I obtained it from the EUCOMM mouse consortium as live mice finally in the middle of 2019 after years of trying to establish this line at our institute from frozen sperm and embryos obtained from the company. This mouse had an insertion upstream of exon 3, containing a cassette, which included *lacZ* and neomycin sequences flanked by *FRT* and *loxP* sites (Figure 5A).

These mice were crossed to FLIR mice obtained from Dr. Klaus Nave. These mice expressed Flp recombinase driven by the *Gt(ROSA)26Sor* promoter (JAX #003946; Farley et al., 2000), removing the cassette at the *FRT* sites and thereby generating a conditional *ANAPC4* knockout mouse (Figure 6 B). This new conditional *ANAPC4* mouse line is designated by the *tm1c* allele by EUCOMM, and I continued to use this same nomenclature throughout this thesis.

The third possible *ANAPC4* allele, *tm1d*, is generated only within neuron cultures obtained from *tm1c/tm1c* mice that were infected with a virus expressing Cre that was driven by the Synapsin promoter (Figure 5C). Generating the *tm1d* allele removed exon

3 of *ANAPC4*, added a premature stop codon, and thereby generated a theoretical protein product of only 80 amino acids.

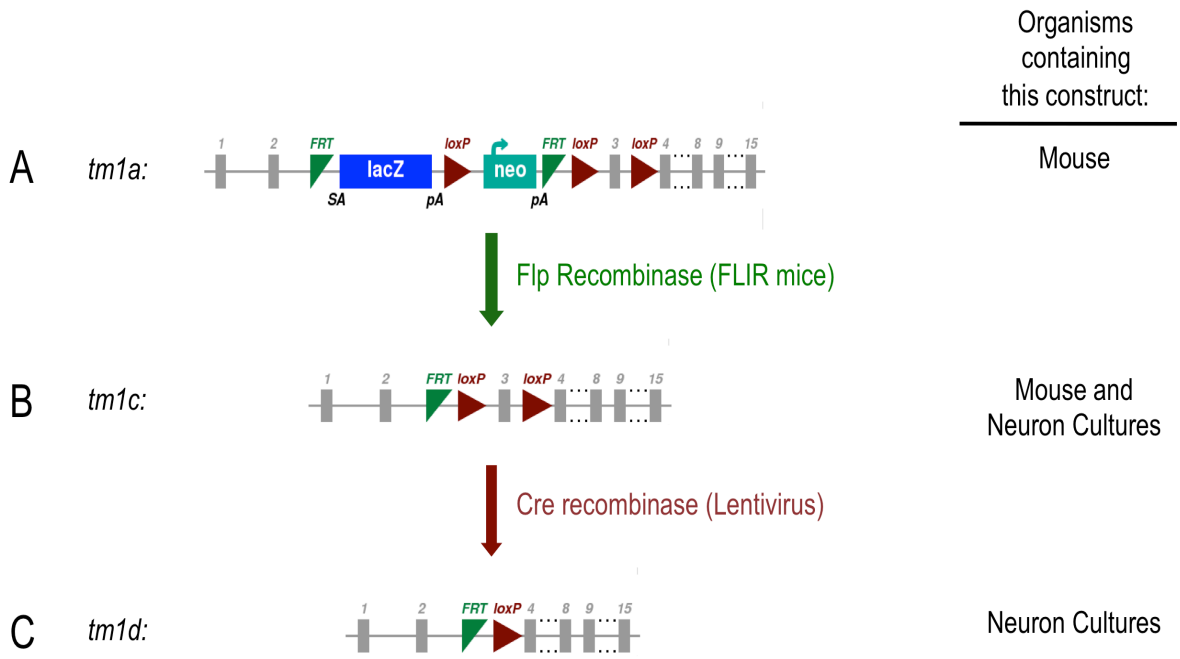

Figure 6. The Schematic Used to Generate a Conditional *ANAPC4* Knockout Mouse Line and to Then Knockout *ANAPC4* in Neuron Cultures. (**A**) The tm1a knockout-first *ANAPC4* mouse was generated by the Sanger Genome Research Institute and supplied by the EUCOMM mouse consortium. This mouse had an insertion upstream of exon 3, which contained a cassette that included *lacZ* and neomycin sequences flanked by *FRT* and *loxP* sites. These mice were crossed to FLIR mice that express Flp recombinase driven by the *Gt(ROSA)26Sor* promoter (JAX #003946; Farley et al., 2000), removing this cassette at the *FRT* sites and thereby generating a conditional *ANAPC4* knockout mouse line expressing the *tm1c* allele (**B**). *ANAPC4* was then knocked out in neuron cultures made from *tm1c/tm1c* mice using lentivirus that expressed Cre-recombinase, thereby generating the *tm1d* allele (**C**) within infected neurons. Generating the *tm1d* allele removed exon 3 of *ANAPC4* and added a premature stop codon, thereby generating in theory a protein product of around 80 amino acids.

3. Results

3.1 Characterization of APC4 SUMOylation Within HEK293 Cells and Cultured Neurons

3.1.1 APC4 is SUMOylated by SUMO1, SUMO2, and SUMO3

APC4 was identified in several proteomic screens as a protein that might be conjugated to SUMO1 (Tirard et al., unpublished) and SUMO2 (Cubeñas-Potts et al., 2015; Hendriks et al., 2018; Matic et al., 2010; Schimmel et al., 2014). While subsequent studies confirmed that APC4 is SUMOylated (Eifler et al., 2018; Lee et al., 2018; Yatskevich et al., 2021), this was not confirmed at the time that I started this study. For this reason, I first sought to confirm that APC4 is SUMOylated and to determine which SUMO paralogs are able to SUMOylate APC4. In order to do this, I analyzed HA-IP eluates obtained from lysates of HEK293 cells that overexpressed Myc-APC4 and either HA-SUMO1, HA-SUMO2, or HA-SUMO3. To block deSUMOylation, all cells were lysed in the presence of NEM, an irreversible cysteine peptidase inhibitor that targets SENPs. WB analysis of IP eluates confirmed that APC4 is SUMOylated, since IP eluates contained size-shifted bands that correspond to APC4-SUMO conjugates (Figure 7 A - C, arrows). This SUMOylation was detected when all SUMO paralogs were overexpressed, including HA-SUMO1 (Figure 7 A, arrows), HA-SUMO2 (Figure 7 B, arrows), and HA-SUMO3 (Figure 7 C, arrows). A smear of proteins in a lysate, which corresponds to all proteins conjugated to SUMO, is normally detected when lysates are blotted with an antibody against SUMO. This smear of SUMOylated proteins was visible when I blotted the Input lysates and IP eluates for HA (Figure 7, brackets in bottom panels), showing that the IP protocol worked as expected.

Some deSUMOylation actively occurred in all Input lysates and IP eluates, even in the presence of NEM. This is evident by the fact that all IP eluates had an intense 100 kDa band that corresponds to non-SUMOylated APC4 (Figure 7, asterisks). Above this band, there was a doublet that correspons to APC4 with either one or two SUMO moieties attached (Figure 7, arrows). These results are consistent with a proteomic

screen showing that SUMO2 can be attached to two different lysine residues of APC4 (Matic et al., 2010).

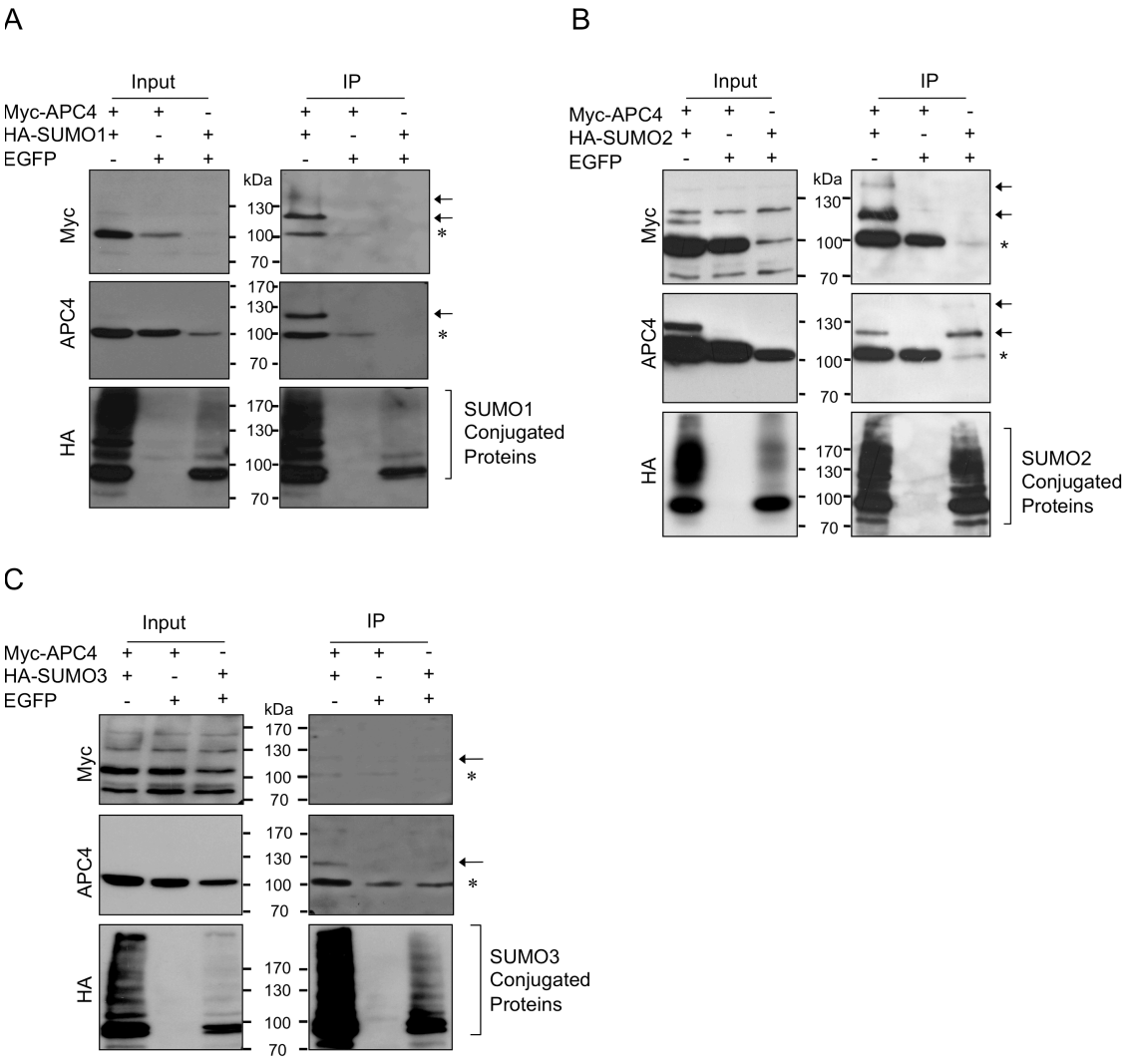

Figure 7. SUMOylation of APC4 by SUMO1, SUMO2, and SUMO3. HEK293 cells were transfected with expression constructs encoding Myc-APC4, EGFP and either HA-SUMO1 (**A**), HA-SUMO2 (**B**), or HA-SUMO3 (**C**). HA-IP was conducted with cell lysates in the presence of NEM. Input and IP eluates were analyzed by SDS/PAGE followed by WB using antibodies directed against Myc (top), APC4 (middle), or HA (bottom). Arrows indicate all APC4-SUMO conjugates, and brackets show the total population of proteins conjugated to the overexpressed SUMO paralog in Input and IP samples. Asterisks show the non-SUMOylated APC4.

Like most in-cell SUMOylation assays, I overexpressed the SUMO constructs because it is difficult to detect SUMOylation otherwise. More importantly, I also had no way to use an antibody to distinguish between SUMO2 and SUMO3 due to their similar amino acid sequence. For this reason, I was unable to determine which SUMO paralogs were primarily responsible for SUMOylating APC4 within cells. However, overexpressing SUMO2 consistently produced a stronger doublet corresponding to SUMOylated APC4 in my assays, SUMO2 was found to bind APC4 in several cell types in proteomic screens (Cubeñas-Potts et al., 2015; Lee et al., 2018; Matic et al., 2010). Based on these facts, I decided to focus on HA-SUMO2 instead of the other SUMO paralogs during the rest of my study. Recently, a paper also suggested that the size of SUMO2 enables it to SUMOylate APC4 better than SUMO1 when the complex is activated by Cdc20 and bound to the MCC (Yatskevich et al., 2021).

3.1.2 The SUMOylation of Mouse APC4 at Lysines 772 and 797

A previous proteomic screen indicated that lysines 772 and 798 of human APC4 (homologous to lysines 772 and 797 in mouse APC4) might be SUMOylated in human cell lines (Matic et al., 2010). In order to confirm which lysines of APC4 are SUMOylated, I generated single and double mutations of these lysines to test them in a SUMOylation assay. In the long-term, I also wanted to study the SUMOylation of APC4 in a mouse model, so I chose to use mouse APC4 instead of the human variant and mutated lysines 772 and 797 to arginine residues.

Corresponding wildtype and mutant Myc-APC4 constructs were overexpressed with HA-SUMO2 in HEK293 cells. I lysed these cells in the presence of NEM, performed HA-IP, and analyzed the IP eluates by WB (Figure 8 A). Upon mutating both of the proposed lysine residues, there was a complete loss of detectable HA-APC4 SUMOylation (Figure 8A, arrows), indicating that the mutating lysines 772 and 797 renders APC4 as SUMOylation-deficient (Figure 8 A, arrows and the lane with Myc-APC4 K772R/K797R). These data also indicate that APC4 is not linked to a chain of SUMO moieties at one lysine residue, but it is instead attached to a single SUMO moiety at two separate lysine resides. This is evident by the fact that the upper

molecular weight band, which corresponds to the attachment of two SUMO moieties to APC4, is not detected when a single lysine residue is mutated (data not shown).

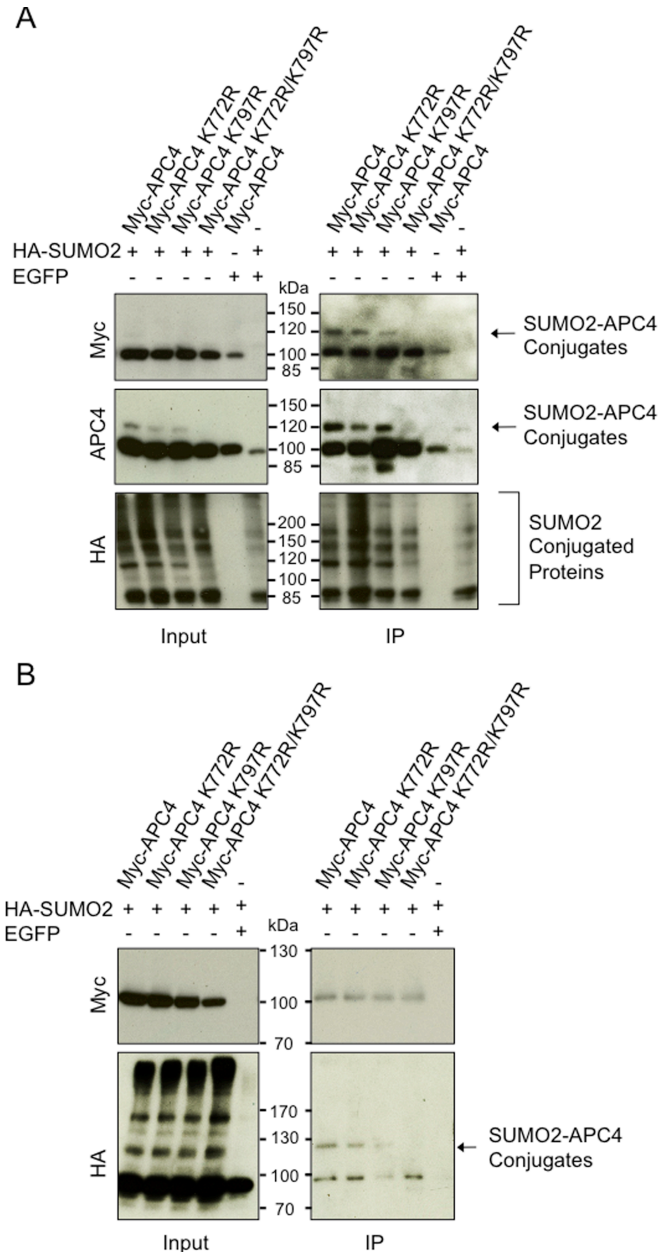

Figure 8. SUMOylation of Wildtype and SUMOylation-Deficient APC4 by SUMO2. HEK293 cells were transfected with wildtype and SUMOylation-deficient (K772R/K797R) Myc-APC4, HA-SUMO2, and EGFP. IP was conducted with cell lysates, and the Input and IP eluates were analyzed by SDS/PAGE followed by WB. (**A**) Cells were lysed in the presence of NEM and HA-IP was conducted with the lysates. The membranes were blotted with antibodies against Myc (top), APC4 (middle), or HA

(bottom). Arrows show APC4 bands conjugated to SUMO2. The bracket indicates SUMO2 conjugates within samples. (**B**) Myc-IP was conducted with cell lysates in the absence of NEM. Membranes were blotted with antibodies against Myc (top) or HA (bottom). Arrows show APC4 bands conjugated to SUMO2.

Unlike most SUMOylated proteins, my preliminary data indicates that APC4 SUMOylation is remarkably stable in the absence of NEM, since I always detected shifted bands in APC4 blots, even when the lysate did not contain NEM (data not shown). In order to properly confirm that APC4 is SUMOylated and that this SUMOylation is stable in the absence of NEM, I completed the reverse Myc-IP in the absence of NEM, using HEK293 cells that overexpressed the Myc-APC4 constructs and HA-SUMO2. I found that while the amount of APC4-SUMO2 conjugates in the eluates was low, the SUMOylation of APC4 remained remarkably stable in the absence of NEM (Figure 8 B, arrows). When observing the Input-banding pattern in the HA-SUMO2 blots (Figure 8 A and B), there is a drastic decrease in the amount of total protein SUMOylation between 100 and 170 kDa when NEM was excluded from the lysate (Figure 8, compare HA Input blots in A and B), and this shows that typically protein SUMOylation does not remain stable in the absence of NEM. As I saw with my prior experiment (Figure 8 A, arrows for the lanes containing Myc-APC4 K772R/K797R), I found that I could generate a SUMOylation-deficient (K772R/K797R) APC4 construct by mutating lysines 772 and 797 (Figure 8 B, arrows in the lanes with Myc-APC4 K772R/ K797R).

3.1.3 APC4 SUMOylation Does Not Influence the Formation of the APC/C

The APC/C is a large complex composed of many different proteins that each must properly be folded for the complex to assemble and function properly (Manchado et al., 2010; McLean et al., 2011; reviewed in Peters, 2006; Sivakumar and Gorbsky, 2015). When the expression of either APC4, APC5, or APC1 alone is depleted, the levels of the respective other two proteins are simultaneously decreased, indicating that the proper folding and assembly of these three proteins is of particular importance for the maintenance of a functional complex (Clark and Spector, 2015; Thornton et al., 2006).

As post-translational modifications may influence the proper folding of proteins and their protein-protein interactions (reviewed in Chen et al., 2017), I first sought to determine if the SUMOylation-deficient (K772R/K797R) APC4 constructs are able to integrate into a functional complex. I also wanted to determine if the APC/C primarily incorporates APC4 in its SUMOylated or non-SUMOylated state.

I first sought to determine if the SUMOylation-deficient (K772R/K797R) Myc APC4 construct integrates into the Cdh1- and Cdc20-activated APC/C. I overexpressed wildtype and SUMOylation-deficient (K772R/K797R) Myc-APC4 constructs, His-SUMO2, and an HA tagged APC/C activator in HEK293 cells. WB analysis of Myc-IP eluates showed that when I conduct an IP for Myc-APC4, I was able to co-IP the APC/C activator, HA-Cdh1 (Figure 9 A, arrows in the HA blots). Similarly, I was able to IP HA-Cdc20 and co-IP all of the Myc-APC4 constructs (Figure 9 B, arrows in the Myc blots). These results confirmed that the tested APC4 constructs all integrate into the activated APC/C, and that APC4 is primarily not SUMOylated within the activated complex.

I originally thought that I might not be able to detect SUMOylated APC4 within the APC/C due to the fact that I was only able to co-IP a small amount of APC4. Previous studies showed that APC4 SUMOylation is increased in cells synchronized in G2/M (Schimmel et al., 2014). I was unable to detect SUMOylated APC4 in the Cdc20-activated APC/C, even when it was purified from cells synchronized in G2/M (data not shown). These data indicate that the Myc-APC4 constructs are all able to integrate into the activated APC/C and that the SUMOylation of APC4 does not affect the formation of the complex (Figure 9 A and B, arrows). I was unable to IP the APC/C in lysates containing NEM, because the complex bound non-specifically to the beads when the lysates contained NEM. Thus, I could not accurately determine how much of the APC4 is SUMOylated within the activated APC/C. However, the SUMOylation of APC4 is moderately stable in lysate lacking NEM (Figure 8 B, arrows). Hence, it is likely that the Cdh1- and Cdc20-activated APC/C primarily contain non-SUMOylated APC4, in accord with the fact that I was never able to detect SUMOylated APC4 within any of the IP eluates (Figure 9 A and 9 B, APC4 blots).

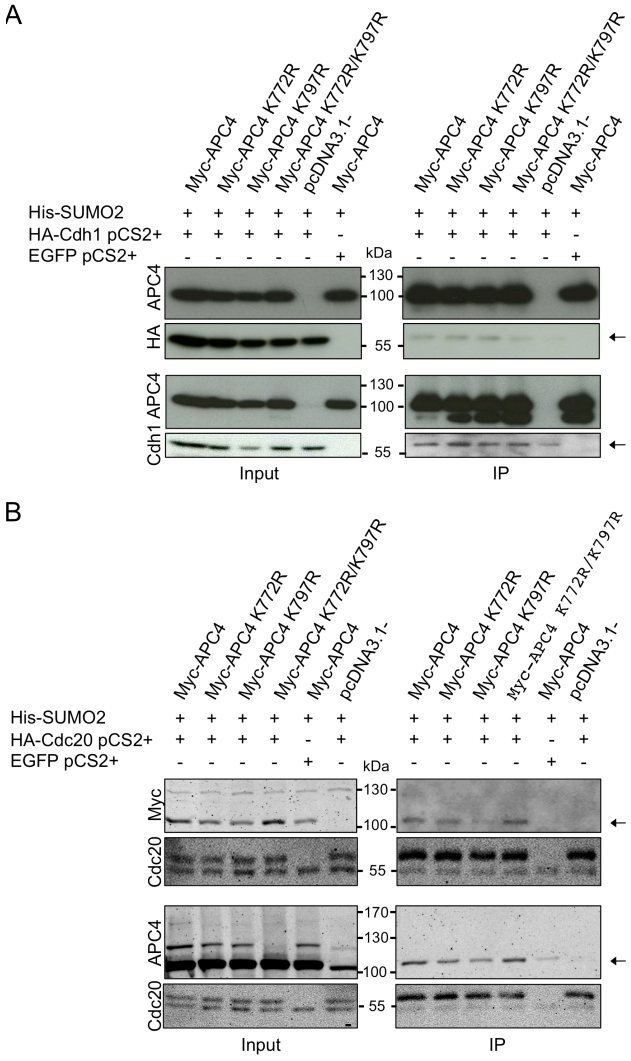

Figure 9. Wildtype and SUMOylation-Deficient APC4 Constructs Integrate Into the Activated Cdh1- and Cdc20-APC/C. HEK293 cells were transfected with wildtype and SUMOylation-deficient (K772R/K797R) Myc-APC4, His-SUMO2, and either HA-CDH1 (**A**) or HA-Cdc20 (**B**). The top two and the bottom two blots in each experiment were from two different membranes. (**A**) Myc-IP was conducted with cell lysates lacking NEM. Input and IP eluates were analyzed by SDS/PAGE and WB using antibodies directed against APC4 (first and third rows), HA (second row), and Cdh1 (fourth row). The arrows indicate complexes where APC4 is bound to Cdh1. (**B**) HA-IP was conducted with cell lysates that contained NEM. Input and IP eluates were analyzed by SDS/PAGE followed by WB using antibodies against Myc (first row), Cdc20 (second and fourth rows), and APC4 (third row). The arrows indicate complexes where APC4 is bound to Cdc20.

As I was unable to detect SUMOylated APC4 in the APC/C when it was bound to an activator, I next wanted to determine if I could detect it within the complex when it was not bound to an activator. In this experiment, I also decided to immunoaffinity purify the endogenous APC/C to ensure that the constructs were integrating into the complex properly. Therefore, I overexpressed HA-SUMO2 and either the wildtype or the SUMOylation-deficient (K772R/K797R) Myc-APC4 constructs in HEK293 cells, and I immunoaffinity purified the endogenous APC/C using an antibody against Cdc27 (Figure 10 A, Cdc27 blots). I found that all of the Myc-tagged APC4 constructs equally integrate into the APC/C (Figure 10 A, Myc blots), but the APC4 within the complex is still primarily in the non-SUMOylated state (Figure 10 A, APC4 and Myc blots). I was also able to co-IP APC5, indicating that I was likely purifying the whole complex (Figure 10 A, APC5 blots). As a final control, I wanted to ensure that adding a N-terminal Myc tag to APC4 did not affect the ability of the constructs to be SUMOylated after they were integrated into the APC/C. For this reason, I decided to conduct Cdc27-IP of lysates generated from HEK293 cells that overexpressed a non-tagged APC4 construct and HA-SUMO2 (Figure 10 B, Cdc27 blots). WB analysis of these IP eluates showed that the APC/C primarily contained non-SUMOylated APC4, as I was unable to detect the non-SUMOylated form in the IP eluates again (Figure 10 B, APC4 blots). The presence of APC5 in IP eluates also confirmed that I was able to immunoaffinity purify the APC/C (Figure 10 B, APC5 blots).

In summary, I found that APC4 SUMOylation is not required for the formation of the APC/C or for the binding of the activators, Cdc20 and Cdh1, to the complex (Figures 9 and 10). My data also indicate that the APC4 in the complex primarily exists in the non-SUMOylated state (Figures 9 and 10, APC4 and Myc blots), even after the activators bind to the complex (Figure 9 A and B, arrows in APC4 and Myc blots). At the time of this study, I was aware of preliminary data in the Vertegaal lab that suggested that APC4 SUMOylation is required for proper cell cycle progression, and that APC4 is the only component of the APC/C that is SUMOylated under normal conditions (Eiflier et al., 2018). Altogether these data suggested that APC4 SUMOylation was affecting the activity of the complex through another mechanism that occurs after the activation of the APC/C. APC4 SUMOylation could affect the binding of other proteins to the APC/C, the

cellular localization of the APC/C, or the enzymatic function of the APC/C. These other potential functions of the SUMOylation will be addressed further in Sections 3.1.4 and 3.1.6.

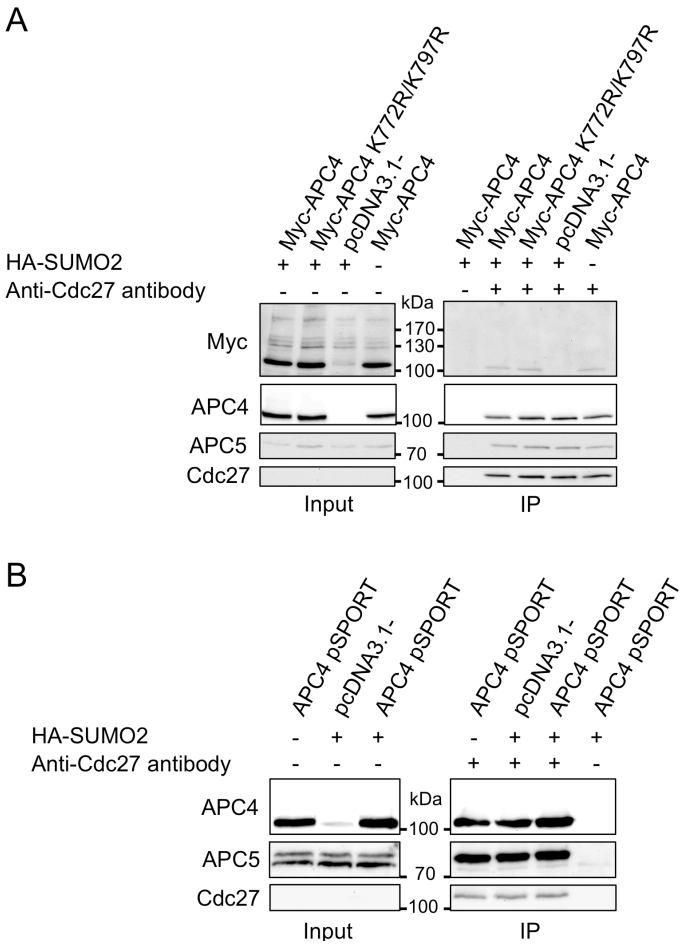

Figure 10. Overexpressed Wildtype and SUMOylation-Deficient Myc-APC4 Constructs Integrate Into the Endogenous APC/C. HEK293 cells were transfected with constructs overexpressing HA-SUMO2 and APC4. Cdc27-IP was conducted with cell lysates lacking NEM. Input and IP eluates were analyzed by SDS/PAGE followed by WB. (**A**) Wildtype and SUMOylation-deficient (K772R/ K797R) Myc-APC4 constructs were transfected into HEK293 cells. WB was conducted with antibodies against Myc (first), APC4 (second), APC5 (third), and Cdc27 (fourth). The wildtype and SUMOylation-deficient (K772R/K797R) mutant constructs both integrate into the endogenous APC/C in a non-SUMOylated state. (**B**) Non-tagged wildtype APC4 and HA-SUMO2 were transfected into HEK293 cells. WB was conducted with antibodies against APC4 (top), APC5 (middle), and Cdc27 (bottom). The non-tagged APC4 construct integrates into the APC/C in its non-SUMOylated state.

3.1.4 APC4 is Localized to Punctate Structures Throughout the Cell Body and this Localization of APC4 is Not Regulated by Its SUMOylation

While the endogenous cellular localization of APC4 was not determined, overexpressed tagged APC4 localizes to the centromere and kinetochores of mammalian cells (Lee et al., 2018) and to the nucleus of Arabidopsis cells (Wang et al., 2012). The APC/C in general is thought to be expressed and function within the nucleus, the kinetochore, the centrosome, and the mitotic spindle within a variety of cell types (Jörgensen et al., 1998; Melloy and Holloway, 2004; Topper et al., 2002; Tugendreich et al., 1995). I next sought to determine the cellular localization of endogenous APC4 and to determine if the SUMOylation of APC4 influences its cellular localization within HEK293 cells and cultured neurons.

I first focused on determining the localization of endogenous APC4 within HEK293 cells. Unfortunately at that time of these experiments, I did not have a way to knockout *ANAPC4* to confirm the specificity of the APC4 antibody, but I later did this and I show the corresponding data in Section 3.2.3. At the time of this study, no APC4 antibodies were known to work effectively for ICC experiments either. For these reasons, I first overexpressed HA-APC4 in HEK293 cells in order to test the antibody specificity and to determine the cellular localization of APC4 within HEK293 cells (Figure 11 A).

When cells were transfected with HA-APC4, the HA and APC4 signals accumulated around the DAPI-stained area of the nucleus (Figure 11 A, APC4 and HA staining in all samples). I also transfected HEK293 cells with an EGPF-expressing construct that had a diffuse EGFP expression, filling the whole cell body with EGFP, and this diffuse pattern was similar to what I observed with the endogenous APC4 signal (Figure 11 A, EGFP images). Both the HA-APC4 (Figure 11 A, HA staining) and endogenous APC4 (Figure 11 A, APC4 staining) expression pattern had a punctate character that filled the whole cell body. Overall these data indicate that endogenous APC4 is localized throughout the whole cell body of HEK293 cells in punctate structures (Figure 11 A, APC4 staining in either the EGFP images or in the non-infected cells within the HA-APC4 images).

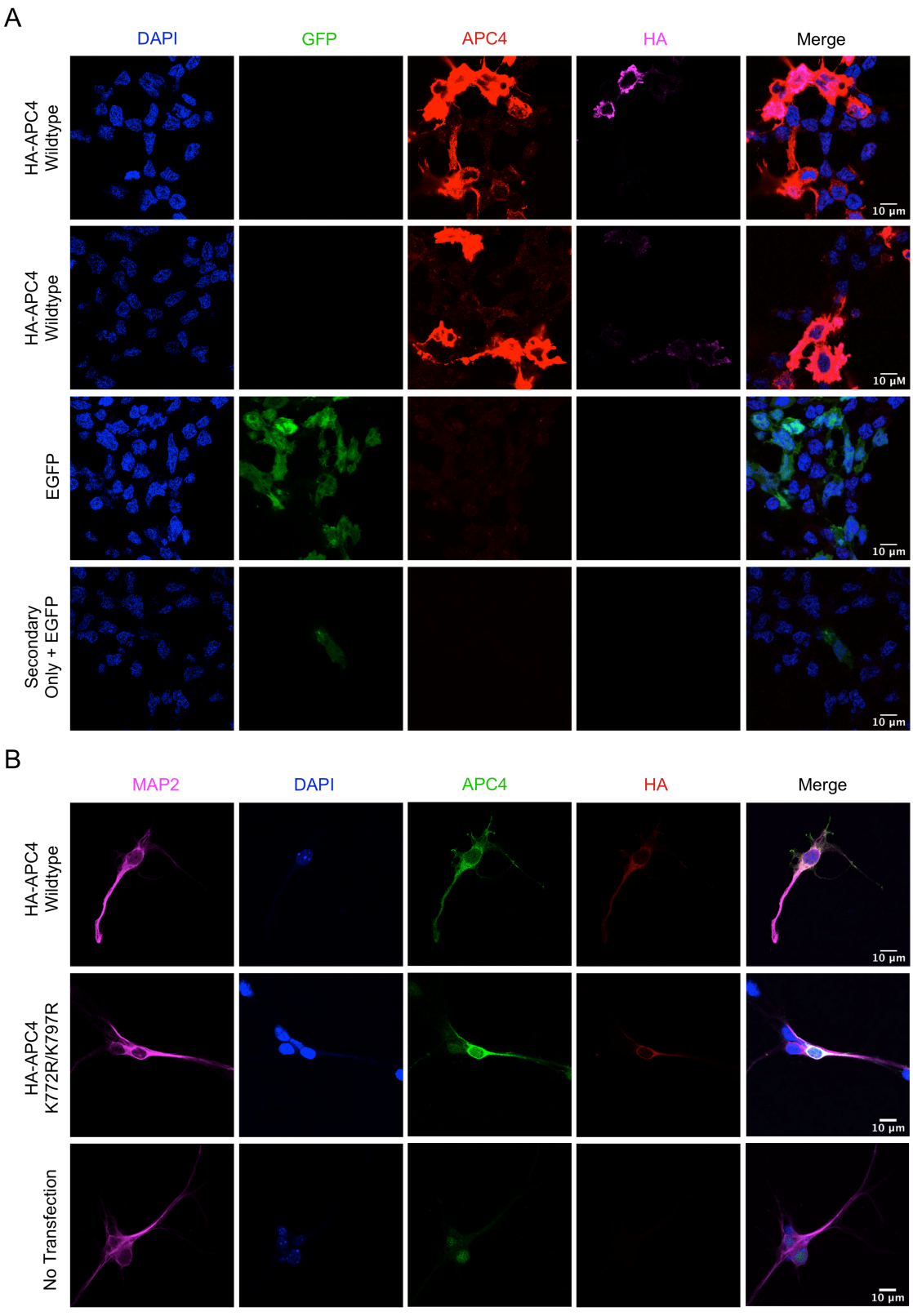
A
DAPI
GFP
APC4
HA
Merge
HA-APC4 Wildtype
HA-APC4 Wildtype
EGFP
Secondary Only + EGFP
10 µm
10 µM
B
MAP2
DAPI
APC4
HA
Merge
HA-APC4 Wildtype
HA-APC4 K772R/K797R
No Transfection

Figure 11. When HA-APC4 Overexpression Is Driven by the CMV Promoter, APC4 Accumulates Outside the Nucleus in Both HEK293 Cells and Neurons. Cells overexpressing HA-APC4 or EGFP were imaged on a confocal microscope. A control sample (Secondary Only) that lacked APC4 primary antibody was used to establish the microscope settings. Scale bars representing 10 μm of distance were added to the merged images (Merge). (**A**) HEK293 cells were fixed two days after transfection and stained with DAPI (blue) and antibodies against GFP (green), HA (magenta), and APC4 (red). (**B**) Wildtype primary hippocampal mouse neuron cultures were transfected with wildtype and SUMOylation-deficient (K772R/ K797R) HA-APC4 at DIV1. Neurons were fixed at DIV5 and stained with DAPI (blue) and antibodies against MAP2 (magenta), HA (red), and APC4 (green).

I next sought to determine the localization of endogenous APC4 within primary hippocampal neuron cultures and to determine if SUMOylation affected this localization (Figure 11 B, APC4 staining). Neuron cultures were transfected with a wildtype or a SUMOylation-deficient (K772R/K797R) HA-APC4 construct that was driven by the CMV promoter. After 5 days, the cells were fixed, stained, and imaged. Similar to what was observed with the HEK293 cells (Figure 11 A, APC4 and HA staining in HA-APC4 overexpression images), the overexpressed HA-APC4 constructs appeared to accumulate outside the nucleus of neurons (Figure 11 B, APC4 and HA staining in the HA-APC4 overexpression images). There were no differences in the expression and localization patterns between the wildtype and the SUMOylation-deficient (K772R/ K797R) HA-APC4 constructs, indicating that SUMOylation does not influence the localization of APC4 (Figure 11 B, APC4 and HA staining in neurons expressing wildtype or the SUMOylation-deficient HA-APC4). The endogenous APC4 staining was also characterized by a weak punctate signal that filled the whole cell body and extended into some of the processes of the transfected neurons. The nuclear signal was increased relative to the rest of the signal in the soma of the neuron (Figure 11 B, APC4 staining in the No transfection images).

In summary, my data indicate that endogenous APC4 is present throughout the cell body of both neurons and HEK293 cells (Figure 11 A and B, APC4 staining). The overexpressed constructs appeared to be partially mislocalized, accumulating mostly around the nucleus while endogenous APC4 localized evenly throughout the whole cell body in both HEK293 cells (Figure 11 A, APC4 and HA staining) and cultured neurons (Figure 11 B, APC4 and HA staining). SUMOylation of APC4 does not have a

noticeable effect on the cellular localization of overexpressed APC4 in neurons based on the fact that the wildtype and SUMOylation-deficient (K772R/K797R) HA-APC4 constructs had a similar localization (Figure 11 B, APC4 and HA staining). This is consistent with the conclusions of another study that recently showed that APC4 SUMOylation does not affect the cellular localization of APC4 during the cell cycle (Lee et al., 2018). While these images were obtained from a single plane on a confocal microscope and it seemed like the overexpressed HA signal was inside the nucleus (Figure 11 A and B, HA and DAPI staining), I was worried that the weak nuclear HA signal was possibly background labeling and perhaps the constructs actually were not able to enter the nucleus (Figure 11 A and B, HA staining). This was important to test, as all of these constructs would need to be able to enter the nucleus in order for them to act in the ubiquitylation of nuclear APC/C substrates.

In order to determine if the overexpressed constructs were able to enter the nucleus, I did a cell fractionation experiment in HEK293 cells that overexpressed HA-SUMO2 and either the wildtype or the SUMOylation-deficient (K772R/K797R) Myc-APC4 constructs. I fractionated HEK293 cell lysates into nuclear and cytoplasmic fractions and analyzed the lysates by WB (Figure 12). To ensure that I obtained relatively pure cellular fractions, I blotted the lysates with antibodies against a cytoplasmic protein, GAPDH, and a nuclear protein, SUMO1 (Figure 12, see the respective labels). The lanes were loaded with equal protein concentrations of the different fractions (Figure 12, lanes E) or an equal cellular proportion of the nuclear fractions when compared to the cytosolic fractions (Figure 12, lanes C). In order to calculate the amount of protein added in the equal cellular proportion samples, I would for example add 1% of the total volume of both the nuclear and the cytoplasmic fractions into each respective well. As I observed on the confocal (Figure 11 A and B, APC4 and HA staining), Myc-APC4 primarily accumulated in the cytoplasm, but a small amount was detected within the nuclear fraction of the Myc blot (Figure 12, Myc (r) blot), indicating that the constructs were able to enter the nucleus and possibly ubiquitylate the APC/C substrates there.

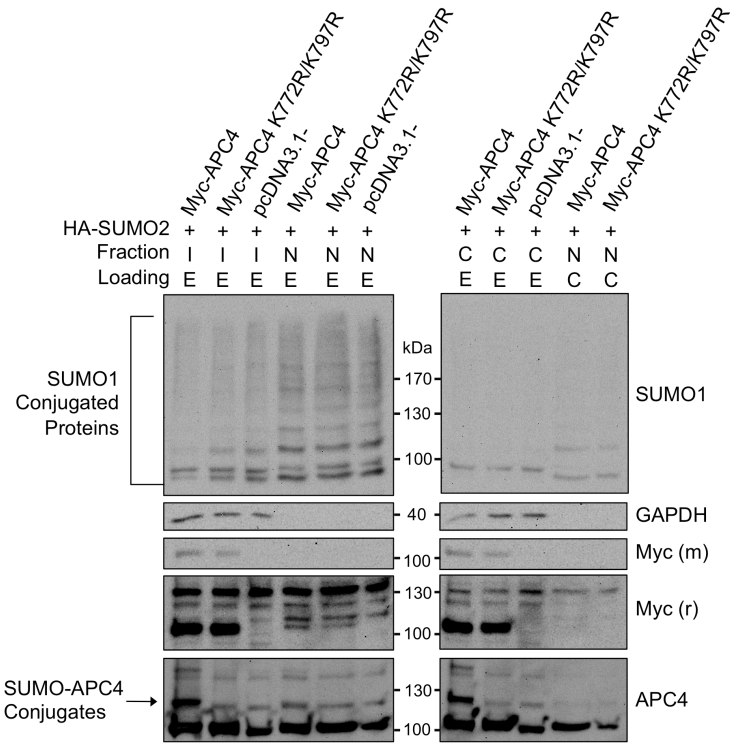

Figure 12. The Overexpressed Myc-APC4 Constructs Are Localized in the Cytosol And the Nucleus of HEK293 Cells. In the presence of NEM, Input (I) cell lysates from HEK293 cells overexpressing HA-SUMO2 and the wildtype or the SUMOylation-deficient (K772R/K797R) Myc-APC4 constructs were fractionated into nuclear (N) and cytosolic (C) fractions. The eluates were analyzed by SDS/PAGE followed by WB using antibodies against SUMO1 (first from top), GAPDH (second), Myc mouse (m; third), Myc rabbit (r; fourth), or APC4 (fifth). The amounts of protein ran on the gel were identical in the Equal Protein Loading samples (E). Cell Equivalent samples (C) were nuclear samples that had an equal percentage of the cell volume loaded onto the gel as was loaded for the corresponding cytosolic E samples. The arrow shows SUMOylated APC4 and the brackets show the total amount of SUMO1 conjugation within the samples. The Myc (r) blots (fourth) indicate that while the Myc-APC4 constructs do accumulate in the cytosol, they both also enter the nucleus.

While I had previously shown that the overexpressed Myc-APC4 constructs are SUMOylated in whole cell lysates (Figure 8 A and B, arrows), I did not know if these constructs would be differentially expressed or SUMOylated between the cytosolic and nuclear fractions. The APC4 blots indicate a substantial proportion of SUMOylated APC4 in both the cytosolic and nuclear fractions (Figure 12, APC4 blots). The endogenous levels of SUMOylated APC4 in different cellular fractions are studied further in Section 3.1.5. Unfortunately, the more sensitive Myc (r) antibody has a lot of

non-specific background (Figure 12, Myc (r) blots), so I was unable to determine if the overexpressed constructs were SUMOylated within the various fractions. However, there was a large difference in the degree of APC4 SUMOylation in the cytosolic fraction when I compared the different constructs, and the increase in the level of APC4 SUMOylation when the wildtype Myc-APC4 construct was overexpressed indicates that the overexpressed construct is likely heavily SUMOylated in the cytosol (Figure 12, upper molecular weight bands in APC4 blots). Further quantification is required to elucidate if this is also true within the nucleus.

When APC4 expression was driven by the CMV promoter, it was mislocalized in both HEK293 cells (Figure 11 A, APC4 staining) and neuron cultures (Figure 11 B, APC4 staining). In order to better understand why this mislocalization occurred, I overexpressed APC4 with the weaker Synapsin promoter in primary hippocampal neuron cultures (Figure 13 B). Cultures were infected by a lentivirus that expressed HA-APC4 driven by the Synapsin promoter at DIV1. After 10 days, the cells were fixed and stained. In contrast to what I observed when I used the stronger CMV promoter (Figure 11 A and B, APC4 staining), driving the expression of APC4 with this weaker promoter resulted in a staining pattern (Figure 13, HA staining) similar to the endogenous APC4 expression observed earlier in neurons (Figures 11 B, APC4 staining in the No Infection Image). While these cells were not stained for APC4 directly, the HA signal filled the entire soma and extended into the processes (Figure 13, HA staining). As I had observed previously (Figure 11 B, APC4 and HA staining), there were no differences in the expression and localization patterns between wildtype and SUMOylation-deficient (K772R/K797R) HA-APC4 constructs, indicating that the SUMOylation of APC4 does not affect the localization of APC4 in neurons (Figure 13, HA staining).

In summary, endogenous APC4 is present in a diffuse punctate pattern that spreads throughout soma of neurons and into the neurites (Figures 11 B and 13, HA staining). In HEK293 cells, it is present in a diffuse punctate pattern that fills the whole cell (Figure 11 A, APC4 and HA signals). In Section 3.2.3, I show that the APC4 antibody is specific for APC4 in neurons. When I overexpressed wildtype or SUMOylation-deficient (K772R/K797R) HA-APC4, there was no difference in the cellular localization of the HA signal (Figures 11 and 13, HA staining for each construct).

Interestingly, when APC4 expression was driven by a CMV promoter it accumulated outside the nucleus in both HEK293 cells (Figure 11 A, APC4 and HA staining) and neuron cultures (Figure 11 B, APC4 and HA staining), but this mislocalization was not detected when APC4 expression was driven by a weaker Synapsin promoter (Figure 13, HA staining). While APC4 was mislocalized when it was driven by the CMV promoter, APC4 was still able to enter the nucleus where it could potentially integrate into the nuclear APC/C and ubiquitylate its substrate proteins there (Figure 12, Myc blots).

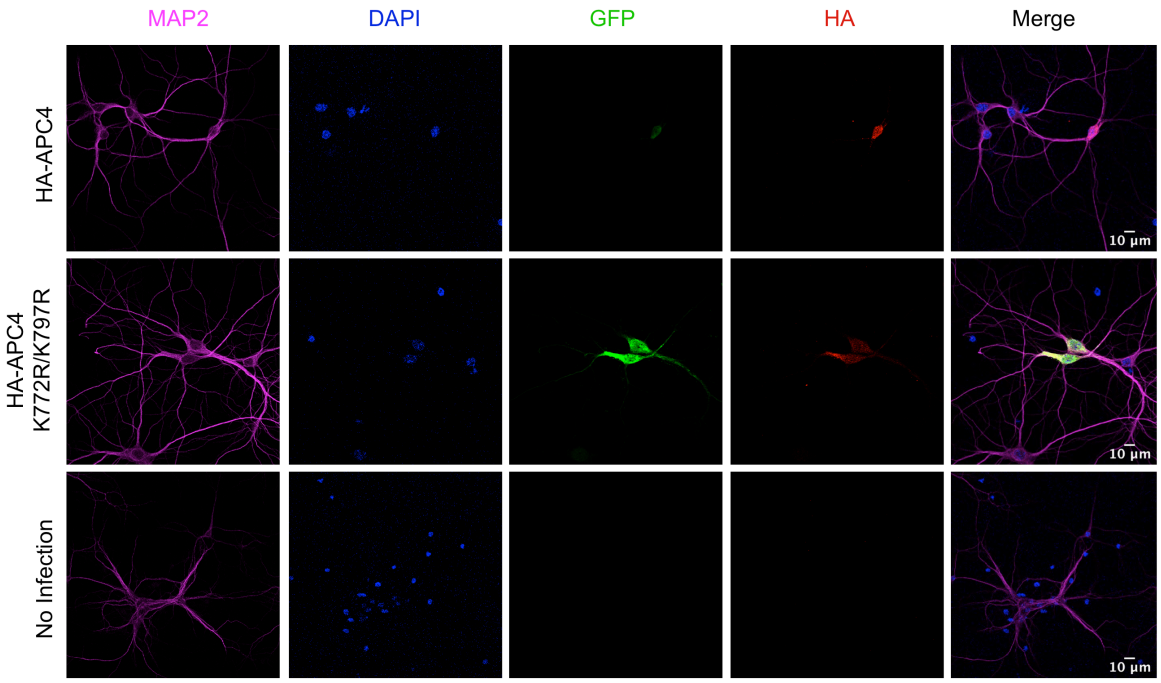

Figure 13. Overexpressed HA-APC4 Does Not Accumulate Outside the Nucleus of Neurons When Driven by the Synapsin Promoter. Wildtype mouse hippocampal neuron cultures were infected at DIV1 with a lentivirus that expressed EGFP and wildtype or SUMOylation-deficient (K772R/K797R) HA-APC4 driven by the weaker Synapsin promoter. Neurons were fixed at DIV11 and stained with DAPI (blue) and antibodies directed against MAP2 (magenta), GFP (green), and HA (red). All stains were merged together and 10 µm long scale bars were added to this image (Merge). All images were obtained on a confocal microscope.

3.1.5 APC4 Is SUMOylated Within a Variety of Different Cellular Fractions

My host lab previously fractioned whole brain lysate and did a proteomic screen for proteins conjugated to SUMO1 within a cytosol-enriched fraction, and identified APC4 in this screen (Tirard et al., unpublished). However, APC4 was not identified in a prior screen from whole cell brain lysate (Tirard and Brose, 2016; Tirard et al., 2012). While proteomic screens are not expected to identify every SUMO-conjugated protein type within a sample, the fact that APC4 was identified only in the cytosolic fraction may also be due to the fact that SUMOylated proteins are enriched within this fraction. I previously showed that APC4 is present in both the cytosol and the nucleus of HEK293 cells that overexpress Myc-APC4 (Figure 12, APC4 and Myc blots). I next sought to further characterize the cellular localization of the SUMOylated and the non-SUMOylated forms of endogenous APC4 in HEK293 cells (Figure 14).

To address the localization of endogenous APC4 and its SUMOylation in HEK293 cells, I fractionated the cells into nuclear and cytosolic fractions in the presence of NEM. To enhance SUMOylation, I transfected the HEK293 cells with HA-SUMO2. Gel lanes were loaded with equal protein concentrations of the different fractions (Figure 14 A, lanes E) or an equal cellular proportion of the nuclear fractions when compared to the cytosolic fractions (Figure 14 A, lanes C). I obtained fairly pure fractions with this procedure, as I was only able to detect the nuclear protein, Histone 3, in the nuclear fraction, and the cytosolic protein, GAPDH, in the cytoplasmic fraction (Figure 14 A, see the respective blots). Endogenous APC4 was detected in both SUMOylated and non-SUMOylated states within the cytosolic and nuclear fractions of HEK293 cells (Figure 14 A, the triplicate bands in the APC4 blot).

I next sought to determine if there were quantitative differences in the degree of APC4 SUMOylation in the different fractions. For each fraction, I determined the ratio of APC4 bound to one SUMO moiety compared to the non-SUMOylated APC4 within the lane. This was calculated for three different experimental replicates and averaged (Figure 14 B, Exp1 - 3 and Average values in the graph). While the ratios between each fraction varied between experiments, there was always an increase in APC4 SUMOylation within the nuclear fraction (Figure 14 B, compare the Cytoplasm and the

Nucleus values), and this difference was found to be statistically significant in a paired t-test ($t = 7.75$, $p < 0.05$).

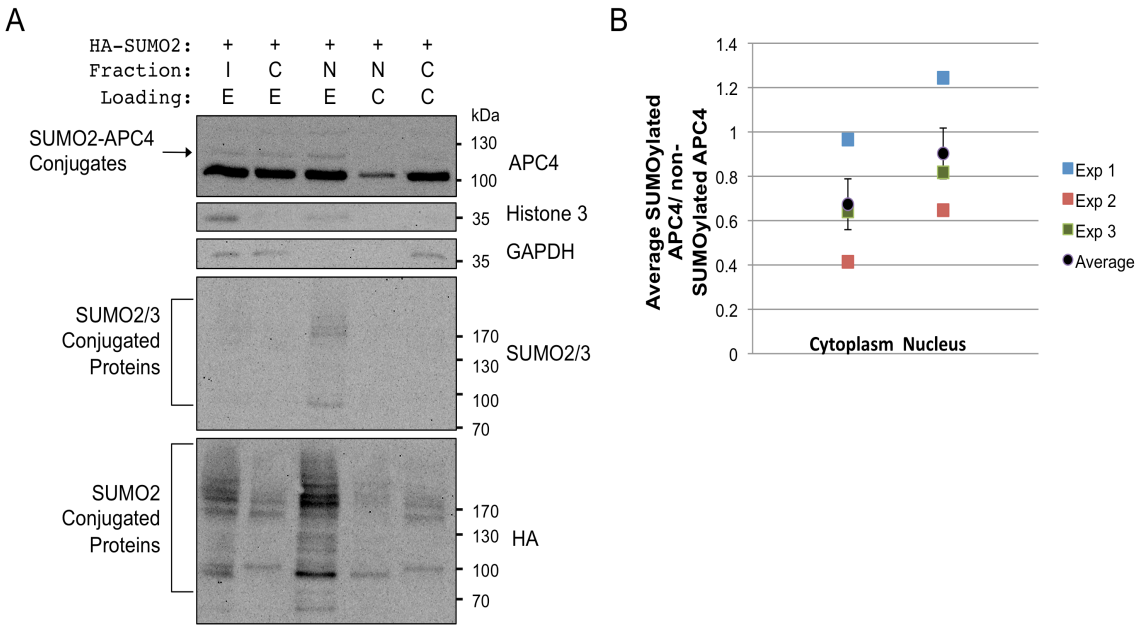

Figure 14. Increased SUMOylation of APC4 in the Nuclear Fraction of HEK293 Cells. Input (I) cell lysates from HEK293 cells overexpressing HA-SUMO2 were fractionated into nuclear (N) and cytosolic (C) fractions in the presence of NEM, and fractions were analyzed by SDS/PAGE and WB. This experiment was completed three separate times. (**A**) The eluates were analyzed by WB using antibodies against APC4 (first from top), Histone 3 (second), GAPDH (third), SUMO2/3 (fourth), or HA (fifth). The amounts of protein ran on the gel were identical in the Equal Protein Loading samples (E). Cell Equivalent samples (C) were nuclear samples that had an equal percentage of the cell volume loaded onto the gel as the corresponding cytosolic E samples. The arrow shows conjugates of SUMO2-APC4 and the brackets show total amounts of SUMO2 conjugation within samples. (**B**) This dot plot shows the quantification of the amount of APC4 conjugated with one SUMO moiety in each fraction after normalizing it to the total amount of non-SUMOylated APC4. The experimental averages were calculated using the ratios of protein in the E lanes on multiple membranes. The average difference for all experiments was calculated, and the SEM was used to draw the error bars. The average difference value of all experiments was compared to a predicted value of 0 in a paired t-test ($p < 0.05$).

While SUMO1 is essentially a nucleus-specific protein (Daniel et al., 2017; Figure 12, SUMO1 blots in C lanes), the exact cellular localization of SUMO2 and SUMO3 is less clear. For this reason, I also blotted the membranes with antibodies against

SUMO2/3 and HA in order to determine which fractions would contain these proteins. The overexpressed HA-SUMO2 construct was enriched in the nuclear fraction, but it was also detected in the cytosol (Figure 14 A, HA blot). Although the SUMO2/3 antibody yielded only weak signal, it detected enriched levels of SUMO2 and SUMO3 in the nucleus (Figure 14 A, SUMO2/3 blot). In general, these data indicate that while there may be some SUMOylated proteins in the cytosol, most of the SUMOylated proteins are localized to the nucleus of HEK293 cells.

I next wanted to elucidate the cellular localization of APC4 within mouse neurons. A wildtype mouse cortex was fractionated into the following fractions: P1 (nuclei), S1 (synaptosomes, cytosol, mitochondria, and organelles), S2 (cytosol, microsomes), P2 (mitochondria and crude synaptosomes), Syn (crude synaptosomes), and SPM (synaptic plasma membranes). WB analysis detected APC4 in all of the fractions tested (Figure 15, APC4 blot). Unlike HEK293 cells (Figure 14 A, APC4 blot), APC4 levels were higher in the cytosol (Figure 15, S2 fraction) as compared to the nucleus (Figure 15, P1 fraction). APC5 was not detected within the SPM or the synaptosome (Syn) fractions, but this could be due to the fact that the anti-APC5 antibody is less sensitive than the APC4 antibody (Figure 15, APC4 and APC5 blots). I was able to detect APC4 within the PSD and synaptosome fractions (Figure 15, APC4 blot), but the corresponding bands were very weak and might represent a contaminate.

However, another study found Cdh1 in the PSD fraction (Pick et al., 2012), and a proteomic screen for proteins within the PSD detected APC1, APC7, and APC12 (Distler et al., 2014). While I completed the current experiment without NEM, I was still able to detect enriched APC4 SUMOylation in the cytosol or the S2 fraction (Figure 15, arrow in the APC4 blot). In contrast to the nucleus of HEK293 cells (Figure 14 A, APC4 blot), I did not detect SUMOylated APC4 in the nuclear fraction, but this may be due to the fact that there was little APC4 in this fraction and that I did not use NEM during the protocol (Figure 15 A, P1 fraction in the APC4 blot).

WB analysis showed that the fractionation worked appropriately. The enrichment of Rab-GDI1 and GAPDH within the S2 fraction showed that this fraction had the expected enrichment of cytosolic proteins (Figure 15, S2 fraction). The presence of NeuN in the cytosolic S2 fraction indicates that this fraction contains nuclear

contaminates, but other studies showed that NeuN is also present in the cytosol of some neurons (Van Nassauw et al., 2005). As expected for the nuclear P1 fraction, there was both an enrichment of the smaller isoform of NeuN and a depletion of Rab-GDI1 and GAPDH. While both Rab-GDI1 and GAPDH are enriched in the cytosol (Figure 15, Rab-GDI1 and GAPDH blots), their expression is not limited to the cytosol in neurons (D'Adamo et al., 2002; Ishitani et al.,1998). The SPM fraction is also fairly pure as it showed an enrichment of PSD-95 but did not contain Rab-GDI1, NeuN, or Synaptophysin (Figure 15, SPM fraction). As expected, the Synaptosome fraction contained both the membrane-associated protein, PSD-95, and cytosolic proteins Rab-GDI1 and Synaptophysin (Figure 15, Syn fraction).

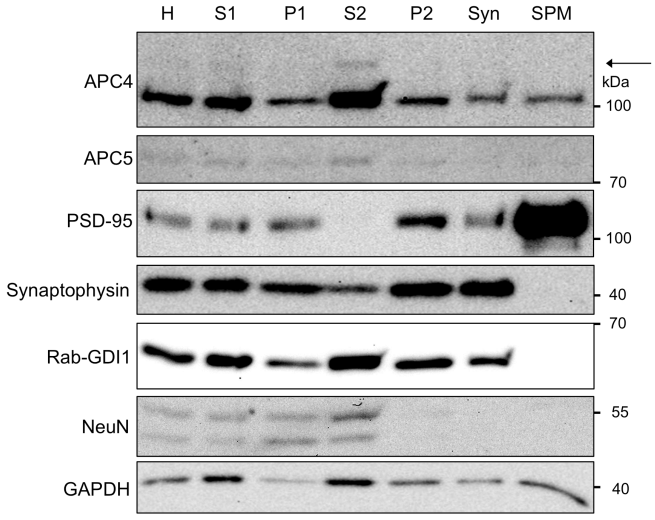

Figure 15. The Subcellular Localization of APC4 in the Wildtype Mouse Cortex. Homogenate (H), S1, P1, S2, P2, Synaptosome (Syn), and SPM fractions were obtained from the cortex of an adult wildtype mouse brain without NEM in the lysate buffer. The fractions were analyzed by SDS/PAGE followed by WB with antibodies against APC4 (first), APC5 (second), PSD95 (third), Synaptophysin (fourth), Rab-GDI1 (fifth), NeuN (sixth), and GAPDH (seventh). The cytosolic fraction (S2) had an enrichment of both SUMOylated (arrow) and non-SUMOylated APC4 when compared to the other fractions. APC4, however, was still detected in all fractions tested, including the Syn and SPM fractions.

3.1.6 APC4 SUMOylation Does Not Influence the Ubiquitylation of GluR1 or ID2 in a HEK293 Cell Ubiquitylation Assay

I previously showed that APC4 SUMOylation does not influence the formation of the APC/C (see Section 3.1.3), binding of the activators to the complex (see Section 3.1.3), or the localization of APC4 (see Section 3.1.6). I next tried to determine if the SUMOylation of APC4 influences the function of the APC/C. I suspected that APC4 SUMOylation likely affected the function of the APC/C because SUMOylation in general is required for the function of the yeast APC/C and proper cell cycle progression (Dieckhoff et al., 2004). While the corresponding studies did not identify the component of the complex that is SUMOylated, they showed that cells with mutations in yeast SUMO and UBC9 homologs have defects in the degradation of Cyclin and Securin (Dieckhoff et al., 2004). APC4 was later confirmed to be the only SUMOylated complex component under normal conditions (Eifler et al., 2018). I was also aware of preliminary data from the Vertegaal lab that showed that APC4 SUMOylation is required for APC/C-dependent cell cycle progression (published later in Eifler et al., 2018). Therefore, I hypothesized that when the APC/C contained SUMOylation-deficient (K772R/K797R) APC4, it would have defects in the ubiquitylation of known substrates. My long-term goal was to study the neuronal APC/C, so I was particularly interested in determining if the SUMOylation of APC4 affected the ability of the APC/C to ubiquitylate its neuronal substrates.

While the typical approach in this context is to purify the APC/C and do *in vitro* ubiquitylation assays to answer these types of questions, these assays can identify substrates that are not physiological substrates of the complex. It also takes a lot of time to set up and troubleshoot this type of assay, as one has to also purify all of the E1 and E2 enzymes involved in the process, which requires knowledge of the actual enzymes that ubiquitylate the specific substrate (Jarvis et al., 2016). I also was unsure which of the proposed neuronal substrates of the APC/C was an actual physiological substrate of the APC/C (see Section 1.6.9; Table 16). For these reasons, I instead tried to establish a simpler ubiquitylation assay that could be done within cells.

Both the wildtype and the SUMOylation-deficient (K772R/K797R) Myc-APC4 constructs were overexpressed in HEK293 cells along with HA-Ubiquitin and the candidate substrates: Flag-ID2 (Figure 16) and untagged GluR1 (Figure 17). HA-ubiquitin was IP (Figures 16 and 17, HA blots), and the candidate substrates were co-IP (Figure 16, Flag blots; Figure 17, GluR1 blots). While I was able to co-IP the substrates, there were no obvious changes in the ubiquitylation of the candidates when I compared the wildtype and the mutant APC4 constructs (Figure 16, Flag blots; Figure 17, GluR1 blots). In order to enhance the ubiquitylation, I also overexpressed the APC/C activator Cdh1 in the GluR1 experiment (Figure 17), but this did not impact the overall ubiquitylation levels of GluR1 (data not shown).

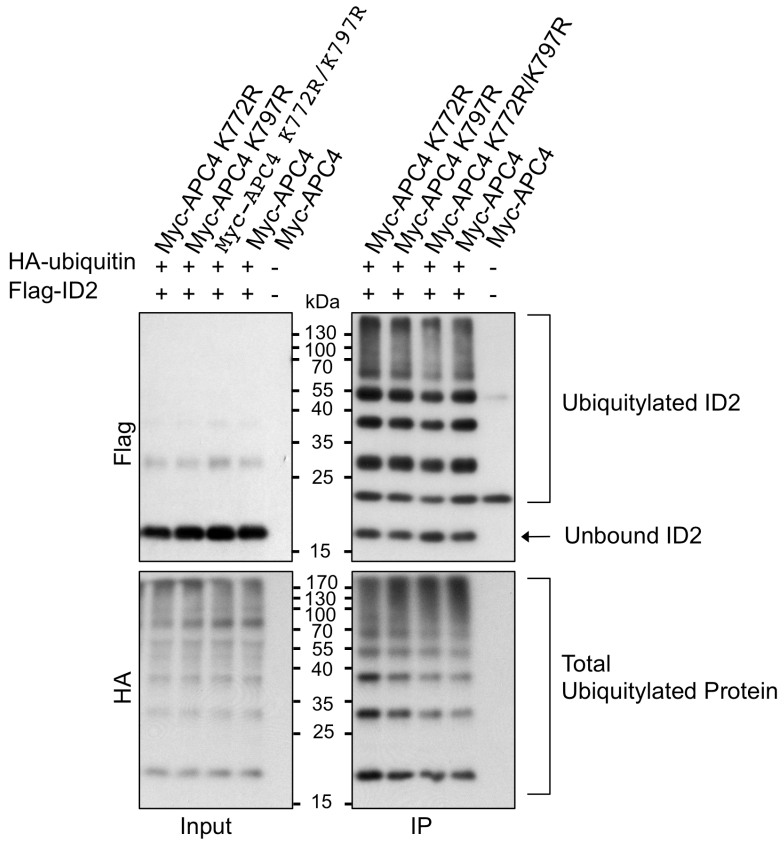

Figure 16. APC4 SUMOylation Does Not Influence the Ubiquitylation of ID2 in a HEK293 Cell Ubiquitylation Assay. HEK293 cells were transfected with constructs that overexpress wildtype and SUMOylation-deficient (K772R/K797R) Myc-APC4, HA-ubiquitin, and Flag-ID2. HA-IP was conducted with cell lysates in the presence of NEM. Input and IP eluates were analyzed by SDS/PAGE and WB with antibodies directed against Flag (top) and HA (bottom). The arrow shows ID2 that is not conjugated to

ubiquitin. The brackets show ubiquitylated ID2 (top) and the total population of ubiquitylated proteins (bottom).

At the time of this experiment, I suspected that the design of this experiment was problematic due to the fact that the cells still had APC/C with the non-mutated form of APC4 and that this remnant complex containing wildtype APC4 that would still be able to ubiquitylate the substrates and mask my ability to see any effect. Little is known about how long the APC/C remains assembled, unfortunately, but APC4 itself is thought to possibly be involved in regulating the stability and assembly of the complex (Clark and Spector, 2015; Thornton et al., 2006; Tran et al., 2010). The half-life of APC4 expression was not determined at that time either, but I later determined it to be around 1.8 days in neuron cultures (see Section 3.2.2). For all of these reasons, I suspected that I was not replacing enough of the APC4 in the cell with the overexpressed Myc-APC4 constructs during the experiments, and this could be why I was unable to see any clear changes in protein ubiquitylation of cognate APC/C substrates in these assays. Additionally, the assay was confounded by the fact that I was also not sure which of the proposed neuronal APC/C substrates were actual substrates of the complex (reviewed in Section 1.6.9; Table 16). For these reasons, I decided that it would be better to knockout *ANAPC4* entirely and then rescue the knockout with the wildype and the SUMOylation-deficient (K772R/K797R) APC4 constructs instead. Thus, I decided to abandon this approach at that time.

Subsequently, I also tried to test EGFP-KIF18B in my HEK293 cell ubiquitylation assay, since KIF18B was identified as a substrate that binds specifically to the SUMOylated APC/C (Eifler et al., 2018). This substrate would allow me to determine if my experimental design would potentially work to screen neuronal substrates of the APC/C. Unfortunately, the KIF18B construct was not soluble in lysate, probably due to the EGFP tag, which prevented me from using the construct in ubiquitylation assays (data not shown).

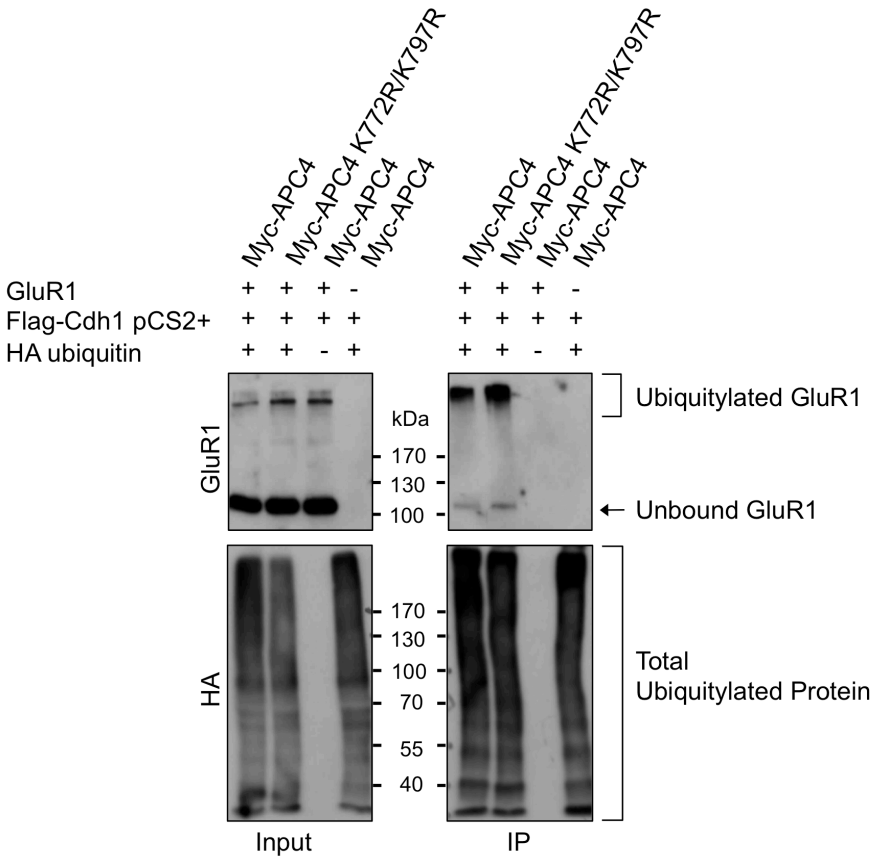

Figure 17. APC4 SUMOylation Does Not Influence the Ubiquitylation of GluR1 in a HEK293 Cell Ubiquitylation Assay. HEK293 cells were transfected with constructs overexpressing wildtype and SUMOylation-deficient (K772R/K797R) Myc-APC4, GluR1, Flag-Cdh1, and HA-ubiquitin. HA-IP was conducted with cell lysates in the presence of NEM. Input and IP eluates were analyzed by SDS/PAGE followed by WB with antibodies against GluR1 (top) and HA (bottom). The arrow shows the GluR1 that is not conjugated to ubiquitin. The brackets show the ubiquitylated GluR1 (top) and total population of ubiquitylated proteins (bottom).

3.2 Elucidating the Function of APC4 Within Neurons

3.2.1 APC4 Is Expressed in Primary Cortical And Hippocampal Neuron Cultures And Integrates Into the Endogenous APC/C

While there are many proposed substrates of the neuronal APC/C, the studies that identified them typically involved the depletion of the activators, Cdh1 and Cdc20; they do not clearly show the role of the APC/C in the ubiquitylation of the proposed substrate

proteins in most cases (reviewed in Eguren et al., 2011). While the APC/C is well studied in other cell types, it is not known if the neuronal APC/C contains the same proteins or if it is regulated by the same mechanisms as in non-neuronal cells. One proposed substrate of the neuronal APC/C, SMURF1, was eventually shown to require Cdh1 by a mechanism that did not involve the APC/C (Wan et al., 2011). Additional proposed neuronal substrates may also require the activators through an APC/C-independent mechanism. For all of these reasons, I decided to systematically study the function of the APC/C within cultured neuron by knocking out the gene that encodes APC4, a core component of the APC/C. In this way, I could really begin to elucidate the function of the APC/C in neurons.

I first tried to determine if APC4 and SUMOylated APC4 could be detected in lysates obtained from wildtype DIV10 hippocampal cultures (Figure 18 C, APC4 blot). As a positive antibody control, I also used lysate obtained from HEK293 cells that overexpressed Myc-APC4. There was a weak APC4 band on the membrane, but I could not detect SUMOylated APC4 in the neuron cultures (Figure 18 C, APC4 blot). The absence of a SUMOylated APC4 band was likely due to the fact that there was too little APC4 in the sample though. As a control, I also blotted for synaptophysin, a neuron marker (Figure 18 C, Synaptophysin blot).

I next wanted to determine if the amount of endogenous APC4 expressed in neuron cultures changes over time. In order to obtain an adequate number of cells to complete this experiment, I decided to instead use wildtype primary cortical neuron cultures. Cells from these cultures were lysed every two days, starting on DIV3, and I found that the levels of APC4 expression within the samples steadily decreased over time (Figure 18 A and B, APC4 blot and graph). APC5, another component of the APC/C, had a similar expression time course (Figure 18 A and B, APC5 blot and graph).

While APC4 is known to be a major component of the APC/C in other cell types, its role in the neuronal APC/C has not been established. In order to establish that APC4 integrates into the endogenous neuronal APC/C, I performed Cdc27-IP from wildtype cortical neuronal cultures at DIV10 (Figure 19, Cdc27 blot). I was able to co-IP a strong APC4 band (Figure 19, APC4 blot) and a weaker APC5 band (Figure 19, APC5 blot),

indicating that I was able to enrich the endogenous neuronal APC/C and that it contains APC4 (Figure 19, APC4 and APC5 blots).

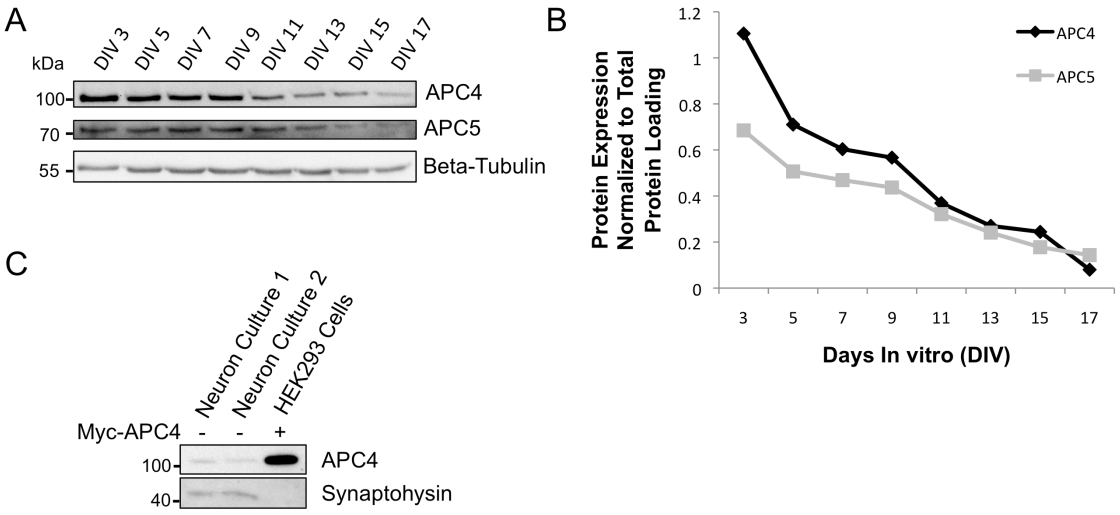

Figure 18. Endogenous APC4 Is Expressed in Wildtype Primary Cortical and Hippocampal Neuron Cultures. (**A** and **B**) APC4 and APC5 expression was analyzed in primary cortical neuron cultures obtained from wildtype mice every two days between DIV3 and DIV17. (**A)** Lysates were analyzed by SDS/PAGE followed by WB with antibodies against APC4 (top), APC5 (middle), and Beta-Tubulin (bottom). (**B**) Line graph depicting the protein expression levels over time of APC4 (black line) and APC5 (gray line), normalized to the total protein MemCode stain. The final ratios were averaged for two separate membranes that contained lysates from the same experiment. (**C**) Endogenous APC4 expression was assessed at DIV10 in two wildtype primary hippocampal neuron cultures. The cultures were lysed in buffer that contained NEM. As an APC4 antibody control, the samples were ran adjacent to HEK293 cell lysate obtained from cells that overexpressed wildtype Myc-APC4. The lysates were analyzed by SDS/PAGE followed by WB with antibodies directed against APC4 (top) and Synaptophysin (bottom). SUMOylated APC4 was not detected in any of these lysates.

Other studies showed co-IP of substrates of the APC/C upon IP of a core component of the APC/C (Stegmüller et al., 2006; Yang et al., 2009). Hence, I also attempted this with two potential substrates of the neuronal APC/C: NEUROD2 and SHANK1 (Figure 19, NEUROD2 and SHANK1 blots). While SHANK1 has not been confirmed as an actual substrate of the APC/C yet (Hung et al., 2010), NEUROD2 is a published substrate (Yang et al., 2009). I was unable to co-IP either SHANK1 or

NEUROD2 with the APC/C in this assay. Subsequent data that I present below indicate that NEUROD2 is not an actual substrate of the neuronal APC/C (see Section 3.2.5). Once definitive substrates of the neuronal APC/C are identified, this type of assay can be tested again to determine if substrates can reliably be screened using this method.

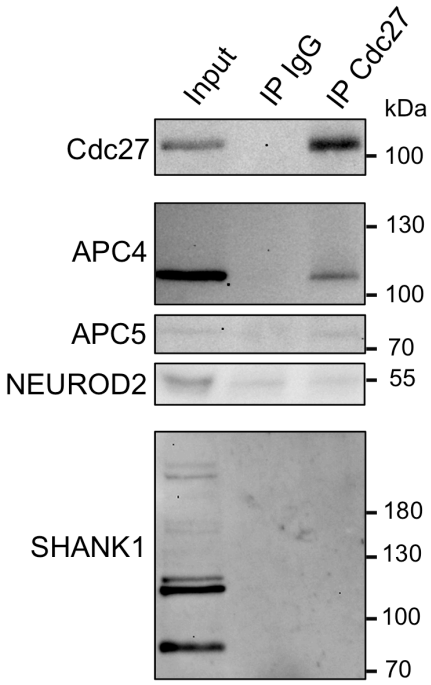

Figure 19. Endogenous APC4 Integrates Into the Cortical APC/C. Wildtype primary cortical neuron cultures at DIV10 were lysed in the absence of NEM. Cdc27-IP was conducted with cell lysates, and an IgG antibody was used as a control. Input and IP eluates were analyzed by SDS/PAGE followed by WB with antibodies directed against Cdc27 (first), APC4 (second), APC5 (third), NEUROD2 (forth), SHANK1 (fifth). Cdc27 and SHANK1 were blotted on separate membranes. APC4 and APC5 co-immunoprecipitated with Cdc27 and the APC/C, but the proposed APC/C substrates NEUROD2 and SHANK1 did not.

3.2.2 APC4 Expression Is Depleted in Neuron Cultures Generated From *tm1c/tm1c* Conditional ANAPC4 Knockout Mice

I had difficulties obtaining a reliable method to knockdown or knockout *ANAPC4* (the gene encoding APC4) within neuron cultures. About one year ago, I finally obtained conditional *ANAPC4* knockout pups that were used to generate neuron cultures (Figure 6 B, *tm1c/ tm1c*). I originally obtained this mouse line in the form of the *tm1a* allele,

which used a knockout-first strategy to knockout *ANAPC4* (Figure 6 A; EUCOMM, MGI: 1098673; IMPC, n.d.). However, this *tm1a* allele may produce an altered mRNA product of the *ANAPC4* gene, meaning that mice with the *tm1a* allele could have a complete or partial loss of APC4 expression (Figure 6 A). Crossing the *tm1a/tm1a ANAPC4* mouse line to a mouse line with Cre expression in the germline, resulted in progeny that were homozygous for a constitutive knockout (*tm1b* allele, scheme is not shown in Figure 6), and these mice died prior to E9.5. Some of the heterozygous mice from this cross also had developmental and hearing defects (IMPC, n.d.).

The MPIEM animal facility initially tried to establish this mouse line for several years from frozen sperm or embryos, but never obtained live mice. Mutant sperm had defects in motility, possibly due to the knockout-first strategy of this *tm1a/tm1a* line (Figure 6 A). In order to finally establish the line at the institute, I eventually obtained live mice from the company (IMPC, n.d.). This *tm1a/tm1a* line was then crossed to a line that expressed Flp recombinase (JAX #003946; Farley et al., 2000) to generate a conditional *tm1c/tm1c ANAPC4* knockout mouse line (Figure 6 B). Once this line was finally established at the institute, it bred normally. I generated primary neuron cultures from the conditional *ANAPC4 tm1c/tm1c* knockout mouse line (Figure 6 B) and infected the neuron cultures from this line with a lentivirus that expresses Cre, resulting in the theoretical knockout of *ANAPC4* only in the infected neurons (*tm1d* allele; Figure 6 C).

After obtaining this mouse line, I first tested whether the expression of APC4 is depleted in the Cre-infected neuron cultures generated from these mice. I found that APC4 protein expression is mostly absent in both primary DIV11 hippocampal (Figure 20 A and B, APC4 blots) and cortical cultures (Figure 20 D, APC4 blots) ten days after infection with a lentivirus that expresses either Cre RFP P2A (Figure 20 A) or Cre NLS RFP (Figure 20 B and D). However, the knockout seemed to work more efficiently in cortical neuron cultures than in hippocampal cultures (Figure 20 B and D, APC4 blots).

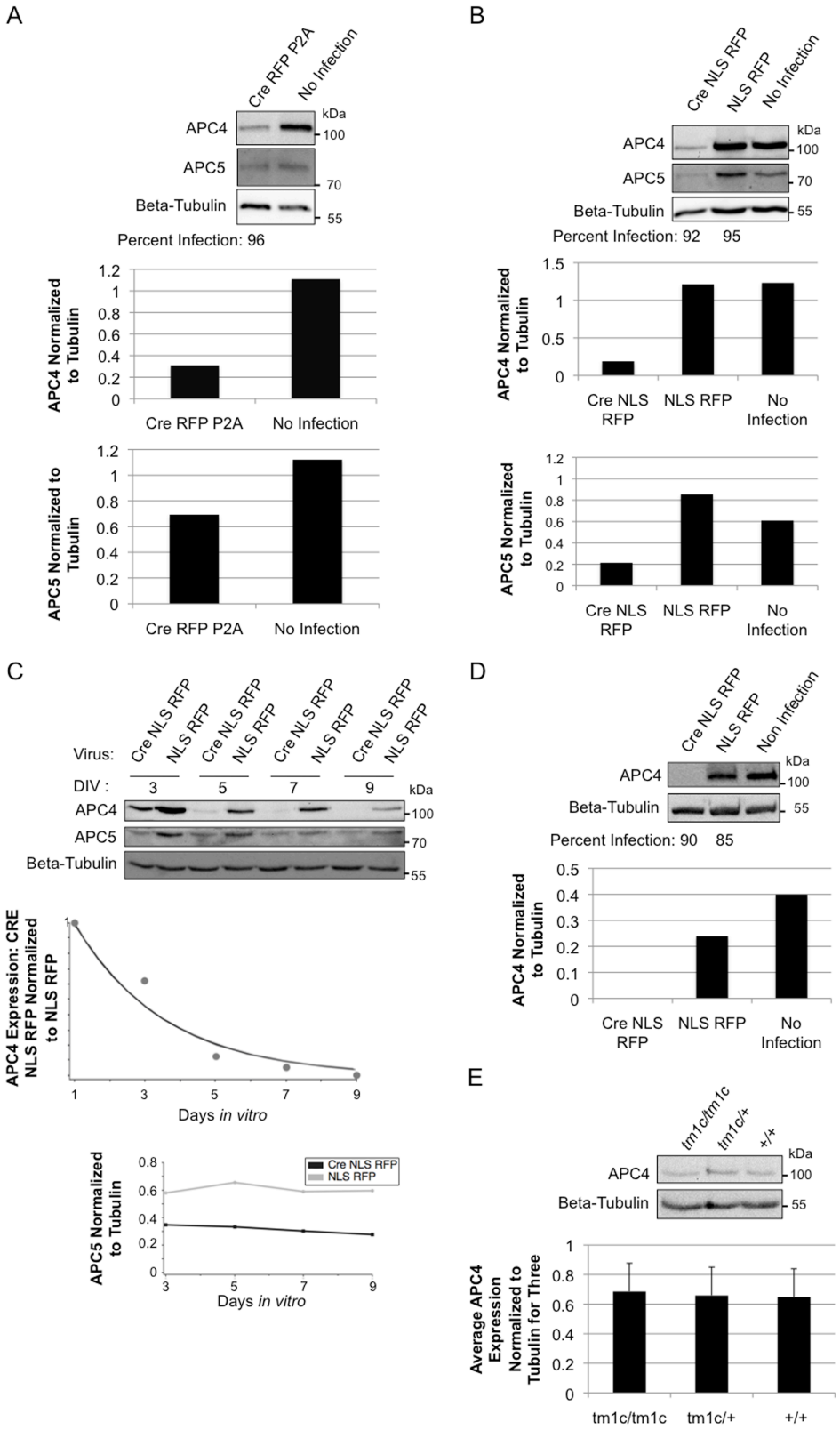
A
Cre RFP P2A
No Infection
kDa
APC4
100
APC5
70
Beta-Tubulin
55
Percent Infection: 96
APC4 Normalized to Tubulin
1.2
1
0.8
0.6
0.4
0.2
0
Cre RFP P2A
No Infection
APC5 Normalized to Tubulin
1.2
1
0.8
0.6
0.4
0.2
0
Cre RFP P2A
No Infection
B
Cre NLS RFP
NLS RFP
No Infection
kDa
APC4
100
APC5
70
Beta-Tubulin
55
Percent Infection: 92 95
APC4 Normalized to Tubulin
1.5
1
0.5
0
Cre NLS RFP
NLS RFP
No Infection
APC5 Normalized to Tubulin
1.2
1
0.8
0.6
0.4
0.2
0
Cre NLS RFP
NLS RFP
No Infection
C
Virus:
Cre NLS RFP
NLS RFP
Cre NLS RFP
NLS RFP
Cre NLS RFP
NLS RFP
Cre NLS RFP
NLS RFP
DIV :
3
5
7
9
kDa
APC4
100
APC5
70
Beta-Tubulin
55
APC4 Expression: CRE NLS RFP Normalized to NLS RFP
1
3
5
7
9
Days in vitro
APC5 Normalized to Tubulin
0.8
0.6
0.4
0.2
0
Cre NLS RFP
NLS RFP
3
5
7
9
Days in vitro
D
Cre NLS RFP
NLS RFP
Non Infection
kDa
APC4
100
Beta-Tubulin
55
Percent Infection: 90 85
APC4 Normalized to Tubulin
0.5
0.4
0.3
0.2
0.1
0
Cre NLS RFP
NLS RFP
No Infection
E
tm1c/tm1c
tm1c/+
+/+
kDa
APC4
100
Beta-Tubulin
55
Average APC4 Expression Normalized to Tubulin for Three
1
0.8
0.6
0.4
0.2
0
tm1c/tm1c
tm1c/+
+/+

Figure 20. APC4 Expression Is Depleted When Cre Is Expressed in Cortical and Hippocampal Neuron Cultures From *tm1c/tm1c* Conditional *ANAPC4* Knockout Mice. Primary hippocampal and cortical neuron cultures were generated from *tm1c/tm1c* conditional *ANAPC4* knockout mice, infected at DIV1, and harvested at various time points. The cultures were lysed without NEM and analyzed by SDS/PAGE and WB. To determine the infection rate, coverslips were fixed and stained at DIV11, and the percentage of DAPI and MAP2-expressing cells that also co-expressed RFP were determined and are displayed for each experiment (top panels in **A, B** and **D**). (**A**) Hippocampal neuron cultures were either infected with Cre-RFP-P2A or not infected, and these cultures were then harvested at DIV11. Cell lysates were analyzed by WB with antibodies against APC4, APC5, and Beta-Tubulin as labeled (top panel). The bar graphs depict the quantification of APC4 (middle panel) and APC5 (bottom panel) expression after normalization to Beta-Tubulin. (**B**) Hippocampal neuron cultures were either not infected or were infected with Cre NLS RFP or NLS RFP. At DIV11, lysates were analyzed by WB with antibodies against APC4, APC5, and Beta-Tubulin as labeled (top panel). The bar graphs depict the quantification of APC4 (middle panel) and APC5 (bottom panel) expression after normalization to Beta-Tubulin. (**C** and **D**) Primary cortical neuron cultures were infected at DIV1 and harvested at DIV 3, 5, 7, 9 (**C**) and 11 (**D**). The infection rate was determined only at DIV11. While the cultures were infected with Cre NLS RFP or NLS RFP at all time points, a No Infection control was collected only at DIV11. Cultures from each time point were lysed together and analyzed by SDS/PAGE followed by WB. (**C**) WB was performed with antibodies against APC4, APC5, and Beta-Tubulin (top panel). For both the CRE NLS RFP and the NLS RFP infected cultures, APC4 expression was first normalized to Beta-Tubulin and these values for both the CRE NLS RFP and the NLS RFP were then normalized to each other. These final values are depicted in the first line graph (middle panel). These values seemed to fit well to an exponential curve, allowing me to calculate the half-life of the APC4 protein within cortical neuron cultures (middle panel; τ = 2.6 days, $t_{1/2}$ = 1.8 days). The second line graph depicts the quantification of APC5 expression levels normalized to Beta-Tubulin (bottom panel). (**D**) WB analysis was conducted using antibodies against APC4 and Beta-Tubulin as labeled (top panel). The bar graph depicts the quantification of APC4 expression normalized to Beta-Tubulin for all conditions (bottom panel). (**E**) Cortical neuron cultures were generated from three mice with the following ANAPC4 genotypes: *tm1c/tm1c*, *tm1c/+*, *+/+*. Lysates were analyzed by SDS/Page followed by WB, using antibodies against APC4 and Beta-Tubulin as labeled (top panel). APC4 expression was normalized to Beta-Tubulin for each lane and the average values for each genotype was calculated (bottom panel). The error bars represent the SEM.

To determine how rapidly APC4 expression was lost, I studied the time course of APC4 expression after infection with Cre NLS RFP, and found that most of the protein was gone by DIV5 and completely gone by DIV7 (Figure 20 C, APC4 blot). I normalized APC4 expression to Beta-Tubulin, and these calculated values for CRE NLS RFP were then normalized to the calculated values for NLS RFP. These final values were plotted,

enabling one to basically determine how APC4 expression changes over time after the infection. These values were fit well by an exponential curve, allowing me to calculate the half-life of APC4 protein turn over to be around 1.8 days in the cortical neuron cultures (Figure 20 C, top graph).

Prior studies indicate that there is an important link between the levels of APC4, APC5, and APC1 expression in cells (Clark and Spector, 2015; Thornton et al., 2006; Tran et al., 2010). It was shown that the knockdown of any of these proteins led to decreased expression of the respective two other proteins. It was hypothesized that when one of these components of the APC/C is absent, the APC/C is not stable, leading to the degradation of the other APC/C components (Clark and Spector, 2015; Thornton et al., 2006). I observed a related phenomenon when I knocked out APC4 in neuron cultures, since I found that both APC4 and APC5 expression was drastically depleted after infection with a Cre-expressing virus (Figure 20 A - C). In hippocampal neuron cultures, a residual amount of both APC4 and APC5 expression remained at DIV11 (Figure 20 A and B, APC4 and APC5 blots). Interestingly in cortical neurons, where APC4 was knocked out more quickly and completely, APC5 levels drastically dropped early but stabilized later. A small amount of APC5 was always detected, even days after the APC4 expression was absent (Figure 20 C, APC5 blot and the second graph).

The conditional *ANAPC4* knockout mouse line has DNA insertions within the non-coding regions of the *ANAPC4* gene. For this reason, I verified that these insertions did not change the endogenous expression of APC4. To do so, heterozygous mice carrying one copy of the *tm1c* allele were interbred, and I generated cortical neuron cultures from their embryos. I completed WB analysis of lysates generated from DIV10 primary cortical neuron cultures obtained from these mice, which were either wildtype, homozygous, or heterozygous for the *tm1c* allele. I blotted the lysates of three individual mice for each genotype (Figure 20 E, see the representative blot for three different mice), and I determined the average normalized APC4 expression for each genotype (Figure 20 E, bottom graph). I found no noticeable differences in the expression of APC4 between these mice (Figure 20 E, APC4 blot and graph), indicating that the insertion of DNA sequences between exon 2 and exon 4 in the *ANAPC4* gene did not affect the expression of APC4.

3.2.3 Validation of the APC4 Antibody For Use in ICC With the *tm1c/tm1c* Conditional *ANAPC4* Knockout Mouse Line

Previously, I had found that endogenous APC4 is localized to puncta within the cell body of both HEK293 cells (Figure 11 A) and neurons (Figure 11 B), but I had no way to determine the specificity of the APC4 antibody in the ICC experiments. Now that I had confirmed that I can efficiently knockout APC4 expression in neuron cultures obtained from *tm1c/tm1c* mice (Figure 20 A - D, APC4 blots), I went on to test the specificity of the APC4 antibody in detecting APC4 within neurons using an imaging approach, and knockout cells as negative control. Primary hippocampal neuron cultures were generated from *tm1c/tmc1* conditional *ANAPC4* knockout mice. Cultures were infected at DIV1 with Cre RFP P2A, fixed and stained on DIV11, and imaged on a confocal microscope (Figure 21). By comparing the RFP and the Cre staining to the MAP2 staining patterns, I found that the coverslips contained a mixture of infected and non-infected cells (Figure 21, see the second Cre RFP P2A panel for an example). Cre and RFP expression was confined to the soma of the neurons (Figure 21, Cre and RFP staining). I later discovered that my RFP signal was not stable if I imaged it over a week after the coverslips were mounted (data not shown), so this is likely the reason that some Cre-infected cells did not have a visible RFP signal in this experiment (Figure 21, second Cre RFP P2A panel). To solve this issue in the other experiments, I either stained with an anti-RFP antibody or I imaged within a week after immunolabeling.

Endogenous APC4 was detected as a weak punctate signal that was confined to the soma of cells that did not express Cre. This signal was entirely absent from cells that expressed Cre (Figure 21, second Cre RFP P2A panel). This indicates that the APC4 antibody does specifically label APC4 in ICC. However, the antibody gave extremely weak signals, even after attempts to optimize the staining with various fixing and staining conditions (data not shown). A second antibody gave a similar weak-staining pattern (data not shown). As the cellular subfractionation studies showed that APC4 is present in the cytosol of HEK293 cells (Figure 14, APC4 blot) and multiple other cellular fractions of the mouse cortex (Figures 15, APC4 blot), I suspect that the current APC4 antibodies do not detect all of the endogenous APC4 expression when

they are used in an ICC approach or the APC4 expression is at a low enough level in the cytoplasm that it is not detected well using an ICC approach.

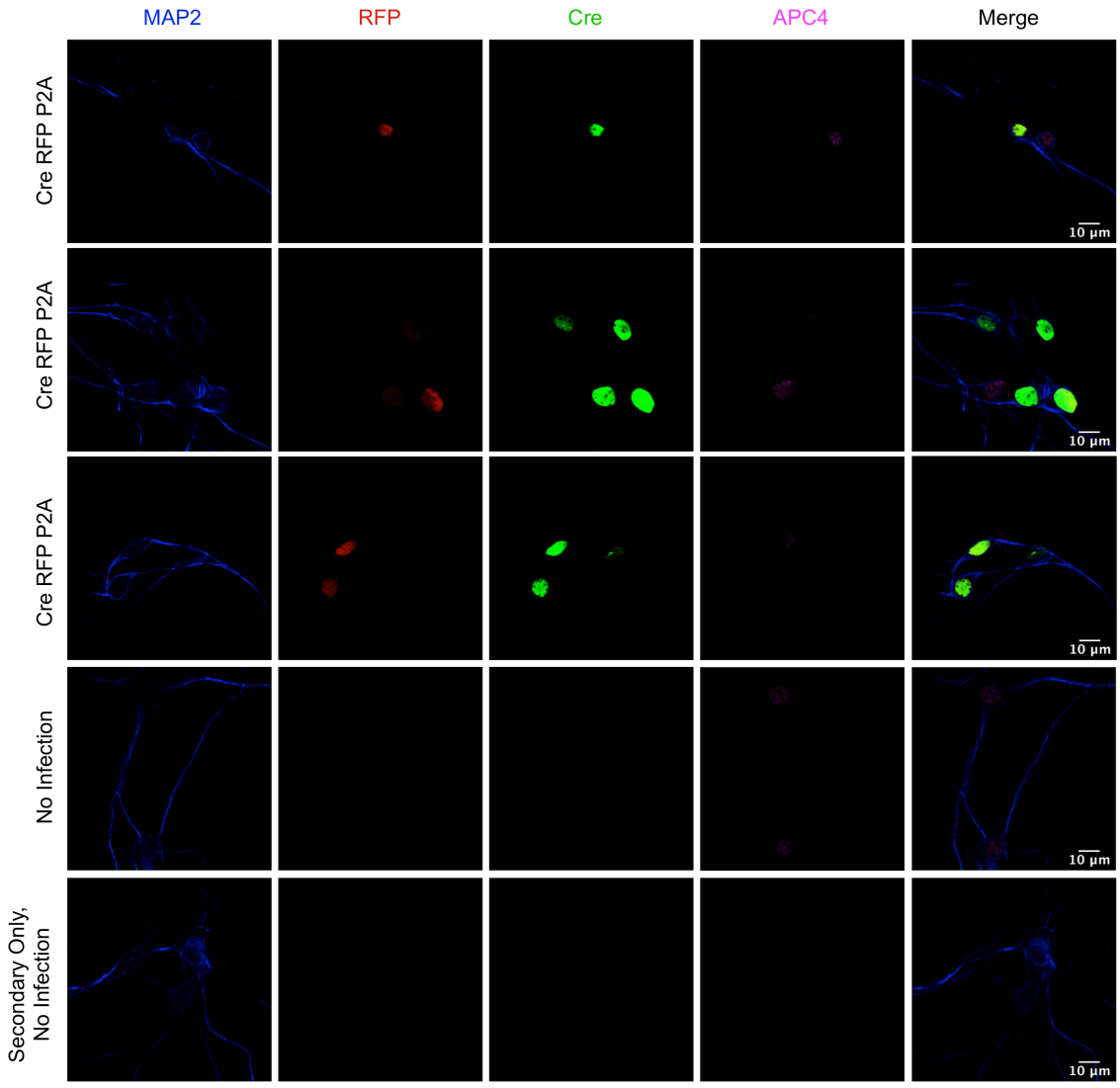

Figure 21. Validating the APC4 Antibody in Neuron Cultures Generated From Conditional *ANAPC4* Knockout Mice. Primary hippocampal neuron cultures were generated from *tm1c/tm1c* conditional *ANAPC4* knockout mice and infected at DIV1 with a lentivirus expressing Cre RFP P2A or a No Infection control. Coverslips were fixed at DIV11 and stained with antibodies against MAP2 (blue), Cre (green), and APC4 (magenta). The RFP expression was also detected (red). The settings on the confocal microscope were determined by using a non-infected control sample that was not stained with the APC4 primary antibody (Secondary Only). Scale bars representing 10 µm are displayed on the merged images (Merge).

3.2.4 Loss of APC4 Expression Affects the Morphology of Cortical Neurons

Cdh1 depletion in neurons doubles the length of axons as compared to control cells (Kannan et al., 2012b; Konishi et al., 2004; Lasorella et al., 2006; Stegmüller et al., 2006). When Cdc20 is depleted, the length of the dendrites decreases, without changing the length of the axons (Kim et al., 2009; Watanabe et al., 2014). SMURF1 was proposed to regulate axon length through a pathway that involves Cdh1, but it surprisingly was suggested to do this via an APC/C-independent mechanism that does not involve SMURF1 protein degradation (Wan et al., 2011). However, this proposed mechanism does not fully explain why SMURF1 is ubiquitylated and why its D box motif, which is typically required for the binding of the Cdh1-APC/C, is required by SMURF1 to regulate axon length (Kannan et al., 2012b). Further studies are required to elucidate how Cdh1 regulates axonal length through SMURF1 and to determine if this actually requires the APC/C in any form. Some of the other proposed substrates of the APC/C that are thought to regulate the morphology of neurons may also require the activators in an APC/C-independent mechanism (Bobo-Jiménez et al., 2017; Kim et al., 2009; Li et al., 2019; Lasorella et al., 2006; Stegmüller et al. 2006; Stegmüller et al., 2008). For this reason, I chose to characterize the morphology of DIV5 cortical neurons after the depletion of APC4, a core component of the APC/C, with the idea to determine if the APC/C is required for regulating neuron morphology.

I analyzed the morphology of DIV5 cortical neurons that were infected with either Cre NLS RFP or NLS RFP. I chose to do the analysis on DIV5 initially, because neuronal morphology is less complex at this age, which makes the analysis easier. APC4 expression is also almost completely depleted by this age (Figure 20 C, APC4 expression on DIV5), indicating that DIV5 is an appropriate age for analyses of *ANAPC4* knockout cells. I generated primary cortical neuron cultures from *tm1c/tm1c* conditional *ANAPC4* knockout mouse embryos, infected the cultures at DIV1, and fixed the cells at DIV5. I initially hoped to be able to reliably distinguish between axons and dendrites of neurons using a SMI-312 and a MAP2 antibody, respectively. Unfortunately the axon and the dendrites were not distinguishable at DIV5 using these stains (Figure 22, MAP2 and SMI-312 staining). For this reason, I decided to do the morphological

analysis on all neurites of each neuron using the Beta III-Tubulin stain, a marker of the microtubule network in all neurites (Figure 22, Beta III-Tubulin staining).

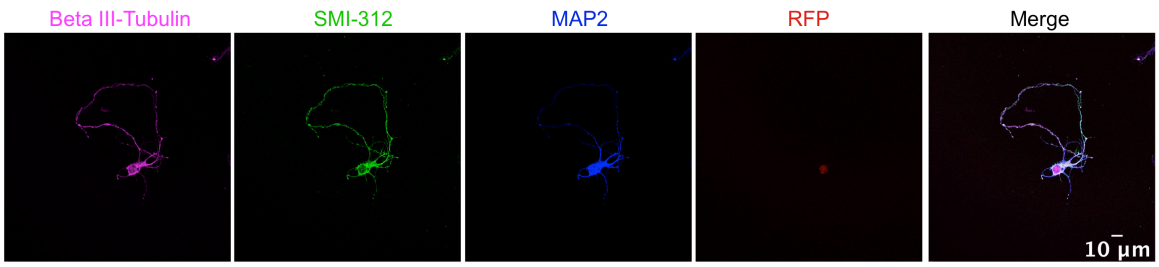

Figure 22. A Representative Cell Shows That the Axon and Dendrites Are Not Easily Distinguishable by DIV5. Primary cortical neuron cultures were generated from *tm1c/tm1c* conditional *ANAPC4* knockout mice, infected with Cre RFP NLS or NLS RFP (not shown) at DIV1, and fixed on DIV5. The neurons were stained for Beta III-Tubulin (purple), neurofilament (SMI-312; green), MAP2 (blue), and RFP (red). The Merge image shows the colocalization of all stainings. This is a representative cell that shows that the axons and dendrites are not easily distinguishable at this stage of development by comparing only the MAP2 (blue) and the SMI-312 (green) staining patterns. This was an issue when the cells were infected with either Cre NLS RFP or NLS RFP. For this reason, the Beta III-Tubulin (magenta) stain was used for the analysis of total neurite complexity. The scale bar denotes 10 µm.

The maximum projection intensities of the Beta III-Tubulin channel were used to trace all of the neurites that were greater than 3 µm using the SNT plugin on Fiji (Tavares et al., 2017). I imaged around 70 neurons in total between two separate experiments, and all of the data for all of these experiments were compiled for the analysis (Figure 23). The neurites were all traced and structures were labeled as a primary neurite, if they directly exited the soma. When the neurite formed a branch, I identified the neurite that was less angled and seemed to be an extension of the primary neurite and I labeled this as the primary neurite. The new neurite branching from the primary neurite was defined as a secondary neurite. Sometimes there was an additional branch point extending from a secondary neurite, and this new neurite extension was labeled a tertiary neurite. The length of all primary, secondary, and tertiary neurites was determined and the number of branch points was recorded. Example neuron traces are displayed for Cre NLS RFP- (Figure 23 A, top panel) and NLS RFP-infected neurons (Figure 23 A, bottom panel). In order to assay neuron complexity, I used the SNT plugin to conduct Sholl analysis (Sholl, 1953; Tavares et al., 2017), which involved putting a

point in the center of the cell body and drawing concentric circles around this point using a 5 μm step size with the SNT program. The number of neurite intersections with each circle was then determined. All of the results and the statistical analysis are displaced in Figure 23 and Table 13.

While this was never described in previous studies, the most striking effect that I observed when I compared Cre NLS RFP- and NLS RFP-infected neurons was a significant increase in the number of processes that extended out of the soma in the Cre NLS RFP-infected neurons (Figure 23 B and C; Table 13). This effect was observed when I either included (Figure 23 B; Table 13; $p < 0.05$) or excluded (Figure 23 C; Table 13; $p < 0.05$) the shorter neurites that were between 3 and 10 μm from the analysis.

The number of branch points increased when Cdc20 was knocked down in one study, but this phenotype was not well examined (Kim et al., 2009). Although, I was unable to definitively distinguish between the axon and dendrites by DIV5, I quantified the total number of branch points (Figure 23 D; Table13, $p > 0.05$) and the total number of branch points that initiated off the primary neurites (Figure 23 E; Table 13; $p > 0.05$), but I found no differences in these measurements when I compared Cre NLS RFP- and NLS RFP-infected neurons.

I expected that neurons obtained from conditional *ANAPC4* knockout mice and infected with Cre NLS RFP or NLS RFP would have differences in the lengths of their neurites, because Cdh1 knockdown increased the axon length (Kannan et al., 2012b; Konishi et al., 2004; Lasorella et al., 2006; Stegmüller et al., 2006), Cdc20 knockdown decreased the dendrite length (Kim et al., 2009; Watanabe et al., 2014), and APC2 knockdown decreased the dendrite length (Kim et al., 2009). Thus, I expected to see similar results when I knocked out *ANAPC4* in cortical neurons. However, I found no substantial difference in neurite lengths when I compared Cre NLS RFP- and NLS RFP-infected cells (Figure 23 F - H; Table 13; $p > 0.05$). I specifically examined the total length of all neurites (primary, secondary, and tertiary combined; Figure 23 F; Table 13; $p > 0.05$), the average length of all primary neurites of a cell (Figure 23 G; Table 13; $p > 0.05$), and the length of the longest neurite of a cell (Figure 23 H; Table 13; $p > 0.05$). I measured the length of the longest neurite to determine if there are differences in the

axon length. However, this seems to not be a good measure of axon length, as I found neurites with axon growth cones on a shorter neurite (data not shown).

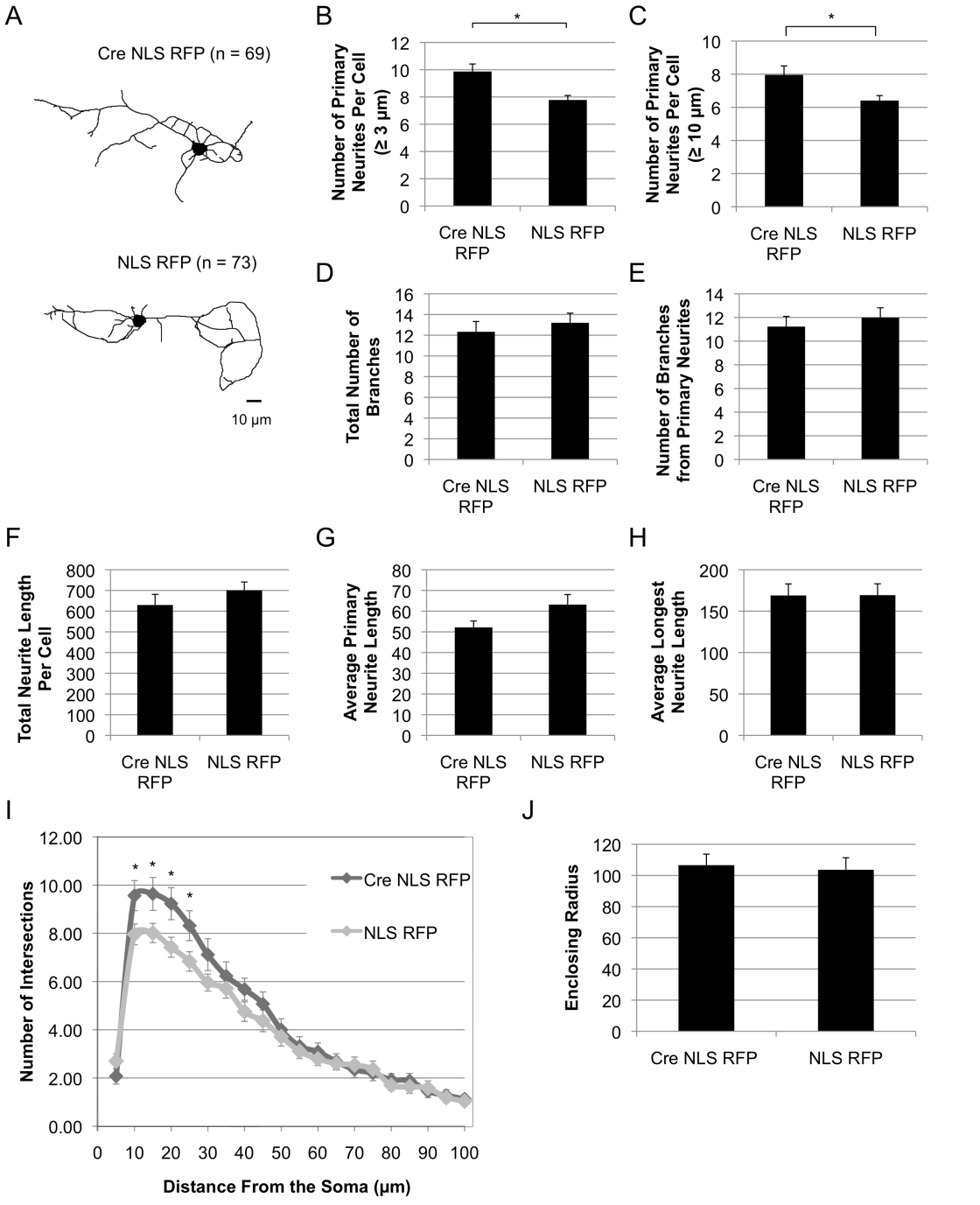

Figure 23. Cortical Neurons Depleted of *ANAPC4* Have More Primary Neurites but the Neurite Length Remains Unchanged. Primary cortical neuron cultures were

generated from conditional *ANAPC4* knockout mice, and the infected neurons were fixed at DIV5, stained, and imaged on a confocal microscope. The maximum projection images of the Beta III-tubulin stain were used to trace the shape of the neurons, and the individual shape of each neuron was analyzed using the SNT program by FIJI. All statistical analysis compare the populations of Cre NLS RFP- (n = 69) and NLS RFP-infected cells (n = 73) using a Welch's t-test, and the values are displayed with an asterisk only if they were significantly different ($p < 0.05$). The error bars all represent the SEM. (**A**) Representative images are displayed of skeletonized neurons that were infected with either Cre NLS RFP (top) or NLS RFP (bottom). The scale bar denotes 10 µm. (**B**) Graph showing the average number of primary neurites extending from the soma that are ≥ 3 µm long (asterisk denotes significant difference; Table 13; $p < 0.05$)**.** (**C**) Bar graph showing the average number of primary neurites extending from the soma that are ≥ 10 µm long (asterisk denotes significant difference; Table 13; $p < 0.05$). (**D**) Graph denoting the total number of branch points per cell after averaging for all cells in each category. (**E**) Graph depicting the total number of branch points within a neuron that break off a primary neurite, averaged for all cells in each condition. (**F**) Bar graph showing the average of the summation of the lengths of all primary, secondary, and tertiary neurites of a cell. (**G**) The average primary neurite length per cell was determined and then averaged for each category and displayed (**H**). The longest neurite length per cell was averaged for all cells. (**I** and **J**) Sholl analysis was conducted with the traced neurons. (**I**) Graph showing the distribution of the intersections relative to the distance from the soma (asterisks show significant difference between conditions at that particular distance; Table 13; $p < 0.05$). (**J**) The average enclosing radius represents the average minimum circle radius that is able to encircle the whole neuron.

Finally, I performed Sholl analysis (Sholl, 1953) on the traced neurons to determine if there were changes in neurite complexity when APC4 was depleted. While the number of intersections were similar between the conditions starting at around 30 µm from the center of the soma (Figure 23 I; Table 13; $p > 0.05$), there were more intersections between the distances of 10 and 25 µm from the center of the soma when APC4 was depleted (Figure 23 I, compare Cre NLS RFP and NLS RFP; asterisks depict significant differences in a Welch's t-test; Table 13; $p < 0.05$). At 5 µm from the center of the neuron, there was a trend at a decrease in the number of intersections when APC4 was depleted (Figure 23 I, compare Cre NLS RFP and NLS RFP at 5 µm), but this distance should not be analyzed as it was often still located within the soma of a neuron. Finally, I determined the radius of the circle that could enclose the full neuron. I compared this average circle radius between conditions, but there was no significant difference (Figure 23 J, compare Cre NLS RFP- and NLS RFP-infected samples within the bar graph, Table 13; $p > 0.05$).

Table 13. Quantification Statistics for the Neuron Morphology Experiment

Measurement	Conclusion	Statistical Values	Cre NLS RFP, Mean, SEM	NLS RFP, Mean, SEM
Number of primary neurites ≥ 3 µm	Significantly different	F(1, 111.91)= 10.56, p=0.002	9.87, 0.55	7.78, 0.33
Number of primary neurites ≥ 10 µm	Significantly different	F(1, 206.26)= 6.246, p=0.014	7.96, 0.54	6.41, 0.30
Number of primary neurites ≤ 3 µm	Not significantly different	F(1, 107.93)= 3.205, p=0.076	1.91, 0.26	1.37, 0.15
Longest neurite length per cell	Not significantly different	F(1, 139.70)= 0.000, p=0.984	168.92, 13.95	169.32, 13.70
Average primary neurite length per cell	Not significantly different	F(1, 120.83)= 3.683, p=0.57	52.18, 3.06	63.16, 4.83
Average summation of the total neurite length per cell	Not significantly different	F(1, 130.812)= 1.174, p=0.281	700.34, 51.25	629.73, 40.28
Average total number of branches per cell	Not significantly different	F(1, 138.244)= 0.605, p=0.438	12.33, 0.99	13.38,0.91
Average number of branches off a primary branch per cell	Not significantly different	F(1, 139.520)= 0.399, p=0.528	11.23,0.86	11.99,0.83
Sholl, intersections at 5 µm	Not significantly different	F(1, 139.053) = 1.976, p=0.162	2.07, 0.32	2.70, 0.32
Sholl, intersections at 10 µm	Significantly different	F(1, 122.207)= 4.492, p=0.036	9.57, 0.62	7.96, 0.43
Sholl, intersections at 15 µm	Significantly different	F(1, 110.252)= 4.208, p=0.043	9.64, 0.68	8.01, 0.40
Sholl, intersections at 20 µm	Significantly different	F(1, 114.993)= 5.341, p=0.023	9.23, 0.66	7.42, 0.41
Sholl, intersections at 25 µm	Significantly different	F(1, 118.033)= 4.006, p=0.048	8.32, 0.62	6.84, 0.40
Sholl, intersections at 30 µm	Not significantly different	F(1, 103.932)= 2.391, p=0.125	7.12, 0.66	5.96, 0.35
Sholl, enclosing radius	Not significantly different	F(1, 139.496)= 0.080, p=0.777	106.59, 7.06	103.63, 7.72

3.2.5 Many Previously Proposed Neuronal APC/C Substrates Are Not Substrates of the Cortical APC/C at DIV11

While most of the proposed neuronal substrates of the APC/C were identified as proteins that require Cdh1 or Cdc20 expression for their degradation, the corresponding studies never went on to confirm that this process actually required the APC/C (see Section 1.6.9; Table 16; reviewed in Eguren et al., 2011). SMURF1 was shown to require Cdh1 for its function in regulating axon length (Kannan et al., 2012b), but SMURF1 requires Cdh1 in an APC/C-independent mechanism (Wan et al., 2011). It is not known how many of the other of neuronal substrates of the APC/C utilize the activator of the complex through a mechanism that is independent from the APC/C.

In order to further characterize the function of APC4 and the APC/C in neurons, I knocked out *ANAPC4* in primary cortical neuron cultures generated from conditional *ANAPC4* knockout mice and analyzed the lysates from DIV11 neuron cultures by WB. I used antibodies directed against several neuronal markers and some of the proposed neuronal substrates of the APC/C with the intent to try to determine if knocking out *ANAPC4* influences the expression level of any of these proteins (Figure 24). To quantify the protein expression, I repeated the experiment three different times. One of the infected wells from each experiment had a coverslip that I used to determine the percentage of the cells infected during the experiment. I had a high infection rate in every experiment, achieving values of at least 92% of the cells being infected during the experiments (Table 14). All protein quantification was completed by determining the ratio of the protein of interest to Beta-Tubulin, and then the average value was determined for all three experiments. The statistical analysis was completed using an independent t-test to compare the distribution of the experimental values when cells were infected with either Cre NLS RFP or NLS RFP. This statistical data for each protein tested are summarized in Table 15.

As I observed previously (Figure 20 C and D), APC4 and APC5 were basically undetectable in all three experiments when Cre was expressed (Figure 24 A, APC4 and APC5 blots), indicating that APC/C is likely not functional within the Cre NLS RFP-infected cells. Interestingly, Cdc27 expression always remained stable in cultures

($p > 0.05$; Figure 24 A, Cdc27 blot; Table 15). I also blotted several neuronal markers to try to identify other proteins with changes in protein expression that might result from the knockout of *ANAPC4* within differentiated neurons. For this reason, I blotted the membranes with antibodies directed against Synaptophysin, Complexin 3, PSD-95, and Synapsin 1/2 (Figure 23 D, see the respective blots), but I was unable to detect any obvious changes in the expression levels of these proteins. However, I was only able to formally quantify the normalized protein expression levels for Synaptophysin and Complexin 3 during this study (Table 15).

Table 14. Infection Rates For Each Biochemistry Experiment

	Cre NLS RFP	**NLS RFP**
Experiment 1	96.6 %	97.6 %
Experiment 2	92.1 %	92.1 %
Experiment 3	92.4 %	96.2 %

I next sought to determine if there were any changes in expression of the proposed neuronal substrates of the APC/C within these cultures. When the APC/C is not functional, there should be a loss of the ubiquitylation and the subsequent degradation of the APC/C substrates. Hence, I expected that the expression of these substrates would increase when the cells were infected with Cre NLS RFP. To my surprise, there were no increases in the expression levels of any of the proposed neuronal substrates that I tested. I found that there were no significant changes at all in the expression of FEZ1 or NEUROD2 (Figure 24 E-H, FEZ1 and NEUROD2 blots; Table 15), and ID1 expression was actually reduced in the Cre NLS RFP-infected cultures ($p < 0.05$; Figure 24 B and C, ID1 blots; Table 15).

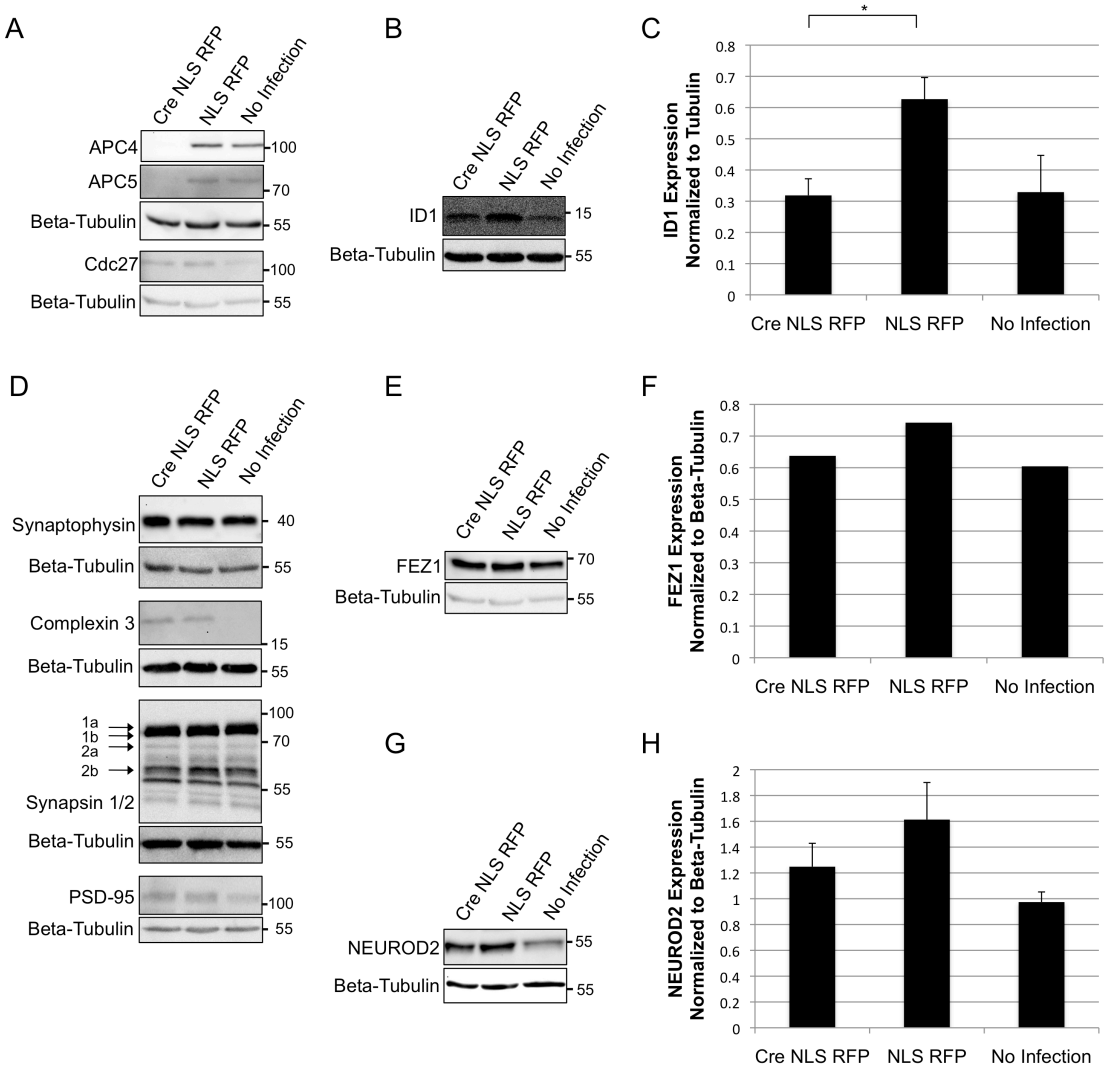

Figure 24. Biochemical Analysis of APC/C Substrates and Neuronal Markers in Neuronal Lysates Depleted of APC4. Primary hippocampal neuron cultures were generated from *tm1c/tm1c* conditional knockout mice, infected at DIV1 with Cre NLS RFP or NLS RFP, and then harvested at DIV11. Lysates were analyzed by SDS/PAGE followed by WB. Unless otherwise stated, three separate experiments were completed in order to quantify the protein expression within the lysates, and this expression was normalized to Beta-Tubulin. Separate membranes are denoted by a large space between the blots, and the Beta-Tubulin control blots are displayed for each membrane. The error bars represent the SEM. (**A**) Example blots from one experiment show that APC4 (first blot from top) and APC5 (second blot) were not detected in Cre NLS RFP infected cells, but there was no difference in the expression of Cdc27 between the samples (fourth blot). (**B**) Lysates were blotted for ID1, a proposed APC/C substrate, and an example blot is depicted. (**C**) ID1 expression was normalized to Beta-Tubulin, and the average of these values was determined for three separate experiments. The ID1 expression was surprisingly reduced in the Cre NLS RFP-infected samples

(asterisk; Table 15; $p < 0.05$). (**D**) Representative blots are shown for several neuronal markers: Synaptophysin (first set), Complexin 3 (second set), Synapsin 1/2 (third set), and PSD-95 (fourth set). The different Synapsin isoforms are denoted with arrows and labeled. There were no detectable differences in the normalized expression of these proteins in the infected samples. (**E**) Lysates were blotted for FEZ1, a proposed APC/C substrate, and an example blot is depicted. (**F**) FEZ1 expression was normalized to Beta-Tubulin, and the average value for two experiments is depicted. While statistical analysis was not conducted, there was no obvious change in the expression of FEZ1. (**G**) Lysates were blotted for NEUROD2, a proposed APC/C substrate. (**H**) The quantification of NEUROD2 expression was normalized to Tubulin for three experiments, and there was no difference between the infected samples.

Surprisingly, lentivirus infection seemed to induce a slight increase in the expression of many of the proteins tested (see NLS RFP-infected cells in Figure 24), but this effect is unrelated to the *ANAPC4* knockout. This was especially noticeable when I blotted for Complexin 3, as I was unable to detect it at all in the non-infected cells, but it was strongly expressed in the infected cells (Figure 24 D, Complexin 3 blot). This trend was also observed when I blotted samples for ID1 (Figure 24 B and C, ID1 blot), Synaptophysin (Figure 24 D, Synpatophysin blot), and NEUROD2 (Figure 24 G and H, NEUROD2 blot and bar graph). As a control, I also repeated the WB analysis with lysates that were obtained from infected wildtype primary cortical neuron cultures, and I observed a similar increase in the expression of all of these proteins within these cultures upon lentivirus infection (data not shown).

There was a slight decrease in the expression of several proteins when Cre was expressed (Figure 24 C, F, and H, compare the Cre NLS RFP and the NLS RFP samples in the graphs), but this slight effect was often observed even when wildtype cultures were infected (data not shown). The slight decrease in the expression of FEZ1 and NEUROD2 within the Cre-infected cultures (Figure 24 F and H, compare the Cre NLS RFP and the NLS RFP samples in the graphs) was also observed with wildtype cultures (data not shown), indicating that it is unrelated to the loss of APC4 expression. However, this decrease was not observed in the ID1 blots of the wildtype-infected cultures (data not shown), indicating that this ID1 effect that I observed within the knockout cultures (Figure 24 B, ID1 blot and graph) is likely due to the loss of *ANAPC4* within the culture.

Table 15. Quantification Statistics: Comparison of the Infected Cells

Protein	N value	Conclusion (Cre RFP NLS compared to NLS RFP)	Statistical Values
APC4	3	Not detected in Cre RFP NLS infected cells; no quantification	-
APC5	3	Not detected in Cre RFP NLS infected cells; no quantification	-
Cdc27	3	No difference	t = -0.76, p = 0.49
ID1	3	Decreased in Cre NLS RFP	t = 3.54, p = 0.02
FEZ1	2	No quantification; no obvious difference; graph shows average of 2 experiments	-
NEUROD2	3	No difference	t = -1.03, p = 0.36
Synaptophysin	3	No difference	t = 0.08, p = 0.94
Complexin 3	3	No difference	t = -1.70, p = 0.16
PSD-95	1	No quantification; no obvious difference	-
Synapsin 1/2	1	No quantification; no obvious difference	-

4. Discussion

4.1 APC4 is SUMOylated

A complex system of post-translational modifications helps to regulate molecular processes in eukaryotic cells, including gene transcription, mRNA translation, protein function, protein-protein interactions, protein localization, and protein stability and turnover (reviewed in Chen et al., 2017). Phosphorylation, a major post-translational modification, is of particular importance in regulating the activity and the function of the APC/C. While still an emerging area of research within the APC/C field, there is a growing body of evidence indicating that the phosphorylation of the activators, Cdh1 and Cdc20, helps to regulate the activation of the complex (Bancroft et al., 2020; Kim et al., 2017; Tanno et al., 2020). In addition to phosphorylation of the activators, the core components of the APC/C have many phosphorylated residues, but the precise function of these phosphorylation events is not well understood. The APC/C has at least 68 different residues that are phosphorylated within the Cdc20-activated complex (Qiao et al., 2016). APC4 itself has three residues that are phosphorylated, and one of these is phosphorylated only during mitosis (Kraft et al., 2003; Qiao et al., 2016). I was excited to learn that APC4 might be SUMOylated adjacent to known residues of APC4 phosphorylation, as this SUMOylation might regulate the phosophorylation of APC4 and the function of the complex (Cubeñas-Potts et al., 2015; Hendriks et al., 2018; Matic et al., 2010; Schimmel et al., 2014; Tirard et al., unpublished). This notion was supported at the time by the fact that SUMOylation itself is required for the activity of the yeast APC/C (Dieckhoff et al., 2004), but eventually yeast SUMOylation was suggested to involve another unidentified mechanism due to the fact that the SUMOylated lysines are not conserved on APC4 (Eifler et al., 2018). For these reasons, I first sought to determine if APC4 is SUMOylated and to better understand the function of this SUMOylation within a variety of different mammalian cell types.

4.1.1 Mouse APC4 is Conjugated to All SUMO Paralogs via Lysines 772 and 798

In the first part of my work, I showed that mouse APC4 is conjugated on lysines 772 and 797 (Figure 8 A and B, APC4 blots) by SUMO1 (Figure 7 A), SUMO2 (Figure 7 B), and SUMO3 (Figure 7 C), indicating that all three SUMO paralogs, when overexpressed, can be conjugated to APC4 in HEK293 cells. Recently, other labs also showed that human APC4 is SUMOylated on lysines 772 and 798 (Eifler et al., 2018; Lee et al., 2018; Yatskevich et al., 2021), but my data was the first study to confirm the SUMOylated residues of the mouse APC4. I generated a SUMOylation-deficient (K772R/K797R) APC4 construct that cannot be SUMOylated (Figure 8 A and B, arrows), and this construct was used during all of my studies. Interestingly, I could never detect any signs of SUMO chains being attached to APC4 (data not shown, but see similar experiments in Figure 8 A and B, the absence of triplicate bands when a single lysine was mutated), so a single SUMO moiety seems to be attached to each of the targeted lysine residues (Figure 8 A and B, arrows). Additionally, mutating one SUMOylation site did not appear to influence the SUMOylation of the other site (Figure 8 A and B, arrows), indicating that the SUMOylation of one of these residues is not dependent on the SUMOylation of the other residue. There seems to be some interplay between the phosophorylation and the SUMOylation of APC4 (Eifler et al., 2018; Yatskevich et al., 2021), but this will be discussed more in depth in Section 4.1.8.

Mostly due to technical limitations, it is not possible to determine with certainty if APC4 is predominately SUMOylated by a single SUMO paralog in cells. First of all, I was not able to reliably detect APC4 SUMOylation in SUMOylation assays without overexpressing a SUMO paralog (data not shown). This is a consistent problem in the SUMO field, so most in-cell SUMOylation assays involve the overexpression of a SUMO paralog (reviewed by Geiss-Friedlander and Melchior, 2007). The second issue is that anti-SUMO antibodies are not very sensitive in WB experiments and none of them can distinguish between SUMO2 and SUMO3. Third, APC4 SUMOylation itself seems to be very weak when SUMO is expressed at endogenous levels (Figure 8 A, APC4 blot, fifth lane in the Input). While it was easier to detect APC4-SUMO2 conjugation upon SUMO overexpression in HEK293 cells, I cannot directly compare the amounts of SUMOylation

between the differently overexpressed SUMO paralogs. For all of these reasons, I was unable to determine which of the different paralogs is primarily responsible for SUMOylating APC4 in cells. This being stated, prior proteomic screens showed that APC4 can be conjugated to either SUMO1 (Tirard et al., unpublished) or SUMO2 (Cubeñas-Potts et al., 2015; Hendriks et al., 2018; Eifler et al., 2018; Lee et al., 2018; Schimmel et al., 2014) in the brain and in human cell lines, respectively, indicating that SUMO1 and SUMO2 are involved in SUMOylating APC4. Recently, SUMO2 was shown to SUMOylate APC4 faster than SUMO1 during in *in-vitro* SUMOylation assays, and the authors argued that APC4 is predominately conjugated to SUMO2 (Yatskevich et al., 2021). However, a faster rate of SUMOylation by a given SUMO paralog *in vitro* does not necessarily imply that this is the predominant SUMO paralog attached to APC4 within cells.

All of the IP samples still had a band corresponding to non-SUMOylated APC4 (Figure 7, asterisks). While NEM is an irreversible inhibitor of SENPs, there often is still residual deSUMOylation activity during the process of an IP, and this might explain some deSUMOylation. As I discussed in this thesis (see Section 3.1.3), the APC/C itself sticks non-specifically to beads during IP. I later adjusted my IP procedure to try to decrease this contamination, but this protocol was not used during the SUMOylation assays. For this reason, it is likely that much of the non-SUMOylated APC4 potentially came from APC/C that bound non-specifically to the beads during the IP.

While I was working on this project, my host lab generated HA-SUMO2 and V5-SUMO3 knockin mouse lines. A follow-up experiment could employ APC4-IP of lysates obtained from HA-SUMO2 and V5-SUMO3 interbred mice, and then these lysates could be analyzed by WB with antibodies against V5, HA, and SUMO1 to determine if all of the endogenous SUMO paralogs SUMOylate APC4 in neurons. It would be interesting to collect tissue from various parts of an interbred HA-SUMO2 and V5-SUMO3 knockin mouse line, and determine if different cell types predominately use different SUMO paralogs in order to SUMOylate APC4. The SUMO2 and SUMO3 knockin mice could also be used to determine if certain SUMO paralogs are primarily responsible for SUMOylating APC4 within different regions of the cell. SUMO1 is predominately a nuclear protein (Daniel et al., 2017; Figure 12, SUMO1 blots in Fraction C lanes), but

SUMO2 can be detected in the cytosol (Figure 14 A, HA blot in Fraction C lanes). For this reason, it would be interesting to use the knockin mice to determine if APC4 is attached to different SUMO paralogs within different cellular subcompartments. While a recent study indicates that the MCC-bound Cdc20-activated APC/C is predominately conjugated to SUMO2 based on the structure of the complex, this does not exclude the other paralogs from SUMOylating APC4 when it is bound to Cdh1 or when the complex is not bound to the MCC (Yatskevich et al., 2021).

While this is discussed more in depth in Section 4.1.3, I found that APC4 is SUMOylated in both the nucleus and the cytosol of HEK293 cells, but there was more SUMOylation in the nucleus (Figure 14 B, compare Cytoplasm and Nucleus values in the graph). On the other hand, there was more APC4 SUMOylation in the cytosol of neurons than in the neuronal nucleus (Figure 15, compare the S2 and P1 fractions respectively). Based on the subcellular localization of the SUMO paralogs, I suspect that different SUMO paralogs could be conjugated to APC4 more prominently within different populations of the complex, which are each then localized to different regions of the cell. For example, the cytoplasmic population of APC4 is less likely to be conjugated to SUMO1 than SUMO2 based on the fact that SUMO1 is predominately a nuclear protein (Daniel et al., 2017; Figure 12, SUMO1 blots in C lanes). However, APC4 was identified in a proteomic screen searching for SUMO1 conjugated proteins within the cytosol of neurons (Tirard et al., unpublished), arguing that SUMO1-APC4 conjugates are still found in the cytosol of neurons. For this reason, this issue should specifically be addressed systematically with our novel SUMO knockin mouse lines.

In summary, I showed that all overexpressed SUMO paralogs are able to be conjugated to APC4 (Figure 7, arrows) on lysines 772 and 797 (Figure 8 A and B, APC4 blots). Single SUMO moieties are attached to each separate lysine residues, and the SUMOylation of one residue does not affect the SUMOylation of the other residue. Future studies are required to determine which SUMO paralog is important for SUMOylating APC4 within cells, but studies suggest that both SUMO1 and SUMO2 might be important for this (Cubeñas-Potts et al., 2015; Hendriks et al., 2018; Eifler et al., 2018; Lee et al., 2018; Schimmel et al., 2014; Tirard et al., unpublished).

4.1.2 APC4 SUMOylation is Not Required for the Assembly or the Activation of the APC/C

After identifying the SUMOylated lysine residues on APC4, I next wanted to test if SUMOylation affects the formation or the activation of the APC/C. For this reason I made a substantial effort to test if the wildtype and the SUMOylation-deficient (K772R/K797R) Myc-APC4 constructs are able to integrate into the core complex of the APC/C (Figure 10 A, Myc blot), the Cdh1-activated APC/C (Figure 9 A, arrows), and the Cdc20-activated APC/C (Figure 9 B, arrows). A control experiment with non-tagged APC4 also had similar results to these other experiments (Figure 10 B, APC4 blots). In total, my data indicate that since the SUMOylation-deficient (K772R/K797R) construct can bind both activated APC/C, APC4 SUMOylation does not affect the formation or the activation of the APC/C. Instead, APC4 SUMOylation is likely involved in a step after complex formation and activation. The binding of the activator to the APC/C is tightly regulated and normally deemed sufficient to define the complex activated, so this is the definition used in this study. However, there are some APC/C inhibitors that bind to the activated complex and block its function, such as the MCC (Alfieri et al., 2016). Therefore, all activated APC/C that I detected in this study cannot be assumed to be fully functional (reviewed in Qiao et al., 2016).

Interestingly, I could never detect SUMOylated APC4 within the APC/C in either HEK293 cells (Figure 10 A, APC4 blots) or in cultured neurons (Figure 19, APC4 blot). While I could not conduct IP experiments with NEM in the lysate, I have other data indicating that APC4 SUMOylation is moderately stable even in lysate lacking NEM (Figure 8 B, arrows). For this reason, I suspect that some APC4 should still remain SUMOylated in this experiment, if it is really SUMOylated in the first place. When I conducted IP of a component of the complex, I only was able to detect a small amount of APC4 within the IP samples (Figure 10 A, APC4 blots), even after loading 1/3 of the IP eluate within the lane. Only a small fraction of the total APC4 protein is SUMOylated within cells (Figure 7 A, arrows). Relative to the amount of APC4 detected in lysates (Figure 7 A, APC4 blot), I probably detect too little APC4 within the complex co-IP experiments to be able to see the SUMOylated form of APC4 on the membrane (Figure

10 A, APC4 blots). Therefore, I believe that this most likely is the reason that I could never detect SUMOylated APC4 within the complex. If this experiment was scaled up or if the SUMOylation was somehow enriched, the SUMOylated form of APC4 might be more easily detectable within the complex.

I initially worried that the accumulation of the APC4 construct in the cytoplasm (Figure 11 A, HA and APC4 staining), where the APC4 population is less likely to be SUMOylated (Figure 14 B), could also compromise my ability to detect SUMOylated APC4 within the APC/C. However, this does not seem to be the case, since I still could not detect SUMOylated APC4 in the sample that was transfected with pcDNA3.1- and HA-SUMO2 alone (Figure 10 A, APC4 blot). I also worried that the Myc-tag could affect the amount of complex containing SUMOylated APC4, but I attempted experiments with a non-tagged version too, producing similar results (Figure 10 B, APC4 blots).

Overall my data indicate that most of the APC/C is formed with APC4 in the non-SUMOylated state, and then a small fraction of it is possibly SUMOylated later. The function of this SUMOylation is still unknown, but it likely affects the function of the complex after the complex is formed and activated (Eifler et al., 2018; Lee et al., 2018; Yatskevich et al., 2021). This topic will be discussed in more depth in Section 4.1.6.

4.1.3 Endogenous SUMOylated and Non-SUMOylated APC4 is Localized to the Cytoplasm and the Nucleus in HEK293 Cells and in Cultured Neurons

The endogenous localization of APC4 was never determined previously, but imaging studies indicate that overexpressed APC4 is localized predominately in the nucleus in Arabidopsis (Wang et al., 2012). In the current study, I characterized the endogenous APC4 localization in HEK293 cells and cultured neurons using biochemistry and imaging approaches. While the anti-APC4 antibody seems to be specific for APC4 (Figure 21, first and second panels have APC4 signal in *ANAPC4* conditional knockout cells that do not express Cre), the APC4 antibody is not very sensitive in the detection of APC4 in HEK293 cells and in neuron cultures (Figure 11 A and B, APC4 staining). In HEK293 cells, the APC4 staining was localized in weak punctate structures that filled the whole cell body (Figure 11 A, APC4 signal in EGFP expressing cells). Hippocampal

neuron cultures showed weak staining located in punctate structures that filled the whole cell body, but there also was a signal in the nucleus (Figure 11 B, APC4 signal in the No Transfection sample).

The HEK293 cell imaging data are consistent with what I observed when I fractionated HEK293 cell lysate into cytoplasmic and nuclear fractions, as APC4 was strongly detected in both fractions (Figure 14 A, APC4 blot). I blotted Cell Equivalent samples that basically contained lysate volumes that corresponded to the same number of cells within each fraction (for example 100 nuclei versus cytoplasm from 100 cells), and these samples indicate that there was more APC4 protein expression in the cytoplasm than in the nucleus (Figure 14 A, C lanes in APC4 blot). APC4 was clearly SUMOylated in each of the fractions (Figure 14 A, arrow), but there was more APC4 SUMOylation within the nucleus than the cytoplasm (Figure 14 B, compare Cytoplasm and Nucleus values in the graph). Regardless, these data indicate a role of APC4 SUMOylation in both the cytoplasm and the nucleus of HEK293 cells. They also show that a large proportion of the APC/C in both fractions remains non-SUMOylated (Figure 14 A, 100 kDa band in APC4 blot).

When I fractionated the mouse cortex into different cellular fractions, I again observed that APC4 is present in all cellular fractions (Figure 15, APC4 signal). Interestingly, it was even detected within the Syn (crude synaptosome) and SPM (purified synaptic plasma membrane) fractions. While corresponding bands were weak and could be a contaminant, other studies also found other APC/C components within the PSD: Cdh1 (Pick et al., 2012), APC1, APC7, and APC12 (Distler et al., 2014). While it is not known if SHANK1 is an actual substrate of the APC/C yet, it is enriched in the PSD fraction (Tobaben et al., 2000) and it could actually be a substrate of the APC/C there (Hung et al., 2010; Jarome et al., 2011; Pick et al., 2012). Potential neuronal substrates of the APC/C are discussed more in depth in Section 4.2.5. Similar to what was observed in HEK293 cells (Figure 14 A, C lanes in APC4 blot), there was more APC4 in the cytoplasm than in the nucleus within the cortex (Figure 15, compare APC4 blot in the nuclear P1 and the cytoplasmic S2 fractions).

While I did not add NEM to the lysates during this fractionation experiment, I was still able to detect an intense band that corresponds to the conjugation of one SUMO

moiety to APC4 in the cytosol (Figure 15, S2 fraction and arrow). This was the opposite of what I observed in HEK293 cells, where there was instead an enrichment of APC4 SUMOylation in the nucleus. Nevertheless, APC4 was strongly SUMOylated in both fractions of HEK293 cells (Figure 14 A, C lanes in APC4 blot). Previously my host lab identified APC4 in a screen for SUMOylated proteins within the cytosol (Tirard et al., unpublished), but they never detected APC4 in their screen that used whole cell brain lysate (Tirard and Brose, 2016; Tirard et al., 2012). The fact that APC4 SUMOylation is enriched within the cytosolic (S2) fraction of the cortex but not within the other fractions (Figure 15, APC4 blot) may explain why APC4 was only identified in the proteomic screen for SUMO1 conjugated proteins from the cytosol. Overall my data indicate that APC4 SUMOylation in particular may be important for the regulation of the function of the cytosolic APC/C within cells of the cortex. However, the specific neuronal substrates of the complex that contains SUMOylated APC4 currently is unclear (see Section 4.2.5).

In conclusion, I found that endogenous APC4 is expressed in both the cytoplasm and the nucleus in HEK293 cells (Figure 14 A, APC4 blot) and in neuron cultures (Figure 15, APC4 blots in nuclear P1 and the cytoplasmic S2 fractions). APC4 SUMOylation occurs in both fractions of HEK293 cells, but the nuclear fraction is more heavily SUMOylated (Figure 14 A, arrow). Alternatively, APC4 SUMOylation appears to be enriched within the cytosol of cells from the mouse cortex (Figure 15, arrow). Future studies must address the function of this SUMOylation, as it is likely important for regulating the ubiquitylation of a variety of different substrates in each cell type.

4.1.4 The Promoter Strength Regulates the Localization of Overexpressed APC4

Surprisingly, overexpressed APC4 accumulates outside the nucleus in both HEK293 cells (Figure 11 A, APC4 and HA staining in cells that expressed HA-APC4) and neuron cultures (Figure 11 B, APC4 and HA staining in transfected cells) when driven by the CMV promoter, but its distribution is more similar to the endogenous pattern when the expression is driven by the weaker Synapsin promoter in neuron cultures (Figure 13, HA staining in the infected cells). While endogenous APC4 localization was previously never studied within any cell types, several labs assessed the localization of

overexpressed APC4 constructs (Lee et al., 2018; Wang et al., 2012). In the first study, Flag-tagged APC4 constructs were expressed with a T7 promoter. While no obvious mislocalization was depicted in these images (no intense accumulation of APC4 as seen in Figure 11 A and B, HA staining), these cells did not have a nuclear envelope due to the fact that they were studying the localization during different stages of the cell cycle (Lee et al., 2018). In a second study, GFP-tagged APC4 was overexpressed in Arabidopsis, but the authors did not indicate the promoter used. Their APC4 stain colocalized with the DAPI stain. There seemed to be some accumulation of APC4 around the nucleus, but the accumulated stain appeared to actually be inside the DAPI-stained area of the nucleus instead of outside it (Wang et al., 2012). However, the DAPI stain was strange in these images when I compared them to similar DAPI staining in Arabidopsis (Liu et al., 2018), because most of the signal was located in ring structures that are not typically seen in DAPI-stained cells (Wang et al., 2012). For this reason, I am uncertain to whether their corresponding data can be taken at face value.

I initially worried that the APC4-expressing construct when driven by the CMV promoter was not being transported to the nucleus at all, but my HEK cell fractionation experiments indicated that these Myc-tagged constructs could still enter the nucleus (Figure 12, nuclear fraction in the Myc(r) blot). This mislocalization effect of APC4 accumulating outside the nucleus was most likely due to the nuclear transport machinery being overwhelmed (reviewed in Stewart, 2007). This mislocalized construct was still used for HEK293 cell biochemistry experiments (Figures 7 - 10, 12, 16, and 17). However, the fact that it was mislocalized should not affect the results or conclusions of the APC4 SUMOylation experiment (Figures 7 and 8). In regards to the complex integration experiments, this should also not affect the conclusions that both the wildtype and the SUMOylation-deficient (K772R/K797R) Myc-APC4 constructs can integrate into the APC/C (Figure 9 A and B, arrows; Figure 10 A, Myc blots).

However, the mislocalization of overexpressed APC4 possibly affects my ability to detect SUMOylated APC4 within the APC/C, because it likely changes the proportion of the APC/C within the cell that comes from the nucleus versus the cytoplasm. SUMO is thought to be a predominately nuclear protein (Daniel et al., 2017; Figure 12, SUMO1 blot in Fraction C lanes), so the cytoplasmic population of the overexpressed APC4

construct might not be SUMOylated as efficiently. Additionally, the APC/C within HEK293 cells had less SUMOylated APC4 in the cytosol in general (Figure 14 B, graph), indicating that I likely enriched the non-SUMOylated APC/C in these experiments. When I conducted Cdc27-IP experiments with lysate that did not overexpress APC4, I was still unable to detect SUMOylated APC4 within the IP eluates (Figure 10 B, APC4 blots), indicating that mislocalization is probably not significantly affecting the proportion of SUMOylated APC4 being incorporated into the APC/C. The mislocalization of overexpressed APC4 likely also affected the HEK293 cell ubiquitylation assays that I conducted, but this will be discussed more in depth in Section 4.1.7. All of these mislocalization issues, however, could be avoided in neurons by expressing HA-APC4 using the weaker Synapsin promoter (Figure 13, HA staining in infected cells).

In summary, I found that when I overexpressed APC4 with a stronger promoter, APC4 expression accumulated outside the nucleus (Figure 11 A, APC4 and HA staining in cells that expressed HA-APC4). This mislocalization effect was not observed when I overexpressed APC4 with the weaker Synapsin promoter (Figure 13, HA staining in the infected cells). Altogether, my data indicate that it is important to overexpress APC4 only with a weaker promoter. While this mislocalization probably did not affect my results for the complex integration experiments or the SUMOylation assay, this mislocalization could easily affect the use of these overexpression constructs in experiments that assess the function of APC4 within a cell.

4.1.5 APC4 SUMOylation Does Not Influence the Localization of APC4

I previously showed that APC4 SUMOylation does not influence the formation or the activation of the APC/C (see Section 4.1.2). I next tested whether APC4 SUMOylation influences the localization of APC4. I overexpressed wildtype and SUMOylation-deficient (K772R/K797R) HA-APC4 constructs in cultured neurons using the CMV promoter. While the HA signal accumulated outside the nucleus, there was no difference in the expression pattern of the HA signal between the two constructs (Figure 11 B, HA staining). Similarly, there was no difference in the expression patterns

between wildtype and SUMOylation-deficient (K772R/K797R) Myc-APC4 when I fractionated HEK293 cells into cytoplasmic and nuclear fractions (Figure 12, Myc (r) blots). Finally, there was no difference in the localization when I overexpressed wildtype or SUMOylation-deficient (K772R/K797R) HA-APC4 driven by the Synapsin promoter in hippocampal neuron cultures (Figure 13, HA staining). Altogether my data indicate that the SUMOylation of APC4 does not substantially affect the localization of APC4 in HEK293 cells and cultured neurons. This is consistent with another study that showed that the overexpression of the SUMOylation-deficient APC4 construct did not result in the mislocalization of APC4 during the cell cycle (Lee et al., 2018).

4.1.6 A SUMO Moiety Conjugated to APC4 Within the APC/C Interacts With APC2 to Regulate the Function of the APC/C

APC4 SUMOylation is strikingly stable in lysates that lack NEM (Figure 8 B, arrows), an irreversible inhibitor of SENP cysteine peptidases that induce deSUMOylation. Generally, the Input banding pattern in HA-SUMO2 blots (Figure 8 A and B) indicate a drastic decrease in the amount of total protein SUMOylation between 100 and 170 kDa when NEM is excluded from the lysate (Figure 8, compare HA Input blots in A and B). Hence, it was surprising when I realized how stable APC4 SUMOylation is in the absence of NEM. At times, I could even detect a triplet band in lysates lacking NEM, indicating that APC4 is still bound to two SUMO moieties in these lysates (data not shown). However, the level of SUMOylation did seem to be weaker in these lysates than those that were treated with NEM. I initially thought the most likely explanation for this is that the SUMOylated residues are unable to be accessed by the SENPs, possibly because these residues are partially hidden within the structure of the APC/C.

Recent studies suggest that the SUMOylated residues of APC4 interact with APC2 (Lee et al., 2018; Yatskevich et al., 2021), and the interaction of APC2 with SUMOylated APC4 probably explains why the SUMOylated APC4 residues are not easily accessible to SENPs. While several groups published cryo-EM structures of the APC/C, the C-terminal end of APC4, including the SUMOylated residues, is disordered and was deleted in corresponding studies (Alfieri et al., 2016; Cronin et al., 2015;

Yamaguchi et al., 2016; Zhang et al., 2016). However, another lab recently showed that the SUMOylated APC4 residues likely directly interact with the SIM of APC2, and it was proposed that APC4 SUMOylation could influence the binding of APC2 to the E2 ligase (Lee et al., 2018). In an additional study, it was argued that this SIM in APC2 decreases the amount of APC4 SUMOylation, but it does not affect the function of the complex. The authors instead proposed another site of interaction between APC2 and the SUMO moiety attached to APC4 (Yatskevich et al., 2021). Regardless of the details, the published data indicate that APC4 SUMOylation does not affect the formation or the activation of the complex, but instead affects the interaction between APC4 and APC2 and thereby the function of the complex (Eifler et al., 2018; Lee et al., 2018; Yatskevich et al., 2021). My data are consistent with this model, as they show that the SUMOylation-deficient (K772R/K797R) APC4 construct can integrate into the APC/C (Figure 10 A and B, APC4 and Myc blots) and bind to both of the activators (Figure 9 A and B, arrows), which indicates that the SUMOylation of APC4 is involved in a step after the activation of the complex.

Due to the fact that I could never detect SUMOylated APC4 within the APC/C, it seems likely that only a small fraction of the complex ever contains SUMOylated APC4 at one time (Figure 9 A and B, arrows; Figure 10 A and B, APC4 and Myc blots). This argues for a model where APC4 SUMOylation affects the ubiquitylation of only a subset of substrates or possibly even helps speed up the ubiquitylation rate to induce the faster degradation of a substrate population when this is required (Eifler et al., 2018; Yatskevich et al., 2021). One proposed model suggests that the SUMOylation of APC4 changes the conformation of the APC/C and allows for a more efficient binding of the E2 ligase to the complex (Lee et al., 2018). Recently, another paper argued against such a model and suggested that APC4 SUMOylation influences the binding of the Cdc20-activated complex to the MCC (a complex that inhibits the Cdc2-activated APC/C), thereby regulating the activity of the APC/C (See Figure 4; Yatskevich et al., 2021). Alternatively, APC4 SUMOylation might instead influence the ability of the APC/C to add ubiquitin chains to substrate proteins or the overall stability of the binding of the substrate and the E2 ligase or other APC/C binding proteins to the complex. Further

studies are required to fully elucidate the function of APC4 SUMOylation in the APC/C and its ability to ubiquitylate substrates.

All these issues notwithstanding, APC4 SUMOylation has been suggested to regulate the ubiquitylation of some but not all substrates of the APC/C (Eifler et al., 2018; Lee et al., 2018; Yatskevich et al., 2021). Initially APC4 SUMOylation was shown to affect the ubiquitylation of KIF18B and Hsl1, but the effect was more profound with KIF18B (Eifler et al., 2018). However, Hsl1 ubiquitylation is not affected by the SUMOylation of the Cdc20-activated APC/C (Yatskevich et al., 2021), so the increased ubiquitylation of Hsl1 by SUMOylation of the complex seemed to only involve the Cdh1-activated APC/C (Eifler et al., 2018). Additional *in vitro* ubiquitylation assays with the Cdc20-activated APC/C showed that SUMOylation does not drastically influence the ubiquitylation of Securin or Cyclin B1, but the ubiquitylation did partially increase when the MCC was also included in the assay. Altogether, these data indicate a model where the affinity of binding between the MCC and the APC/C is reduced but not eliminated by APC4 SUMOylation. The corresponding structural data indicate that the addition of the SUMO moiety likely shifts the position of APC2 within the complex. The addition of this SUMO requires the transition of the MCC-Cdc20-activated APC/C from a completely closed state to a more functional state that is only partially blocked by the MCC. Unfortunately, it is not known how adding two SUMO moieties would affect the structure and function of the complex. The corresponding data were obtained from *in vitro* ubiquitylation assays that lacked the complex responsible for disassembling the MCC (Yatskevich et al., 2021). If this complex that disassembles the MCC had been incorporated into the study, the amount of ubiquitylation detected when APC4 was SUMOylated might have increased in this assay, perhaps blocking the activity of the MCC more efficiently. This should be addressed specifically in the future. Interestingly the MCC components are expressed within neurons, but their function there is unclear at this time (Meng et al., 2012; Yang et al., 2017).

While APC4 SUMOylation seems to regulate the inhibition of the Cdc20-activated APC/C by the MCC (Yatskevich et al., 2021), this SUMOylation is likely also affecting other aspects of the function of the complex for several reasons. First, the ubiquitylation of Hsl1 increased when the Cdh1-activated complex was SUMOylated (Eifler et al.,

2018). Second, the Cdh1-activated complex is more likely to be the SUMOylated complex in the nucleus, where there is a high level of APC4 SUMOylation in HEK293 cells (Figure 14 A and B, APC4 blot and graph). Finally, neurons have a lot of APC4 SUMOylation (Figure 15, S2 fraction) but very little Cdc20 expression, so the Cdh1-activated APC/C is more likely to be at least partially SUMOylated within neurons (Gieffers et al., 1999; Kim et al., 2009). A recent paper argued that the size of SUMO2 is better fit to function within the Cdc20-activated APC/C than SUMO1. SUMO1 is predominately a nuclear protein (Figure 12, SUMO1 blots; Daniel et al., 2017) and is conjugated to APC4 in neurons (Tirard et al., unpublished). It is possible that SUMO1 is more involved in SUMOylating the Cdh1-activated APC/C while SUMO2 is more involved in regulating the Cdc20-activated complex, but this question needs to be addressed further during future studies.

There is one huge caveat with the original paper that showed that SUMOylated APC4 binds to APC2 (Lee et al., 2018), and this is the fact that adding a C-terminal tag to mouse APC4 seemed to affect the folding of APC4 in my hands. I initially generated both N- and C-terminal HA-APC4 constructs, and I always detected a strong band of an appropriate size in the HA blots of lysates that overexpressed these constructs (data not shown). While the APC4 blots showed an expected increase in APC4 expression when the N-terminally tagged construct was expressed, the expression of the C-terminally tagged APC4 was very low (data not shown). The anti-APC4 antibody I used a polyclonal antibody that is directed to the C-terminus of APC4, so I suspected that the antibody was no longer able to detect the C-terminally tagged APC4 construct. Interestingly, I never observed similar issues with the SUMOylation-deficient (K772R/K797R) Myc-APC4 construct (Figure 10 A, Inputs in the APC4 and Myc blots), suggesting that mutating lysines 772 and 797 in the C-terminus of APC4 did not drastically impact the structure of the protein like the C-terminal HA tag did. While I did not study the cause of the issues with the C-terminal HA construct in depth, I worry that tagging the C-terminus of APC4 with SUMO potentially affects the folding of APC4, which in turn likely affects the binding of APC4 to other components of the APC/C.

Recently, another paper argued in opposition to this original paper and suggested that the SIM site of APC2 is not required for the function of the complex, but

instead affects the efficacy by which APC4 becomes conjugated to SUMO2 (Yatskevich et al., 2021). This would be consistent with my finding that tagging the C-terminus of APC4 with HA likely affects the folding of APC4 (data not shown), and the described binding to the SIM of APC2 could be an artifact to APC4 not being folded correctly (Lee et al., 2018). However, this original paper did show that mutating the SUMOylation sites of APC4 or the SIM motif of APC2 both induces a dramatic increase in the length of metaphase and the observed phenotype was similar for both mutants (Lee et al., 2018). Hence, these two papers are in disagreement as to how this particular SIM site on APC2 operates and whether it is important for regulating the activity of the APC/C (Lee et al., 2018; Yatskevich et al., 2021). It may be that this particular SIM on APC2 interacts with a SUMO moiety on APC4 when the complex is not bound to the MCC or when it is instead activated by Cdh1.

SUMOylation was initially found to be required for the ubiquitylation of substrates by the yeast APC/C, but the SUMOylated components of the APC/C were not identified. While corresponding studies only covered a few substrates of the yeast complex, they showed that SUMOylation affects the level of ubiquitylation of all substrates tested, indicating that SUMOylation affects the overall function of the yeast APC/C (Dieckhoff et al., 2004). Unfortunately, yeast APC4 is not even an ortholog of mammalian APC4, so the SUMOylated lysines are not conserved in yeast (Eifler et al., 2018). Further studies are required in yeast to determine if APC4 is the SUMOylated component of the complex that is required for the activity of the APC/C.

In conclusion, the papers utilizing a mammalian model within this field argue that the SUMOylation of APC4 only affects the ubiquitylation of a subset of the substrates of the APC/C (Eifler et al., 2018; Lee et al., 2018). While APC4 SUMOylation affects substrates of both complexes (Eifler et al., 2018; Yatskevich et al., 2021), it is unknown yet if APC4 SUMOylation affects the levels of ubiquitylation of all substrates of the Cdh1-activated APC/C or only a subset of them. APC4 SUMOylation impacts Hsl1 ubiquitylation directly when it is ubiquitylated by the Cdh1-activated APC/C (Eifler et al., 2018) but not the Cdc20-activated APC/C (Yatskevich et al., 2021). Further studies are required to elucidate how the SUMOylation of APC4 impacts the ubiquitylation of all of the substrates of the APC/C. It seems likely that targeting APC4 SUMOylation and its

interaction with APC2 could potentially provide a promising drug target, especially if it can affect the ubiquitylation of only a subset of the APC/C substrates. As I mentioned earlier, there is a disagreement in the literature about the interaction sites between SUMO and APC2 (Eifler et al., 2018; Yatskevich et al., 2021), and this could be explained by SUMO binding to different regions of APC2 depending on the activation pathway or other post-translational modifications of the complex. If this were the case one could for example try to develop drugs that interfere with the interaction sites between SUMO and APC2 when the complex is bound to the MCC. These drugs likely would not affect the other APC/C within the cell when the APC/C does not bind the MCC, but they could potentially be used to slow down the rate of cell division within cancer cells by stabilizing the inactivation of the APC/C by the MCC.

4.1.7 The Development of Ubiquitylation Assays to Test the Impact of APC4 SUMOylation on the Function of the APC/C

I attempted to develop two different approaches to study the substrates and the function of the neuronal APC/C. In the first approach, I performed Cdc27-IP and then WB of IP eluates with antibodies against neuronal substrates of the APC/C. Unfortunately I could not detect NEUROD2 or SNANK1 within the IP eluates (Figure 19, NEUROD2 and SHANK1 blots). I think this is most likely due to the fact that these proteins are actually not substrates of the APC/C in the system that I used for this study. NEUROD2 does not seem to be a substrate of the neuronal APC/C at all (Figure 24 G and H, NEUROD2 blot and graph; Malureanu et al., 2010). SHANK1 is probably at best an activity-dependent substrate of the APC/C (Jarome et al., 2011), but this should be studied further. Once a bona fide APC/C substrate is identified in neuron cultures, I can test to see if this approach works. However, some sort of ubiquitylation assay would still be required in addition to this, because this approach would not be able to distinguish between substrates and other APC/C binding proteins (Man et al., 2008; Wang et al., 2008). However, this approach could be very beneficial as fast method to screen candidate substrates if it worked and to possibly elucidate the effects of APC4 SUMOylation on the binding of the complex to the substrates.

In the second approach, I overexpressed the substrates and wildtype or SUMOylation-deficient (K772R/K797R) Myc-APC4 constructs in HEK293 cells in order to study the ubiquitylation of these substrates by WB. I found no difference in the amounts of ID2 (Figure 16, ID blots) or GluR1 (Figure 17, GluR1 blots) ubiquitylation in these assays, but I was not sure if the assay would be sensitive enough to detect changes for several reasons. First, the mislocalization and the overexpression itself of APC4 could affect the results of the ubiquitylation assay. While this is not well studied, the activated APC/C is likely functioning in different regions of the cell and ubiquitylating different sets of proteins in each subcompartment (Jörgensen et al., 1998; Melloy and Holloway, 2004; Topper et al., 2002; Tugendreich et al., 1995). Due to the fact that I had little of the overexpressed APC4 constructs getting into the nucleus (Figure 12, Myc (r) blots), it is probably difficult to detect changes in the ubiquitylation of nuclear substrates like ID2 in this assay especially (Figure 16, ID blots; Figure 17, GluR1 blots). Second, I thought that some wildtype APC/C would still exist, and it could still ubiquitylate the substrate and mask my ability to see any effects due to the fact that the wildtype APC4 is not depleted. Finally, I was not sure how stable the APC/C is in cells typically and how long it takes to replace most of the existing complex with the SUMOylation-deficient (K772R/K797R) Myc-APC4 construct. Overall it seems like APC4 needs to remain in complex consistently to avoid degradation that quickly happens when APC4, APC5, or APC1 are depleted (Clark and Spector, 2015; Thornton et al., 2006; Tran et al., 2010). From my data in neuron cultures, I concluded that APC4 has a half-life of around 1.8 days (Figure 20 C, middle graph and legend), which indicates that the APC4 could remain within the complex for longer periods of time. Hence, I am not sure how much of the APC/C was actually replaced in this experiment with the SUMOylation-deficient (K772R/K797R) Myc-APC4 construct, since the cells were lysed only two days after the transfection (Figure 16, ID blots; Figure 17, GluR1 blots).

While I attempted to develop two different approaches to study the substrates and the function of the neuronal APC/C, these experiments were confounded by the fact that I am unsure which of the proposed neuronal substrates of the APC/C are bona fide substrates. For this reason, I was unable to determine if the approaches described below worked in principle. For this reason, I did not focus further on these approaches. I

instead decided that it would be better to focus on identifying the function of the neuronal APC/C using an *ANAPC4* knockout mouse line, which then could be rescued with the SUMOylation-deficient (K772R/K797R) HA-APC4 constructs in order to determine the function of APC4 SUMOylation in the context of the mutant phenotypes.

4.1.8 The Interplay of APC4 SUMOylation And Phosphorylation in Regulating the Function of the APC/C

The APC/C contains a complex network of different residues that are phosphorylated during different stages of the cell cycle. The APC/C contains over 120 different phosphorylated residues, and at least 68 of these are only phosphorylated when the complex is activated by Cdc20, indicating that the phosphorylation pattern of the APC/C might be important for the function of the complex (Qiao et al., 2016). Only one phosphorylation site on APC1 is actually required for the activation of the complex by Cdc20, suggesting that this vast phosphorylation network is not actually involved in the activation of the complex, but instead is potentially involved in regulating the function of the APC/C (Qiao et al., 2016). APC4 itself contains at least three different residues that are phosphorylated (Kraft et al., 2003; Qiao et al., 2016; Yatskevich et al., 2021), and two of these are located adjacent to a SUMOylation site (Eifler et al., 2018; Yatskevich et al., 2021). Human APC4 serine 779 is phosphorylated during mitosis specifically (Kraft et al., 2003; Qiao et al., 2016), and serine 777 is phosphorylated within the Cdc20-activated APC/C (Qiao et al., 2016).

The attachment of a SUMO moiety to lysine 772 of APC4 seems to be affected by the phosphorylation of two neighboring serine residues on APC4 (Eifler et al., 2018). When serines 777 and 779 were mutated in human cell lines, the amount of APC4 SUMOylation at lysine 772 was diminished, indicating that there is interplay between the phosphorylation and the SUMOylation of APC4 (Eifler et al., 2018). Unfortunately, the authors did not seek to further understand this connection. Even in their subsequent paper they only showed that artificial phosphorylation of the APC/C increased the level of APC4 SUMOylation *in vitro* (Yatskevich et al., 2021). Further studies are required to understand the interplay between the sites of phosphorylation and SUMOylation. One of

the major problems in their argumentation (Eifler et al., 2018) is that the authors do not determine if the total amount of APC4 SUMOylation is altered when the phosphorylation sites are alone mutated. Second, they did not assess if mutating the phosphorylation sites on APC4 alters the SUMOylation of APC4 on lysine 798. Finally, it would be interesting to determine if either a single or a double mutation of lysines 772 and 798 (the SUMOylation sites) on APC4 alters the amount of APC4 phosphorylation at all.

While the function of APC4 phosphorylation has not been elucidated, APC4 SUMOylation is required for the proper timing of metaphase and some functions of the APC/C (Eifler et al., 2018; Lee et al., 2018). For this reason, further studies are required to fully understand the function and the interplay between APC4 phosphorylation and SUMOylation. The targeting of these sites could potentially be an excellent drug target, especially if these modifications only impact the ability for the APC/C to ubiquitylate a subset of its substrate proteins (Eifler et al., 2018; Lee et al., 2018; Yatskevich et al., 2021). The development of such drug targets may be of particular importance in the treatment of neurological disorders such as ischemia (Zhang et al., 2019), pain disorders (Li et al., 2020; Tan et al., 2015), and Alzheimer's disease (Fuchsberger et al., 2016), as these disorders are characterized by the loss of Cdh1 expression (Fuchsberger et al., 2016; Li et al., 2020; Tan et al., 2015; Zhang et al., 2019). The development of APC/C drug targets that only affect the ubiquitylation of a subset of substrate proteins is preferred over a target that would affect more APC/C activity, as these drugs would likely have fewer side effects.

4.2 Determining the Function of APC4 In Neuron Cultures

4.2.1 APC4 Expression is Depleted in Primary Cortical Neuron Cultures Generated From *tm1c/tm1c* Conditional *ANAPC4* Knockout Mice

The APC/C is well known for its function in regulating the cell cycle (reviewed in Peters, 2006; reviewed in Sivakumar and Gorbsky, 2015; Pfleger and Kirschner, 2000; Robbins and Cross, 2010), but its function in non-dividing cells like neurons is much less well understood (reviewed in Cajigas et al., 2010). Surprisingly, various components of the

complex are highly expressed in neurons (Gieffers et al., 1999), indicating that the APC/C has a function in these non-dividing cells. Over the past few decades, multiple potential neuronal substrates of the APC/C were identified in neurons (reviewed in Cajigas et al., 2010). However, the function of the complex has not been systematically studied in neurons, and most of the studies conducted to date failed to definitively show that the proposed substrates are ubiquitylated by the APC/C (see Section 4.2.5).

For this reason, I sought to develop a method to study the function of the APC/C in neurons by specifically knocking out or knocking down *ANAPC4*. I picked *ANAPC4* in particular for this study for several reasons. First, very little is known about the function of APC4 in the complex, beyond the fact that it is a core component of the complex and required for cell cycle progression (Eifler et al., 2018; Furuta et al., 2000; Lee et al., 2018; Yamashita et al., 1999). Second, the stability several proteins within the complex are lost when *ANAPC4* is deleted (Clark and Spector, 2015; Thornton et al., 2006; Tran et al., 2010), implying that the complex is not functional at all when APC4 expression is lost. Finally, the development of a method to deplete APC4 from neurons would enable further studies on the function of APC4 SUMOylation in neurons. Unfortunately, I ran into multiple difficulties developing a method to deplete APC4 protein expression in cultured neurons, but I finally obtained a conditional *ANAPC4* knockout mouse line towards the end of my thesis work that I used to study the function of APC4 within neuron cultures.

I first showed that when neurons generated from *tm1c/tm1c* conditional *ANAPC4* knockout mice were infected with a virus that expressed Cre, APC4 protein expression was depleted (Figure 20 A - D, compare cultures infected with Cre to either the non-infected or NLS RFP-infected cultures). The mouse line that I obtained had an insertion of DNA sequences between exons 2 and exons 4, but these insertions did not affect the overall expression of APC4 in *tm1c/tm1c* and *tm1c/+* mice (Figure 20 E, APC4 expression). Hence, the expression of Cre NLS RFP and the subsequent removal of exon 3 in the *ANAPC4* gene in these cells was responsible for the loss of expression of APC4 in the infected knockout neurons (Figure 20 A - D, APC4 blots and graphs). Interestingly, the depletion of APC4 occurred more quickly in cortical neuron cultures (Figure 20 D, compare Cre NLS RFP to NLS RFP) than in hippocampal neuron cultures

(Figure 20 B, compare Cre NLS RFP to NLS RFP). In one pilot experiment, I found that there was very little Cre expression by DIV3 within infected hippocampal neuron cultures (data not shown). Altogether these data indicate that the rate of APC4 depletion is different between cortical (Figure 20 D, compare Cre NLS RFP to NLS RFP) and hippocampal (Figure 20 B, compare Cre NLS RFP to NLS RFP) neuron cultures, and this is likely in some extent due to the fact that Cre was expressed more slowly within hippocampal neuron cultures (data not shown).

I found that the half-life of APC4 is 1.8 days in cortical neuron cultures (Figure 20 C, second panel and figure legend), so the depletion of APC4 happens fairly fast in these neurons. While the APC4 half-life determined is an estimate of the half-life during the first 7 days of development (Figure 20 C, second panel and figure legend), the half-life seems like it will actually change over time with the age of the cultures. This is evident by the fact that both APC4 and APC5 expression levels drop drastically over time, which included an even larger drop in the expression of APC4 between DIV3 and DIV5 (Figure 18 A and B, observe the APC4 and APC5 expression over time). A prior study used a mass spectrometry approach to determine the half-life of proteins in different types of primary cultures, and found that APC4 had a half-life of around 1.7 days in mouse embryonic neurons. Monocytes and B cells had APC4 half-lives of around 1.3 days and 2.5 days respectively. The authors were also able to determine the half-life of several other components of the APC/C in neurons, which included APC1 (2.0 days), APC2 (1.6 days), APC5 (2.6 days), and APC7 (1.1 days). The calculated half-life for APC5 (Mathieson et al., 2018) is similar to the data that I observed during my time course, as a little less than half of the APC5 expression remained by DIV5 (Figure 20 C, APC5 expression in the top and bottom panels).

My data also matched (Figure 20 C, observe both the APC4 and APC5 expression) previous observations made upon APC1, APC4, or APC5 knockdown in fibroblasts. While the authors had a little residual APC4 left after 4 days, they never determined the percentages of cells that expressed the shRNA (Clark and Spector, 2015), and different cell types seem to have slightly different APC4 half-life (Mathieson et al., 2018). With the exception of APC/C activators that can have a half-life as low as 40 minutes (Yen and Yang, 2010), the core components of the APC/C seem to be more

stable in a variety of different cell types (Mathieson et al., 2018). This overall is consistent with the model in the field that poses that the APC/C remains assembled most of the time, but post-translational modifications and the binding of additional proteins to the APC/C help to regulate the activity of the complex (Kraft et al., 2003; Qiao et al., 2016; Robbins and Cross, 2010; Pfleger and Kirschner, 2000; Zachariae et al., 1998).

Altogether, my data suggested that I could utilize *tm1c/tm1c* conditional *ANAPC4* knockout mice infected with a virus that expressed Cre to knockout APC4 expression in cortical neuron cultures by DIV5 (Figure 20 C, APC4 blot). During the rest of this study, I used these cortical cultures to study how *ANAPC4* knockout affects the morphology (see Section 4.2.4) and the biochemistry of neurons (see Sections 4.2.3 and 4.2.5).

4.2.2 APC4 Depletion Results in the Partial Degradation of APC5 Within Neuron Cultures

HCMV viral infection results in the inactivation of the APC/C, and this likely involves the degradation of APC4, APC5, and APC1 in infected cells (Tran et al., 2010). While the precise mechanism by which the virus induces the degradation of these proteins within a cell is undetermined, the depletion of any one of these three proteins within a cell line results in the parallel degradation of all of these proteins (Clark and Spector, 2015). The authors speculated that all of these proteins are marked for degradation if any one of them is missing from the APC/C (Clark and Spector, 2015; Thornton et al., 2006; Tran et al., 2010). My data with neuron cultures is consistent with this notion (Clark and Spector, 2015; Thornton et al., 2006; Tran et al., 2010), as I found that APC5 expression is depleted when *ANAPC4* is knocked out in primary hippocampal (Figure 20 A and B, APC4 and APC5 blots and graphs) and cortical neurons (Figure 20 C, APC4 and APC5 blots and graphs). While the loss of APC4 expression seems to induce a loss in APC5 expression (Figure 20 C, APC4 and APC5 blots and graphs), Cdc27 expression is not affected by the knockout of *ANAPC4* (Figure 24 A, Cdc27 blot). Thus, the effect on APC4 and APC5 stability in neurons does not affect all proteins that constitute the APC/C, similar to what was observed with other proteins in the complex in

fibroblasts (Clark and Spector, 2015). Interestingly, there was always some residual APC5 expression left in neuron cultures upon APC4 knockout (Figure 20 A - C, APC5 expression and graphs), while prior studies on depleted APC4 in fibroblasts showed stronger depletion of APC5 four days after transfection (Clark and Spector, 2015). While this is probably just due to experimental variations, there is some evidence that the half-life of APC4 is longer than the half-life of APC5 in some cell types and that the reverse relationship is seen in other cell types (Mathieson et al., 2018).

It would be interesting to rescue the knockout in the *tm1c/tm1c* conditional *ANAPC4* knockout neuron cultures with a SUMOylation-deficient (K772R/K797R) HA-APC4 construct in order to see if this construct is able to fully rescue the loss of APC5 expression that is typically observed when APC4 is depleted (Figure 20 A - C, APC5 blots). I suspect that it would at least partially rescue it, since the SUMOylation-deficient (K772R/K797R) Myc-APC4 mutant is able to fully integrate into the APC/C (Figure 9 A and B, HA and Myc blots respectively; Figure 10 A, Myc blots) and purified complex that contains a SUMOylation-deficient APC4 can ubiquitylate substrates in an *in vitro* ubiquitylation assay (Eifler et al., 2018). However, this still needs to be addressed specifically, as this mutation could still affect protein-protein interactions and therefore affect the stability of the complex.

In summary, I showed that when I knockout *ANAPC4*, I loose the expression of APC5 within neuron cultures. Due to the fact that the expression of APC4 and APC5 is basically eliminated (Figure 20 B - D, APC4 and APC5 blots and graphs) and that the expression of APC4 is required for the proper function of the APC/C (Eifler et al., 2018; Furuta et al., 2000; Lee et al., 2018; Yamashita et al., 1999), the APC/C is probably not functional in *ANAPC4* knockout neuron cultures. This enabled me to use these cultures to study the function of APC4 and the APC/C in general in primary neuron cultures generated from conditional *ANAPC4* knockout mice.

4.2.3 ID1 Is Not a Direct Substrate of the APC/C, but Its Expression Is Instead Regulated Downstream of the APC/C

ID1 is thought to normally be polyubiquitylated and degraded constantly, keeping ID1 levels low. The E3 ligase responsible for this polyubiquitylation is not known. While several studies indicated that ID1 might be ubiquitylated by the APC/C (Kim et al., 2009; Man et al., 2008; Wang et al., 2008), the picture is not clear and complicated by the fact that ID1 also seems to bind to and regulate the activity of APC/C (Figure 25; Man et al., 2008; Wang et al., 2008). The main bit of evidence that supports the notion that Cdh1 might be a substrate too is the fact that there are two different sites of interaction between Cdh1 and ID1 that seem to both be used separately from each other; these include the C-terminus of ID1 and the typical D box motif that is normally used by the Cdh1-activated APC/C to bind to and ubiquitylate substrates (Man et al., 2008). If ID1 is in fact a substrate of the APC/C, I would expect that it would accumulate when *ANAPC4* is knocked out in cultured neurons. However, I found that ID1 expression is instead drastically reduced (Figure 24 B and C, ID1 blot and graph), which implies that ID1 is not a physiological substrate of the APC/C in primary cortical neurons (Figure 24 B and C, ID1 blot and graph). An *in vitro* ubiquitylation assay would be helpful to confirm that ID1 is actually ubiquitylated by the APC/C, but this surprisingly was not published to date.

ID1 is continuously ubiquitylated and degraded in cells by an E3 ubiquitin ligase. My data indicate that this E3 ligase is not the APC/C within cortical neuron cultures (Figure 24 B and C, ID1 blot and graph), implying that the actual E3 ligase responsible for ID1 ubiquitylation remains unknown. When ID1 expression is required in a cell, it is stabilized by USP1, an enzyme that removes ubiquitin chains from ID1 (Jung et al., 2016; Mistry et al., 2013). USP1 itself is a substrate of the Cdh1-activated APC/C (Cataldo et al., 2013; Cotto-Rios et al., 2011). Cancer cells often express high levels of both USP1 and ID1, showing again that the expression of these two proteins is interconnected (reviewed in García-Santisteban et al., 2013; reviewed in Zhao et al., 2020). While I did not assess USP1 expression itself, I hypothesize that its expression accumulates in *ANAPC4* knockout neuron cultures, due to the fact that it is a substrate

of the APC/C (Cataldo et al., 2013; Cotto-Rios et al., 2011). As I will discuss further in Section 4.2.4, depletion of USP1 results in a decrease in the number of primary neurites extending from the soma of neurons. While the authors did not analyze the neuron morphology when USP1 is overexpressed (Anckar and Bonni, 2015), these neurons will likely have an increase in the number of primary neurites. Surprisingly, I too found an increase in the number of primary neurites when I knocked out *ANAPC4* (Figure 23 B and C), so future studies should determine if the levels of USP1 are also affected. However, the increased expression and activity of USP1 should induce an accumulation of ID1, even if ID1 is also a direct substrate of the APC/C. This is the opposite of what I observed (Figure 24 B and C, ID1 blot and graph), indicating that there are problems with the current model in the field.

The most likely explanation for what occurs is that there is another E3 ligase responsible for the ubiquitylation of ID1, and the activity of this E3 ligase increases in response to the increased expression of another substrate of the APC/C. This E3 ligase could either be a direct substrate of the APC/C or it may be a downstream target of an APC/C substrate. These types of feedback loops are commonly used to regulate the activity of the APC/C, and the most famous example of this is the Cdh1-activated APC/C function in ubiquitylating Cdc20 (Robbins and Cross, 2010; Pfleger and Kirschner, 2000). If the model that I propose is correct, this E3 ligase is activated by the accumulation of an unknown APC/C substrate, and this activation results in the increase of ID1 ubiquitylation and the subsequent loss of ID1 protein expression. USP1 would need to deubiquitylate ID1 at a higher rate, but the final protein level would depend on the simultaneous rates of ID1 ubiquitylation and deubiquitylation. According to my data, the ubiquitylation rate is faster within cortical neurons. While I would first need to confirm that USP1 protein expression is increased when I knockout *ANAPC4* in cortical neuron cultures, this model could be partially confirmed by knocking down USP1 in *ANAPC4* knockout cells. I would expect to observe a decrease in the expression levels of ID1 in this case.

Alternatively the decreased ID1 protein levels could result from changes in the transcription or translation of ID1 in cells that lack *ANAPC4*. The signaling pathways themselves also could be entirely different within neurons, as the ID1 protein regulation

pathway was only deduced in dividing cell lines. While I gave a few ideas that may explain my results, there are many different possibilities that could explain my data, and further studies are required to really understand why ID1 expression is depleted when *ANAPC4* is knocked out in cortical neurons (Figure 24 B and C, ID1 blot and graph).

ID1 associates with both Cdh1 and Cdc20 (Man et al., 2008; Wang et al., 2008), and there is growing evidence that ID1 regulates the activation of both the Cdh1-activated APC/C and Cdc20-activated APC/C (Figure 25; Wang et al., 2008). The C-terminus of ID1 in particular is important for the binding of Cdh1, resulting in the activation of the Cdh1-APC/C and the degradation of substrates like Aurora A (Man et al., 2008). The fact that Aurora A and ID1 are not physically associated with each other in the complex (Man et al., 2008) supports a model where ID1 helps to inhibit the binding of Cdh1 to the APC/C (Figure 25). This model is supported by the fact that ID1 overexpression results in a decrease in the association between Cdh1 and Aurora A (Man et al., 2008). The following substrates have been implicated in this pathway downstream of ID1: Cyclin B1, Plk1, Aurora A, Cdc20, SKP2, and Survivin (Figure 25; Man et al., 2008; Whitehurst et al., 2008). At another stage of the cell cycle, ID1 binds RASSF1A, allowing for the activation of the complex by Cdc20 (Chow et al., 2012; Wang et al., 2008) and the resulting degradation of CyclinB1 and Securin (Figure 25; Wang et al., 2008). Cdc20, RASSF1A, and ID1 are physically associated with each other and the association of these proteins into a complex inhibits the activation of the APC/C by Cdc20 (Figure 25; Chow et al., 2012; Wang et al., 2008). Aurora A phosphorylation of RASSF1A induces the degradation of RASSF1A and helps to induce the switch from the Cdh1-activated APC/C to the Cdc20-activated APC/C and the subsequent progression of the cell cycle (Figure 25; Chow et al., 2012). My data and the other published data to date in general fit this proposed model, but the role of the APC/C in ubiquitylating ID1 itself is questionable based on the current evidence (Figure 25; Figure 24 B and C, ID1 blot and graph; Chow et al., 2012; Man et al., 2008; Wang et al., 2008; Whitehurst et al., 2008).

None of my data from neuron cultures generated using the conditional *ANAPC4* knockout mouse line (Figure 23 F, G and H; Figure 24 B and C, ID1 blot and graph) resemble the data obtained by in previous studies on ID1 (Kim et al., 2009). First, my

data indicate that ID1 is not a substrate of the Cdc20-activated APC/C, as ID1 expression is depleted instead of stabilized in the knockout cells (Figure 24 B and C, ID1 expression in Cre NLS RFP and NLS RFP). Second, it was suggested previously that this pathway regulates dendrite length and the number of branch points in dendrites of DIV5 neurons. Interestingly, the knockdown of either Cdc20 or APC2 resulted in a decrease in the length of dendrites, but this was not seen in the Cdh1 knockdown (Kim et al., 2009). Unlike these results, I did not detect any significant changes in the length of neurites or the total number of branches upon *ANAPC4* knockout (Figure 23 D - H, compare Cre NLS RFP to NLS RFP). Thus, the model that was previously published to explain the interplay between ID1 and the neuronal Cdc20-activated APC/C (Kim et al., 2009) should be modified to better incorporate the data found in other cell types (Figure 25; Chow et al., 2012; Man et al., 2008; Wang et al., 2008) and my data (Figure 24 B and C, ID1 expression in Cre NLS RFP and NLS RFP). Then this model must then be confirmed within neurons. While Cdc20 does bind to ID1 using a D box, a site normally used by the APC/C, the simultaneous binding of both of these proteins to the rest of the APC/C was never confirmed (Kim et al., 2009; Lasorella et al., 2006). The data shown in these studies are consistent though with the proposed model developed based on other cell types (Figure 25; Chow et al., 2012; Man et al., 2008; Wang et al., 2008). From the point of view of this neuronal study (Kim et al., 2009) and the model from other cell types (Figure 25; Chow et al., 2012; Wang et al., 2008), ID1 depletion results in the loss of ID1 binding to RASSF1A, freeing the binding of Cdc20 to the APC/C (Figure 25), and the activation of the APC/C. This activation of the APC/C then results in increased degradation of an unidentified substrate that controls dendritic grown. Other problems with this model will be discussed further in Section 4.2.4 when I discuss my morphology data.

In summary I found that ID1 expression levels were depleted when *ANAPC4* was knocked out in neuron cultures (Figure 24 B and C, ID1 expression in Cre NLS RFP and NLS RFP). The full mechanism of how this works is not well understood, but the current proposed model is described in Figure 25. The fact that ID1 protein expression is decreased in neuron cultures depleted of APC4 will be of interest to the cancer research field, as identifying a mechanism to deplete ID1 expression seems to be a 'hot topic'

there (Mistry et al., 2013). Further studies elucidating the mechanism by which APC4 depletion results in the loss of ID1 expression will improve our understanding of how ID1 protein expression is regulated, and it may enable the development of novel drug targets that affect ID1 protein stability. While this is not well studied currently, this information could also potentially shed light on new treatments for neurological disorders (Lee et al., 2015; reviewed in Chen et al., 2020).

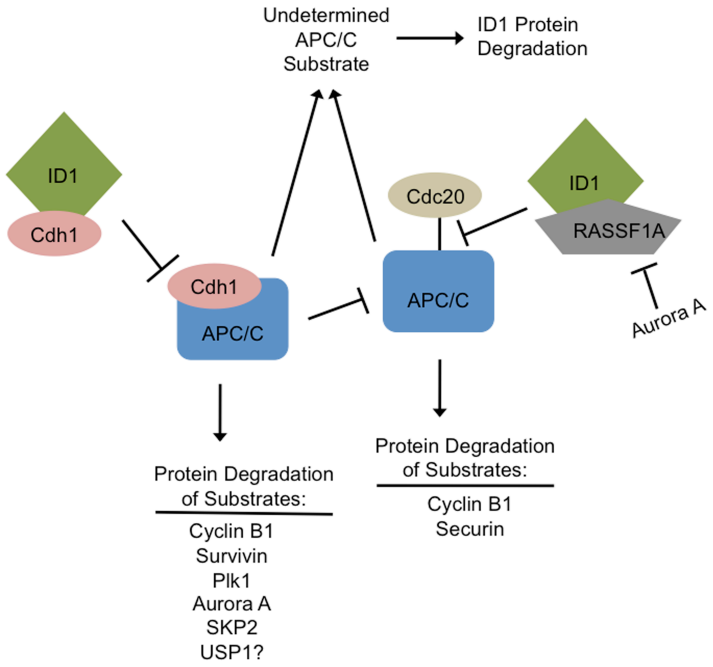

Figure 25. ID1 Regulates the Activation of the APC/C. ID1 (Green) binds to both Cdc20 (tan) and Cdh1 (pink) during the cell cycle, where it helps to regulate the activation of the APC/C (blue). ID1 (green) and RASSF1A (gray) together bind Cdc20 (tan), inhibiting it from activating the complex (blue), where it is proposed to ubiquitylate Cyclin B1 and Securin. Alternatively, ID1 (green) binds to Cdh1 (pink) and inhibits the activation of the APC/C by Cdh1. This then blocks the ubiquitylation of Cyclin B1, Survivin, Plk1, Aurora A, SKP2, and possibly USP1. USP1 is known to regulate the deubiquitylation of ID1. While ID1 is constantly ubiquitylated and degraded, the E3 ubiquitin ligase involved in this is unknown, but it seems to likely be regulated by a substrate of the APC/C and is not degraded directly by the APC/C itself.

4.2.4 APC4 Regulates the Morphology of Cortical Neurons

The most famous proposed substrates of the neuronal APC/C are thought to regulate the morphology of neurons (reviewed in Cajigas et al., 2010). When Cdh1 was depleted

from cerebral granule neurons, the length of the axons increased in cerebral granule cells (Li et al., 2019; Lasorella et al., 2006; Stegmüller et al. 2006; Stegmüller et al., 2008). Cdh1 depletion also induced changes in the length of neurites *in vivo* (Bobo-Jiménez et al., 2017). Cdc20 depletion did not affect the length of axons at all, but it instead reduced the length of the dendrites and the number of branch points within the dendrites of cerebellar granule, cortical, and hippocampal neuron cultures (Kim et al., 2009; Watanabe et al., 2014). While these studies all tie the neuronal phenotypes to the APC/C activators, the substrates and phenotypes were typically never linked to central components of the APC/C (see Section 4.2.5). There was one exception where the gene encoding APC2 was knocked down in cerebral granule neurons, leading to decreases in dendrite length (Kim et al., 2009). However, the APC/C substrate proposed in this study does not seem to be an actual substrate, and it instead seems to regulate the activation of the APC/C. Therefore, the substrates of the APC/C that regulate dendrite length remained unknown (see Section 4.2.3; Kim et al., 2009).

In this current study, I sought to determine if neuron morphology is affected by the loss of APC4 or the loss of the APC/C in general from neurons. Based on what was known in the literature, I expected to find a substantial decrease in the complexity of the neurons, an overall decrease in the length of the dendrites (Kim et al., 2009) and neurites (Bobo-Jiménez et al., 2017), and an increase in the axon length (Li et al., 2019; Lasorella et al., 2006; Stegmüller et al. 2006; Stegmüller et al., 2008). To my surprise, I was unable to identify any significant changes in any of these parameters in cortical neurons depleted of APC4 (Figure 23). As an estimate of axon length, I calculated the average longest neurite length per condition, and I found that there was no significant difference (Figure 23 H). These results overall indicate that including the axon and dendrites together for analysis is realistically not masking my ability to detect an effect. Typically the total axon or the dendrite length was the main measurements assayed in prior studies (Bobo-Jiménez et al., 2017; Kim et al., 2009; Li et al., 2019; Lasorella et al., 2006; Stegmüller et al. 2006; Stegmüller et al., 2008; Watanabe et al., 2014), but I found no differences in the total length of the neurites (Figure 23 F). I also saw no differences in the average length of primary neurites (Figure 23 G), the average length of the longest neurite (Figure 23 H), or the number of branch points (Figure 23 D and

E). The main difference that I was able to detect in my study was an increase in the total number of neurites extending out of the soma of the cells depleted of APC4 (Figure 23 B and C), but this effect was never recorded previously when Cdh1 or Cdc20 were depleted (Bobo-Jiménez et al., 2017; Kim et al., 2009; Li et al., 2019; Lasorella et al., 2006; Stegmüller et al. 2006; Stegmüller et al., 2008; Watanabe et al., 2014).

My Sholl analysis results show that when the conditional *ANAPC4* knockout neurons expressed Cre NLS RFP, there is an increase in the complexity of the neuron for the first 30 μm of distance from the soma (Figure 23 I, compare Cre NLS RFP and NLS RFP for the first 30 μm). This effect is entirely explained by the fact that there were on average two additional neurites extending from the soma in the cells that expressed Cre (Figure 23 B and C), and it does not seem to be due to an increase in the number of branches (Figure 23 D and E). This overall is inconsistent with the Cdc20 knockdown data that depicted an overall decrease in the complexity of neurons (Kim et al., 2009)

As with the previous study (Kim et al., 2009), I characterized neurons on DIV5, but I studied the morphology of mouse cortical neurons instead of rat cerebral granule neurons that were used in the previous study. Unlike the previous study, I was unable to look at the dendrite length specifically, due to the fact that axons and dendrites in my cells were not entirely differentiated at the time of my analysis. Even if I had been able to reliably distinguish between the axon and the dendrites in my morphology analysis (Figure 22, SMI-312 and MAP2 staining respectively), this likely would not have drastically affected the results of the morphology analysis based on the fact that the longest neurites (likely the future axons) had similar lengths in both conditions (Figure 23 H). While the knockdown of APC2 induced a very drastic decrease in the length of dendrites in cerebral granule neurons (Kim et al, 2009), I only saw a slight trend of a decrease, and this would not be greatly affected by removing the axons. Additionally, the fact that I see a decrease in ID1 expression (Figure 24 B and C, ID1 blot and graph) should lead to an increase in the length of dendrites based on previous models, which is the opposite of what I observed (Figure 23 F – H, graphs). One potential explanation for the fact that I am unable to detect any changes in the lengths of neurites is that I saw an overall increase in the number of processes leaving the soma of neurons depleted of APC4 (Figure 23 B and C, compare Cre NLS RFP and NLS RFP). This effect was never

described previously with either the Cdh1 or Cdc20 knockdown. However, the increase in the number of dendrites could potentially mask any dendritic length effects observed because there were essentially two extra neurite lengths added to this measurement when APC4 was depleted. The fact that other studies observed changes in dendrite length upon *APC2* knockout indicates that discrepant findings could have arisen due to the use of different cell types, different species, or different time courses of APC/C inactivation. In the future, all of my experiments should be repeated with cerebral granule neurons cultures obtained from *ANAPC4* knockout mice. Future morphological analysis can also include neurons at later time points in order to try to better distinguish between axons and dendrites in the analysis.

As I discuss further in Section 4.2.5, there are many proposed substrates of the APC/C, but the corresponding studies typically only involved the depletion of the activators but did not directly tie the results to the APC/C itself. Recently, the proposed APC/C substrate SMURF1 was shown to require Cdh1 through its D box motif (Kannan et al., 2012b), but it uses this motif via an APC/C-independent mechanism (Wan et al., 2011). It is likely that this phenomenon is also occurring with some of the other proposed APC/C substrates identified after activator perturbation, and this is most likely the reason that I did not observe the same morphological effects when I knockout *ANAPC4* in neuron cultures.

The fact that I observed changes in the number of neurites but not the length of the neurites argues that the APC/C is regulating some aspect of early neurite initiation but not neurite elongation. However, this process is not well understood presently (reviewed in Flynn, 2013). I previously indicated that USP1 might be regulating ID1 levels (see Section 4.2.3), and this is supported by the fact that I saw an increase in the number of neurite extensions when APC4 was depleted (Figure 23 B and C). USP1 is known to be a substrate of the APC/C within other cell types (Cataldo et al., 2013; Cotto-Rios et al., 2011). When cerebral granule neurons were depleted of USP1, they also had an increase in the length of the longest neurite and a decrease in the number of primary and secondary neurites. While the authors did not attempt to look at what happened to the neuron morphology when USP1 was overexpressed (Anckar and Bonni, 2015), it is expected that it would likely have the opposite effect due to the fact

that the enzyme will just be more active in deubiquitylating proteins (Cataldo et al., 2013; Cotto-Rios et al., 2011). While this needs to be confirmed, I hypothesize that USP1 protein levels are stabilized when *ANAPC4* is knocked out, and this likely leads to an increase in the number of neurites in the infected cells. This model is consistent with my morphology data too (Figure 23 B and C, graphs).

However, there is one major issue with this model of USP1 being responsible for regulating the number of neurites. USP1 stabilization should result in the stabilization of ID1 expression (Cataldo et al., 2013; Cotto-Rios et al., 2011) instead of the depletion that I observed (Figure 24 B and C, ID1 blot and graph). This effect could be explained though by ID1 also being ubiquitylated by an E3 ubiquitin ligase that is directly or indirectly activated by the loss of APC/C function (see Section 4.2.3). Additionally, the phenotype could be regulated by USP1-mediated deubiquitylation of other proteins in neurons (reviewed in Lim et al., 2020).

In summary, I was unable to confirm (Figure 23, all morphology data) the prior studies when the APC/C activators were depleted from neurons and found that the neurite length was decreased and there were fewer branches (Bobo-Jiménez et al., 2017; Kim et al., 2009; Li et al., 2019; Lasorella et al., 2006; Stegmüller et al. 2006; Stegmüller et al., 2008; Watanabe et al., 2014). I instead observed that there was an increase only in the number of the neurites extending from the soma of cortical neurons that lacked APC4 expression (Figure 23 B and C, graphs). Future studies are required to fully understand the function of USP1 and ID1 ubiquitylation and how this affects neuron morphology and physiology, possibly through the activity of the APC/C. Additional studies should repeat all of these experiments in cerebral granule neuron cultures generated from the conditional *ANAPC4* knockout mice in order to determine if the cell type may explain some of the discrepancies seen between my data (Figure 23, all morphology data; Figure 24 B and C, ID1 blot and graph) and prior publications (Bobo-Jiménez et al., 2017; Kim et al., 2009; Li et al., 2019; Lasorella et al., 2006; Stegmüller et al. 2006; Stegmüller et al., 2008; Watanabe et al., 2014).

4.2.5 The Majority of the Tested Neuronal Substrates of the APC/C Are Not Actual APC/C substrates

The majority of studies that discovered 'neuronal substrates' of the APC/C only showed that the substrate binds to the activator of the APC/C, but they failed to show that it actually binds to the other components of the APC/C or is ubiquitylated by APC/C (Table 16, see Substrate Status: Prior Published Status). There were two major exceptions to this notion. One study conducted Cdc27-IP and showed that ID1 and ID2 both associate with Cdc27 (Lasorella et al., 2006). Similarly, APC2 was knocked down and the affected cells had a similar morphology to cells depleted of Cdc20 (Kim et al., 2009). However, studies from the cell cycle field indicate that ID1 is instead regulating the activation of the APC/C (Figure 25; Chow et al., 2012; Man et al., 2008; Wang et al., 2008; Whitehurst et al., 2008), and my data indicate that it is probably not an APC/C substrate. Before my study (see Section 4.2.3; Figure 24 B and C, ID1 blot and graph), the status of ID1 as a substrate of the APC/C was debated. While it does have a D box motif to bind to the APC/C, it also binds to Cdh1 using the C-terminal domain of ID1 (Figure 25; Table 16; Man et al., 2008). Beyond ID1 and ID2 (Kim et al., 2009), authors within the neuronal APC/C field typically did not try to show that any of the neuronal phenotypes that they described actually require the APC/C (Table 16; reviewed in Cajigas et al., 2010).

The most famous proposed substrates of the neuronal APC/C were previously thought to regulate the length of neurites and the number of branch points of neurites (reviewed in Cajigas et al., 2010). While these phenotypes were properly linked to either Cdh1 or Cdc20, they were typically not confirmed to require the APC/C. In contrast to what I expected if these morphology effects were controlled by the APC/C, *ANAPC4* knockout neurons (Figure 20 C, APC4 blot and graph; Figure 24 A, APC4 blot) on DIV5 showed no changes in the length or the branching of their neurites (see Section 4.2.4; Figure 23 D - H). I also was not able to detect the expected accumulation of major proposed neuronal APC/C substrates after *ANAPC4* knockout, such as ID1 (Figure 24 B and C, ID1 blot and graph), FEZ1 (Figure 24 E and F, FEZ1 blot and graph), and NEUROD2 (Figure 24, G and H). Interestingly, ID1 expression actually decreased upon

ANAPC4 knockout (Figure 24 B and C, ID1 blot and graph), which indicates that it is instead regulated indirectly by the APC/C (see Section 4.2.2 for this discussion). In accord with my data, a prior study was unable to detect any changes in the protein expression levels of proposed APC/C substrates GluR1, SHANK1, or SnoN when the gene encoding *APC2* was conditionally knocked out in excitatory neurons of the forebrain (Kuczera et al., 2010). *APC2* knockout in hematocytes is required for the function of the APC/C though (Wirth et al., 2004). When a hypomorphic mouse line was generated that had less Cdc20 expression, cerebral granule neuron cultures generated from this line showed no changes in Synapsin expression, in dendrite length, or in NEUROD2 expression levels. However, other cell types obtained from these mice had clear defects in metaphase, in proper chromosome alignment, and in the degradation of Cyclin B1 (Malureanu et al., 2010), indicating that the knockout approach did affected APC/C activity. The one major study refuting my results is that when the gene encoding APC2 was knocked down, rat neurons had a similar morphology to Cdc20 knockdown cells (Kim et al., 2009), but this finding was not reproducible in my hands when I knocked out *ANAPC4* in mouse cortical neuron cultures. Overall, my data and the cumulative account in the literature call into question the assumption that many of the proposed APC/C substrates that require Cdh1 or Cdc20 actually require the APC/C too.

Similar to what was observed with SMURF1 (Wan et al., 2011), my data (Figure 24 B, C, and E - H, ID1, FEZ1, and NEUROD2 blots and graphs) indicate that the activators are likely regulating the various proposed cellular processes contributed to the APC/C using an APC/C-independent mechanism. This was confirmed to be the case with SMURF1, which also seems to require a D box motif to bind to Cdh1, even through its APC/C-independent mechanism (Wan et al., 2011). This could also explain why many of the proposed substrates of the APC/C still require a D box motif (Fu et al., 2011; Kannan et al., 2012b; Kim et al., 2009; Stegmüller et al., 2016; Wu et al., 2007; Yu et al., 2011) but not the APC/C. A crystal structure study showed how the Cdh1-activated APC/C binds to the D box motif of the substrate, demonstrating that an outer region of Cdh1 associates with the residues corresponding to the D box motif (da Fonseca et al., 2011), so it is imaginable that this same interaction could occur in the absence of the APC/C in the case of these proposed substrates that also bind to the D

box motif. Interestingly, a region of APC10 also interacts with the substrate (da Fonseca et al., 2011), so this binding may need to be replaced with other proteins when an APC/C-independent mechanism is used. Further studies are required to identify the other proteins involved in these APC/C-independent mechanisms.

Other points of potential discrepancies between my data and the prior findings are discussed in Section 4.2.4. These include the fact that I used different cell types and species to generate the cultures, I used neurons of different ages to generate the cultures, or the time courses of APC/C perturbation could be different. Furthermore, off-target effects of the knockdown approach could have played a role, given that these are notorious to induce morphological defects in neurons (Alvarez et al., 2006). The ubiquitylation of some proteins like SHANK1 seems to be regulated by activity (Jarome et al., 2011), so there is a good chance that this is the reason that there were no changes in SHANK1 expression when the gene encoding APC2 was knocked out previously (Kuczera et al., 2010). SHANK1 ubiquitylation should specifically be studied after the induction of activity, but other substrates could also be studied using this paradigm.

Alternatively, it is unlikely but possible that there is a functional APC/C within neurons that does not require APC4 and APC5. The proteins that constitute the APC/C have not actually been confirmed to date within neurons (reviewed in Cajigas et al., 2010), but there is no evidence of such alternative complexes in other cell types. APC4 expression is required for the activity of the APC/C in other cell types (Clark and Spector, 2015; Eifler et al., 2018; Furuta et al., 2000; Lee et al., 2018; Tran et al., 2010; Yamashita et al., 1999; Wang et al., 2012). To rule out this possibility, I am urgently still trying to find an actual neuronal substrate of the APC/C that I can use to show that the APC/C is not functional. I plan to look at the expression of SnoN and Cyclin B1 in Cre NLS RFP- and in NLS RPF-infected cells. While I am skeptical that SnoN is a substrate based on the fact that it did not appear to be one when the gene encoding APC2 was knocked out (Kuczera et al., 2010), I think that Cyclin B1 will be a reliable substrate to study in neurons (Almeida et al., 2005; Maestre et al., 2008). Additionally, SKP2 may also be a good substrate to address (Harmey et al., 2009).

Table 16. Proposed Mammalian Substrates of the Neuronal APC/C

Substrate	Activator	Location in the cell	Phenotype (Complex or Activator Was Lost)	Substrate Status: Prior Published Status	Substrate Status: *ANAPC4* Knockout in Cortical Neurons
Synapse-Related Substrates					
FMRP (1)	Cdh1	Cytosol	Synapses: translation regulator	Co-IP with Cdh1 only	Untested
GluR1 (2)	Cdh1	Unknown	Synapses: receptor	More likely a substrate in rats but not *C. elegans*	Untested, (*APC2* knockout: likely not a substrate)
SHANK1 (proposed only, suggested activity dependent substrate) (3)	Cdh1	Unknown	Synapse formation	Unconfirmed for both the complex and activators (APC2 knockout: suggests not but did not test with activity induction)	Untested (activity dependent test required)
Dendritic Growth					
FEZ1 (4)	Cdc20	Centrosome	Decreased dendrite length and complexity	Co-IP with Cdc20, does not use D box	Not a substrate
ID1 (5)	Cdc20	Centrosome	Decreased length of dendrites	Co-IP with Cdc27 in HeLa Cells	APC/C substrate regulates ID1 levels, but it is not a substrate
ROCK2 (6)	Cdh1	Cytoplasm	Cell death, decreased neurite length	Co-IP with Cdh1 only	Untested

Substrate	Activator	Location in the cell	Phenotype (Complex or Activator Was Lost)	Substrate Status: Prior Published Status	Substrate Status: *ANAPC4* Knockout in Cortical Neurons
Axon Growth					
ID2 (7)	Cdh1	Nucleus	Increased axon growth	Co-IP with Cdc27 in HeLa cells	Untested
P250GAP (8)	Cdh1	Cytosol	Increased axon growth	Likely not a substrate	Untested
SMURF1 (9)	Cdh1	Cytosol	Increased axon growth	Requires D box, APC/C independent	Untested
SnoN (10)	Cdh1	Nucleus	Increased axon growth	Requires D box, Co-IP with Cdh1 only	Untested, (*APC2* knockout: likely not a substrate)
Glycolysis, Apoptosis, and Development					
MOAP-1 (11)	Cdh1	Unknown	Regulates Apoptosis	Confirmed in HEK293, unknown in neurons	Untested
NEUROD2 (12)	Cdc20	Nucleus	Transcription factor; fewer synapses	Co-IP with Cdc20 only	Not a substrate
PFKFB3 (13)	Cdh1	Trans-located from nucleus to cytosol	Glycolysis, oxidative stress pathway	Downstream of Cdh1, substrate not directly confirmed	Untested

This table lists by functional category the proposed mammalian substrates of the neuronal APC/C. For each substrate, it lists the activator of the complex involved, the cellular localization, the proposed function, and a summary of what was learned about this substrate in the current study (Figure 24). The references for the information in this table are denoted by number at the bottom of each respective cell in column 1. (**1**) Valdez-Sinon et al., 2020. (**2**) Fu et al., 2011; Juo and Kaplan, 2004; Kuczera et al., 2010. (**3**) Kuczera et al., 2010; Jarome et al., 2011; Pick et al., 2012. (**4**) Watanabe et al., 2014. (**5**) Kim et al., 2009; Lasorella et al., 2006. (**6**) Bobo-Jiménez et al., 2017. (**7**) Lasorella et al., 2006; Yu et al., 2011. (**8**) Kannan et al. 2012b; Wan et al., 2011. (**9**) Kannan et al. 2012a. (**10**) Kuczera et al., 2010; Li et al., 2019; Stegmüller et al. 2006; Stegmüller et al., 2008. (**11**) Huang et al., 2012. (**12**) Yang et al., 2009. (**13**) Rodriguez-Rodriguez et al., 2012.

Lentiviral infection in general induced an increase in the expression of Complexin 3 (Figure 24 D, Complexin 3 blot), ID1 (Figure 24 B and C, ID1 blot and graph), and NEUROD2 (Figure 24 G and H, NEUROD2 blot and graph). Important physiology within a neuron could be influenced by some of these changes. For this reason, I always compared Cre NLS RFP- and NLS RFP-infected samples when I assessed the effect of the *ANAPC4* knockout on neuron physiology. Unfortunately, this increased expression alone could possibly alter the signaling pathways that I am testing and may confound my ability to see accumulation of the protein of interest. Cre expression itself could also influence the results, but I ruled out this possibility by repeating all of the experiments shown in Figure 24 with neuron cultures generated from wildtype mice (data is not shown).

In summary, I found that most of the neuronal substrates and phenotypes that I tested do not seem to directly involve the activity of the cortical APC/C (see Sections 4.2.3 to 4.2.5). In the future, when trying to identify a substrate of the neuronal APC/C, one needs to take the time to actually determine if it is a bona fide substrate of the complex, using a more stringent experimental approach. IP experiments should always be conducted using an antibody directed against a core component of the APC/C, such as Cdc27, instead of using only antibodies against the activators of the complex. Functional experiments, such as characterizing neuron morphology, should be conducted with perturbations of both, the activator and a core component of the APC/C. While *in vitro* ubiquitylation assays are not optimal, they actually are beneficial for determining if a binding protein is an actual substrate. This is especially true in cases like ID1, where the potential substrate is also a candidate regulator of the APC/C (Man et al., 2008; Wang et al., 2008). Typically, studies outside the neuronal APC/C field have focused on showing that the identified substrate is actually a substrate of the APC/C (Huang et al., 2012), and this more stringent experimental approach must be adopted within the neuronal APC/C field. This can potentially be done using a knockout approach like I have done in the present study, or by doing additional biochemistry experiments. While it seems now that many of the currently proposed candidate neuronal APC/C substrates have to be dismissed, we are left with the important question of what the complex is actually doing in non-dividing cells like neurons.

Interestingly, this also opens up a whole new direction of research that involves determining how Cdh1 and Cdc20 influence neuron morphology and physiology (reviewed in Cajigas et al., 2010) indepentent of the APC/C.

4.3 Conclusions and Outlook

The APC/C regulates many complex cellular processes like the cell cycle (reviewed in Peters, 2006; reviewed in Sivakumar and Gorbsky, 2015, 2015; Pfleger and Kirschner, 2000; Robbins and Cross, 2010). It is able to differentially regulate these processes through a complex regulatory network that includes post-translational modification of the many components of the APC/C, enabling the complex to bind different proteins and to facilitate the transfer of ubiquitin chains to different substrates (Kraft et al., 2003; Qiao et al., 2016). In the current study, I first focused on a novel post-translational modification of the APC/C that involves the conjugation of SUMO to APC4. I identified the sites of mouse APC4 SUMOylation as lysines 772 and 797, and I designed an APC4 variant that is SUMOylation-deficient (K772R/K797R; Figure 8 A and B, arrows). I then showed that APC4 SUMOylation does not influence the formation (Figure 10 A, Myc blots) or the activation of the APC/C (Figure 9 A and B, arrows). APC4 SUMOylation also did not influence the subcellular localization of APC4 (Figure 13, HA staining; Figure 12, Myc blots). APC4 is localized to the cytoplasm and the nucleus of HEK293 cells (Figure 14, APC4 blot) and neurons (Figure 15, APC4 blot), and it is SUMOylated in both of these compartments (Figure 14, APC4 blot; Figure 15, APC4 blot; Tirard et al., unpublished).

While I was not able to confirm that APC4 SUMOylation affects the function of the APC/C, this is most likely the case based on evidence from the cell cycle field (Eifler et al., 2018; Lee et al., 2018; Yatskevich et al., 2021). It was previously hypothesized that APC4 SUMOylation affects the ability of the APC/C to ubiquitylate a subset of its substrates (Eifler et al., 2018; Lee et al., 2018; Yatskevich et al., 2021), but this needs to be studied more systematically. If it is indeed affecting the ubiquitylation of only a subset of the substrates of the APC/C, drugs targeting this modification may be of great interest for the treatment of cancer (Mistry et al., 2013) and neurological diseases

(Fuchsberger et al., 2016; Lee et al., 2015; Li et al., 2020; reviewed in Chen et al., 2020; Tan et al., 2015; Zhang et al., 2019).

The sheer complexity of the APC/C enables it to regulate complex cellular processes that require the fast degradation of different sets of proteins, as in the cell cycle (reviewed in Peters, 2006; reviewed in Sivakumar and Gorbsky, 2015; Pfleger and Kirschner, 2000; Robbins and Cross, 2010). While the components of the complex are rather abundant in neurons (Gieffers et al., 1999), the function of the APC/C it in these non-dividing cells is not well understood. To date there are several publications that suggested a role for the APC/C activators of Cdh1 and Cdc20 within neurons, but these studies did not tie the corresponding phenotypes to APC/C function directly (reviewed in Cajigas et al., 2010).

In this current study, I knocked out the gene encoding APC4, a core component of the APC/C, and I characterized the consequences of this knockout biochemically (Figure 24). I also studied the effects of the knockout on the morphology of cortical neurons (Figure 23). In contrast to previously published data (Table 16; Kim et al., 2009; Lasorella et al., 2006; Watanabe et al., 2014; Yang et al., 2009), my results indicate that ID1 (Figure 24 B and C, ID1 blot and graph), FEZ1 (Figure 24 E and F, FEZ1 blot and graph), and NEUROD2 (Figure 24 G and H, NEUROD2 blot and graph) are not substrates of the APC/C. Interestingly, ID1 seems to be a downstream target of the APC/C, as its levels are actually decreased when APC4 expression is abolished (Figure 24 B and C, ID1 blot and graph). Additionally, cortical neurons depleted of APC4 did not have changes in the length of their neurites (Figure 23 F - H) or in the number of neurite branches (Figure 23 D and E), which contradicts earlier findings that were based on the depletion of the APC/C activators (Bobo-Jiménez et al., 2017; Kim et al., 2009; Li et al., 2019; Lasorella et al., 2006; Stegmüller et al. 2006; Stegmüller et al., 2008; Watanabe et al., 2014). However, I did observe that neurons depleted of APC4 have a novel phenotype that involves an increase in the number of neurites extending from their soma, indicating that the APC/C likely plays a role in regulating early steps in the initiation of neurite formation (Figure 23 B and C). Overall my data indicate that the APC/C is important for neuron physiology, but that many of the previously published substrates and phenotypes that are associated to the neuronal APC/C (reviewed in

Cajigas et al., 2010) may not involve the activity of the APC/C at all. In the future, studies identifying neuronal substrates of the APC/C must involve more stringent analyses to show that the core components of the complex are actually involved in inducing any observed effects instead of just characterizing the APC/C activators.

The *ANAPC4* conditional knockout mouse line (Figure 6) is a powerful tool for studying the neuronal APC/C, and it can be used in future studies to better understand how APC4 SUMOylation affects the neuronal APC/C and neuron physiology. The extent by which the APC/C is involved in regulating neuron physiology outside of its function in controlling the cell cycle and the apoptotic pathways is unclear. However, its function in these processes alone deems this a pertinent pathway to study in neurons due to its disease implications. More specifically, the development of APC/C drug targets that affect its ability to ubiquitylate a subset of proteins will be of great interest for the development of treatments for cancer and for other diseases that injure the nervous system (Fuchsberger et al., 2016; Lee et al., 2015; Li et al., 2020; reviewed in Chen et al., 2020; Tan et al., 2015; Zhang et al., 2019). However, our ability to tackle this task requires a more complete understanding of all of the substrates of the APC/C and a deeper understanding of how post-translational modifications regulate the activity of the APC/C.

5. References

Abramoff, M.D., Magalhaes, P.J., and Ram, S.J. (2004). Image Processing with ImageJ. *Biophotonics International* 11: 7: 36-42.

al-Khodairy, F., Enoch, T., Hagan, I.M., and Carr, A.M. (1995) The Schizosaccharomyces pombe hus5 gene encodes a ubiquitin conjugating enzyme required for normal mitosis. *J Cell Sci* 108: 475–486.

Alfieri, C., Chang, L., Zhang, Z., Yang, J., Maslen, S., Skehel, M., and Barford, D. (2016). Molecular basis of APC/C regulation by the spindle assembly checkpoint. *Nature* 536: 431-436.

Almeida A., Bolanos J.P., and Moreno, S. (2005). Cdh1/Hct1-APC is essential for the survival of postmitotic neurons. *J Neurosci* 25: 8115–21.

Alvarez, V.A., Ridenour, D.A., and Sabatini, B.L. (2006). Retraction of synapses and dendritic spines induced by off-target effects of RNA interference. *The Journal of neuroscience : the official journal of the Society for Neuroscience*, *26*(30), 7820–7825.

Anckar, J., and Bonni, A. (2015). Regulation of neuronal morphogenesis and positioning by ubiquitin-specific proteases in the cerebellum. *PloS one,* 10(1), e0117076.

Bancroft, J., Holder, J., Geraghty, Z., Alfonso-Pérez, T., Murphy, D., Barr, F. A., and Gruneberg, U. (2020). PP1 promotes cyclin B destruction and the metaphase-anaphase transition by dephosphorylating CDC20. *Molecular biology of the cell*, *31*(21), 2315–2330.

Barford, D. (2011). Structural insights into anaphase-promoting complex function and mechanism. *Philos Trans R Soc Lond B Biol Sci*., 366(1584): 3605-3624.

Bentley, A.M., Williams, B.C., Goldberg, M.L., and Andres, A.J. (2002). Phenotypic characterization of Drosophila ida mutants: defining the role of APC5 in cell cycle progression. *Journal of cell science*, 115 (Pt 5), 949–961.

Biggins, S., Bhalla, N., Chang, A., Smith, D.L., and Murray, A.W. (2001). Genes Involved in Sister Chromatid Separation and Segregation in the Budding Yeast *Saccharomyces cerevisiae*. *Genetics* 159: 453–470

Bobo-Jiménez, V., Delgado-Esteban, M., Angibaud, J., Sánchez-Morán, I., de la Fuente, A., Yajeya, J., Nägerl, U.V., Castillo, J., Bolaños, J.P., and Almeida, A. (2017). APC/C^{Cdh1}-Rock2 pathway controls dendritic integrity and memory. *Proceedings of the National Academy of Sciences of the United States of America*, *114*(17), 4513–4518.

Borchert, G.M., Holton, N.W., Edwards, K.A., Vogel, L.A., and Larson, E.D. (2010). Histone H2A and H2B are monoubiquitinated at AID-targeted loci. *PloS one*, 5(7), e11641.

Boulet, G.A., Micalessi, I.M., Horvath, C.A., Benoy, I.H., Depuydt, C.E.,and Bogers, J.J. (2010). Nucleic acid sequence-based amplification assay for human papillomavirus mRNA detection and typing: evidence for DNA amplification. *Journal of clinical microbiology*, *48*(7), 2524–2529.

Burton, J.L., Xiong, Y., and Solomon, M.J. (2011). Mechanisms of pseudosubstrate inhibition of the anaphase promoting complex by Acm1. *The EMBO journal*, 30(9), 1818–1829.

Cajigas, I.J., Will, T., and Schuman, E.M. (2010). Protein homeostasis and synaptic plasticity. *The EMBO journal*, *29*(16), 2746–2752.

Carlin, R.K., Grab, D.J., Cohen, R.S., and Siekevitz, P. (1980). Isolation and characterization of postsynaptic densities from various brain regions: enrichment of different types of postsynaptic densities. *The Journal of cell biology*, *86*(3), 831–845.

Cataldo, F., Peche, L.Y., Klaric, E., Brancolini, C., Myers, M.P., Demarchi, F., and Schneider, C. (2013). CAPNS1 regulates USP1 stability and maintenance of genome integrity. *Molecular and cellular biology*, *33*(12), 2485-2496.

Chan, S.J., Zhao, H., Hayakawa, K., Chai, C., Tan, C.T., Huang, J., Tao, R., Hamanaka, G., Arumugam, T.V., Lo, E.H., Yu, V., and Wong, P.H. (2019). Modulator of apoptosis-1 is a potential therapeutic target in acute ischemic injury. Journal of cerebral blood flow and metabolism: *official journal of the International Society of Cerebral Blood Flow and Metabolism*, 39(12), 2406–2418.

Chau, V., Tobias, J.W., Bachmair, A., Marriott, D., Ecker, D.J., Gonda, D.K., and Varshavsky, A. (1989). A multiubiquitin chain is confined to specific lysine in a targeted short-lived protein. *Science* 243, 1576–1583

Chen, B.J., Lam, T.C., Liu, L.Q., and To, C.H. (2017). Post-translational modifications and their applications in eye research (Review). *Molecular medicine reports*, *15*(6), 3923–3935.

Chen, S.D., Yang, J.L., Lin, Y.C., Chao, A.C., and Yang, D.I. (2020). Emerging Roles of Inhibitor of Differentiation-1 in Alzheimer's Disease: Cell Cycle Reentry and Beyond. *Cells*, *9*(7), 1746.

Chow, C., Wong, N., Pagano, M., Lun, S.W., Nakayama, K.I., Nakayama, K., and Lo, K.W. (2012). Regulation of APC/CCdc20 activity by RASSF1A-APC/CCdc20 circuitry. *Oncogene*, *31*(15), 1975-1987.

Clark, A.E., and Spector, D.H. (2015). Studies on the Contribution of Human Cytomegalovirus UL21a and UL97 to Viral Growth and Inactivation of the Anaphase-Promoting Complex/Cyclosome (APC/C) E3 Ubiquitin Ligase Reveal a Unique Cellular Mechanism for Downmodulation of the APC/C Subunits APC1, APC4, and APC5. *Journal of virology*, *89*(13), 6928–6939.

Collingridge, G.L., Peineau, S., Howland, J.G., and Wang, Y.T. (2010). Long-term depression in the CNS. *Nature reviews. Neuroscience*, *11*(7), 459–473.

Cotto-Rios, X.M., Jones, M.J., Busino, L., Pagano, M., and Huang, T.T. (2011). APC/CCdh1-dependent proteolysis of USP1 regulates the response to UV-mediated DNA damage. *The Journal of cell biology*, *194*(2), 177-186.

Cubeñas-Potts, C., Srikumar, T., Lee, C., Osula, O., Subramonian, D., Zhang, X. D., Cotter, R.J., Raught, B., and Matunis, M.J. (2015). Identification of SUMO-2/3-modified proteins associated with mitotic chromosomes. *Proteomics*, *15*(4), 763–772.

Cronin, N.B., Yang, J., Zhang, Z., Kulkarni, K., Chang, L., Yamano, H., and Barford, D. (2015). Atomic-Resolution Structures of the APC/C Subunits Apc4 and the Apc5 N-Terminal Domain. *Journal of molecular biology*, *427*(20), 3300–3315.

D'Adamo, P., Welzl, H., Papadimitriou, S., Raffaele di Barletta, M., Tiveron, C., Tatangelo, L., Pozzi, L., Chapman, P.F., Knevett, S.G., Ramsay, M.F., Valtorta, F., Leoni, C., Menegon, A., Wolfer, D.P., Lipp, H.P., and Toniolo, D. (2002). Deletion of the mental retardation gene Gdi1 impairs associative memory and alters social behavior in mice. *Human molecular genetics*, *11*(21), 2567–2580.

da Fonseca, P.C., Kong, E.H., Zhang, Z., Schreiber, A., Williams, M.A., Morris, E.P., and Barford, D. (2011). Structures of APC/C(Cdh1) with substrates identify Cdh1 and Apc10 as the D-box co-receptor. *Nature,* 470(7333), 274–278.

Daniel, J.A., Cooper, B.H., Palvimo, J.J., Zhang, F.P., Brose, N., and Tirard, M. (2017). Analysis of SUMO1-conjugation at synapses. *eLife*, *6*, e26338. https://doi.org/10.7554/eLife.26338

de Boer, H.R., Guerrero Llobet, S., and van Vugt, M.A. (2016). Controlling the response to DNA damage by the APC/C-Cdh1. *Cellular and molecular life sciences : CMLS*, *73*(5), 949–960.

Delgado-Esteban, M., García-Higuera, I., Maestre, C., Moreno, S., and Almeida, A. (2013). APC/C-Cdh1 coordinates neurogenesis and cortical size during development. *Nature communications*, *4*, 2879.

Dieckhoff, P., Bolte, M., Sancak, Y., Braus G.H., and Irniger, S. (2004). Smt3/SUMO and Ubc9 are required for efficient APC/C-mediated proteolysis in budding yeast. *Mol Microbiol*. 51:1375–1387.

Dimova, N.V., Hathaway, N.A., Lee, B.H., Kirkpatrick, D.S., Berkowitz, M.L., Gygi, S.P., Finley, D., and King, R.W. (2012). APC/C-mediated multiple monoubiquitylation provides an alternative degradation signal for cyclin B1. *Nature cell biology*, *14*(2), 168–176.

Distler, U., Schmeisser, M.J., Pelosi, A., Reim, D., Kuharev, J., Weiczner, R., Baumgart, J., Boeckers, T.M., Nitsch, R., Vogt, J., and Tenzer, S. (2014). In-depth protein profiling of the postsynaptic density from mouse hippocampus using data-independent acquisition proteomics. *Proteomics*, 14(21-22), 2607–2613.

Do, J.L., Bonni, A., and Tuszynski, M.H. (2013). SnoN facilitates axonal regeneration after spinal cord injury. *PloS one*, *8*(8): e71906.

Eguren, M., Manchado, E., and Malumbres, M. (2011). Non-mitotic functions of the Anaphase-Promoting Complex. *Semin. Cell. Dev. Biol*., 22(6): 572-578.

Eifler, K., Cuijpers, S.A., Willemstein, E., Raaijmakers, J.A., El Atmioui, D., Ovaa, H., Medema, R.H., and Vertegaal, A.C. (2018). SUMO targets the APC/C to regulate transition from metaphase to anaphase. *Nat Commun*., 9(1):1119.

Erpapazoglou, Z., Walker, O., and Haguenauer-Tsapis, R. (2014). Versatile roles of k63-linked ubiquitin chains in trafficking. *Cells*, *3*(4), 1027–1088.

Ertych, N., Stolz, A., Stenzinger, A., Weichert, W., Kaulfuß, S., Burfeind, P., Aigner, A., Wordeman, L., and Bastians, H. (2014). Increased microtubule assembly rates influence chromosomal instability in colorectal cancer cells. *Nature cell biology*, *16*(8), 779–791.

Everett, R.D., Boutell, C., and Hale, B.G. (2013). Interplay between viruses and host sumoylation pathways. *Nature Reviews Microbiology*, 11, 400-411.

Fagerland, M.W., and Sandvik, L. (2009). Performance of five two-sample location tests for skewed distributions with unequal variances. *Contemporary clinical trials*, *30*(5), 490–496.
Farley FW, Soriano P, Steffen LS, Dymecki SM. Widespread recombinase expression using FLPeR (flipper) mice. Genesis. 2000 Nov-Dec; 28(3-4):106-10.
Felgner, P. L., Gadek, T. R., Holm, M., Roman, R., Chan, H.W., Wenz, M., Northrop, J.P., Ringold, G.M., and Danielsen, M. (1987). Lipofection: a highly efficient, lipid-mediated DNA-transfection procedure. *Proceedings of the National Academy of Sciences of the United States of America*, *84*(21), 7413-7417.
Flynn K.C. (2013). The cytoskeleton and neurite initiation. *Bioarchitecture*, *3*(4), 86-109.
Fontes, A., Macarthur, C.C., Lieu, P.T., and Vemuri, M.C. (2013). Generation of human-induced pluripotent stem cells (hiPSCs) using episomal vectors on defined Essential 8™ Medium conditions. *Methods in molecular biology (Clifton, N.J.)*, *997*, 57–72.
Fu, A.K., Hung, K.W., Fu, W.Y., Shen, C., Chen, Y., Xia, J., Lai, K.O., and Ip, N.Y. (2011). APC(Cdh1) mediates EphA4-dependent downregulation of AMPA receptors in homeostatic plasticity. *Nature neuroscience*, *14*(2), 181–189.
Fuchsberger, T., Martínez-Bellver, S., Giraldo, E., Teruel-Martí, V., Lloret, A., and Viña, J. (2016). Aiña, J. (2016). Aartínez-Bellver, S., Giraldo, E., letion That Can Be Prevented by Glutaminase Inhibition Promoting Neuronal Survival. *Scientific reports*, 6, 31158.
Furuta, T., Tuck, S., Kirchner, J., Koch, B., Auty, R., Kitagawa, R., Rose, A.M., and Greenstein, D. (2000). EMB-30: an APC4 homologue required for metaphase-to-anaphase transitions during meiosis and mitosis in Caenorhabditis elegans. *Mol Biol Cell*, 11(4): 1401-1419.
García-Higuera, I., Manchado, E., Dubus, P., Cañamero, M., Méndez, J., Moreno, S., and Malumbres, M. (2008). Genomic stability and tumour suppression by the APC/C cofactor Cdh1. *Nature cell biology*, *10*(7), 802–811.
García-Santisteban, I., Peters, G.J., Giovannetti, E., and Rodríguez, J.A. (2013). USP1 deubiquitinase: cellular functions, regulatory mechanisms and emerging potential as target in cancer therapy. *Molecular cancer*, *12*, 91.
Gareau, J.R. and Lima, C.D. (2010). The SUMO pathway: emerging mechanisms that shape specificity, conjugation, and recognition. *Nat. Rev. Mol. Cell. Biol.*, 11, 861-871.
Garnett, M.J., Mansfeld, J., Godwin, C., Matsusaka, T., Wu, J., Russell, P., Pines, J., and Venkitaraman, A.R. (2009). UBE2S elongates ubiquitin chains on APC/C substrates to promote mitotic exit. *Nature cell biology*, *11*(11), 1363–1369.
Geiss-Friedlander, R and Melchior, F. (2007) Concepts in sumoylation: a decade on. *Nat. Rev. Mol. Cell. Biol*., 12, 947-956.
Gieffers, C., Peters, B.H., Kramer, E.R., Dotti, C.G., and Peters, J.M. (1999). Expression of the CDH1-associated form of the anaphase-promoting complex in postmitotic neurons. *Proc. Natl. Acad. Sci. U S A*., 96(20): 11317-11322.
Golebiowski, F., Matic, I., and Tatham, M. (2009). System-wide changes to SUMO modification in response to heat shock. *J. Sci. Signal:* 2(72): ra24.

Gomez, J.F., Brioso, M.A., Machado, J.D., Sanchez, J.L., and Borges, R. (2002). New approaches for analysis of amperometrical recordings. *Annals of the New York Academy of Sciences*, *971*, 647–654.

Graham FL, Smiley J, Russell WC, and Nairn R. (1977). Characteristics of a human cell line transformed by DNA from human adenovirus type 5. *J Gen Virol*. 36(1):59-74.

Gunaseelan, S., Wang, Z., Tong, V., Ming, S., Razar, R., Srimasorn, S., Ong, W.Y., Lim, K.L., and Chua, J. (2021). Loss of FEZ1, a gene deleted in Jacobsen syndrome, causes locomotion defects and early mortality by impairing motor neuron development. *Human molecular genetics*, ddaa281.

Harmey, D., Smith, A., Simanski, S., Moussa, C.Z., and Ayad, N.G. (2009). The anaphase promoting complex induces substrate degradation during neuronal differentiation. *The Journal of biological chemistry*, *284*(7), 4317–4323.

Hendriks, I.A., Lyon, D., Su, D., Skotte, N.H., Daniel, J.A., Jensen, L.J., and Nielsen, M.L. (2018). Site-specific characterization of endogenous SUMOylation across species and organs. *Nature communications*, *9*(1), 2456.

Herrero-Mendez, A., Almeida, A., Fernández, E., Maestre, C., Moncada, S., and Bolaños, J.P. (2009). The bioenergetic and antioxidant status of neurons is controlled by continuous degradation of a key glycolytic enzyme by APC/C-Cdh1. *Nat. Cell Biol*., 11(6): 747-752.

Hou, L., Antion, M.D., Hu, D., Spencer, C.M., Paylor, R., and Klann, E. (2006). Dynamic translational and proteasomal regulation of fragile X mental retardation protein controls mGluR-dependent long-term depression. *Neuron*, *51*(4), 441–454.

Huang, J., Ikeuchi, Y., Malumbres, M., and Bonni, A. (2015). A Cdh1-APC/FMRP Ubiquitin Signaling Link Drives mGluR-Dependent Synaptic Plasticity in the Mammalian Brain. *Neuron*, *86*(3), 726–739.

Huang, J.Y., and Raff, J.W. (2002). The dynamic localisation of the Drosophila APC/C: evidence for the existence of multiple complexes that perform distinct functions and are differentially localized. *Journal of Cell Science*, 115: 2847-2856.

Huang, N.J., Zhang, L., Tang, W., Chen, C., Yang, C.S., and Kornbluth, S. (2012). The Trim39 ubiquitinligase inhibits APC/C Cdh1-mediated degradation of the Bax activator MOAP-1. *J. Cell Biol*., 197: 361–367.

Hung, A.Y., Sung, C.C., Brito, I.L., and Sheng, M. (2010). Degradation of postsynaptic scaffold GKAP and regulation of dendritic spine morphology by the TRIM3 ubiquitin ligase in rat hippocampal neurons. *PloS one*, 5(3), e9842.

Ikeuchi, Y., Stegmüller, J., Netherton, S., Huynh, M.A., Masu, M., Frank, D., Bonni, S., and Bonni, A. (2009). A SnoN–Ccd1 pathway promotes axonal morphogenesis in the mammalian brain. *J Neurosci* 29, 4312–4321.

IMPC (n.d.) *Gene Anapc4*. International Mouse Phenotyping Consortium. https://www.mousephenotype.org/data/genes/MGI%3A1098673

Inkscape. (n.d.). Inkscape. http://www.inkscape.org/.

Ishitani, R., Tanaka, M., Sunaga, K., Katsube, N., and Chuang, D. M. (1998). Nuclear localization of overexpressed glyceraldehyde-3-phosphate dehydrogenase in cultured cerebellar neurons undergoing apoptosis. *Molecular pharmacology*, *53*(4), 701–707.

Jarome, T.J., Werner, C.T., Kwapis, J.L., and Helmstetter, F.J. (2011). Activity dependent protein degradation is critical for the formation and stability of fear memory in the amygdala. *PloS one*, *6*(9), e24349.

Jarvis, M.A., Brown, N.G., Watson, E.R., VanderLinden, R., Schulman, B.A., and Peters, J.M. (2016). Measuring APC/C-Dependent Ubiquitylation In Vitro. *Methods in molecular biology (Clifton, N.J.)*, *1342*, 287–303.

Jin, L., Williamson, A., Banerjee, S., Philipp, I., and Rape, M. (2008). Mechanism of ubiquitin-chain formation by the human anaphase-promoting complex. *Cell*, *133*(4), 653–665.

Jiang, M., and Chen, G. (2006). High Ca2+-phosphate transfection efficiency in low-density neuronal cultures. *Nature protocols*, *1*(2), 695–700.

Johnson, E.S. and Blobel, G. (1997). Ubc9p is the conjugating enzyme for the ubiquitin-like protein Smt3p. *J Biol Chem.*, 272(43): 26799-802.

Jörgensen, P.M., Brundell, E., Starborg, M., an Höög, C. (1998). A subunit of the anaphase-promoting complex is a centromere-associated protein in mammalian cells. *Molecular and cellular biology*, 18(1), 468–476.

Jung, J.K., Jang, S.W., and Kim, J.M. (2016). A novel role for the deubiquitinase USP1 in the control of centrosome duplication. *Cell cycle (Georgetown, Tex.)*, *15*(4), 584-592.

Juo, P., and Kaplan, J.M. (2004). The anaphase-promoting complex regulates the abundance of GLR-1 glutamate receptors in the ventral nerve cord of C. elegans. *Current biology*, 14(22), 2057–2062.

Kannan, M., Lee, S.J., Schwedhelm- Domeyer, N., and Stegmüller, J. (2012a). The E3 ligase Cdh1-anaphase promoting complex operates upstream of the E3 ligase Smurf1 in the control of axon growth. *Development (Cambridge, England)*, *139*(19), 3600–3612.

Kannan, M., Lee, S.J., Schwedhelm-Domeyer, N., Nakazawa, T., and Stegmüller, J. (2012b). p250GAP is a novel player in the Cdh1-APC/Smurf1 pathway of axon growth regulation. *PloS one*, *7*(11), e50735.

Kaplow, M.E., Korayem, A.H., and Venkatesh, T.R. (2008). Regulation of glia number in Drosophila by Rap/Fzr, an activator of the anaphase-promoting complex, and Loco, an RGS protein. *Genetics*, 178(4), 2003–2016.

Kelly, A., Wickliffe, K.E., Song, L., Fedrigo, I., and Rape, M. (2014). Ubiquitin chain elongation requires E3-dependent tracking of the emerging conjugate. *Molecular cell*, *56*(2), 232–245.

Kim, A.H., Puram, S.V., Bilimoria, P.M., Ikeuchi, Y., Keough, S., Wong, M., Rowitch, D., and Bonni, A. (2009). A centrosomal Cdc20-APC pathway controls dendrite morphogenesis in postmitotic neurons. *Cell*, 136(2): 322-336.

Kim, T., Lara-Gonzalez, P., Prevo, B., Meitinger, F., Cheerambathur, D. K., Oegema, K., and Desai, A. (2017). Kinetochores accelerate or delay APC/C activation by directing Cdc20 to opposing fates. *Genes & development*, *31*(11), 1089–1094.

King, R.W., Peters, J.M., Tugendreich, S., Rolfe, M., Hieter, P. and Kirschner, M.W. (1995). A 20S complex containing CDC27 and CDC16 catalyzes the mitosis-specific conjugation of ubiquitin to cyclin B. *Cell* 81, 279–288

Kirkpatrick, D.S., Hathaway, N.A., Hanna, J., Elsasser, S., Rush, J., Finley, D., King, R.W., and Gygi, S.P. (2006). Quantitative analysis of in vitro ubiquitinated cyclin B1 reveals complex chain topology. *Nat Cell Biol,* 8: 700–710.

Konishi, Y., Stegmüller, J., Matsuda, T., Bonni, S., and Bonni, A. (2004). Cdh1-APC controls axonal growth and patterning in the mammalian brain. *Science*, 303(5660): 1026-1030.

Kowalski, J.R., Dube, H., Touroutine, D., Rush, K.M., Goodwin, P.R., Carozza, M., Didier, Z., Francis, M.M., and Juo, P. (2014). The Anaphase-Promoting Complex (APC) ubiquitin ligase regulates GABA transmission at the C. elegans neuromuscular junction. *Mol Cell Neurosci.*, 58: 62-75.

Kraft, C., Herzog, F., Gieffers, C., Mechtler, K., Hagting, A., Pines, J., and Peters, J.M. (2003). Mitotic regulation of the human anaphase-promoting complex by phosphorylation . *The EMBO Journal* 22(24): 6598-6609.

Kroeger, C.M., Ejima, K., Hannon, B.A., Halliday, T.M., McComb, B., Teran-Garcia, M., Dawson, J.A., King, D.B., Brown, A.W., and Allison, D.B. (2021). Persistent confusion in nutrition and obesity research about the validity of classic nonparametric tests in the presence of heteroscedasticity: evidence of the problem and valid alternatives. *The American journal of clinical nutrition*, *113*(3), 517–524.

Kuang, C., Golden, K.L., Simon, C.R., Damrath, J., Buttitta, L., Gamble, C.E., and Lee, C.Y. (2014). A novel fizzy/Cdc20-dependent mechanism suppresses necrosis in neural stem cells. *Development*, 141(7), 1453–1464.

Kuczera, T., Stilling, R.M., Hsia, H. E., Bahari-Javan, S., Irniger, S., Nasmyth, K., Sananbenesi, F., and Fischer, A. (2010). The anaphase promoting complex is required for memory function in mice. *Learning & memory (Cold Spring Harbor, N.Y.)*, *18*(1), 49–57.

Kumar, A and Zhang, K.Y. (2015). Advances in the Development of SUMO specific protease (SENP) inhibitors. *Comput Struct Biotechnol J.,* 13, 204-211.

Kumar, B.V., Lakshmi, M.V., and Atkinson, J.P. (1985). Fast and efficient method for detection and estimation of proteins. *Biochemical and biophysical research communications*, *131*(2), 883–891.

Lasorella A., Stegmüller, J., Guardavaccaro, D., Liu, G., Carro, M.S., Rothschild, G., de la Torre-Ubieta, L., Pagano, M., Bonni, A., and Iavarone A. (2006). Degradation of Id2 by the anaphase-promoting complex couples cell cycle exit and axonal growth. *Nature*, 442: 471–474.

Lee, C.C., Li, B., Yu, H., and Matunis, M.J. (2018). Sumoylation promotes optimal APC/C Activation and Timely Anaphase. *eLife*, *7*: e29539.

Lee, J.C., Chen, B.H., Cho, J.H., Kim, I.H., Ahn, J.H., Park, J.H., Tae, H.J., Cho, G.S., Yan, B.C., Kim, D.W., Hwang, I.K., Park, J., Lee, Y.L., Choi, S.Y., and Won, M.H. (2015). Changes in the expression of DNA-binding/differentiation protein inhibitors in neurons and glial cells of the gerbil hippocampus following transient global cerebral ischemia. *Molecular medicine reports*, *11*(4), 2477-2485.

Li J., Chen X., Li, X, Hu, R., Yao, W., Mei, W., Wan, L., Gui, L., and Zhang, C. (2020). Upregulation of Cdh1 in the trigeminal spinal subnucleus caudalis attenuates trigeminal neuropathic pain via inhibiting GABAergic neuronal apoptosis. *Neurochem Int*., 133: 104613.

Li, M., Shin, Y.H., Hou, L., Huang, X., Wei, Z., Klann, E., and Zhang, P. (2008). The adaptor protein of the anaphase promoting complex Cdh1 is essential in maintaining replicative lifespan and in learning and memory. *Nature cell biology*, *10*(9), 1083–1089.

Li, X., Wei, K., Hu, R., Zhang, B., Li, L., Wan, L., Zhang, C., and Yao, W. (2017). Upregulation of Cdh1 Attenuates Isoflurane-Induced Neuronal Apoptosis and Long-Term Cognitive Impairments in Developing Rats. *Frontiers in cellular neuroscience*, *11*, 368.

Li, Z., Zhang, B., Yao, W., Zhang, C., Wan, L., and Zhang, Y. (2019). APC-Cdh1 Regulates Neuronal Apoptosis Through Modulating Glycolysis and Pentose-Phosphate Pathway After Oxygen-Glucose Deprivation and Reperfusion. *Cellular and molecular neurobiology*, *39*(1), 123–135.

Liang, Y.C., Lee, C.C., Yao, Y.L., Lai, C.C., Schmitz, M.L., and Yang, W.M. (2016). SUMO5, a Novel Poly-SUMO Isoform, Regulates PML Nuclear Bodies. *Scientific reports*, *6*, 26509.

Lim, K.H., Joo, J.Y., and Baek, K.H. (2020). The potential roles of deubiquitinating enzymes in brain diseases. *Ageing research reviews*, *61*, 101088.

Ling, F., Kang, B., and Sun, X.H. (2014). Id proteins: small molecules, mighty regulators. *Current topics in developmental biology*, *110*, 189–216.

Liu, B., Bai, W., Ou, G., and Zhang, J. (2019). Cdh1-Mediated Metabolic Switch from Pentose Phosphate Pathway to Glycolysis Contributes to Sevoflurane-Induced Neuronal Apoptosis in Developing Brain. *ACS chemical neuroscience*, *10*(5), 2332–2344.

Liu, L., Li, C., Song, S., Teo, Z., Shen, L., Wang, Y., Jackson, D., and Yu, H. (2018). FTIP-Dependent STM Trafficking Regulates Shoot Meristem Development in Arabidopsis. *Cell reports*, *23*(6), 1879–1890.

Lois, C., Hong, E.J., Pease, S., Brown, E.J., and Baltimore, D. (2002). Germline transmission and tissue-specific expression of transgenes delivered by lentiviral vectors. *Science (New York, N.Y.)*, *295*(5556), 868–872.

López-Murcia, F.J., Reim, K., Jahn, O., Taschenberger, H., and Brose, N. (2019). Acute Complexin Knockout Abates Spontaneous and Evoked Transmitter Release. *Cell reports*, *26*(10), 2521–2530.e5.

Maestre, C., Delgado-Esteban, M., Gomez-Sanchez, J.C., Bolaños, J.P., and Almeida, A. (2008). Cdk5 phosphorylates Cdh1 and modulates cyclin B1 stability in excitotoxicity. *The EMBO journal*, 27(20), 2736–2745.

Malureanu, L., Jeganathan, K.B., Jin, F., Baker, D.J., van Ree, J.H., Gullon, O., Chen, Z., Henley, J.R., and van Deursen, J.M. (2010). Cdc20 hypomorphic mice fail to counteract de novo synthesis of cyclin B1 in mitosis. *The Journal of cell biology*, *191*(2), 313–329.

Man, C., Rosa, J., Yip, Y.L., Cheung, A.L., Kwong, Y.L., Doxsey, S.J., and Tsao, S.W. (2008). Id1 overexpression induces tetraploidization and multiple abnormal mitotic phenotypes by modulating aurora A. *Molecular biology of the cell*, *19*(6), 2389-2401.

Manchado, E., Eguren, M., and Malumbres, M. (2010). The anaphase-promoting complex/ cyclosome (APC/C): cell-cycle-dependent and -independent functions. *Biochem. Soc. Trans*., 38, 65–71.

Mathieson, T., Franken, H., Kosinski, J., Kurzawa, N., Zinn, N., Sweetman, G., Poeckel, D., Ratnu, V. S., Schramm, M., Becher, I., Steidel, M., Noh, K.M., Bergamini, G., Beck, M., Bantscheff, M., and Savitski, M.M. (2018). Systematic analysis of protein turnover in primary cells. *Nature communications*, *9*(1), 689.

Matic, I., Schimmel, J., Hendriks, I.A., van Santen, M.A., van de Rijke, F., van Dam, H., Gnad, F., Mann, M., and Vertegaal, A.C. (2010). Site-specific identification of SUMO-2 targets in cells reveals an inverted SUMOylation motif and a hydrophobic cluster. SUMOylation motif. *Mol. Cell*, 39:641-652.

McLean, J.R., Chaix, D., Ohi, M.D., and Gould, K.L. (2011). State of the APC/C: Organization, function, and structure. *Critical Reviews in Biochemistry and Molecular Biology,* 46(2): 118–136.

Melloy, P.G., and Holloway, S.L. (2004). Changes in the localization of the Saccharomyces cerevisiae anaphase-promoting complex upon microtubule depolymerization and spindle checkpoint activation. *Genetics*, 167(3), 1079–1094.

Meng, X., Tian, X., Wang, X., Gao, P., and Zhang, C. (2012). A novel binding protein of single-minded 2: the mitotic arrest-deficient protein MAD2B. *Neurogenetics*, *13*(3), 251–260.

Meyer, H.J., and Rape, M. (2014). Enhanced protein degradation by branched ubiquitin chains. *Cell* 157, 910–921.

Mistry, H., Hsieh, G., Buhrlage, S.J., Huang, M., Park, E., Cuny, G.D., Galinsky, I., Stone, R.M., Gray, N.S., D'Andrea, A. D., and Parmar, K. (2013). Small-molecule inhibitors of USP1 target ID1 degradation in leukemic cells. *Molecular cancer therapeutics*, *12*(12), 2651-2662.

Naldini, L., Blömer, U., Gallay, P., Ory, D., Mulligan, R., Gage, F.H., Verma, I.M., and Trono, D. (1996). In vivo gene delivery and stable transduction of nondividing cells by a lentiviral vector. *Science (New York, N.Y.)*, *272*(5259), 263–267.

Neuert, H., Yuva-Aydemir, Y., Silies, M., and Klämbt, C. (2017). Different modes of APC/C activation control growth and neuron-glia interaction in the developing Drosophila eye. *Development*,144(24), 4673–4683.

Oh, E., Akopian, D., and Rape, M. (2018). Principles of Ubiquitin-Dependent Signaling. *Annual review of cell and developmental biology*, *34*, 137–162.

Owerbach, D., McKay, E.M., Yeh, E.T., Gabbay, K.H. and Bohren, K.M. (2005). A proline-90 residue unique to SUMO-4 prevents maturation and sumoylation. *Biochem. Biophys. Res. Commun.,* 337, 517–520.

Pelisch, F., Bel Borja, L., Jaffray, E.G., and Hay, R.T. (2019). Sumoylation regulates protein dynamics during meiotic chromosome segregation in *C. elegans* oocytes. *Journal of cell science*, *132*(14), jcs232330.

Peters, J.M. (2006). The anaphase promoting complex/cyclosome: a machine designed to destroy. *Nature Reviews Molecular Cell Biology* 7, 644-656**.**

Pfleger, C.M. and Kirschner, M.W. (2000). The KEN box: an APC recognition signal distinct from the D box targeted by Cdh1. Genes Dev, 14(6): 655–665.

Pfleger, C.M., Lee, E., and Kirschner, M.W. (2001). Substrate recognition by the Cdc20 and Cdh1 components of the anaphase-promoting complex. *Genes & development*, *15*(18), 2396– 2407.

Preibisch, S., Saalfeld, S., and Tomancak, P. (2009). Globally optimal stitching of tiled 3D microscopic image acquisitions. *Bioinformatics (Oxford, England)*, *25*(11), 1463–1465.

Pick, J.E., Malumbres, M., and Klann, E. (2012). The E3 ligase APC/C-Cdh1 is required for associative fear memory and long-term potentiation in the amygdala of adult mice. *Learning & memory (Cold Spring Harbor, N.Y.)*, *20*(1), 11–20.

Pick, J.E., Wang, L., Mayfield, J.E., and Klann, E. (2013). Neuronal expression of the ubiquitin E3 ligase APC/C-Cdh1 during development is required for long-term potentiation, behavioral flexibility, and extinction. *Neurobiology of learning and memory*, *100*, 25–31.

Porter, L.A., Cukier, I.H., and Lee, J.M. (2003). Nuclear localization of cyclin B1 regulates DNA damage-induced apoptosis. *Blood*, *101*(5), 1928–1933.

Puram, S.V., Kim, A.H., Ikeuchi, Y., Wilson-Grady, J.T., Merdes, A., Gygi, S.P., and Bonni, A. (2011). A CaMKII β signaling pathway at the centrosome regulates dendrite patterning in the brain. *Nature neuroscience*, 14(8), 973–983.

Qiao, R., Weissmann, F., Yamaguchi, M., Brown, N. G., VanderLinden, R., Imre, R., Jarvis, M. A., Brunner, M. R., Davidson, I. F., Litos, G., Haselbach, D., Mechtler, K., Stark, H., Schulman, B. A., and Peters, J. M. (2016). Mechanism of APC/CCDC20 activation by mitotic phosphorylation. *Proceedings of the National Academy of Sciences of the United States of America*, *113*(19), E2570–E2578.

Reim, K., Mansour, M., Varoqueaux, F., McMahon, H.T., Südhof, T. C., Brose, N., and Rosenmund, C. (2001). Complexins regulate a late step in Ca2+-dependent neurotransmitter release. *Cell*, *104*(1), 71–81.

Robbins, J.A., and Cross, J.R. (2010). Regulated degradation of the APC-coactivator Cdc20. *Cell Division*, 5:23-31.

Rodrigo-Brenni, M.C., and Morgan, D.O. (2007). Sequential E2s drive polyubiquitin chain assembly on APC targets. *Cell*, *130*(1), 127–139.

Rodriguez-Rodriguez, P., Fernandez, E., Almeida, A., and Bolaños, J.P. (2012). Excitotoxic stimulus stabilizes PFKFB3 causing pentose-phosphate pathway to glycolysis switch and neurodegeneration. *Cell Death Differ.*, 19(10): 1582-1589.

Roger, B., Al-Bassam, J., Dehmelt, L., Milligan, R.A., and Halpain, S. (2004). MAP2c, but not tau, binds and bundles F-actin via its microtubule binding domain. Current biology, 14(5), 363–371.

Saritas-Yildirim, B., and Silva, E.M. (2014). The role of targeted protein degradation in early neural development. *Genesis* (New York, N.Y.: 2000), 52(4), 287–299.

Schell, M.A., and Wilson, D.B. (1979). Cloning and expression of the yeast galactokinase gene in an Escherichia coli plasmid. *Gene*, *5*(4), 291–303.
Schimmel, J., Eifler, K., Sigurðsson, J.O., Cuijpers, S.A.G., Hendriks, I.A., Verlaan-de Vries, M., Kelstrup, C.D., Francavilla, C., Medema, R.H., Olsen,J.V., and Vertegaal, A.C.O. (2014). Uncovering SUMOylation Dynamics during Cell-Cycle Progression Reveals FoxM1 as a Key Mitotic SUMO Target Protein. *Molecular Cell*, 6: 1053-1066.
Seufert, W., Futchert, B., and Jentsch, S. (1995). Role of a ubiquitin-conjugating enzyme in degradation of S and M phase cyclins. *Nature*: 373: 78-81
Schindelin, J., Arganda-Carreras, I., Frise, E., Kaynig, V., Longair, M., Pietzsch, T., Preibisch, S., Rueden, C., Saalfeld, S., Schmid, B., Tinevez, J. Y., White, D. J., Hartenstein, V., Eliceiri, K., Tomancak, P., and Cardona, A. (2012). Fiji: an open-source platform for biological-image analysis. *Nature methods*, *9*(7), 676–682.
Schneider, C.A., Rasband, W.S., and Eliceiri, K.W. (2012). NIH Image to ImageJ: 25 years of image analysis. *Nature methods*, *9*(7), 671–675.
Sholl D.A. (1953). Dendritic organization in the neurons of the visual and motor cortices of the cat. *Journal of anatomy*, *87*(4), 387–406.
Shteinberg, M., Protopopov, Y., Listovsky, T., Brandeis, M., and Hershko, A. (1999). Phosphorylation of the cyclosome is required for its stimulation by Fizzy/cdc20. *Biochem Biophys Res Commun.*, 260(1):193-198.
Silies, M., and Klämbt, C. (2010). APC/C(Fzr/Cdh1)-dependent regulation of cell adhesion controls glial migration in the Drosophila PNS. *Nature Neuroscience*, 13(11), 1357–1364.
Sivakumar, S. and Gorbsky, G.J. (2015). Spatiotemporal regulation of the anaphase-promoting complex in mitosis. *Nat Rev Mol Cell Biol*., 16(2): 82-94.
Skovlund, E., and Fenstad, G.U. (2001). Should we always choose a nonparametric test when comparing two apparently nonnormal distributions?. *Journal of clinical epidemiology*, *54*(1), 86–92.
Slack, C., Overton, P.M., Tuxworth, R.I., and Chia, W. (2007). Asymmetric localisation of Miranda and its cargo proteins during neuroblast division requires the anaphase-promoting complex/cyclosome. *Development (Cambridge, England)*, 134(21), 3781–3787.
Stegmüller, J., Huynh M.A., Yuan, Z., Konishi, Y., and Bonni, A. (2008). TGF β -Smad2 signaling regulates the Cdh1–APC/SnoN pathway of axonal morphogenesis. *J Neurosci*, 28: 1961–1969.
Stegmüller, J., Konishi, Y., Huynh, M.A., Yuan, Z., Dibacco, S., and Bonni, A. (2006). Cell-intrinsic regulation of axonal morphogenesis by the Cdh1–APC target SnoN. *Neuron*, 50: 389–400.
Stewart M. (2007). Molecular mechanism of the nuclear protein import cycle. *Nature reviews. Molecular cell biology*, *8*(3), 195–208.
Sudakin, V., Ganoth, D., Dahan, A., Heller, H., Hershko, J., Luca, F.C., Ruderman, J.V. and Hershko, A. (1995). The cyclosome, a large complex containing cyclin-selective ubiquitin ligase activity, targets cyclins for destruction at the end of mitosis. *Mol. Biol. Cell* 6, 185–197.

Swaiman, K.F., Neale, E.A., Fitzgerald, S.C., and Nelson, P.G. (1982). A method for large-scale production of mouse brain cortical cultures. *Brain research*, 255(3), 361–369.

Tan, W., Yao, W.L., Hu, R., Lv, Y.Y., Wan, L., Zhang, C.H., and Zhu, C. (2015). Alleviating neuropathic pain mechanical allodynia by increasing Cdh1 in the anterior cingulate cortex. *Molecular pain*, *11*, 56.

Tanaka K, Nishide J, Okazaki K, Kato H, Niwa O, Nakagawa T, Matsuda H, Kawamukai M, and Murakami Y. (1999). Characterization of a fission yeast SUMO-1 homologue, Pmt3p, required for multiple nuclear events, including the control of telomere length and chromosome segregation. *Mol Cell Biol.,* 19: 8660–8672.

Tanno, N., Kuninaka, S., Fujimura, S., Takemoto, K., Okamura, K., Takeda, N., Araki, K., Araki, M., Saya, H., and Ishiguro, K. I. (2020). Phosphorylation of the Anaphase Promoting Complex activator FZR1/CDH1 is required for Meiosis II entry in mouse male germ cell. *Scientific reports*, *10*(1), 10094.

Tatham, M.H., Jaffray, E., Vaughan, O.A., Desterro, J.M.P. Botting, C.H., Naismith, J.H., and Hay, R.T. (2001). Polymeric Chains of SUMO-2 and SUMO-3 Are Conjugated to Protein Substrates by SAE1/SAE2 and Ubc9. *J. Biol. Chem*., 276, 35368-35374.

Tavares, G., Martins, M., Correia, J.S., Sardinha, V.M., Guerra-Gomes, S., das Neves, S.P., Marques, F., Sousa, N., and Oliveira, J. F. (2017). Employing an open-source tool to assess astrocyte tridimensional structure. *Brain structure & function*, *222*(4), 1989–1999.

Thornton, B.R., Ng, T.M., Matyskiela, M.E., Carroll, C.W., Morgan, D.O., and Toczyski, D.P. (2006). An architectural map of the anaphase-promoting complex. *Genes & development*, *20*(4), 449–460.

Tirard, M., and Brose, N. (2016). Systematic Localization and Identification of SUMOylation Substrates in Knock-In Mice Expressing Affinity-Tagged SUMO1. *Methods in molecular biology (Clifton, N.J.)*, *1475*, 291–301.

Tirard, M., Hsiao, H.H., Nikolov, M., Urlaub, H., Melchior, F, and Brose, N. (2012). In vivo localization and identification of SUMOylated proteins in the brain of His_6-HA-SUMO1 knock-in mice. *Proc. Natl. Acad. Sci.,* 109: 21122-21127.

Tobaben, S., Südhof, T.C., and Stahl, B. (2000). The G protein-coupled receptor CL1 interacts directly with proteins of the Shank family. *The Journal of biological chemistry*, *275*(46), 36204–36210.

Tomomori-Sato, C., Sato, S., Conaway, R.C., and Conaway, J. W. (2013). Immunoaffinity purification of protein complexes from Mammalian cells. *Methods in molecular biology* (Clifton, N.J.), 977, 273–287.

Topper, L.M., Campbell, M.S., Tugendreich, S., Daum, J.R., Burke, D.J., Hieter, P., and Gorbsky, G.J. (2002). The dephosphorylated form of the anaphase-promoting complex protein Cdc27/Apc3 concentrates on kinetochores and chromosome arms in mitosis. *Cell cycle (Georgetown, Tex.)*, 1(4), 282–292.

Tran, K., Kamil, J.P., Coen, D.M., and Spector, D.H. (2010). Inactivation and disassembly of the anaphase-promoting complex during human cytomegalovirus infection is associated with degradation of the APC5 and APC4 subunits and does not require UL97-mediated phosphorylation of Cdh1. *J. Virol*., 84(20), 10832-10843.

Tugendreich, S., Tomkiel, J., Earnshaw, W., and Hieter, P. (1995). CDC27Hs colocalizes with CDC16Hs to the centrosome and mitotic spindle and is essential for the metaphase to anaphase transition. *Cell*, 81(2), 261–268

Uemura, H., Rogers, M.J., Swanson, R., Watson, L., and Söll, D. (1988). Site-directed mutagenesis to fine-tune enzyme specificity. *Protein engineering*, 2(4), 293–296.

Van Nassauw, L., Wu, M., De Jonge, F., Adriaensen, D., and Timmermans, J.P. (2005). Cytoplasmic, but not nuclear, expression of the neuronal nuclei (NeuN) antibody is an exclusive feature of Dogiel type II neurons in the guinea-pig gastrointestinal tract. *Histochemistry and cell biology*, *124*(5), 369–377.

Valdez-Sinon, A.N., Lai, A., Shi, L., Lancaster, C.L., Gokhale, A., Faundez, V., and Bassell, G.J. (2020). Cdh1-APC Regulates Protein Synthesis and Stress Granules in Neurons through an FMRP-Dependent Mechanism. *Science*, 23(5), 101132.

Van Roessel, P., Elliott, D.A., Robinson, I.M., Prokop, A., and Brand, A.H. (2004). Independent regulation of synaptic size and activity by the anaphase-promoting complex. *Cell*, 119(5): 707-178.

Vardar, G., Chang, S., Arancillo, M., Wu, Y.J., Trimbuch, T., and Rosenmund, C. (2016). Distinct Functions of Syntaxin-1 in Neuronal Maintenance, Synaptic Vesicle Docking, and Fusion in Mouse Neurons. *The Journal of neuroscience : the official journal of the Society for Neuroscience*, *36*(30), 7911–7924.

Wan, L., Zou, W., Gao, D., Inuzuka, H., Fukushima, H., Berg, A.H., Drapp, R., Shaik, S., Hu, D., Lester, C., Eguren, M., Malumbres, M., Glimcher, L.H., and Wei, W. (2011). Cdh1 regulates osteoblast function through an APC/C-independent modulation of Smurf1. *Molecular cell*, 44(5), 721–733.

Wang, C.H., Wu, C.C., Hsu, S.H., Liou, J.Y., Li, Y.W., Wu, K.K., Lai, Y.K., and Yen, B.L. (2013). The role of RhoA kinase inhibition in human placenta-derived multipotent cells on neural phenotype and cell survival. *Biomaterials*, *34*(13), 3223–3230.

Wang, L., Wansleeben, C., Zhao, S., Miao, P., Paschen, W., and Yang, W. (2014). SUMO2 is essential while SUMO3 is dispensable for mouse embryonic development. *EMBO Rep*., 8: 878-885.

Wang, X., Di, K., Zhang, X., Han, H.Y., Wong, Y.C., Leung, S.C., and Ling, M.T. (2008). Id-1 promotes chromosomal instability through modification of APC/C activity during mitosis in response to microtubule disruption. *Oncogene*, *27*(32), 4456-4466.

Wang, Y., Hou, Y., Gu, H., Kang, D., Chen, Z.L., Liu, J., and Qu, L.J. (2012). The Arabidopsis APC4 subunit of the anaphase-promoting complex/cyclosome (APC/C) is critical for both female gametogenesis and embryogenesis. *Plant J*., 69(2), 227-240.

Watanabe, Y., Khodosevich, K., and Monyer, H. (2014). Dendrite development regulated by the schizophrenia-associated gene FEZ1 involves the ubiquitin proteasome system. *Cell reports*, *7*(2), 552–564.

Whitehurst, A.W., Ram, R., Shivakumar, L., Gao, B., Minna, J.D., and White, M.A. (2008). The RASSF1A tumor suppressor restrains anaphase-promoting complex/cyclosome activity during the G1/S phase transition to promote cell cycle progression in human epithelial cells. *Molecular and cellular biology*, *28*(10), 3190-3197.

Wirth, K.G., Ricci, R., Giménez-Abián, J.F., Taghybeeglu, S., Kudo, N.R., Jochum, W., Vasseur-Cognet, M., and Nasmyth, K. (2004). Loss of the anaphase-promoting complex in quiescent cells causes unscheduled hepatocyte proliferation. *Genes & development*, *18*(1), 88-98.

Wise, A., Schatoff, E., Flores, J., Hua, S.Y., Ueda, A., Wu, C.F., and Venkatesh, T. (2013). Drosophila-Cdh1 (Rap/Fzr) a regulatory subunit of APC/C is required for synaptic morphology, synaptic transmission and locomotion. Int. J. Dev. Neurosci., 31(7): 624-633.

Wu, G., Glickstein, S., Liu, W., Fujita, T., Li, W., Yang, Q., Duvoisin, R., and Wan, Y. (2007). The anaphase-promoting complex coordinates initiation of lens differentiation. *Molecular biology of the cell*, *18*(3), 1018–1029.

Yamaguchi, M., Vander Linden, R., Weissmann, F., Qiao, R., Dube, P., Brown, N.G., Haselbach, D., Zhang, W., Sidhu, S.S., Peters, J.M., Stark, H., and Schulman, B.A. (2016). Cryo-EM of mitotic checkpoint complex-bound APC/C reveals reciprocal and conformational regulation of ubiquitin ligation. *Molecular Cell* 63: 593–607.

Yamano H. (2019). APC/C: current understanding and future perspectives. *F1000 Research*, 8, F1000 Faculty Rev-725.

Yamashita, Y.M., Nakaseko, Y., Kumada, K., Nakagawa, T., and Yanagida, M. (1999). Fission yeast APC/cyclosome subunits, Cut20/Apc4 and Cut23/Apc8, in regulating metaphase-anaphase progression and cellular stress responses. *Genes Cells*, 4(8): 445-463.

Yang, Y., Kim, A.H., Yamada, T., Wu, B., Bilimoria, P.M., Ikeuchi, Y., de la Iglesia, N., Shen, J., and Bonni, A. (2009). A Cdc20-APC ubiquitin signaling pathway regulates presynaptic differentiation. *Science*, 326(5952): 575-578.

Yang, Z., Jun, H., Choi, C.I., Yoo, K.H., Cho, C.H., Hussaini, S., Simmons, A.J., Kim, S., van Deursen, J.M., Baker, D.J., and Jang, M.H. (2017). Age-related decline in BubR1 impairs adult hippocampal neurogenesis. *Aging cell*, *16*(3), 598–601.

Yatskevich, S., Kroonen, J.S., Alfieri, C., Tischer, T., Howes, A.C., Clijsters, L., Yang, J., Zhang, Z., Yan, K., Vertegaal, A.C.O, and Barford, D. (2021). Molecular mechanisms of APC/C release from spindle assembly checkpoint inhibition by APC/C SUMOylation. *Cell Reports* 34(13), 108929

Yau, R., and Rape, M. (2016). The increasing complexity of the ubiquitin code. *Nature cell biology*, 18(6), 579–586.

Yen, A.H., and Yang, J.L. (2010). Cdc20 proteolysis requires p38 MAPK signaling and Cdh1-independent APC/C ubiquitination during spindle assembly checkpoint activation by cadmium. *Journal of cellular physiology*, *223*(2), 327–334.

Yu P., Zhang Y.P., Shields, L.B., Zheng, Y., Hu, X., Hill, R., Howard, R., Gu, Z., Burke, D.A., Whittemore, S,R., Xu, X., and Shields, C.B. (2011). Inhibitor of DNA binding 2 promotes sensory axonal growth after SCI. *Exp Neurol* 231: 38–44.

Yu, S., Galeffi, F., Rodriguiz, R.M., Wang, Z., Shen, Y., Lyu, J., Li, R., Bernstock, J. D., Johnson, K.R., Liu, S., Sheng, H., Turner, D.A., Wetsel, W.C., Paschen, W, and Yang, W. (2020). Small ubiquitin-like modifier 2 (SUMO2) is critical for memory processes in mice. *FASEB journal: official publication of the Federation of American Societies for Experimental Biology*, 34(11), 14750–14767.

Yuan, Y.F., Zhai, R., Liu, X.M., Khan, H. A., Zhen, Y.H. and Huo, L.J.(2014). SUMO-1 plays crucial roles for spindle organization, chromosome congression, and chromosome segregation during mouse oocyte meiotic maturation. *Mol. Reprod. Dev*., 81: 712-724.

Zachariae, W., Schwab, M., Nasmyth, K., and Seufert, W. (1998). Control of cyclin ubiquitination by CDK-regulated binding of Hct1 to the anaphase promoting complex. *Science*, 282(5394): 1721-1724.

Zhang, B., Chen, X., Lv, Y., Wu, X., Gui, L., Zhang, Y., Qiu, J., Song, G., Yao, W., Wan, L., and Zhang, C. (2019). Cdh1 overexpression improves emotion and cognitive-related behaviors via regulating hippocampal neuroplasticity in global cerebral ischemia rats. *Neurochemistry international*, 124, 225–237.

Zhang, F.P., Mikkonen, L., Toppari, J., Palvimo, J.J., Thesleff, I., and Jänne, O.A. (2008). Sumo-1 function is dispensable in normal mouse development. *Mol Cell Biol*., 28(17): 5381–5390.

Zhang, L., Park, C.H., Wu, J., Kim, H., Liu, W., Fujita, T., Balasubramani, M., Schreiber, E.M., Wang, X.F., and Wan, Y. (2010). Proteolysis of Rad17 by Cdh1/APC regulates checkpoint termination and recovery from genotoxic stress. *The EMBO journal*, 29(10), 1726–1737.

Zhang, S., Chang, L., Alfieri, C., Zhang, Z., Yang, J., Maslen, S., Skehel, M., and Barford, D. (2016). Molecular mechanism of APC/C activation by mitotic phosphorylation. *Nature* 533: 260–264.

Zhao, Z., Bo, Z., Gong, W., and Guo, Y. (2020). Inhibitor of Differentiation 1 (Id1) in Cancer and Cancer Therapy. *International journal of medical sciences*, *17*(8), 995-1005.

Zhou, W., Zhu, P., Wang, J., Pascual, G., Ohgi, K.A., Lozach, J., Glass, C.K., and Rosenfeld, M.G. (2008). Histone H2A monoubiquitination represses transcription by inhibiting RNA polymerase II transcriptional elongation. *Molecular cell,* 29(1), 69–80.

Acknowledgements

I am extremely thankful for the instruction given, the assistance provided, and the meaningful discussions that I had during my time in Göttingen at the Max Plank Institute for Experimental Medicine. My time at the institute has been very rewarding, and I would like to appreciate many of these colleagues and my mentors now.

First of all, I would like to thank Dr. Nils Brose for the opportunity to work in his lab. I appreciated his continued patience and encouragement while working on this project, even though I experienced many experimental setbacks. Dr. Brose was always willing to help me quickly resolve any issues that arose and I enjoyed our thoughtful discussions. In spite of working on a project that was entirely unrelated to the research conducted in our lab, he was always helpful and supportive.

I am grateful for Dr. Marilyn Tirard's assistance and discussions throughout the years. She supplied me with useful experimental advice and taught me experimental techniques, such as cortical neuron cultures and IP. She provided me with assistance whenever I had technical issues with an experiment or equipment in our laboratory.

I would like to thank Dr. Holger Bastians for his willingness to serve on my thesis committee and the numerous helpful suggestions that he gave me over the years. His expertise on the cell cycle was very helpful in shaping the direction of portions of this thesis. He gave me useful protocols for techniques like synchronizing cells in G2/M, and he gave me different antibody recommendations. Finally, he is providing me with a Cyclin B1 antibody that I will use to wrap up this project.

I would like to acknowledge all of my extended members of my committee for taking time to be involved in my exam committee and for the useful input they will provide. This includes the following people: Dr. Markus Bohnsack, Dr. Thomas Dresbach, Dr. Ira Milosevic, and Dr. Tiago Outeiro.

I would like to express gratitude to Dr. James Daniel for all of his willingness to help me in the lab. He was one of my best resources for troubleshooting experiments, and he gave me many protocols. I would like to thank Dr. Hiroshi Kawabe for many useful discussions during my first few years in the lab. He always gave me great experimental advice, and he supplied me with the ubiquitin overexpression constructs.

I would like to appreciate Dr. Silvia Ripamonti for teaching me how to make neuron cultures and how to design imaging experiments. Dr. Mišo Mitkovski and Heiko Roehse were always willing to discuss experiments with me and fix problems that I had with the confocal microscope.

I am grateful to Dr. Erinn Gideons for helping guide me with the cell fractionation of the mouse cortex experiment, and Dr. Dilja Krüger-Burg also provided me with useful suggestions to complete this experiment. In general, Dr. Krüger-Burg provided me with good advice and discussions over the years, including recently when I tried to determine the best way to do the statistical analysis for the neuron morphology experiment.

Dr. Holger Taschenberger and Dr. Francisco Jose Lopez Murcia instructed me on how to do the half-life experiment and quantification. While I repeated the quantification myself, Holger did an initial quantification with my data. Dr. Carolina Thomas gave me a lot of useful advice on completing the Sholl Analysis, and she always provided helpful advice and good scientific discussions.

Aisha Ahmad and Anja Günther assisted me with resolving issues encountered occasionally with the virus making protocol. Klaas Hellman in our lab was always willing to give helpful information and reagents to me. I had many insightful discussions and great advice throughout the years from Dr. Nandhini Sivakumar, Dr. Trayana Stankova, Dr. Sonja Wojcik, Dr. Hong Jun Rhee, Dr. Hung-En Hsia, and Dr. Kwon Nok Mimi Man. I finally am grateful to all other members of the Brose Department that I did not name here. I appreciate all of you for all of your assistance and discussions over the years.

I would like to acknowledge the assistance of Dr. Dieter Heineke from the Dean's Office and Dr. Dirk Kamin from the GAUSS. My appreciation is also extended to all of the other staff within their offices and within the other offices at the University that provided me with any assistance, including Dr. Anke Schürer and Rebecca Willhardt.

I am grateful to Dr. Judith Stegmüller for her willingness to always supply me with DNA constructs and to recommend the use of different APC/C-related antibodies. Dr. Klaus Nave's lab supplied me with the FLIR mice and the Histone 3 antibody. Dr. John Chua provided the FEZ1 antibody. Dr. Marilyn Tirard provided the homemade SUMO1 and SUMO2/3 antibodies. Dr. Frauke Melchior provided many of our SUMO constructs, including the HA-SUMO2 construct that I used regularly in this study. Dr. Marc

Kirschner (Pfleger et al., 2001) provided the APC/C activator constructs. Dr. Christian Rosenmund (Vardar et al., 2016) provided the Cre RFP P2A lentivirus construct. EUCOMM provided me with the *ANAPC4* conditional knockout mouse.

I am thankful for the care provided to my mice by all the technicians within the Barrier and Quarantine mouse facilities at the MPIEM; this includes the following people: Stefan Roeglin, Nadja Hoffmeister, Lina Tyra Leunig, Katharina Rathmann, Ann-Kathrin Willige, Alissa Sölter, and Dorothee Rittmeier. I would especially like to thank Ursula Fuenfschilling and Dr. Anke Schraepler for all of their help setting up this colony at the institute. Ursula Fuenfschilling and Nicole Weber were responsible for freezing sperm from all of my lines, re-deriving the line outside of quarantine, and trying to establish the lines initially from the frozen material at our institute.

I am grateful for our institute's DNA core facility, which is under the guidance of Fritz Benseler. Within this lab, Ivonne Thanhäuser, Christiane Harenberg, and Dayana Warnecke were responsible for making all of the primers, doing the sequencing, and doing the genotyping. The other technicians in our lab helped to prepare the DNA for the mouse genotyping. I would also like to thank Astrid Zeuch for cloning some rescue contracts that I will use after my thesis submission.

In regards to actually writing this thesis, I am extremely thankful for the helpful comments and discussions provided by Dr. Marilyn Tirard and Dr. Nils Brose. I also appreciate the help of Dr. James Daniel and Carol Day in editing parts of this thesis. I would like to also like to thank Dr. Xiaomin Zhang for her feedback in regards to Figure 3, and Aisha Ahmad for her discussion of Table 1.

Finally, I would like to especially thank my best friend for their support and help over the years, because without them none of this was possible. I would like to appreciate all of my friends here in Göttingen and abroad that helped make this new country my home during my time here and encouraged me throughout this process too. I have developed many friendships that will hopefully last for a lifetime, and we shared many fond memories over the years. My family has also been incredibly supportive of me over the years and encouraged me to follow my career goals, even when this forced me to move to another continent! I will be forever grateful to them for this.